Carotenoids and Life, Femtoseconds and Light

Kloz, M.

2013

document version
Publisher's PDF, also known as Version of record

promotor: prof.dr. R. van Grondelle

copromotor: dr. J.T.M. Kennis

VRIJE UNIVERSITEIT

Carotenoids and Life, Femtoseconds and Light,

transient absorption

and femtosecond stimulated Raman spectroscopy

of free and bound carotenoids

ACADEMISCH PROEFSCHRIFT

ter verkrijging van de graad Doctor aan
de Vrije Universiteit Amsterdam,
op gezag van de rector magnificus
prof.dr. L.M. Bouter,
in het openbaar te verdedigen
ten overstaan van de promotiecommissie
van de Faculteit der Exacte Wetenschappen
op maandag 11 februari 2013 om 15.45 uur
in de aula van de universiteit,
De Boelelaan 1105

door

Miroslav Kloz

geboren te Jablonec nad Nisou, Tsjechie

Dedicated to all gifted who never got the opportunity

To all contributors who never been recognized

And to all who helped me and never got repaid

Carotenoids and Life, Femtoseconds and Light

***

Transient absorption

and femtosecond stimulated Raman spectroscopy

of free and bound carotenoids

Contents

Reader's guide:

The thesis consists of two parts. The Introductory Section and the Focused section.

The Introductory section contains two chapters. First chapter is an essay describing my personal view of Biophysics and its position in the context of Physics. There I dared to expresses my opinion on some very fundamental issues of science in order to reveal my motivations and driving forces that made me to take the direction in science I have taken. The second chapter of the introductory section is a brief, however within my possibilities, exhausting theoretical background to all problems covered during my graduate studies. This chapter in any way does not supplement the results and introductions presented in the following Focused section, but it is rather written with the intention to build a reasonable starting point from which the other parts of the thesis can be read and understood for a non specialist. Additionally I tried to focus on the parts of the theory which I myself found difficult to understand. So rather than repeating the established statements that left me puzzled I described everything the way I understand it now. This way the rigorosity was perhaps bit compromised but it was the intention to express my view as an experimentalist. The longest section dealing with the stimulated Raman process was written with the additional intention to express the most up to date view of these phenomena. This subchapter goes a little bit beyond the space of the already published and reviewed work and opinions. I stressed the parts concerning the problems of femtosecond Raman spectroscopy with the intention that this text will be a useful tool to anybody (hopefully another graduate student) who would like to get a quick contact with the front research in the field without digesting hundreds of pages of already published papers. I hope that my belief will be at least partially fulfilled.

The Focused section is collection of my articles in the order of publication. It contains all the papers published during my graduate work (it is always mentioned just below the title in which journal the work was published) but also it includes some of the work which is still in preparation for publication. This section maintains a more formal writing style which is now a consensus for scientific publications and each chapter represents a self standing piece of finished work. There was no effort invested in unifying the formats so each chapter mirrors the requirements of the journal in which it was published or to which it is prepared to be published. However the references were unified over the entire thesis in order to safe pages as the references are largely overlapping among the chapters. All the reference numbers in the text refer to the same list at the end of the thesis.

Introductory Section

1. Physics, biophysics, life, femtosecond, and photosynthesis

I dare to state that everybody who was given the opportunity to get at least a basic insight into the marvelous depth with which modern physics interprets the phenomena underlying the physical world would agree that this creation represents one among the highest achievements of human spirit so far. Not in its seeming entirety (I will get to this slippery issue later), but especially in unprecedented courage in shedding of the limiting boundaries and prejudices of any type of our common life intuition. Boundaries that turned out to be lethal for otherwise amazingly insightful science of antiquity. Through this the modern fundamental physics became a genuine discipline of philosophy and perhaps even the most prolific one. Practical application of modern physical laws led to a technological outburst that surpassed even the most fanciful 19th century Sci-Fi visions of the future. It can be argued that the outburst of literally all human faculties noticed over the last 150 years, from engineering to psychoanalysis, is directly or indirectly rooted in the success of physics. Is there still space for physics to expand? Is it realistic to expect even more from the fundamental physical research? It is hard to say, but I am certainly not the only one who strongly believes that there is still a "lot at the bottom". And this bottom does not necessarily have to be reached by hadron super-colliders.

In fact there is a great collection of questions to which even the most recent physical theories cannot give satisfying answers. Unfortunately, a lot of these mysteries are actually considered quite relevant for our human existence, such as the origin of cancer or distinguishing between good and evil. If we analyze all these tricky questions we will find that what they have in common is almost always their link with the unusual mysterious and enormously complex form of matter which we call "life". When it comes to the issue of life the only thing that the modern physicists are quite sure about is that all processes within living objects do not violate any of known physical laws. In other words life appears to be a part of the same physical reality as all the inanimate rest of the universe. But nevertheless there is still something "special" about life. First of all, its shameless richness in variation of forms, richness so vast that many respectable scientific disciplines are devoted to the sole collection and cataloging of mere fractions of this variation. The second is a contrast in surprising unity of the essential building blocks from which all the life seems to be derived. Besides nucleotides, amino acids, there is just a handful of cofactors and other molecules. It seems that all the life on Earth can be decomposed in just a few tens of building blocks! However difficult it is to set this number precisely, it is almost certainly smaller than for example the number of known subatomic particles. How can we explain that it was possible to find quite satisfying, universal and truly predictive models both for the jiggling world of subatomic particles and the equally mysterious world of spinning galaxies and black holes? How can we explain that there is no particular solution of our celebrated equations clearly

explaining the existence and evolution of life? How can the tremendous complexity of life be a product of our fundamental laws of the physics, known for its simplistic beauty rooted in countless experimental verifications often performed with a stunning precision and sensitivity? There are certainly many viewpoints from which we can tackle this, including fatalistic religious perspectives, however my personal opinion is on the side of perhaps the most trivial explanation: there is still a lot of work to be done when it comes to the formulation and understanding of the fundamental laws of the physics. The most obvious crack in the laws of physics lies in the very important fact, that for different scales of time and space we have a different set of laws of physics. For small scales the so called "Quantum physics", for medium scales the so called "Classical/special relativity physics" and for large scales the physics of "General relativity". We somewhat hypocritically assume that all of these "Physics" hold all the time and just at certain scales some became the dominant one. The fact is that theorists failed in finding any reasonable harmony between quantum and general relativistic principles. Perhaps the inertia in early 20th century based confidence of theorists led to the focusing especially on the challenging junction between the most extreme aspects of the relativistic and quantum physics, discussing issues such as miniature black holes or the early Big bang. I call it a "string theory junction". Unfortunately this (at least temporarily) stolen attention from another junction, to my belief quite equal to its sibling when it comes to the potential to drive a theoretician crazy: The junction between the classical and the quantum physics.

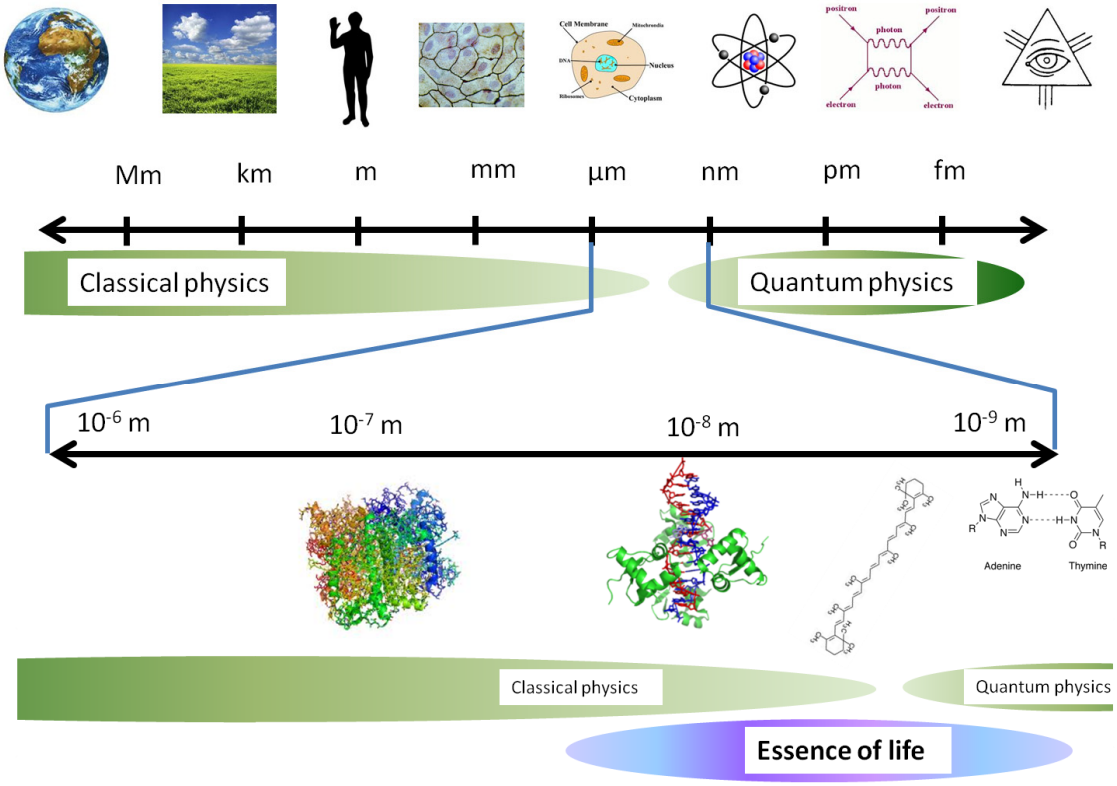

Figure 1

Different biological processes on a logarithmic spatial scale. Huge biological molecules such as proteins are unquestionably a biological material, too complex to be in any way assembled spontaneously. Such large systems are currently almost impossible to be understood in a fully quantum way. They belong to the world of classical physics. Small organic molecules such as DNA bases can be synthesized spontaneously and they can be understood in a quantum way, however they cannot be considered as a something living. Most simple bio-molecules such as tRNA or carotenoids lay almost exactly on the junction between the classical and the quantum worlds.

To illustrate this issue just a little bit more in detail I tried in figure 1 to illustrate, on a logarithmic scale, which processes occur at various spatial scales. As a biophysicist I dared to truncate the axis at large scales as cosmic distances seem to be irrelevant to the issue of life (this is not necessary true, but let's quit the debate on the topic for a while). On the scales of micrometers we can find the most primitive self sustainable organisms or organelles of eukaryotic cells. However simple and defined these small objects are in comparison to a human being, they are not entirely deterministic and display individual properties varying among the specimens. Crucial life processes operating at this scale level such as diffusion, aggregation, locomotion, osmotic pressure or electrostatic potential over the membrane can be efficiently described in a purely classical way. On the other hand the most basic building blocks of life, spanning the nanometer scales, such as DNA bases or amino acids are well defined molecules whose structures and properties can be very well calculated out of current quantum mechanical approaches. These objects are fully deterministic and undistinguishable from their copies in a deep quantum mechanical manner. Everything seems to be quite in order but is this enough for the development of a proper physical theory of life? Certainly not! The reason is that the true magic of life is hidden in amazingly flexible and powerful (mostly catalytic) activities of proteins and RNAs. Their activity is a result of processes that bridge the quantum world of molecules with the semi-classical world of large biopolymers. These catalysts appear to actively control the geometry at which the substrate, cofactor, and the protein moiety interact, achieving an acceleration of reaction rates by many orders of magnitude in comparison with the situation when the substrate and the cofactor would be freely dispersed in a test tube. The trick is that the quantum objects do not have perfectly defined positions so it is difficult to talk about the geometry of their interaction. Biological catalysts are true "nano-machines" with all the magic it may imply. Beautiful example is nitrogen gas fixation. A process which readily happens in soil or ambient water at room temperature and atmospheric pressure we have to perform under literary volcanic conditions of 20 MPa and 500˚C. What sort of physics do we need to describe and understand enzymatic activity of proteins? My strong personal belief is that it is far from a coincidence that these processes happen exactly at scales where the systems are too small to be treated classically but still having too many degrees of freedom to be handled by the full quantum mechanical treatment. Physical origin of life

seems to be safely hidden in a quite tiny interval of scales where we still struggle in formulating a powerful and reliable theories. In the interval where the uncertain world of time-spatially delocalized and fundamentally undistinguishable (or distinguishable) objects communicates with the mundane world of well defined individual objects.

Is there any way how to escape from this conundrum? Surprisingly yes! In comparison to the above mentioned "string theory junction" considering conditions such as 10^{-42} s after Big bang, we can investigate the "life junction" experimentally! This is of course not a trivial goal, but biophysics got a powerful ally. It is one of those human creations which were literarily unthinkable just a single generation before: The femtosecond laser.

The Femtosecond laser opened the doors for an explicit investigation of molecular and atomic motions. Light triggered reactions can be synchronized in an ensemble for a large number of identical molecules creating a macroscopic polarization of the sample. Quantum dynamics can then be analyzed by means of a macroscopic experimental apparatus. To get at least some feeling how fast timescales we can probe, now let's make this comparison: It is strongly believed that all processes in Universe started by the so called Big Bang about 13.7 billion years ago. This makes a formidable 7.2 x 10^{15} minutes since this event. But let's make a similar calculation from the other side: How many femtosecond events we have to pile up to make one minute? Well not less than 6 x 10^{16}, almost ten times more! In other words the difference between a second and a femtosecond is quite comparable with the difference between a second and the age of the Universe! In this context I can't resist to share another one of my speculations. From simple calculations I just spelled out we can see that the duration of the most essential manifestation of life – self replication – takes a time surprisingly quite close to the middle between the ultrafast period of quantum coherence in life relevant processes (~10^{-15} s) and age of the universe (~4.3 x 10^{17} s). In fact, essential processes of molecular biology such as DNA replication, or amino acid polymerization have a duration of one cycle almost exactly in the middle between these two extremes. May be it is just a coincidence that we got such a full taste of the universe at this time of its evolution. In any way these numbers are illustrated in figure 2 in order to get a visual impression of an amazing depth to which we can nowadays probe the ultrafast processes:

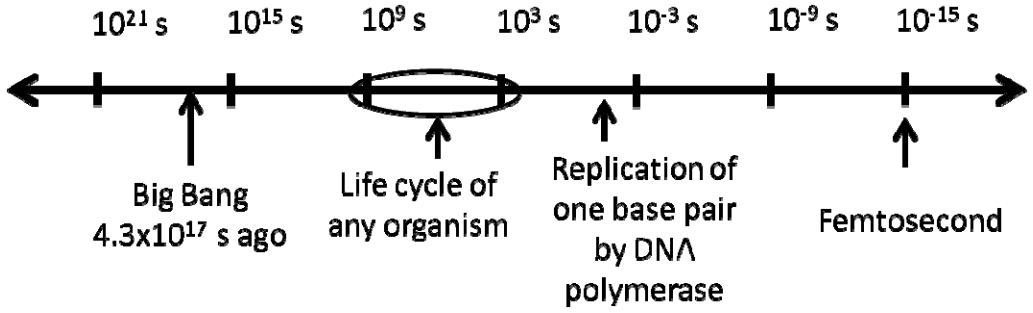

Figure 2

On the logarithmic scale we can see that a femtosecond (which we can nowadays handle experimentally!) is even more distant to our common life time scales than the Big Bang! Interestingly, the difference between the time scale of essential molecular processes of life such as DNA replication to femtoseconds is almost equal to the distance the age of the universe has to these processes.

But perhaps it is not an accident that we – intelligent living creatures – perceive the world on the scale from seconds to years rather than in microseconds or eons as some other organisms do. Importantly nowadays we can continuously probe all the time scales from years down to the femtosecond! This experimental possibility to trace life from quantum processes up to the lifetime of entire organisms is a unique opportunity. Most branches of physics can only dream about such a vast unexplored land waiting for an experimental colonization.

These cosmic thoughts brought us to the most essential aspect of biophysics which I skipped in the paragraph discussing the spatial scales. It is the link between the life processes on Earth and the thermodynamic legacy of the Big Bang. There is a huge and painfully underestimated misconception in the understanding of life processes among our society including our political leaders. This misconception is the belief that life processes (including our meta-organic technical civilization) require energy for its function! The truth is that energy cannot be produced neither be consumed in any way! What life really needs is a very specific flow of energy commonly described by means of a bit mysterious quantity called Entropy. This misconception is far from being just a word play. The essential difference is that the concept of entropy inevitably works with a difference between the System and its Surrounding. Thinking by means of entropy contains an important fact that life requires receiving of something “high grade” from outside and producing something “low grade” as waste. In fact there are many ways how this can be achieved but prior to the ascent of Man, more than 99.9% of life was directly or indirectly maintained by receiving “high grade” hot photons from the Sun and as a waste irradiated “low grade” cold photons into the extremely cold Space background. Everything else remained practically constant on Earth. This extreme difference between the temperature of a source and sink is in fact the reason why living organisms have enough potential to execute processes such as the mentioned nitrogen gas fixation. This “space entropy socked” feeding an absolute majority of life on Earth for more than a billion years without necessarily altering high grade parts of our planet into the low grade waste is called photosynthesis. This is illustrated in figure 3:

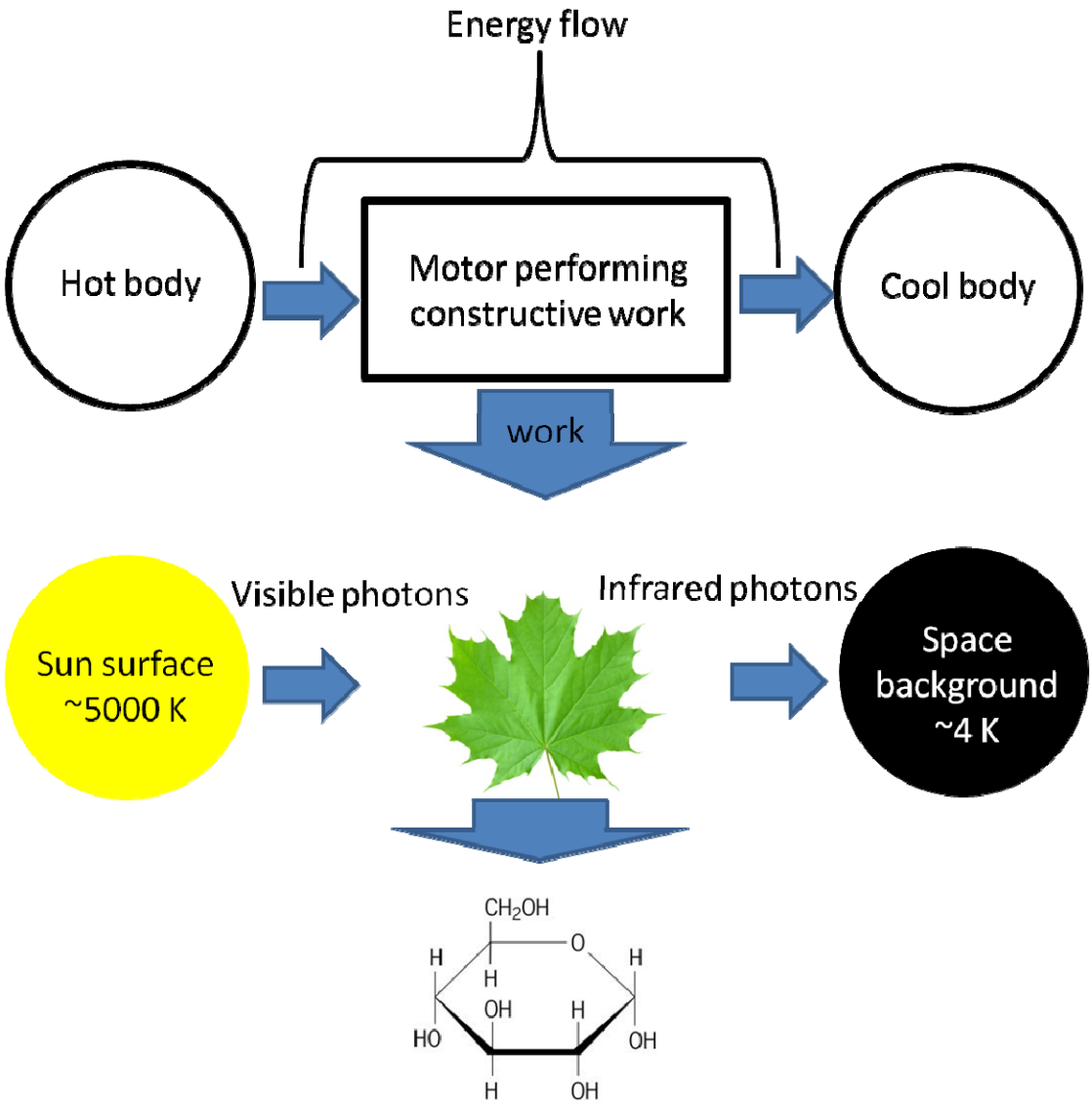

Figure 3

Photosynthesis can be viewed as a typical motor using two thermal baths of a different temperature. The potential efficiency and power of any engine is known to depend on the temperature difference between the baths. For photosynthesis this difference is actually more than 5000 ˚C (more than in any man made engine or power plant, despite the light gets cooled down by atmosphere catching the high energy radiation). Quantities such as temperature are in a way restricted to the macroscopic world, but in a very simple way we can say that the pigment in a photosynthetic organism that just absorbed a visible photon is extremely hot and in fact the organism has to handle this "exciton" with the similar safety regulations as we would have to handle something thousands ˚C hot. Some other parts of this thesis deals with this "photo protection" issue.

The most common opinion is that photosynthesis did not play a role in the origin of life. I think that it is largely based on the fact that photosynthesis is already understood to be just too complicated to arise spontaneously, but the same holds for practically any aspect of life.

In fact the origin of life as well as of photosynthesis is still a huge mystery. But it is quite sure, that photosynthesis is certainly the physically most advanced form of life processes, at least in a sense of the underling molecular biology. In a bit trivial way we can say that the switching from heterotrophy to an autotrophy was a progress from the fuel based combustion engine culture to the solar electricity based culture, just within the biological rather than industrial framework. Unfortunately biological structures have problems with making macroscopic electric circuits (similar as they have with macroscopic rotational motion) so they need a constant supply of electrons when executing photosynthesis. The most advanced photosynthetic organisms sorted out this problem by a mechanism almost equally influential as the photosynthesis itself: Splitting of the most abundant molecule on Earth surface: water. The fact that living organisms can perform this four-electron process at room temperatures using only moderately rare elements is (together with few other similar achievements such as mentioned splitting of nitrogen molecule) a true wonder of life. Study of processes like this should stand and fortunately already stands in the center of attention of molecular biophysics.

What message can we take home from all these ideas? First of all that there is still a lot of work for physicists to be done. It is a very philosophical question if ever we will be able to tackle issues such as a meaning of life by the unforgivingly exact and materialistic intellectual machinery of physics. But there are plenty of perfectly reproducible and physically well defined processes going on all around us that call for a real physical understanding. There is a well established belief that all biology can be reduced to chemistry, that all chemistry can be reduced to physics, and that physics explains everything by just a handful of 100% valid laws of the material world. The truth is that none of these reductions is firmly established. Especially when it comes to biomolecules there are countless properties waiting for a deep fundamental physical understanding. What comes first to my mind are for example processes such as a protein folding, all sorts of a weak signal sensing of animals and plants such as a magnetic field sensing, or protein catalysis in general. There seem to be no reason why these processes should be beyond our grasp and recently lot of progress was noticed in this direction, but yet they are largely a mystery at the moment.

The second message is the importance of experiments. Some people can disagree with me, but I believe that biophysics is just in its beginnings. History is written in words and so the people who gave things their names, and those are the theorists, are the most recalled. However a careful investigation clearly points out that the driving force of a progress in physics was always an experiment. In fact it took quite a long time for experimentalists to undermine the classical physics to the state when theorists eventually moved forward. It seems to us to be almost confusing how the late 19^{th} century physicists could be so fatalistic about their theories when they literary excluded things such as a stability of matter from their attention! A theory made by pure theoreticians and mathematicians always inclines towards the rigidity but especially often tends to design stronger and stronger microscopes

while missing the possibility of telescope (or the other way around) if I may use such a metaphor.

Let's mobilize the joint effort of experimentalists and theorists to challenge the "little big gap" between the classical and the quantum world. I will not be surprised if the progress in this direction will bring into the question even some very fundamental building blocks of our current physical theories. There are hidden the true origins of life! And don't forget that we and our ideas and models are just a part of it. I hope that my graduate work, focused on femtosecond spectroscopy, may contribute to this great mission by at least the tiniest piece.

2. Theoretical and practical background of works presented in the focused section

2.1. Molecular quantum mechanics and the femtosecond

It is generally accepted that quantum processes dominate at small scales, usually far beyond the resolution of any optical microscope. Many classical books put forward particular explanations for it but the question why we do not perceive any of the crazy quantum physics effects at large scales is actually very complicated, perhaps largely even not understood. In a way we perceive the quantum physics all around us in the form of the variety in matter. All properties of materials, such a conductivity of metals or a stiffness of diamonds are purely quantum effects. The "static effects" of quantum mechanics are actually very well manifested in the macroscopic world. So the question should be perhaps reduced to: why we do not observe any macroscopic quantum dynamics? Without going deep into the problem (which would be interesting, however beyond the scope of this thesis) we, physicists, generally believe that the quantum dynamics kind of "average out" among the individual microscopic parts of the macroscopic objects. But how does it happen? It is a result of two quite independent aspects. The first aspect is that the quantum effects are generally governed by periodic functions, in the simple cases literary wave-like functions. This is a direct result of the quantum mechanical equations such as the Schrödinger equation. The second aspect is that the quantum processes are extremely fast and the period of quantum oscillations is in most cases remarkably short. This is a direct result of the extremely small value of the Plank constant ħ.

In a very crude way we can imagine this as if we would be sitting in a bullet proof tank and receiving hits from hundreds of AK-47 assault rifles behind the hill. The individual parts of the "enemy" communicate with us exclusively by an exchange of particles (as the quantum systems do), however we would perceive the "enemy" just as a macroscopic repelling force field as all the bullets would hit us so fast that their only manifestation would be a constant pressure. It is important that if we would be able to record the pressure on our tank with extremely high time resolution, we would be able to record hits from individual bullets and resolve the quantum nature of the process. This is what the ultrafast spectroscopy is about. In fact we do not necessarily need any microscope to study the quantum dynamics of molecules and molecular complexes. Practically equally deep insight can be achieved by performing macroscopic experiments just with femtosecond time resolution!

2.2. Transient absorption experiment

2.2.1. Semi classical picture

Thanks to the advent of ultrafast lasers, capable to generate just a few optical cycle pulses, the spectroscopic experiments became the first experiments we can perform at the truly quantum time resolution. I will explain the basics of these experiments by the transient absorption experiment, however the fundamental basis is always the same: One pulse, commonly called a pump (Pu), is used to trigger a reaction for many molecules in the sample at the same time in a highly synchronized way. After a carefully controlled time delay the system is interrogated, in case of a transient absorption experiment by another ultrashort optical pulse denoted as a probe (Pr). Changes of the studied system during its reaction are manifested by changes of its absorption/emission properties. This approach is often called a "pump-probe" experiment and it is visualized in figure 1. Because it is practically almost impossible to have a precise control over the exact number of excited molecules (and so to separate the signal from the excited and the relaxed molecules), what it is usually recorded is not the absorption spectrum of an excited molecule, but the so called "transient absorption spectra". This is simply the difference between absorption spectra of pumped and un-pumped sample. This quantity can be recorded with a high reproducibility and also high sensitivity. The drawback is that the transient absorption spectra display both negative and positive signals and therefore are a bit more difficult to read.

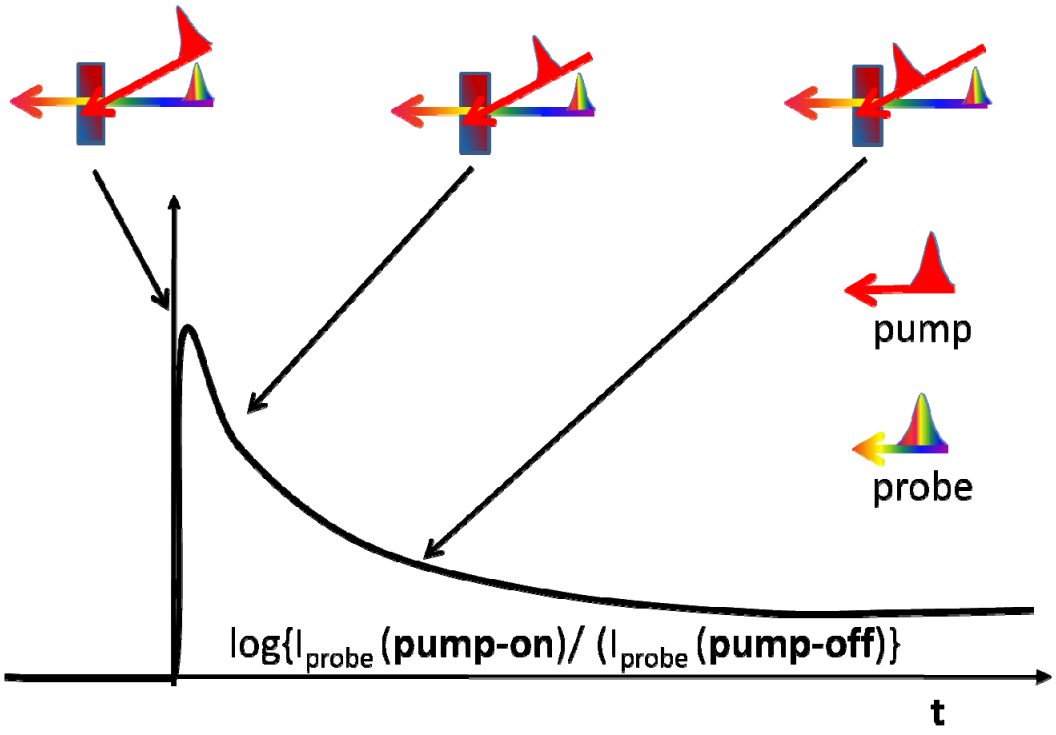

Figure 1

The basis of the ultrafast spectroscopy is to trigger some reaction at an extremely well defined moment by a laser pulse (usually called Pump) and then investigate the spectral property of the system after a certain delay, usually by another pulse called Probe. The response of simple molecules is often manifested as a sum of exponential decays of transient absorption spectra.

The most essential effects usually encountered in this type of experiment can be fortunately explained by the so called "semi-classical" picture without recalling too much of quantum theory. The semi classical picture is basically a classical point of view where the "only" component we take from the quantum physics is the fact that electrons in the system can occupy only specific states with a defined energy. While the relaxed sample manifests only absorption of light in the HOMO-LUMO transition, the excited sample displays three essential phenomena when interacting with light. Those are: excited state absorption (further absorption of already excited moleculess), stimulated emission (forced transition of an excited molecule to the ground state associated with the amplification of the probe light at the corresponding wavelength), and ground state bleach (drop in a ground state absorption due to electrons missing in the ground state). In a simple scheme the ground state bleach and the stimulated emission should be manifested in a same way but in real systems the stimulated emission differs from the ground state bleach by the stokes shift originating in vibronic and solvation effects. This is illustrated in figure 2.

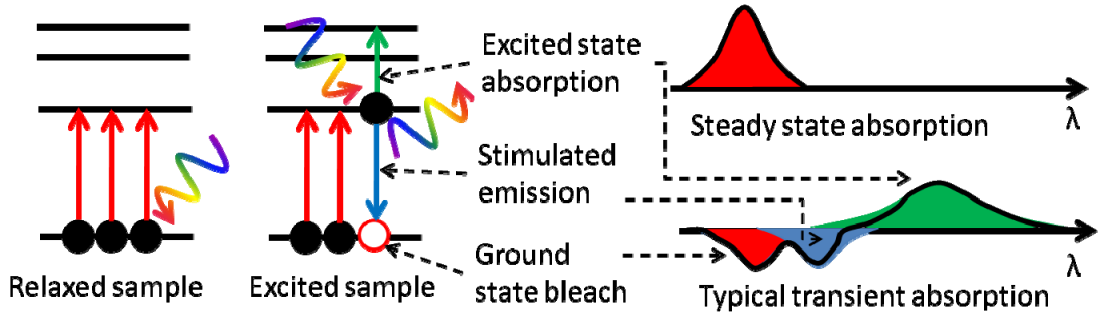

Figure 2

The main signals we can recognize in the transient absorption spectra. Two are negative: ground state bleach, and stimulated emission. One is positive: excited state absorption.

2.2.2. Technical realization of pump probe experiment

There is an important technical aspect to the femtosecond pump probe experiment. Because no electronic shutter or trigger system can operate with femtosecond precision, the only way to perform the experiment is to prepare all the involved pulses from one original pulse. All the logic, pulse manipulation and timing control have to be realized in a purely optical way. In fact this is the main reason why it is so difficult to make a pump probe

experiment into a “turn-key” box as it is very common for the majority of steady-state or low time resolution spectrometers. The problem will be most probably solved by an extensive use of a fiber optics, adaptive optics, and automated feedback loops, but at the moment the common optical fibers cannot stand the field intensities usually encountered during experiments and still induce a large spectral dispersion into the propagating pulses. Luckily at least for those who are not frightened to play with the optics at a daily basis the necessity of preparing all pulses from a one original “seed” is realizable thanks to several phenomena exclusive for ultra short pulses.

A great event for the development of ultrafast spectroscopy was the invention of a technique called chirped pulse amplification (1). The principle is that the ultrashort pulse is intentionally severely spectrally dispersed, amplified in this stretched form, and then again recompressed. In this way extremely strong pulses can be generated. Nowadays there are commercially available lasers producing mJ pulses, while home-built system can generate pulses with energies more than 1 J. This perhaps does not seem to be so impressive, however given the ultra short nature of the pulses the peak power of the pulse is in the range of TW! Field intensities inside the pulse are so strong that the pulse interacts in a non-linear way with virtually any type of matter. This allows using nonlinear optical devices combining parametric amplification with higher harmonic generation and sum (difference) frequency generation in a way that literary any wavelength from UV to mid IR can be prepared out of the fundamental laser wavelength (usually around 800 nm or 1064 nm depending on the type of working medium) with an efficiency often exceeding 10%. The high peak power of the pulses also allows harnessing a phenomenon called a “supercontinuum generation”. When the femtosecond pulse is focused into some medium ecord></Cite></EndNote>(18) in exceptionally fast. Thanks to it this Raman active vibration with lifetime as short as few picoseconds became a sort of etalon for testing ultrafast Raman techniques ADDIN EN.CITE pulses spectrally spanning more than a whole octave that is more than the entire visible light region. This white light is excellent as a probe for a majority of experiments. Complete transient spectra from near UV to near IR can be then recorded without any type of scanning and alteration of the experimental equipment.

2.3. Global fitting analysis

In the previous chapter I have shown how we can recognize excited states in the transient spectra. But we usually want to know more than the spectra of excited states and their lifetimes. In fact the biophysicists are interested especially in mutual interactions of parts of complex biological macromolecules. One of the most thoroughly understood processes of this kind is the energy flow in light harvesting proteins and also in charge separating photosystems. In cases like this we face signals from multiple chromophores often with largely overlapping spectra. There is a valuable signal processing tool for disentangling all the recorded entwined signals. It is called “global fitting analysis”.

The global fitting analysis is in fact a multiple stage process often working in a target approaching spiral (2). First an assumption about the system is made, in case of a photosynthetic protein an assumption about energy transfer pathways and rates. According to this assumption a so called “compartment model” is constructed. The concept of compartment models is largely used in many fields such as a pharmacology, where it models how the concentration of a drug evolves in organs and tissues. The system is modeled as a sum of compartments which are connected via simple linear differential equations (which basically means that compartments tends to exponentially decay into each other). This produces a model consisting of n compartments which can have in a most general way n^2 rate constants describing all possible flows between the compartments. In case of a spectroscopic experiment the energy tends to cascade downwards so in reality we have to consider hardly a half of the flows, but usually even less. The important property of these models is that they always have a solution in the form of n spectral components each evolving in parallel to each other as a simple exponential (this is entirely true under certain conditions considering sources and sinks, but in the spectroscopic experiments we face a sufficiently simple scenery). The recorded time resolved data (a temporal evolution of the transient spectra) then can be fitted as a linear superposition of exponentially evolving spectral components (this fit is sometimes called the Decay Associated Spectra - DAS). The fitting of DAS is a difficult however numerically doable task. Importantly the fitted spectral components and the associated rates can be linked with the model and used to recalculating backwards the spectra of the assumed compartments and the rates among them. For simple cases such as compartments linearly following each other (the so called “sequential model” or the “sequential scheme” or evolution associated decay spectra “EADS”) there is even a direct algebraic solution linking the fitted DAS with EADS we are interested in. The procedure is illustrated in the figure 3:

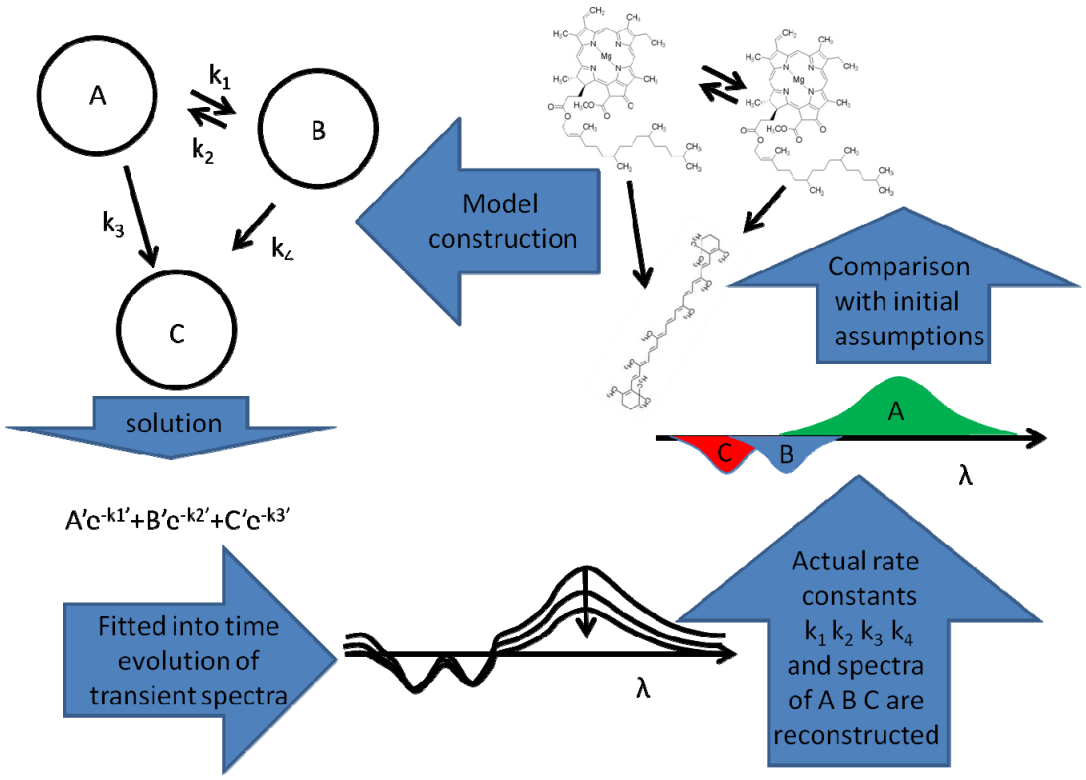

Figure 3

A global fitting analysis is a circular process. A real system is first simplified into a compartment model. Solution of the model is fitted to the time resolved spectra. This allows to derive back the spectra associated with compartments and rates connecting them. This result is compared with the real system. When the result is found to be inconsistent with reality it can be used as a starting point for a different model. This process is repeated until we have a model that at the same time perfectly fits the experimental data and does not contradict the physics or the knowledge about the system. In this case the model probably reflects the true processes inside.

In fact multiple rounds through the process have to be usually made until we find a model that perfectly fits the experimental data and does have a reasonable physical sense at the same time. The second condition is very important. Especially when the model contains many branchings at a certain number of compartments it can reach a level of complexity where it is capable to fit practically any experimental data. Models more complex than the sequential scheme are usually fitted with many parameters (such as branching ratios) artificially fixed to certain values. In this case we can keep the model safe from fitting unrealistic values but we still have to be sure that we made the restrictions correctly. A general rule of thumb is that we have to be very critical to any effects which are extracted by the fit but do not show any sign in the raw data. To use the global fitting correctly, recognize artifacts, and avoid typical pitfalls needs a certain experience, but everybody can learn it from practice.

However complicated the procedure seems to be nowadays we can use software that will do all the math for us. There is a publically available fitting R package called TIMP (3) (developed by former and current members of our group in Amsterdam) specially designed to fit the compartment models to time resolved data. Now it exists also with a GUI extension allowing a highly user friendly fitting. This freeware can be found under the name GLOTARAN (4). Despite the risk of "over fitting" the global fitting analysis represents an extremely valuable tool for the analysis and understanding of the time resolved spectra.

2.4. Crucial elements from advanced theory of non linear spectroscopy

2.4.1. Density matrix

So far we practically thought about the experiment as if the ensemble of synchronized molecules would behave the same way as a single molecule, however this is at a certain point an unbearable simplification. I will try to illustrate this for the most simple case when the sample would consist just of a pair of two level systems:

Imagine first an experiment on a single molecule having just two states |1> and |2> and for simplicity let's assume that we can repeatedly prepare the molecule in the same quantum state. If we would record the molecule being for 50% in state |1> and for 50% in state |2> then the only possible state of the molecule that can explain such an observation is a wave function that has an equal amplitude for being in state |1> or in state|2>. For example:

$$\psi = 1/\sqrt{2}(\,|1> + |2>)$$

For an ensemble of two molecules the same result of the experiment can be explained in two quite different ways: one possibility is similar to the one mentioned above: a pair of particles in superposed states:

State of particle 1: $\psi_1 = 1/\sqrt{2}(\,|1> + |2>)$

State of particle 2: $\psi_2 = 1/\sqrt{2}(\,|1> + |2>)$

But it may be also just one particle in state |1> and the other in state |2>:

State of particle 1: $\psi_1 = |1>$

State of particle 2: $\psi_2 = |2>$

Both states of the ensemble give the same result of the measurement when we randomly choose a particle and perform a measurement on it. However these two states of the system are fundamentally quite different. The former is traditionally called a

"superposition" state the latter is described as a so called "mixed" state. In fact mixed states do not have a meaning in a pure quantum mechanical treatment because the strictly applied quantum mechanics does not permit to treat one part of the system independently from another. For this reason theorists prefer to work with the so called "density matrix". The density matrix is formally a convolution of a wave function with itself and does not longer represent quantum amplitudes but rather already the explicit probabilities. On the diagonal are the actual probabilities to find the system in a certain state, those are called the "populations". Interpretation of the off-diagonal terms is a somewhat more complicated, but they represent kind of probabilities of the system being in a certain selected pair of states at the same time (in a quantum sense). The off-diagonal elements then serve for kind of a bookkeeping of correlations between the states. In practice they usually periodically oscillate in time as the system evolves and are called the "coherences". A comparison between the wave function and the density matrix formalism is summarized in the table 1:

	Common shortcut	For Dirac	For Heisenberg	obey equation
Wave function	ψ	|ψ> or <ψ|	vector	$i\hbar\dot{\psi} = \hat{H}\psi$
Density matrix	ρ	|ψ><ψ|	matrix	$i\hbar\dot{\rho} = \left[\hat{H}, \rho\right]$

Table 1

A comparison of a notation and the main properties of a wave function and a density matrix formalism. Note that the density matrix evolution is determined by a so called Liouville-Von Neumann equation rather than the Schrodinger equation. This equation contains Hamiltonian in a commutator.

If we compare the two above mentioned states represented in the form of the density matrix the first (superposed state) is:

$$\begin{matrix} 1/2 & 1/2 \\ 1/2 & 1/2 \end{matrix}$$

while the second (mixed) state is:

$$\begin{matrix} 1/2 & 0 \\ 0 & 1/2 \end{matrix}$$

The superposed and the mixed states are distinguishable. The density matrix then serves as a kind of "bookkeeping" of the extent to which each measured probability is a result of superposed states or a mere mixture of molecules in different states. The more diagonal the

density matrix is, the more the system is in a mixed state. Additionally, the fact that the density matrix is explicitly linked with the measured probabilities (in contrast to a wave function containing quantum amplitudes rather than explicit probabilities) allows incorporating many phenomenological terms into the calculation. Those are especially a so called “dephasing” and a “population relaxation”. It is far beyond the scope of this thesis to describe these issues in a detail, and none of the works in the following chapters deals with these issues. But we can briefly characterize their meaning. At the beginning of this chapter it was mentioned that most quantum properties are described by periodic functions. When the period of these oscillations slightly varies among the individual molecules in the sample, after a certain time they become to oscillate out of phase and the sample does no longer behave in a quantum way on a macroscopic scale. This process is commonly compared to a long distance race in an athletic stadium. At the beginning all runners move in a swarm, but after a couple of rounds they become spread all over the stadium as their speed is not an exactly equal. There are multiple causes of these variations among the molecules, but we divide them into two large groups: “homogenous”, and “inhomogeneous”. In the most simple way the homogeneous are those that change speed quickly in time while the inhomogeneous stays the same for a period of time longer than the dephasing. This distinction is made for the reason, that the inhomogeneous dephasing can be experimentally reduced, while the homogeneous cannot. In the density matrix formalism the dephasing is usually included via artificially forcing the off-diagonal elements of the density matrix to decay to zero. The population relaxation is associated with an intrinsic transition of molecules to the ground state. Regardless if the system is in a superposition or a mixed state, after a certain time all molecules have to relax to the state defined by thermal equilibrium (for electronic states at room temperature it is simply the ground state). Again this effect is usually treated phenomenologically by plugging-in exponential terms forcing populations to decay.

2.4.2. Interaction of density matrix with electric field

I have shown above that we can understand the essentials of a pump-probe experiment without bothering with the quantum nature of an interaction between the system and the field. However, more complex phenomena such as stimulated Raman scattering cannot be fully understood this way. First of have to inspect the dynamical equation for the density matrix (the so called Liouville-Von Neumann equation shown in table 1) more deeply. Formally it is nothing but a reformulation of the Schrödinger equation for the density matrix. The essential difference from the Schrodinger equation is the presence of a commutator:

Equation 1.1 $i\hbar\dot{\rho} = \left[\widehat{H}, \rho\right] = \widehat{H}\rho - \rho\widehat{H}$

This means that any interaction with the field happens in two ways, with each of the two complex conjugates forming the density matrix independently. This is usually somewhat magically shortened as an "interaction with the |ket>" or "interaction with the <bra|". For those who are fond of fancy interpretations of quantum mechanics, it can be understood as an interaction with the system propagating "forward in time" or "backward in time". I always wondered why in the Schrödinger picture we can live without this strange property, especially because it has such an important consequences! The way I understand this conundrum is that problems where all the degrees of freedom are treated in an entirely quantum way always result in periodic solutions (such as motion of electrons in hydrogen atom). In this case the direction of time does not have a meaning and the complex conjugates are just phase shifted identical twins. Working with the density matrix and the Liouville-Von Neumann equation is then just a complicated way leading eventually to the same results as the Schrödinger picture. So the necessity to work with a matrix rather than with a vector and the necessity to consider the forward and backward interactions independently is a price we have to pay for the fact that we simulate huge systems with in exceptionally fast. Thanks to it this Raman active vibration with lifetime as short as few picoseconds became a sort of etalon for testing ultrafast Raman techniques ADDIN EN.CITEopic.

Importantly we can (and we have to) think about the electric field in a similar way. The real sinusoidal electromagnetic wave consists of two complex conjugates:

Equation 1.2 $cos(\omega t) = 1/2\left(e^{i\omega t} + e^{-i\omega t}\right)$

and the system can interact with the field only by an exchange of one quantum ħω.

So the system evolves simultaneously in two quite opposite ways and the field can also interact in two opposite ways. It is an essential property of the quantum mechanical formalism that the full response of a system to the interaction with a field can be calculated only by considering all the possibilities how these, in a way indistinguishable, alternatives get entangled (in an approximate approach called the "perturbative expansion of density matrix" (5)). What is a forward interaction for the |ket> is a backward interaction for the <bra| and the other way round. It perhaps sounds over-engineered and complicated (and perhaps it is), but it works and in fact there are beautiful ways how to keep track of all the possibilities and at the same time inspect their qualitative properties. I will describe two of the approaches: the "double sided Feynman diagrams" and the "wave mixing energy level diagrams" (WMEL). Feynman diagrams are certainly seen more often in the literature, however I find the wave mixing diagrams easier to be read and inspected, at least for simple processes. For this reason I am not surprised that they are becoming more popular nowadays and they will dominate in this thesis. The choice certainly depends on the purpose but I cannot resist to speculate that the dominance of double sided Feynman diagrams is partially caused by the fact that people feel more "fancy" while using them.

In the Feynman diagram formalism the system evolves in successive steps. Because these steps cannot be explicitly considered as an evolution in time this evolution is commonly called a “vertex”. In each step the system undergoes just a one interaction with field either with the |ket> or the <bra| side. This interaction can be an absorption and excitation of the system or an emission and associated de-excitation of the system. When the left and the right side of the density matrix are not in balance, the system is in a “coherence” and kind of oscillate between the two states. When the both sides of density matrix are at the same state, the system is described as being in a “population” and sits firmly in this state. In this formalism the system has to always end up in a population state so the last interaction is kind of “predestined” by the state in which the system is left after all previous interactions. This last interaction is commonly called a “free induction decay” (FID) and usually represents the signal we get from the sample. The detailed guidelines for the use of the Feynman diagrams can be found in many textbooks (5, 6). In figure 4 I displayed Feynman diagrams and corresponding wave mixing diagrams for the most common process encountered in the transient absorption spectroscopy. Note that all pathways exist in two mirror images so the usual convention is to plot just pathways that ends with the emission (FID) from |ket>. These two mirror images represent merely the complex conjugate of the same process.

Wave mixing energy level diagrams are fundamentally the same formalism with the only difference that the vertex is going from left to right rather than vertically and the states are not denoted by indexes but rater visualized by vertical lines in a Jablonski-like energy level diagram. The <bra| interactions are distinguished by a dashed arrow from the|ket> interactions plotted as a full arrow. WMEL can be viewed as two Jablonski diagrams (one for <bra| and another for |ket>) merged into the one in order to incorporate the density matrix formalism. Formally in Feynman diagrams only the interactions are depicted schematically while in WMEL both interaction and energy levels are plotted schematically so Feynman diagrams are more abstract and general. This makes Feynman diagrams better suited for those who prefer the algebra and a general view on the processes and WMEL for those who prefer visualizations and connection with a specific system under study. Figure 4 displays both Feynman diagrams and WMEL in order to facilitate establishing a link among them.

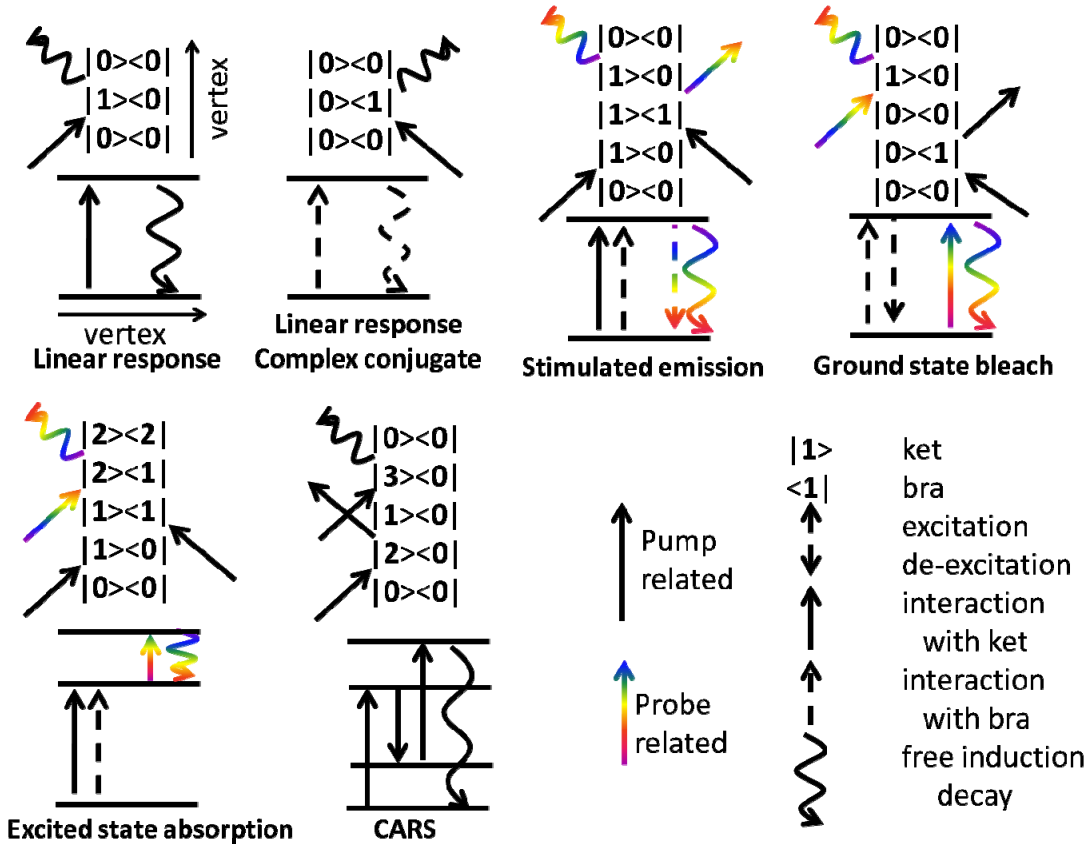

Figure 4

Feynman diagrams and corresponding wave mixing energy level diagrams (WMEL) for the most common processes encountered in the pump probe transient absorption spectroscopy plus a diagram for the CARS as an example. In the WMEL the <bra| interaction is distinguished from the |ket> by a dashed arrow and the vertex is horizontal rather than vertical. The free induction decay (FID) is displayed as a wavy arrow. In Feynman diagrams states are numbered from bottom starting with 0. Note that many processes can be described without considering the right side at all such as CARS or the linear response.

2.4.3. Pump probe spectroscopy in the light of Feynman diagram

In the light of the full formalism of nonlinear spectroscopy, the pump-probe phenomena described in chapter 2.2.1 in a semi-classical way look somewhat more complicated. I would like to point out what new aspects we can actually learn by accepting these complications. First of all, the pump probe experiment is actually a so called “four wave mixing” process (the three wave mixing processes cancel out in the isotropic medium). It means we force three interactions between the field and the system to create the free induction decay

emitting the desired signal. When we perform the experiment by an arbitrary crossing of the pump and the probe beams in the sample and measure the signal as changes in the outgoing probe intensity, we actually perform a very restrictive selection among the Feynman diagrams that can contribute to our signal. This is due the process called a “phase matching”. Each quantum of field carries not only the scalar energy but also the vector of momentum. Momentum has to be conserved as well as energy and so the direction of the emitted signal is in general dependent on the direction of fields that prepare the free induction decay (as long as decoherence did not occur and the sample is large in comparison to the wavelength of the applied field). In fact, the signal field can be emitted in a direction which does not coincide with any of input fields. When we look for the signal in the probe pulse direction in the noncollinear experiment, we automatically select for the nonlinear phenomena where momenta from the other pulses except the probe cancel out. A most simple way to achieve this is to have two opposite interactions with the pump. Figure 5 illustrates how the stimulated emission or the ground state bleach appears in a pump probe signal while the CARS signal generally should not, despite it is a two pulse mediated four wave mixing signal as well. Effects emitting the signal field in the probe direction are usually a way more convenient for measurement than the others and we call them “self heterodyned”.

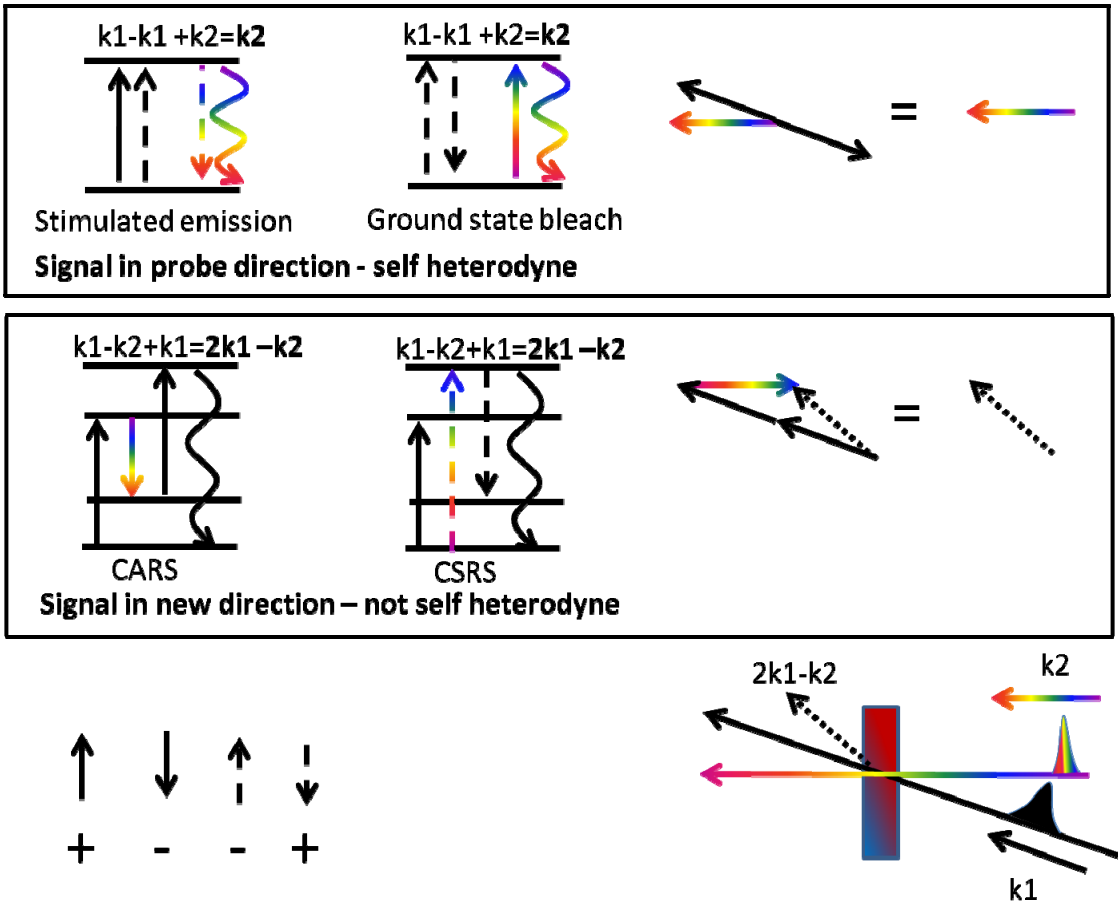

Figure 5

Photons carry also a momentum. In coherent experiments (the pulse sequence is executed within the decoherence time) the direction of the emitted signal depends on the bulk momentum exchanged between the field and the sample. The processes leading to emission of a signal into the probe pulse direction are described as a self heterodyned.

The reason is that in practice we almost always have to work with detectors that, rather than the field, record the light intensity which is the square of the field. The square of a something small is even smaller, so the recorded signal is very weak. However, when the field is emitted along the probe pulse direction it interferes with the probe pulse field and makes a part of the signal linear in the intensity:

Equation 1.3 $$I = \left(E_{Pr} + E_{sig}\right)^2 = {E_{Pr}}^2 + 2E_{Pr}\boldsymbol{E_{sig}} + {E_{sig}}^2$$

As a surplus the recorded intensity is sensitive to the phase of the signal. For basic pump probe processes the intermediate state between the pump and probe is a static population so the phase sensitivity does not have an effect, but it is useful in more complex experiments such as the multidimensional experiments (6). When we want to get all of this for a non self heterodyne process, we have to add a one extra pulse perfectly coinciding with the signal vector, which is a significant additional effort and a technical difficulty for the experimentalist.

2.5. Femtosecond stimulated Raman experiment

2.5.1. Stimulated Raman scattering

Raman scattering is a nonlinear optical process where one or more of the intermediated states is a vibrational state. In fact there are multiple processes of this kind. I have shown in figure 5 that the four wave mixing coherent Raman processes such as the CARS or CSRS do not contribute to a signal in experiments performed in a so called pump probe geometry. However there is one four wave mixing Raman process producing a self heterodyne signal in the pump probe geometry. It is called “stimulated Raman scattering” (SRS). Later I will explain why the spontaneous Raman scattering can be considered just as a special kind of the SRS. In the most simple way, SRS can be viewed as an exchange of a photon between two fields where a vibrational transition of the molecule is used as a resonator and a sink for the energy and momentum lost in the process (figure 6). Because none of the intermediate states is a population and the pump and probe originating interactions are alternating over the vertex, SRS is manifested only when the pump and probe pulses are overlapped in time. Later, when discussing the theory of femtosecond SRS in detail, I will show that this brings a

necessity to actually include a few more four wave mixing pathways than the one shown in the figure 6 in order to understand all the SRS related phenomena.

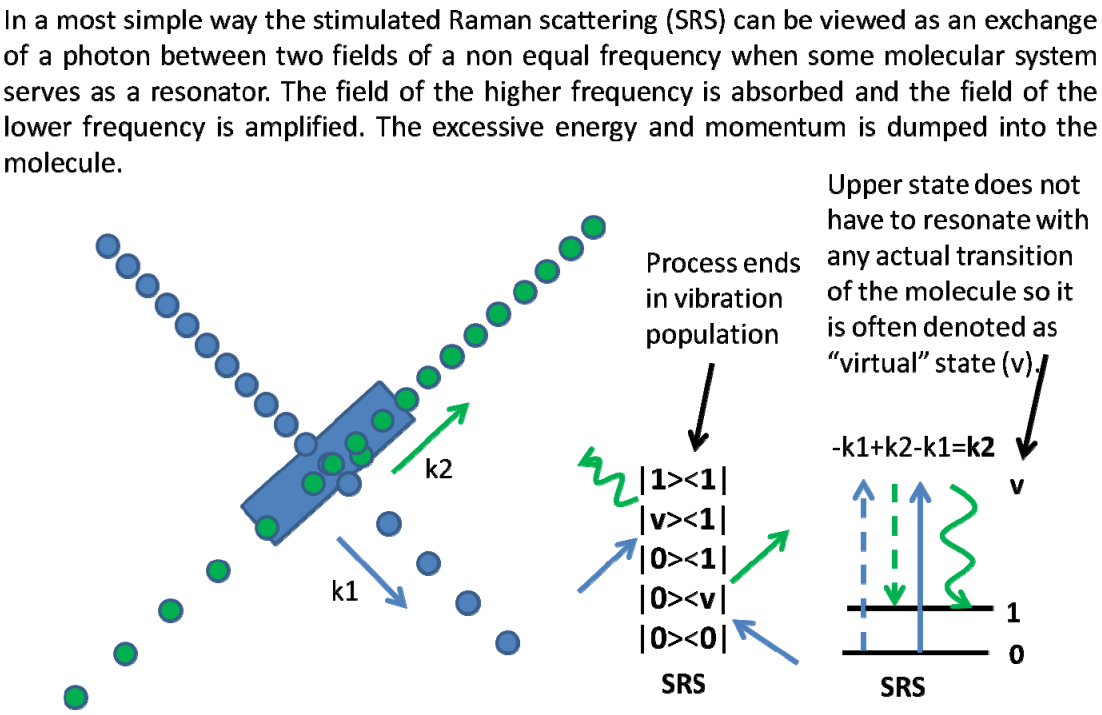

Figure 6

SRS is a process where two fields exchange a photon using a molecule as a resonator. When one field is considered as the pump and the other as the probe the SRS can be described as a self heterodyned pump probe process. The underling mechanism is actually a four wave mixing process related to the ground state bleach (figure 4) but with partially swapped ordering of fields.

We can see that the amplified field contributes to the process only via a one <bra| de-excitation (green dashed arrow in the figure 6). This de-excitation can be mediated also by the vacuum field fluctuations. This is the origin of spontaneous Raman scattering. Because the vacuum fluctuations are not oriented, the spontaneous Raman scattering photons are emitted to all directions in a similar way as a fluorescence.

The SRS phenomena have been known for many decades. One of the elementary uses is the tunable conversion of laser light towards longer wavelengths by Stokes shifting chosen narrowband pulses in Raman active medium. However, prior to the rise of femtosecond lasers, SRS was practically never used for the actual recording of Raman spectra. In SRS, the Raman resonances are manifested just by an amplification of the low frequency field, so the SRS signal generated in a thin sample has to be resolved on top of a strong baseline light intensity (7). For CARS or CSRS emitting non-collinearly with any input field, the Raman resonance is manifested as a convenient rise of the signal from zero. Mostly for this reason, CARS and CSRS dominated over SRS in the field of coherent Raman spectroscopy during the

era of ultrafast spectroscopy performed with non-spectrally resolved detection. A quick and massive outburst of femtosecond experiments employing the broadband super-continuum generated probes and fully spectrally resolved detection gave SRS a new dimension in so-called femtosecond stimulated Raman scattering spectroscopy.

2.5.2. Femtosecond Stimulated Raman scattering – experiment

Figure 7 shows a phenomenological description of Femtosecond stimulated Raman scattering (FSRS). The essence of the FSRS experiment is performing SRS with one spectrally narrow pulse (historically called the Raman pump - Rp) and one ultra short and broadband pulse (called the probe - Pr). In this configuration, the broadband pulse is amplified at all the wavelengths Raman shifted from the Rp pulse in the Stokes direction ("Raman gain") and absorbed at all the wavelength Raman shifted in the anti-stokes direction ("Raman loss"). All possible Raman resonances are then investigated at the same time and even in two different ways.

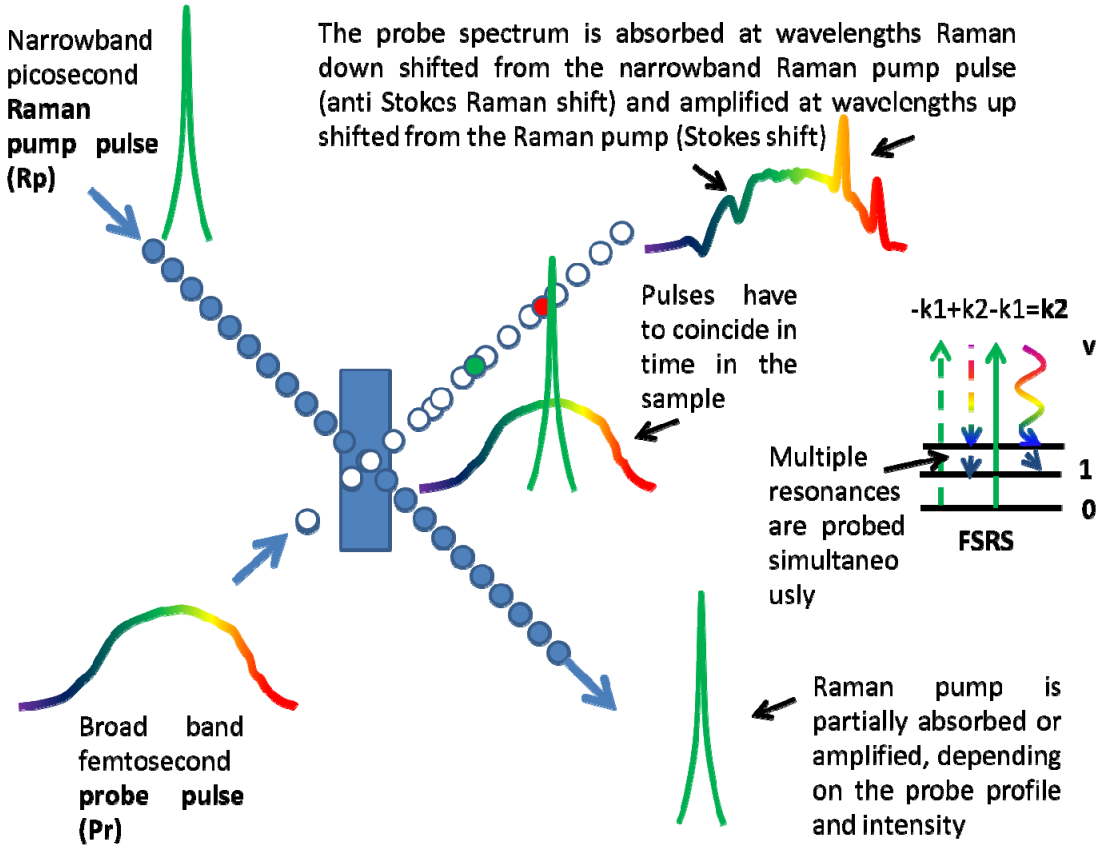

Figure 7

Femtosecond stimulated Raman scattering (FSRS) is SRS performed with a one pulse narrow and a one pulse ultra short and broadband. This leads to multiple SRS phenomena at the same time hereby probing an entire Raman spectrum as a spectrally dependent amplification and absorption of the broadband pulse.

In a most elementary way (difficulties will be discussed later in the thesis) the actual Raman spectrum can be extracted from the probe profile by calculating a logarithmic intensity gain in the probe intensity when the Rp pulse is applied:

Equation 1.4 $Raman\ gain = log\left({I_{Pr}}^{Rp-on}/{I_{Pr}}^{Rp-off}\right); \qquad I_{Pr} = I_{Pr}(\lambda)$

It should be noted that the detection in transient absorption experiments is usually set to calculate the inverse ratio:

Equation 1.5 $Raman\ gain = log\left({I_{Pr}}^{pump-off}/{I_{Pr}}^{pump-on}\right); \quad I_{Pr} = I_{Pr}(\lambda)$

The purpose is to plot the absorption as a positive signal and the emission as a negative signal (see figure 2). In this case the Raman spectrum is seen as a negative signal, which is not an issue as long as the signals are interpreted correctly. This way we obtain the Raman spectra usually almost identical to those acquired in a spontaneous Raman experiment. Unusual peak shapes can be the result of an improper time overlap of pulses, spectral dispersion of the Rp pulse or an asymmetrical time profile of the Rp pulses.

2.5.3. Time resolution and time resolved FSRS

In fact, given the cost of a femtosecond laser system, FSRS is a rather expensive way of recording Raman spectra, but there are multiple advantages of the FSRS apart from a capability to record an entire Raman spectrum within the single interaction of two pulses with a large gain. The crucial advantage of the FSRS process is that the recording of Raman spectra is time gated with femtosecond precision. It is commonly believed that the FSRS time resolution is determined only by the duration of the femtosecond probe pulse despite the inevitably long duration of the narrowband Rp pulse participating in the process. This means that the time spectral resolution of the FSRS is breaking the traditional uncertainty principle:

Equation 1.6 $\Delta E \Delta \tau \sim h$

I am personally still a bit worried about such a strong statements, but for example the superresolution microscopic techniques such as STED are already broadly approved to break the diffraction limits in a similar way by combining several pulses of drastically different characteristics. The “secret” of the time resolution is illustrated in figure 8. The

conundrum can be lumped into the statement that the "Heisenberg principle is circumvented rather than explicitly broken":

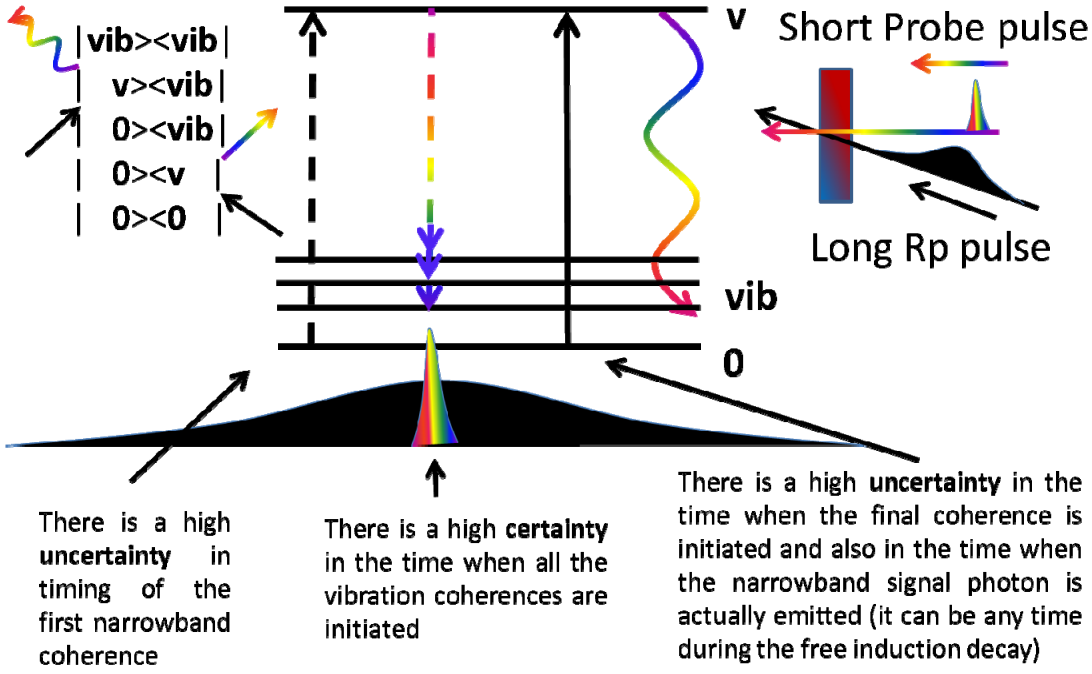

Figure 8

An illustration how FSRS can carry fs time resolution despite its spectral resolution depends on the picosecond Rp pulse. Despite there is a time uncertainty in timing of both virtual state coherences the triggering of the vibration coherences is perfectly defined.

I personally do not question interpretations summarized in figure 8. If I may express my opinion, the main problems start when we include the actual ultrafast changes in the vibrational structure of the studied molecule. When the vibrational manifold of the molecule changes on a time scale of the involved coherences, the picture starts to be quite complicated in terms of the interpretation of the recorded data. A nice example is a vibrational signature of the ultrashort lived (lifetime below 200 fs in the β-carotene) carotenoid S2 state (see chapter 2.6.1.). We can really record its vibrational structure, but so far it appears to be just one extremely broad featureless peak (8, 9). Assigning a true time constant to the processes that happen faster than the Rp pulse duration is also the issue (10). An understanding of the time resolution still needs to be settled within the FSRS community and the interpretation of spectra acquired from the extremely fast reactions will probably always be a challenge. Because the super resolution feature is one of the "best selling" aspect of FSRS, the general agreement among the FSRS community cannot be considered as the final proof. But it is sure that FSRS is really an extraordinary form SRS,

certainly competing for the position of being the spectroscopy offering the highest possible time-vibronic structure resolution.

This high “time gating” capability of FSRS is used in the time-resolved FSRS experiment. It can be viewed as a pump probe experiment where FSRS is used as a probe. Because the FSRS and transient absorption signals can be generated at practically the same spectral region, both signals can be recorded simultaneously which is a great advantage in comparison to IR experiments. However, there is an important difference between transient absorption pump probe (regardless if UV, VIS or IR) and time resolved FSRS. While all transient absorption experiments are in general four wave mixing processes (formally can be viewed as depending on a third order nonlinearity of the system), time resolved FSRS is a six wave mixing process (formally probing a fifth order nonlinearity!). This is illustrated in the figure 9:

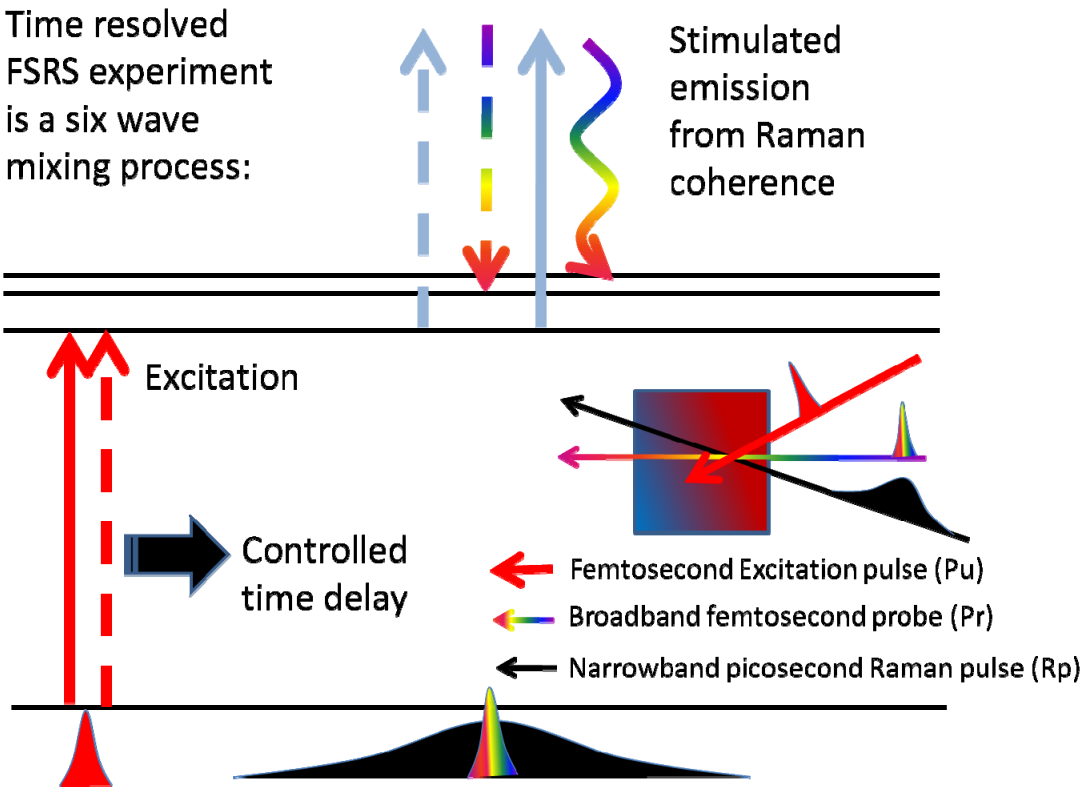

Figure 9

An illustration of the time resolved FSRS experiment. It can be seen that it is actually a six wave mixing process.

Such a high nonlinearity generally results in a very weak time resolved FSRS signal. Additionally, there is a large space for parasitic processes producing undesired nonlinear responses and signals. The extent and number of these process depend largely on the relation between the exact experimental realization of FSRS and the studied system, but

usually at least a few of them apply. The most common of them is the dumping of an excited state population by the Rp pulse. This is illustrated in the figure 10:

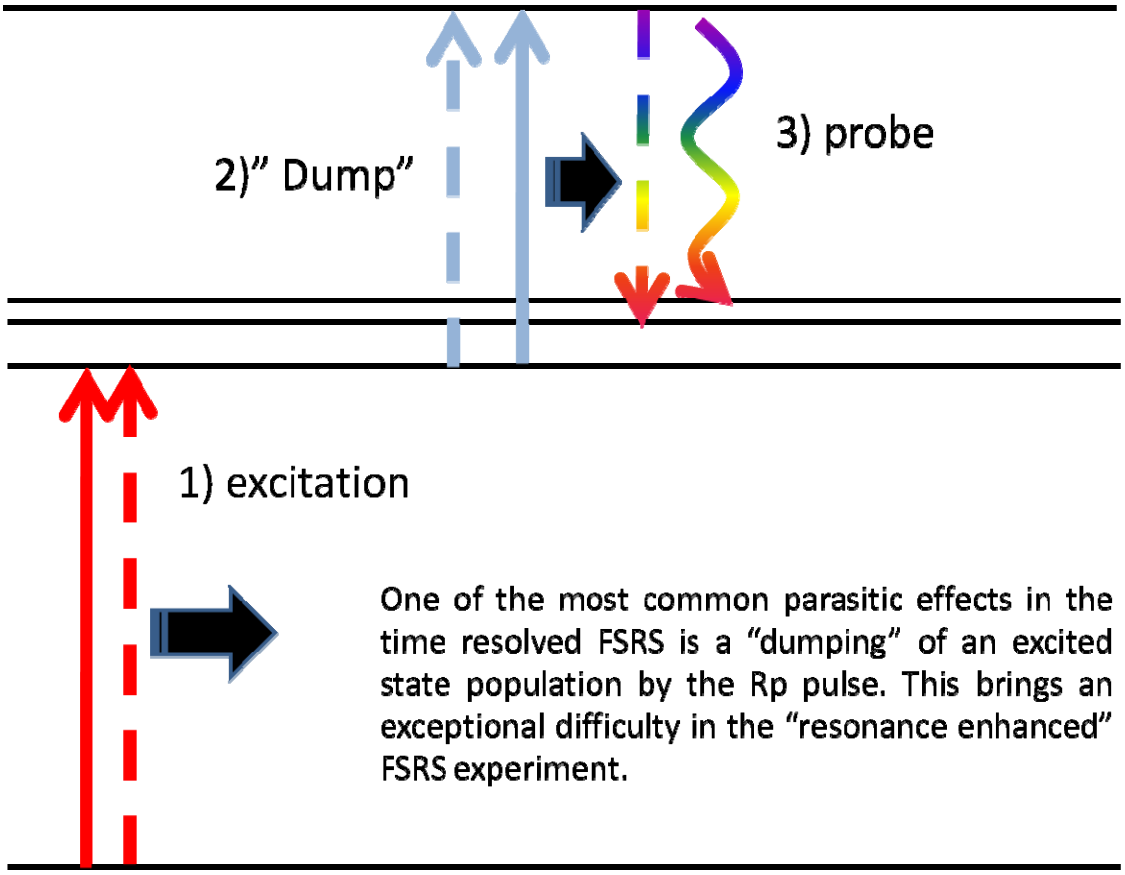

Figure 10

Exactly the same experiment as described in figure 9 can actually generate a so called pump-dump probe signal. Where Rp pulse causes repumping of excited states to even higher states or their depletion to the ground state.

The excited states generally manifest very broad absorption spectra so usually it is impossible to tune the Rp pulse out of the resonance. Additionally the long duration of the Rp pulse gives it a very strong dumping or repumping capability. This process causes an exceptional difficulty when a resonance enhancement of the Raman signal is attempted as it means to tune the Rp pulse explicitly into the resonance. This produces an inevitable trade-off between the resonance enhancement and the time resolved signal loss due to the dumping of an excited state population and unpredictable results of repumping of excited states. As a result the resonance enhanced FSRS can be used for selecting of desired signals however not for the actual signal amplification in the time resolved experiment.

Despite these difficulties the time resolved FSRS experiments are readily attempted both in a resonance and an off resonance realization. Some of them map the structural changes of reactions happening on a sub-picosecond time scale (8, 11).

2.5.4. Elements from the more complete theory of FSRS

In the previous chapters we discussed the FSRS as if it was just a single nonlinear process that we can describe by a one single Feynman diagram. In fact, when the narrowband and broadband pulses are overlapped in time in a medium a whole class of phenomena contributes to the recorded signal (12). These processes can be divided in two large groups: Processes that produce narrowband signals and processes producing a broadband background. Figure 11 shows wave mixing diagrams of the main processes contributing to the bulk FSRS signal:

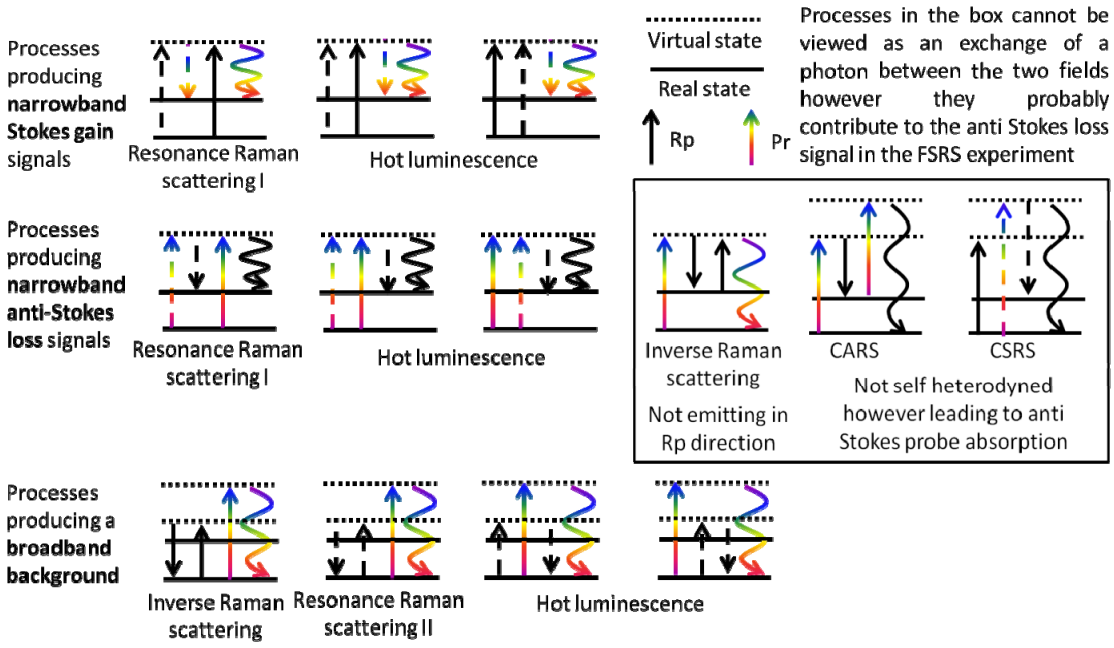

Figure 11

The FSRS experiment as illustrated in the figure 7 in fact produces a whole class of self heterodyned signals. Some of them leads to the narrowband Raman peaks, but some of them produces only a broadband background. Note also that the anti Stokes signal (the so called Raman anti Stokes loss) is bit different in nature form the Stokes signal. It contains contributions both form SRS and the other coherent Raman phenomena at the same time.

Process that resonate with the actual vibration state lead to a narrowband signal, processes that depend solely on virtual states produce a broadband background signal. Interestingly,

we can notice that there are more pathways contributing to the anti Stokes Raman loss than processes contributing to the Stokes Raman gain. The reason is that the gain signal depends solely on the processes that end at a vibration population and emit a self heterodyned signal in the probe direction. In these processes no photons are lost, they are merely downshifted in energy and redirection to the low frequency field. Contrary, in the anti Stokes Raman loss region we observe not only the absorption of the high energy probe photons that are red shifted and emitted in the Rp pulse direction but also photons that are absorbed to form a virtual electronic state population leading to an incoherent scattering of light to all the directions (the inverse Raman scattering) and probably also processes that emit a coherent signal in new directions such as CARS. A deep understanding of the anti Stokes Raman loss signals still needs to be established, but my arguments of variability in the nature of the anti Stokes signal can partially explain the readily observed experimental phenomena of the anti Stokes signal being stronger in the intensity than the Stokes signal and also manifesting more complex peak shapes (13). However, the anti Stokes signal was experimentally discovered to depend also on the probe spectra in the Stokes region which cannot be easily explain by any of diagrams in the figure 11. The nature of the complete FSRS signal is probably even more complicated that what is illustrated in the figure 11. A robust theory of the FSRS is still under construction!

2.5.5. Impulsive Raman scattering

Interestingly, because the Raman gain processes leads to an absorption of the Rp pulse and at least some Raman loss processes to an amplification of the Rp pulse, it seems that the FSRS experiment performed with a probe spectrum symmetric around the Rp pulse wavelength would probably lead to a maintaining of the Rp pulse intensity. In this configuration, FSRS can be viewed as a conversion of high energy photons to low energy photons within the probe pulse. The Rp field and the molecular transitions then serve as resonators greatly enhancing the efficiency of this process for the certain narrow wavelengths. In this picture the FSRS experiment with the Rp pulse placed in the center of the probe pulse can be viewed as a special type of an enhanced “impulsive Raman scattering”. This is displayed in figure 12:

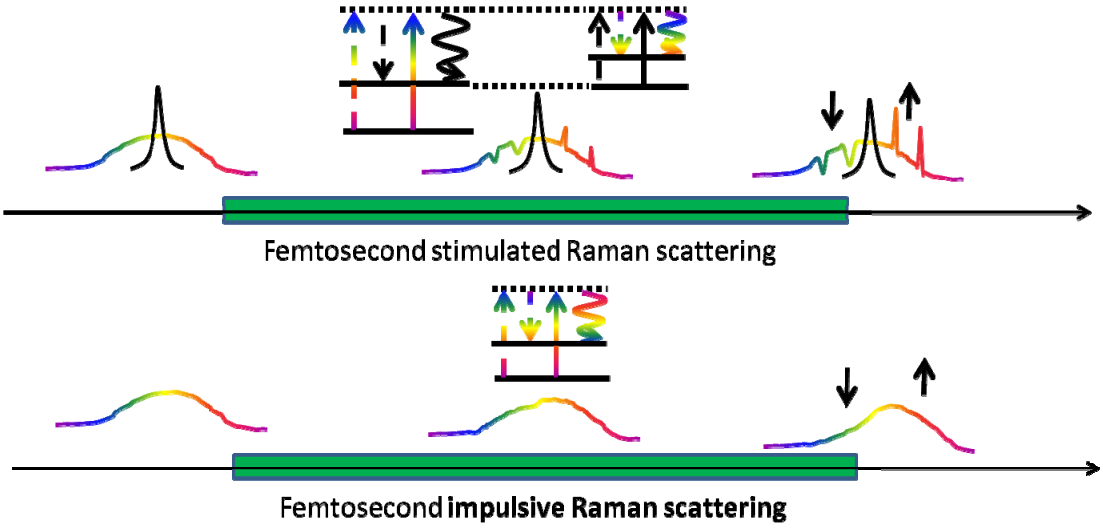

The impulsive Raman scattering is a special case of the femtosecond stimulated Raman scattering where all interactions happen within a single pulse. It can be used for coherent excitation of vibration modes.

Raman pump pulse should be yellow rather than black in this configuration but its color was mad black to gain visibility and distinct it from the probe pulse .

Figure 12

When the Rp pulse is placed in the center of the Pr pulse an exchange of photon between the blue and the red part of the Pr pulse is mediated. In fact this can occur also without the Rp pulse. However in this case the process does not depend on any sharply defined virtual state and the Pr pulse is only continuously amplified at its red part while absorbed at the blue part. This is called an impulsive Raman scattering (IRS).

It is common to consider as impulsive Raman scattering only the first two coherences forming interactions out of the entire four wave mixing process producing the vibration population. I think that all phenomena where SRS happens within a single pulse can be called impulsive Raman scattering. It is important to note that SRS phenomena can be used both for a coherent (phase sensitive) and non-coherent excitation of vibrational states via an impulsive scattering. This property means that FSRS can be used not only to probe the system at the femtosecond time scale, but also to manipulate its vibrational manifold at the femtosecond scales. This property is now intensively investigate in order to develop the so called “multidimensional Raman spectroscopies”.

2.5.6. 2D Raman spectroscopy

2.5.6.1. Frequency versus time domain experiment and the spectral window of 2D FSRS

In a most simple way, the nature of multidimensional spectroscopies is recording maps reflecting correlations between the states of the system. This can be performed in two quite distinct ways. One way is the scanning of highly selective excitation performed by narrowband pulses and recording of the spectral response of the system. This is a so called "frequency domain experiment". An alternative is to impulsively excite all the states of the system simultaneously and then scan the time response of the system. The Fourier transform of the oscillatory time response then yields the 2D spectra. This is a so called "time domain experiment". Because the time domain experiment requires tailoring and phase sensitive handling of extremely short pulses (ideally below 10 fs) it is usually experimentally dramatically more challenging. In fact, most of the 2D experiments nowadays described by authors as time domain experiments can be viewed as hybrid frequency-time domain experiments, as they are performed with pulses significantly longer than ideal for time domain experiment, however providing a certain spectral selectivity in the excitation.

Both of these 2D spectroscopies can in principle be realized via the SRS processes. This is particularly tempting as the otherwise very well established 2D IR experiments can be currently realized only for a very small spectral window. This is illustrated in figure 13:

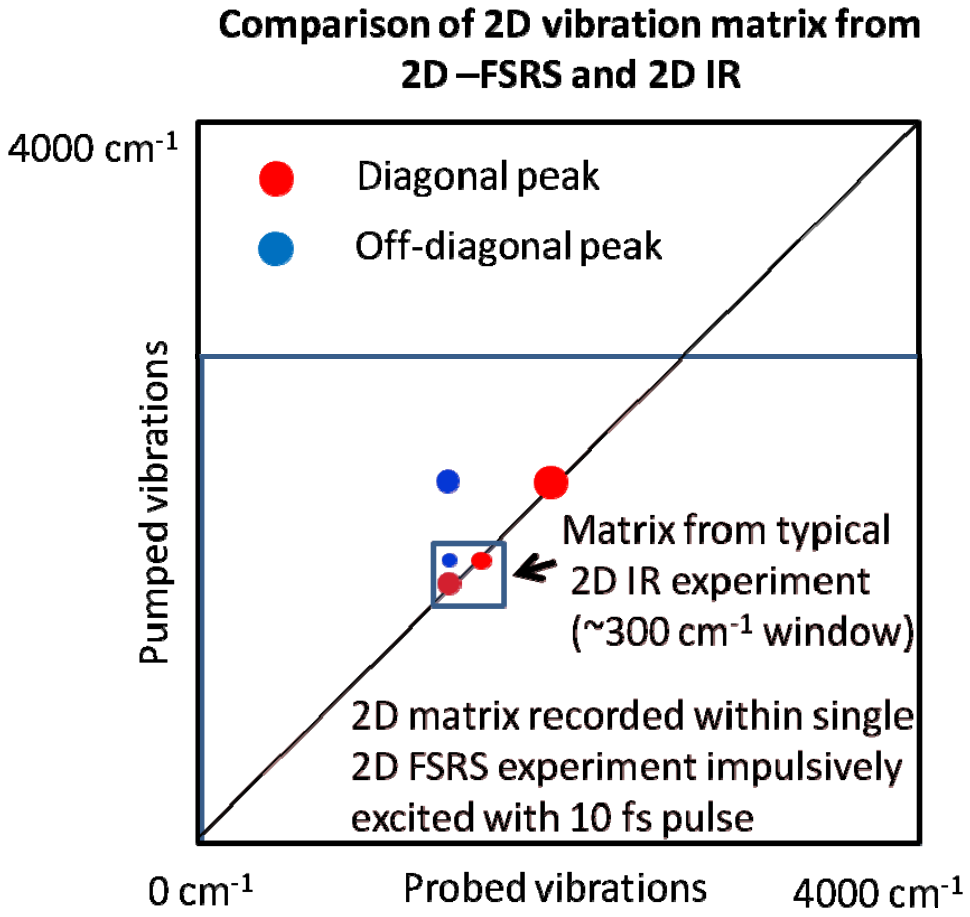

Figure 13

The comparison of the spectral window of the typical 2D IR experiment and a potential window of the 2D FSRS experiment.

The reason is that we cannot probe the entire IR vibration spectra in a single window and we also cannot prepare good 10 fs pulses (required in order to achieve a broad excited range) in the mid IR region. Despite this very promising prospect of the 2D Raman experiment, there are many difficulties. While the basic 2D IR (or VIS) experiment is still just a four wave mixing process, 2D Raman is always at least a six wave mixing process. This is associated with the broad range of parasitic effects in a similar way as the time resolved FSRS experiment described in chapter 2.5.3. In fact, no truly reliable and fruitful 2D Raman experiment has been performed so far. The field can be described as being in the state of "proof of the principle" experiments.

2.5.6.2. Time domain 2D FSRS

The basis of time domain 2D FSRS experiment is employing impulsive Raman scattering for coherent excitation of vibrational modes. This type of a 2D Raman spectroscopy was the first to be attempted (14) experimentally. The excited vibration coherences evolve over the experimentally controlled time and then they are probed by the FSRS process. The self heterodyned nature of FSRS causes that when the FSRS signal is scanned over the time delay between the impulsive excitation and the probe, periodic oscillations of coherences are manifested in the intensity of the signal. A Fourier transform of these oscillations gives the 2D spectra. In figure 14 the basic scheme of the frequency domain 2D Raman experiment is displayed. The shown scheme is just an example. Several similar diagrams can be drawn, but I am not going to attempt to describe the theory of the 2D FSRS in an exhaustive way. Despite the fact that it is just a three pulse experiment, it is actually a six wave mixing process formally probing a fifth order nonlinearity of the system:

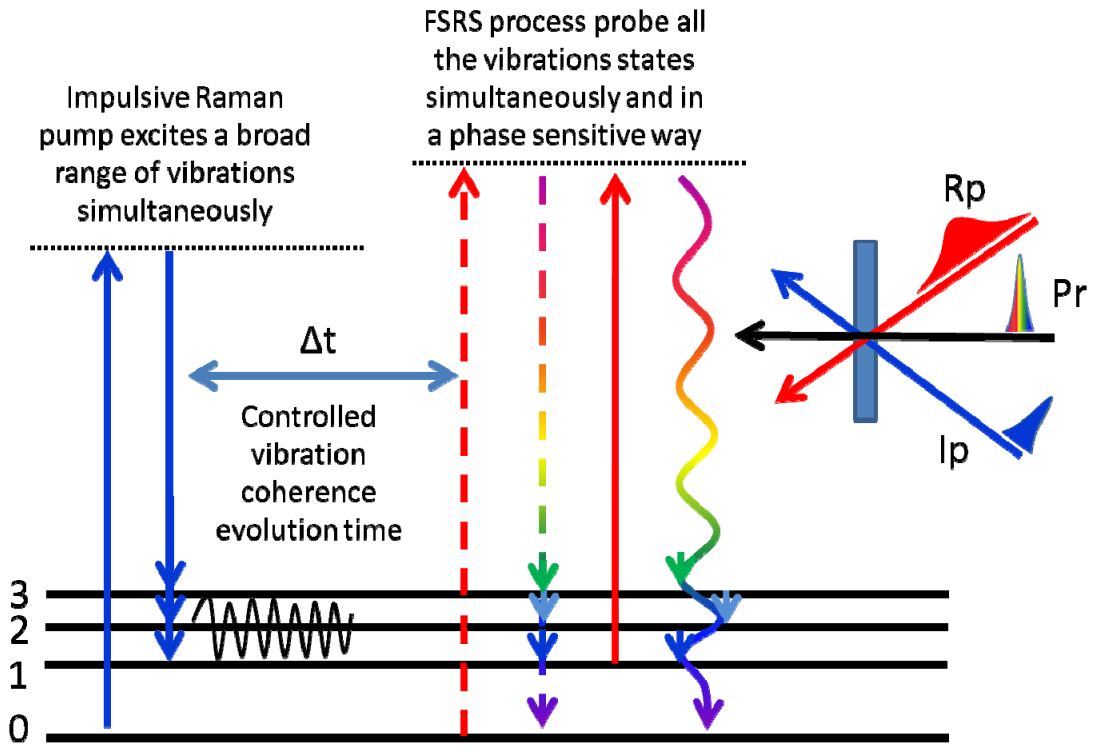

Figure 14

The frequency domain 2D FSRS is performed when a broad range of vibrations is excited by the IRS process prior to recording of FSRS spectra. When the time delay between the impulsive excitation and the probe is scanned a coherent oscillations of the system are recorded in the FSRS signal. A Fourier transform of the temporal evolution of FSRS spectra then gives the 2D FSRS spectra which should contain peaks associated with an anharmonic coupling of vibration modes.

The extent of the 2D spectral window is asymmetric in comparison to the typical 2D IR experiment. The FSRS process can easily scan en entire vibration manifold (or at least it can be easily tuned to any range of interest), however the range of excited vibrations depends on the inverse duration of the impulsive pump. A 15 fs pulse can excite vibrations up till 1500 cm^{-1}. To excite an entire vibration range (0 – 4000 cm^{-1}) would require a sub 10 fs pulse. This is difficult, however not impossible as slightly sub 10 fs pulses can be generated without unbearable difficulties in VIS-near-IR region. This dependence of the excited range on the pulse duration means that time-domain 2D FSRS is easily performed for low frequency modes excitation, but technically difficult for higher frequency vibrational excitation. In this sense, time domain 2D FSRS is somewhat complementary to the 2D IR spectroscopy typically having difficulties with very low frequencies excitation.

The time domain 2D FSRS spectra were repeatedly recorded and observation of sidebands which looked very promisingly as peaks from an anharmonic coupling of modes caused a lot of optimism (15). Unfortunately it was discovered that rather than coupling of modes, so-called cascading signals were recorded (16). The fact that cascading signals are generated at exactly the same Raman shifts where the true 2D peaks are expected is still severely strangling the 2D FSRS experiment.

2.5.6.3. 2D Raman spectroscopy – cascading signals

The reason why a possibility of cascading signals was initially overlooked in the FSRS community (to certain communities it was know for a long time (17)) is partially because cascades cannot be directly derived from the blind application of theoretical formalism of the perturbative expansion of the density matrix and the corresponding Feynman diagrams. This demonstrates how careful the scientist has to be when developing brand new experiments. Every working theory carries a bunch of hidden assumptions. In new conditions, something negligible can become important. The problem of the cascade is that we cannot consider it while focusing solely on the interaction between a single molecule and the field. The cascade is a mutual interaction among the fields originating in the different neighboring molecules. This signal is fundamentally still a third order nonlinearity of the molecule so it easily overcomes the 2D signal which can be regarded as a fifth order nonlinearity. But painfully the cascade signal is manifested at regions of the 2D matrix where the actual 2D signal is expected. The cascading mechanism is depicted in the figure 15 where the link between the molecules is visualized as a merge of two four-wave mixing diagrams:

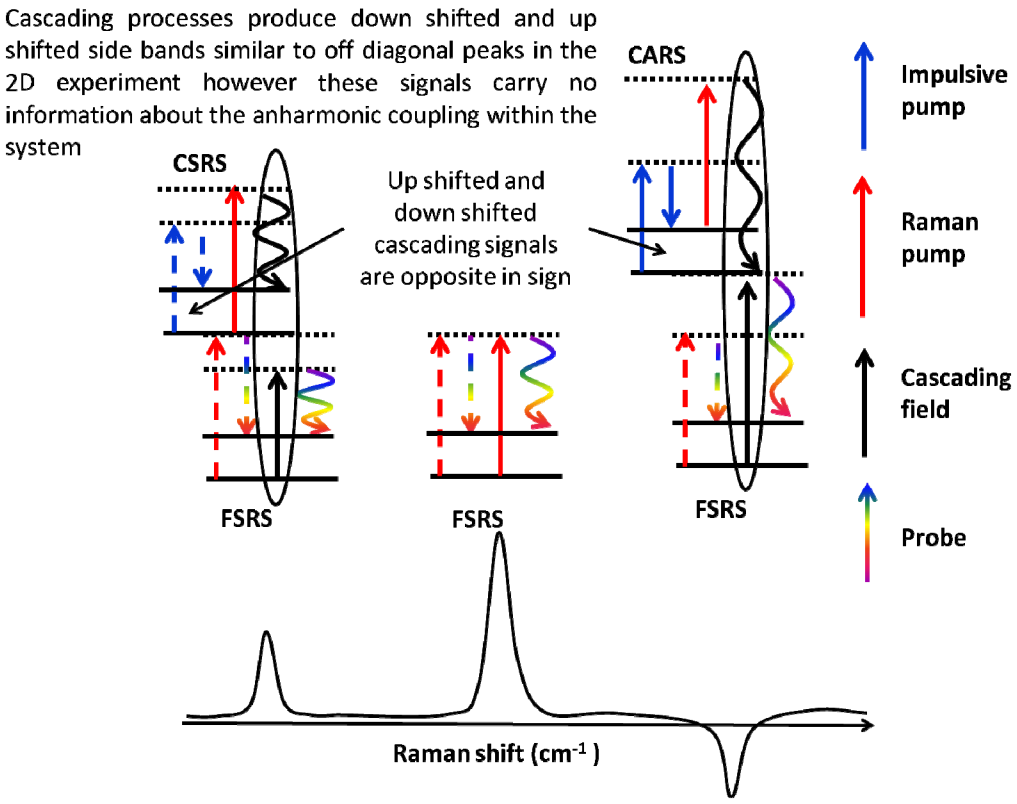

Figure 15

A schematic formation of the cascading signals. By a merge of two WMEL diagrams it is illustrated how the up shifted and down shifted signals can be generated without probing any intra molecular coupling just by connecting two “ground state” coherent Raman processes. Because the CARS and CSRS is based on a different sign of the initial vibration coherence the up shifted signal has and opposite phase from the down shifted signal.

The fact that cascades originate in the interaction of neighboring molecules means that they can be relatively reduced by diluting the sample, however this reduces the desired fifth order signal as well. Unfortunately, nowadays it is not possible to perform a 2D Raman experiment at dilutions where the fifth order signal is expected to overcome the signal from the cascade. By application of rules from chapter 2.4.3, it can be derived that the cascade signal should not be perfectly self heterodyned (emitted in the probe pulse direction). This means that the phase matching principle can be harnessed in designing an experimental geometry where the cascade signal is suppressed. At the moment of writing this text it is not generally known to which extent it can be done. Personally I am afraid that efficient suppression of cascades will require deeper understanding of a mechanism and conditions at which the cascades are formed, or perhaps a completely different way of 2D Raman experiment in general. In any way at the moment it is not clear if any of the time domain 2D Raman experiments conducted so far succeeded in recording of coupling of different vibration modes as they are hidden under cascading signals.

2.5.6.4. 2D Raman spectroscopy – frequency domain experiment

An alternative to the time domain experiment where an ultrashort pulse excites coherently all the vibrations simultaneously, is excitation of a single vibration specifically by a pair of narrowband pulses. This process is depicted in figure 16:

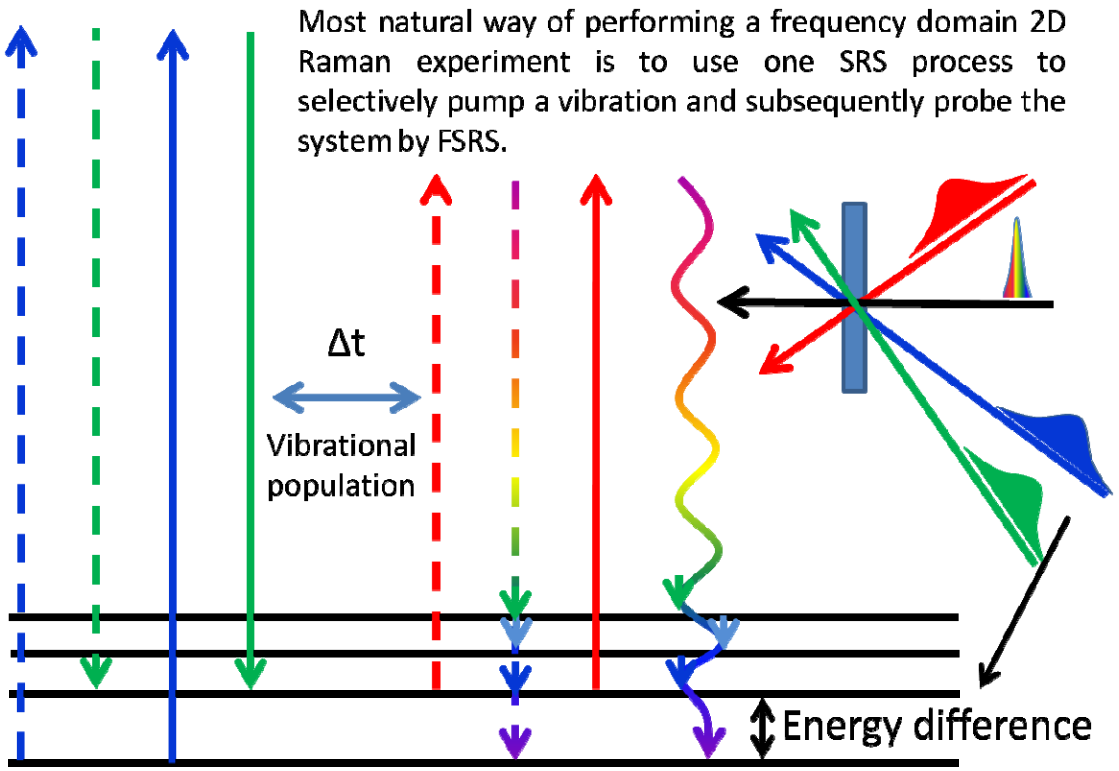

Figure 16

A pair of narrowband pulses can be used for a selective excitation of a certain vibration state. This can be used for recording of a frequency domain 2D Raman spectra via a four pulse experiment. In this case both excitation and probing is independently perfectly self heterodyned.

Such an experiment is an eight-way mixing process probing a 7^{th} order nonlinearity. It sounds a bit scary (to me it does), but from the quantum perspective it disconnects the double vibration transitions necessary to produce an off-diagonal peak into a pair of strongly allowed single vibration transitions. In this sense the recorded signal can easily overcome the 2D signal from the time domain fifth order process depicted in figure 14, where a double quantum transition is required to generate an off-diagonal peak. Additionally, frequency domain 2D is not expected to generate the cascading signals and if it would, then only at the one Raman shift as only one transition is excited at the same time. Unfortunately, this experiment requires one pulse more in contrast to the described

frequency domain experiment. Additionally, the high spectral selectivity means a rather long pulse. Given the quite short vibrational population times, this experiment will have to be performed at such a short time delay between excitation and probing of vibrations that practically all involved pulses will be overlapped at certain time and will give rise to many parasitic signals. But it is still interesting to attempt this experiment as it should produce 2D signal which will be not necessarily entirely overwhelmed by cascading signals. It also does not require ultrashort pulses to excite the high energy vibrations. In the frequency-domain experiment any vibrational level can be excited without difficulties.

As the pulses are generally rather long there is an interesting possibly to link the excitation and the probing into a single pulse operating in either ways: once mixed with the pump pulse for the excitation purpose and once mixed with the femtosecond probe pulse for probing. This is schematized in the figure 16:

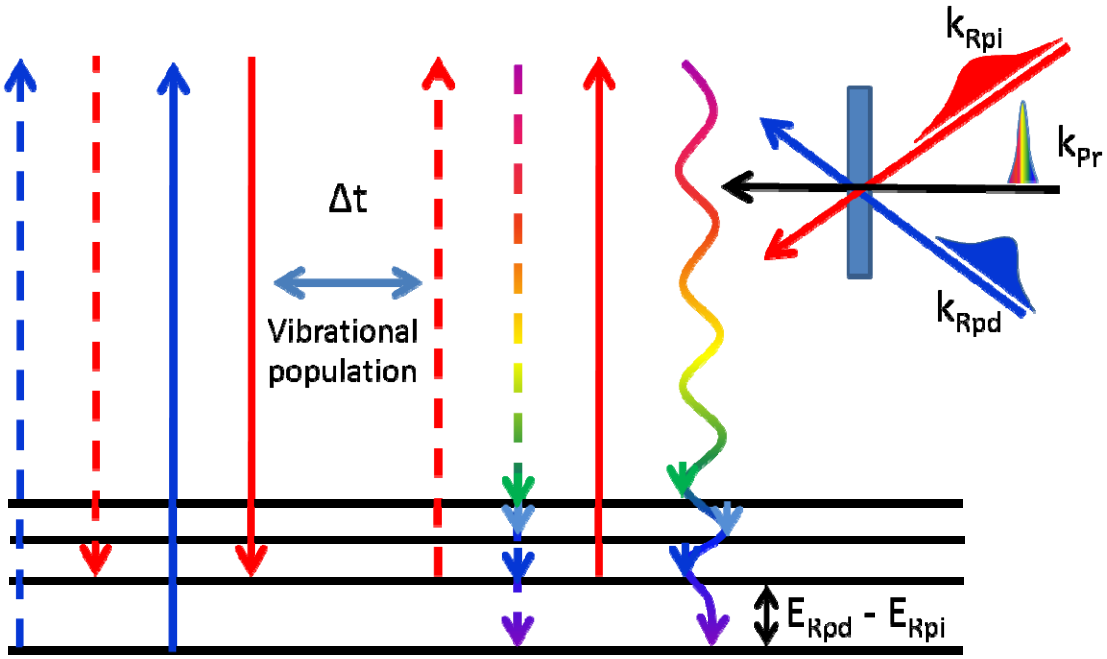

Figure 17

There is a possibility to use a one long narrowband pulse both for the excitation and probing. This way a frequency domain 2D Raman experiment can be conducted based just on 3 pulses.

When the time length of the solely pumping Rpd pulse is chosen reasonably short, the excitation and the detection of vibrations can be still well separated. The generation of sufficiently short narrowband picoseconds pulses is technically among the most difficult aspects of FSRS experiment (2.5.7.) so reduction towards the three pulse experiment in contrast to the realization depicted in figure 16 makes the experiment substantially more realistic. The usefulness of this experiment and frequency domain experiments in general,

as well as in case of the time domain experiment, still waits for clear experimental evaluation.

2.5.7. Generation of narrowband picoseconds pulses out of Femtosecond pulses

All the power of the FSRS experiment originates in a perfectly timed interaction between a strong narrowband picosecond field and a femtosecond probe. The required precision in timing can be achieved only by preparing all the pulses out of one initial pulse. It is a bit counterintuitive fact that the generating of a few-picoseconds spectrally narrowband pulses is technically more complicated than the generating of femtosecond pulses. The reason is that the Q-switch mechanism is technically unrealistic for ultrashort pulses (typically producing nanosecond pulses) while mode locking and the parametric amplification is in contrast restricted to the ultra short pulses.

The easiest but inefficient way to prepare a picoseconds pulse out of a femtosecond pulse is to filtrate the femtosecond pulse via a spectral filter, usually a pulse shaper. All the power except the chosen narrow spectral region is rejected. However trivial it sounds, thanks to huge powers at which we can obtain femtosecond pulses nowadays and high robustness of the approach, it is still a very common approach. Additionally, the technological demand for efficient gratings for femtosecond pulse compressors allows nowadays the building of highly transmissive pulse shapers where the losses except the intended spectral rejection are below 40%. A scheme of the pulse shaper commonly called a “grating filter” is in figure 18:

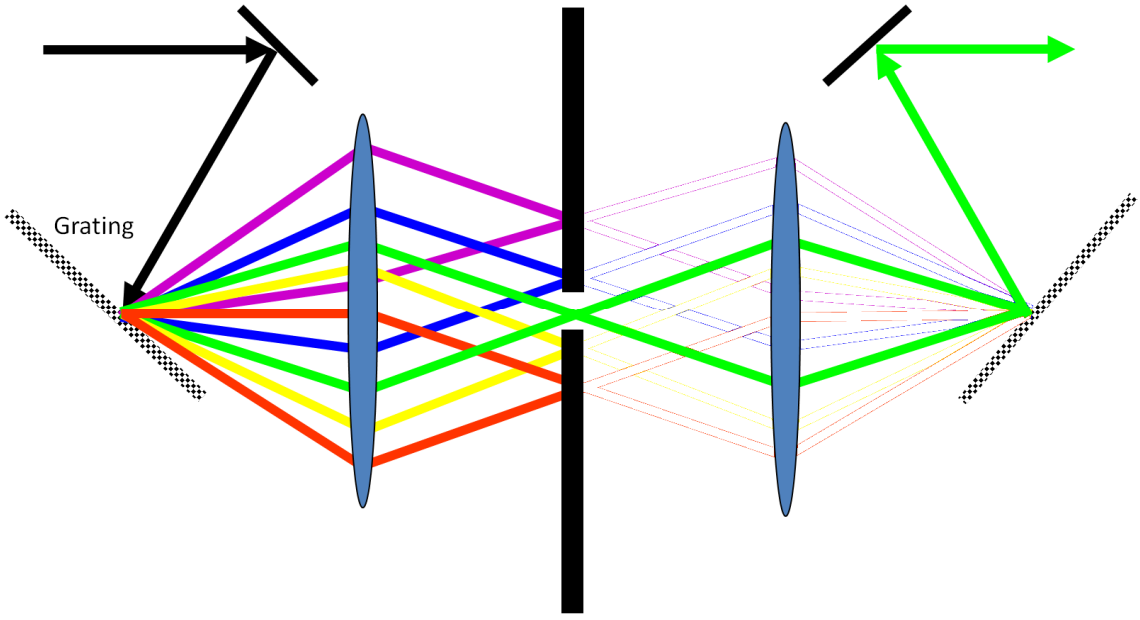

Figure 18

In a pulse shaper the pulse is spectrally decomposed and again composed. By placing a slit into the plane where the frequencies are separated a completely tunable selection of the spectral bandwidth can be achieved.

An alternative to filtration is a bandwidth compression. This is usually performed by second harmonic generation from deliberately strongly chirped pulses. When the pulses are stretched in a typical "pulse stretcher" both a positive and negative chirp can be introduced. This allows generation of the close to Fourier transform limited pulses with both spectral and time profile being close to Gaussian. Unfortunately the apparatus is usually rather complicated. An easy alternative is to generate the second harmonics in a crystal so thick that it introduces a sufficient chirp itself. Unfortunately this approach produces picoseconds pulses of less symmetrical temporal and spectral profile. Both approach are illustrated in the figure 19:

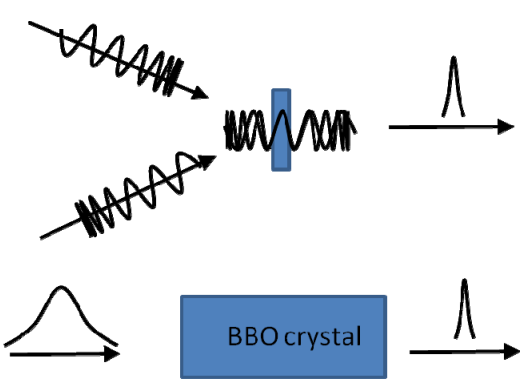

Second harmonic generation from two femtosecond oppositely strongly chirped pulses produces narrowband picosecond pulses. Introducing of controllable chirp require passing the pulses through the pulse stretcher.

When a very thick nonlinear crystal is used the chirp can be generated already within the nonlinear crystal. The simplicity of the approaches is contra balanced by the fact that the pulse has an asymmetrical time profile.

Figure 19

A second harmonic generation from the pair of strongly chirped (spectrally dispersed) pulses results in bandwidth compression. A spectral bandwidth compression by two orders of magnitude can be produced with a high efficiency (~30%).

Because the experimental systems are usually pumped by a 800 nm operating Titanium:Sapphire amplifiers, the bandwidth compression produces the relatively impractical 400 nm centered pulses, but the spectrally compressed pulses can be used to pump a picosecond OPA, OPG or NOPA. Unfortunately the picoseconds OPAs are significantly less robust than the femtosecond OPAs. Given that we feed the OPA by pulses already generated by a nonlinear process the generation of tunable narrowband picosecond pulses from broadband femtosecond pulses is extremely sensitive to the stability of our femtosecond amplifier. Despite this the entire system can be nowadays purchased commercially.

2.5.8. Future prospects for FSRS

The pump-probe transient absorption experiments are nowadays very well established and capable of studying very complex systems such as proteins while recording a very weak signal (μOD). At the beginning, FSRS was viewed as the same thing just for vibrational states. After initial optimism, the FSRS experiments were discovered to face both technical and fundamental problems. In contrast to the other femtosecond spectroscopies, FSRS is an extremely nonlinear process. Even the most basic time resolved Femtosecond stimulated Raman spectroscopies depend on least a fifth order nonlinearity (they require five correctly ordered interactions with the field). The 2D Raman experiment is at least a 5^{th} order nonlinearity as well. So, when performed on an actinically pumped (photo-activated) sample the recording of the 2D Raman spectra is at least a 7^{th} order nonlinearity! In fact, serious difficulties were encountered already during the steady state 2D Raman experiments.

So what are the prospects? My view is certainly not entirely optimistic. However a few issues have to be considered. FSRS was from the very beginning plagued by the burden of its predecessors. Especially the experimental aspects were initially considered to be almost identical to the pump-probe transient absorption experiments. Many problems encountered in FSRS can be probably solved by different approaches to the pulse preparation, signal collection, data processing, the experimental geometry etc. An additional burden is that it was believed that we will simply obtain a signal identical to the steady state Raman just with the time resolution. This is just not true. In fact in chapter 2.2.1. I briefly shown that also the transient absorption spectra contain features unknown to the steady state absorption spectroscopy. A link between FSRS and spontaneous Raman can be established, however the FSRS experiment is associated with many processes that can never happen in the steady-state experiment. A good example of phenomena which dramatically differs in the FSRS as compared to spontaneous Raman spectroscopy is the resonance enhancement. It is a very powerful tool in spontaneous Raman experiments, it is, however, very problematic in FSRS both in terms of complicated peak shapes and achieving an actual signal enhancement. For these reasons, FSRS represents an interesting challenge for theorists as well. A truly deep understanding of all the phenomena associated with the FSRS experiment can show directions for overcoming many difficulties. The high nonlinearity of stimulated Raman spectroscopies is certainly an issue, however FSRS works specifically with molecular resonances and at such intensities that to view the molecular states as “balls on the springs” cannot be applied anymore. The order of nonlinearity does not explicitly define signal intensity. Also, the principal freedom in the choice of wavelength at which the FSRS experiment is performed allows using all the great technological advances in the photonic technology. So there is certainly a space for expansion. From the purely fundamental perspective the 2D Raman experiment with its literary exhaustive vibration window, higher specificity than IR absorption and probably even unbeatable time resolution

is a candidate for the most universal and powerful optical analog of the NMR! This is something certainly worth of trying. But most importantly, some very interesting and informative FSRS experiments were already conducted so at least a particular usefulness of the FSRS is already unquestionable. There is already quite something to build upon! I can only speculate how far a patient and continuous effort of the quickly growing FSRS community will push the possibilities of the Femtosecond Raman experiments in the future.

2.6. Carotenoids

2.6.1. General properties and their excited states

Carotenoids are certainly extraordinary molecules present in probably all known self sustainable organisms. To a various extent, all the focused works presented in this thesis deal with carotenoids and for this reason they deserve special attention in the introduction. In the first chapter I mentioned that the complexity of carotenoids lies very close to the junction between the classical and the quantum world. Now I will try to clarify it a little bit deeper. Carotenoids have three important features which, when combined together, are responsible for their extraordinary properties.

First they are relatively large molecules; typically they consists of about 100 atoms. This gives them space for a high variability within their basics structural core, and it forms a complex vibrational and conformational manifold. Many isomers (such as cis-trans) can be derived from a carotenoid of the same stoichiometry. Importantly, the large number of degrees of freedom makes carotenoids already very difficult molecules for the fully “ab initio” quantum calculations.

The second characteristic of carotenoids is that in contrast to their size, they are an extraordinarily symmetric molecules! Some carotenoids such as β-carotene fit perfectly into C_{2h} symmetry group. Symmetry causes that their generally complex vibrational and excited state manifolds are dominated by simple schemes quite strictly bounded by selection rules. This is illustrated in figure 20:

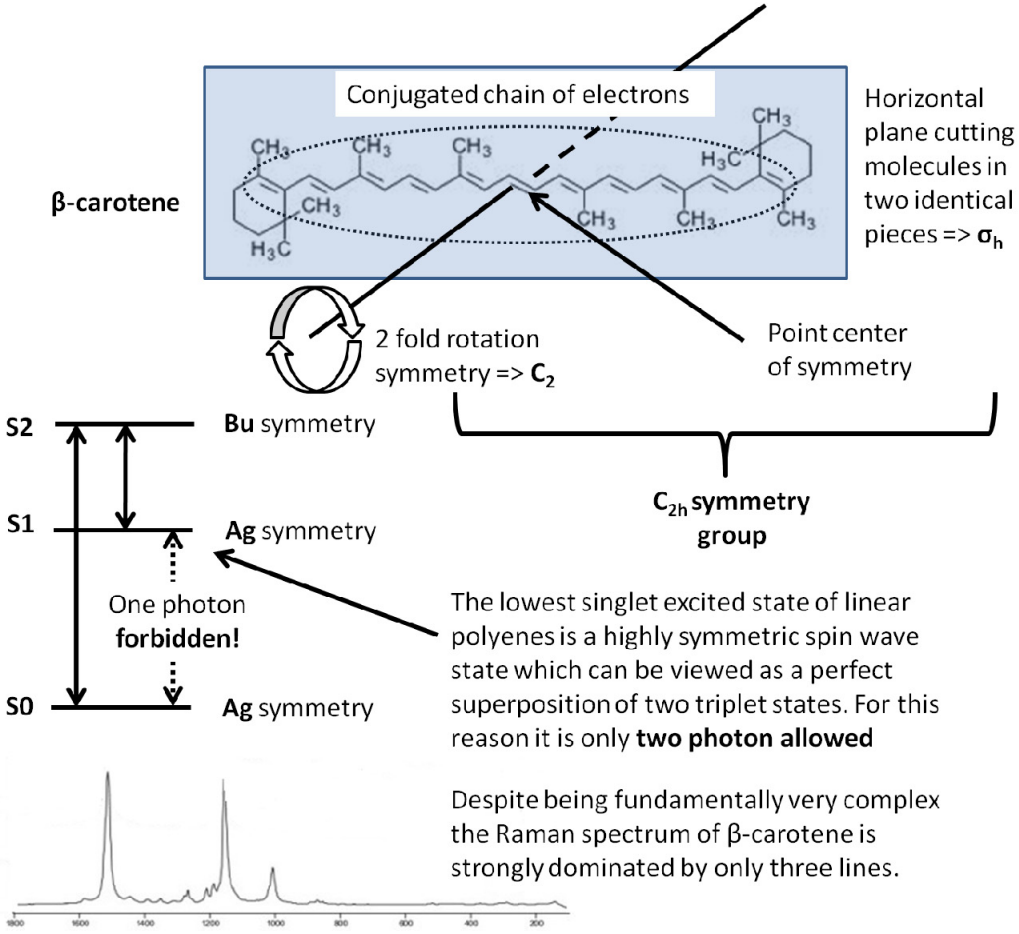

Figure 20

An important characteristics of carotenoids is that their lowest singlet excited state (usually shortened simply as the "S1") is symmetry forbidden for the one photon transitions. However, this state is quickly populated from the first allowed state "S2". A lot of functionality of carotenoids can be derived from it. The vibrational spectrum is dominated by only three transitions. All these features originate in conjugated chain forming the backbone of every carotenoid.

The backbone of carotenoid is formed by a highly symmetrical conjugated chain which is responsible for the dominant electronic and vibration characteristics. This chain produces two lowest unoccupied states of a different symmetry making the transition from the ground state to the first excited state highly forbidden for a single photon absorption. This perfectly non-polarized state, usually described as the S1, can be understood as a superposition of two triplet states that are inseparable as long as the symmetry is maintained. The first allowed state, usually denoted as the S2, has an extremely high transition moment and it is responsible for typical blue-green light absorption of carotenoids leading to the characteristic orange color of most carotenoids. Transition between the S2 and the S1 state is strongly allowed and so the S2 state usually quickly

(<300fs) relaxes to the S1 state from which the energy dissipates to heat as the transition to ground state is again a one photon forbidden. This causes that carotenoids has extremely low fluorescence. The lifetime of the S1 state greatly varies among the carotenoids from about 1 ps up to hundreds of ps usually being shorter for the longer carotenoids (for the β-carotene it is about 10 ps).

The third characteristics of carotenoid is their relative flexibility. The linear nature of carotenoids gives a space for a small, however important distortions of their structure out of the ideal C_{2h} symmetry described in the figure 20. As a result carotenoids, when incorporated in proteins, manifest drastically different properties from their behavior in vapors or when they are freely dissolved in solvents. Among the most important properties observed on bound carotenoids is the appearance of new states (18) and extraordinarily fast triplet formation (19). The most experimentally observed "hidden" state is a so called S* state (20). Its name is purely historical simply originating in the fact that there is no certainty about the nature of the state. The attempts for interpretation of S* state can be divided into two groups. First an assumption is that the S* is an independent state of a similar nature as the S1 state. To this I also count the interpretation that the S* state is a different minimum of the same potential surface as the S1 state. Another large class of interpretations assumes that S* state is just a hot S0 or S1 state. The signatures of the hot S1 state are quite understood now and they differ from the S*, so the center of mass is now in the hot S0 (ground state) as being responsible for S*. This is summarized in figure 21:

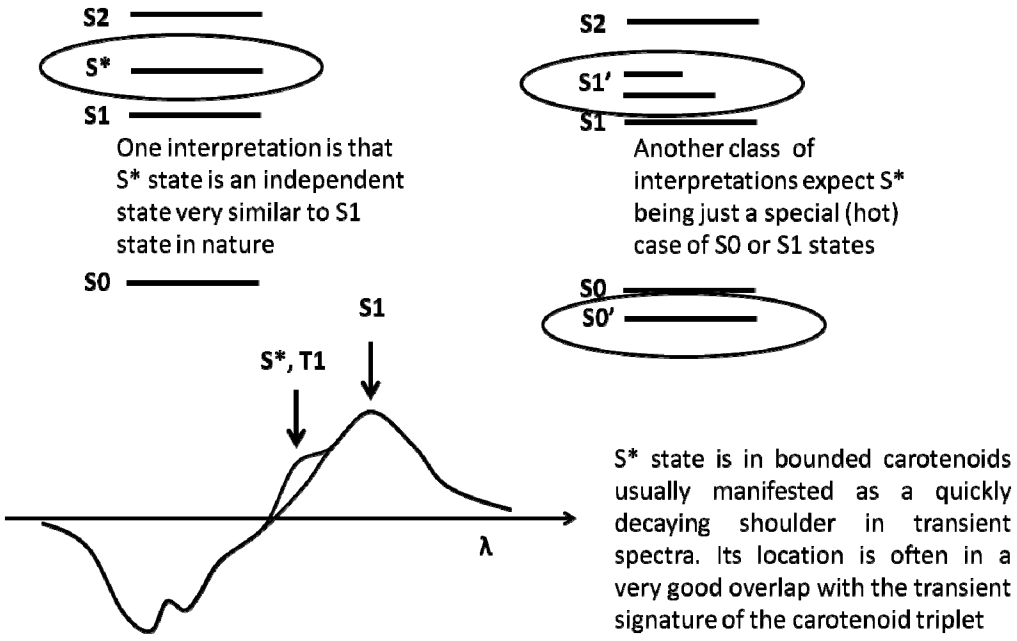

Figure 21

The nature of S* state is still not known. However its signature in the transient absorption spectra is very well established.

I personally incline to believe that the S* state is a quite independent state, perhaps of a very similar nature as the S1 state, whose presence is allowed by a conformational change of the carotenoid. The S* state was first discovered in LH1 complexes together with an ultrafast triplet formation (19, 21). Interestingly, S* was manifested by an excited state absorption peak at almost exactly the same position as the transient absorption of a triplet. This led to the up to nowadays popular assumption that the S* state is a triplet precursor. In fact, since then the S* state was observed on a large number of other systems including some free carotenoids. In none of these following cases a connection of S* with the triplet was observed. So, its relation to the triplet remains unclear. However the interpretation of the S* state is not the objective of this chapter, neither a subject of any following focused works. Let's just conclude that the S* state is a phenomenological feature of carotenoids demonstrating the hidden complexity of the seemingly simple characteristics of carotenoids. I personally strongly believe that it is related to bending or twisting of carotenoid backbone. This process can also make two triplets forming the S1 state separable (22). It is then no surprise that both the S* and the triplet phenomena can occur simultaneously.

2.7.2. Carotenoids in photosynthesis

Carotenoids play many roles in biological systems, however I will briefly describe only their role in photosynthesis as it is a subject of two presented focused works in this thesis. As time resolved experiments were first capable of resolving the somewhat slower world of triplet states, the first discovered photo protective property of carotenoid was that they serves as a sink for the triplet states (triplets in photosynthesis have to be avoided as they can generate an extremely destructive single oxygen). A little bit later it was discovered that carotenoids actually play probably an equally important role in avoiding the triplet formation in general (23, 24). In the previous chapter I briefly showed that carotenoids are usually excited into the so called S2 state and that this state quickly relaxes into the hidden non-emissive S1 state. This property was discovered to play an essential role in photo protection operating on the singlet state level. When carotenoids and chlorophylls are in an appropriate distance the carotenoid S2 state can very efficiently (within less than 100 fs) transfer energy to chlorophyll. However when the excitation on chlorophyll is not immediately transferred or processed (as it happens when the machinery is still busy with processing the previous photon) it is transferred back to the carotenoid via its S1 state on a picosecond scale (a normal lifetime of chlorophyll excited state is in 1 ns). As a result carotenoids not only feed the system with excitation when they absorb a photon, but they also immediately remove any excitation back when it is not used. When the unlikely triplet formation yet happens, the triplet can be transferred to carotenoid as a last resort .The extent of these photo protective roles of carotenoids of course strongly varies among the specific photosynthetic proteins and their parts. This is illustrated in the figure 22:

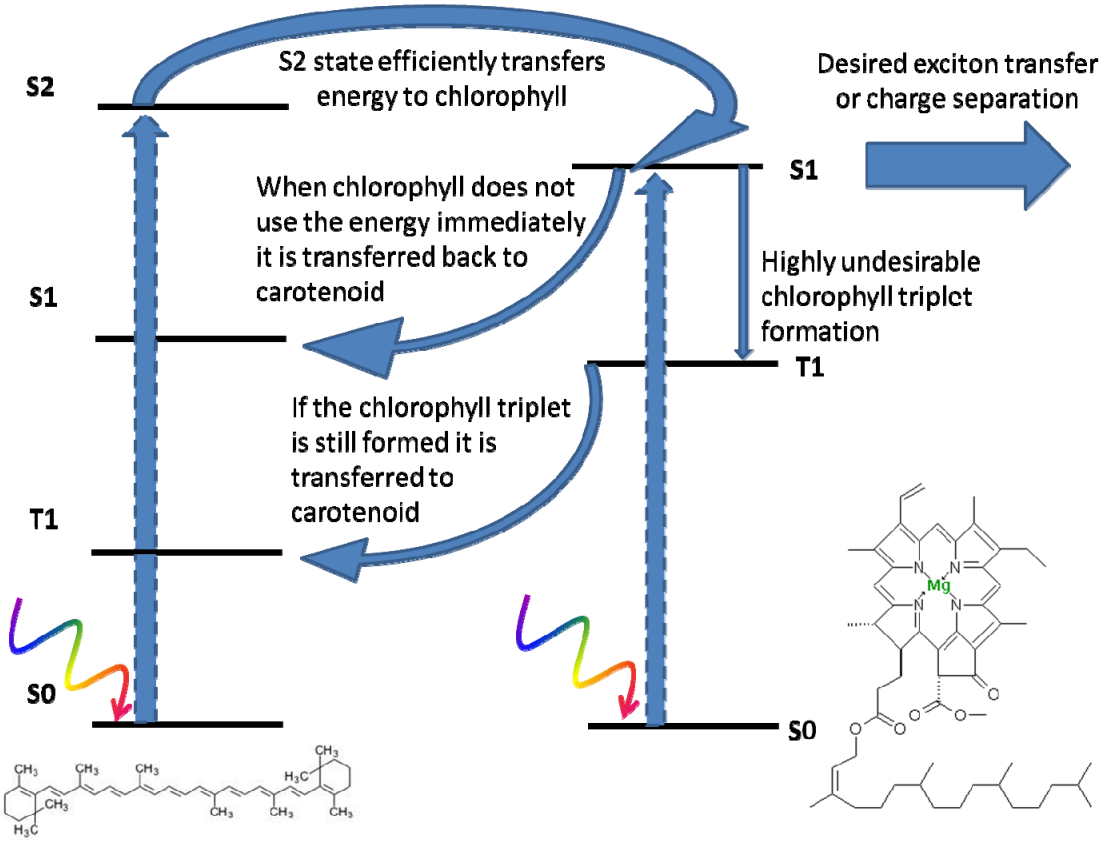

Figure 22

Carotenoids transfer energy to chlorophylls but interestingly they also suck the energy back at a high rate. This guarantee that excitation does not stay on the chlorophyll more than just a few ps. This way they drastically reduce the probability of triplet formation. The intensity of the effect increases with the length of the carotenoid as it pushes the S1 and S2 state energy downwards.

The whole story is in fact even more complex and in a way ingenious. Various carotenoids have their S1 state at different energies. Generally longer carotenoids have the S1 state lower (18). This holds similarly for the S2 state, just the S2 state energy drops slower with the length of carotenoids. This means that the longer the carotenoid, the less it transfers its energy to a chlorophyll, and the more it sucks the energy from the chlorophyll. By choice of the carotenoid, plants can tune the photo protection mechanism to optimum! Nowadays there is a vivid debate about the detailed mechanism of the described processes in various organisms and an active role of the carotenoid exchange in the switching among state of a different photo protection activity. The problem is that incorporation of a different carotenoid into the protein moiety can mean a change in the overall structure of the protein. As result despite the exchange of carotenoids in overexcited plants is known for more than two decades (25), there is still no consensus if the drop in the carotenoid S1 state energy is the only reason for plant to synthesize longer carotenoids when overexcited. The fact remains that on the primitive artificial systems consisting just out of a single carotenoid

and a single tetrapyrrole a switch from carotenoid with 9 double bonds to carotenoid with 10 double bonds can mean change in triplet yield in a ratio of 30:1 (26-28)! A part of my focused works section deals with the issue. Despite many controversial details (often originating in the different experimental methods adopted by the different groups) the photo protection role of carotenoids in the photosynthesis seems to be not only unquestionable and extremely efficient, but probably even irreplaceable!

Focused Section

3. Carotenoid Photoprotection In Artificial Photosynthetic Antennas

Miroslav Kloz, Smitha Pillai, Gerdenis Kodis, Devens Gust, Thomas A. Moore, Ana L. Moore, Rienk van Grondelle, John T.M. Kennis

This work was published in: Journal of the American Chemical Society

Abstract

A series of phthalocyanine-carotenoid dyads in which a phenylamino group links a phthalocyanine to carotenoids having 8 to 11 backbone double bonds were examined by visible and near infrared femtosecond pump-probe spectroscopy combined with global fitting analysis. The series of molecules has permitted investigation of the role of carotenoids in the quenching of excited states of cyclic tetrapyrroles. The transient behavior varied dramatically with the length of the carotenoid and the solvent environment. Clear spectroscopic signatures of radical species revealed photoinduced electron transfer as the main quenching mechanism for all dyads dissolved in a polar solvent (THF), and the quenching rate was almost independent of carotenoid length. However, in a non-polar solvent (toluene), quenching rates displayed a strong dependence on the conjugation length of the carotenoid and the mechanism does not include charge separation. The lack of any rise time components of a carotenoid S_1 signature in all experiments in toluene suggests that an excitonic coupling between the carotenoid S_1 state and phthalocyanine Q state , rather than a conventional energy transfer process, is the major mechanism of quenching. A pronounced inhomogeneity of the system was observed and attributed to the presence of a phenyl-amino linker between phthalocyanine and carotenoids. Based on accumulated work on various caroteno-phthalocyanine dyads and triads, we have now identified three mechanisms of tetrapyrrole singlet excited state quenching by carotenoids in artificial systems: (i) Car–Pc electron transfer and recombination; (ii) ^{1}Pc to Car S_1 energy transfer and fast internal conversion to the Car ground state; (iii) excitonic coupling between ^{1}Pc and Car S_1 and ensuing internal conversion to the ground state of the carotenoid. The dominant mechanism depends upon the exact molecular architecture and solvent environment. These synthetic systems are providing a deeper understanding of structural and environmental effects on the interactions between carotenoids and tetrapyrroles and thereby better defining their role in controlling natural photosynthetic systems.

Introduction

Non-photochemical quenching (NPQ) is a biological control system that allows plants and some other photosynthetic organisms to adapt to changing light levels(29, 30). It prevents photodamage by dissipating excess energy under conditions of moderate to high light levels where the non-photochemical, downstream biochemical processes cannot keep pace with the rate of photo-generated chemical potential. In doing so it necessarily limits photosynthetic efficiency, i.e., biomass production. Anticipating that research aimed at addressing the rate-limiting downstream processes will be successful, it is essential to understand the control system in depth so that it can be "reset" to allow higher fluxes of photogenerated redox potential.

Carotenoid chromophores play a crucial role in the energy dissipation process by quenching chlorophyll singlet excited states in photosynthetic antennas. They have an additional crucial function by quenching Chl triplet excited states and singlet oxygen(31, 32). Generally, there is no single mechanism of NPQ for natural photosynthetic systems, as different classes of organisms have their own particular ways of carrying out photoprotection. Controversy persists regarding the precise molecular mechanism of the 'classical' NPQ mechanism in plant PSII. There is evidence for both energy and electron transfer quenching in NPQ of higher plants; the mechanism could depend on the type of pigment-protein complex and its position in the antenna system(23, 24, 33-40). Diatoms are an important class of marine algae that show a very strong NPQ response(41, 42). Their light-harvesting complexes (LHCs) differ from those of plants and bind Chl-a and -c, fucoxanthin and diadinoxanthin. Diatoms have a diadinoxanthin cycle alongside a xanthophyll cycle,(43) which is reminiscent of but differs in an important way from the latter. In cyanobacteria, excess energy in the PSI/PSII antenna is believed to be dissipated via the IsiA protein under certain circumstances.(44, 45) The orange carotenoid protein (OCP) is believed to directly quench excitations in the phycobilosome antenna of cyanobacteria.(46, 47)

In a synthetic model system reported earlier, it was demonstrated that the S_1 state of a cyclic tetrapyrrole (phthalocyanine, Pc) is quenched by energy transfer to the S_1 state of a carotenoid provided the system of the carotenoid includes at least 10 conjugated double bonds.(26) Unexpectedly for energy transfer, the quenching was much stronger in polar solvents. These results were interpreted in terms of charge-transfer states arising from carotenoid carbonyl groups strongly coupled to the carotenoid S_1 state and thereby mediating the energy transfer(26). Indeed, the transient spectra of the S_1 state of the model carotenoids resemble those of fucoxanthin and peridinin, which also have carbonyl groups conjugated to the polyene. The S_1 states of fucoxanthin and peridinin have considerable charge-transfer character(48) that was demonstrated to be vitally important for their efficient light harvesting function.(49, 50)

The present work addresses the question of whether carotenoids lacking the terminal carbonyl group, but in dyads otherwise structurally similar to the molecules studied previously, can act as quenchers of the excited states of tetrapyrroles. The study of these carotenoids is pertinent to NPQ, since the xanthophylls involved in NPQ of higher plants do not contain carbonyl groups.(51) For this purpose a new series of dyads have been prepared which feature a secondary amine group as a linker between the carotenoid (Car) and the Pc. Dyads **1**, **2**, **3** and **4** contain carotenoid moieties of 8, 9, 10 and 11 conjugated double bonds, respectively, in addition to a phenyl group (Fig. 1). For convenience, dyads **1**, **2**, **3** and **4** are referred to as Dyad-8, Dyad-9, Dyad-10 and Dyad-11.

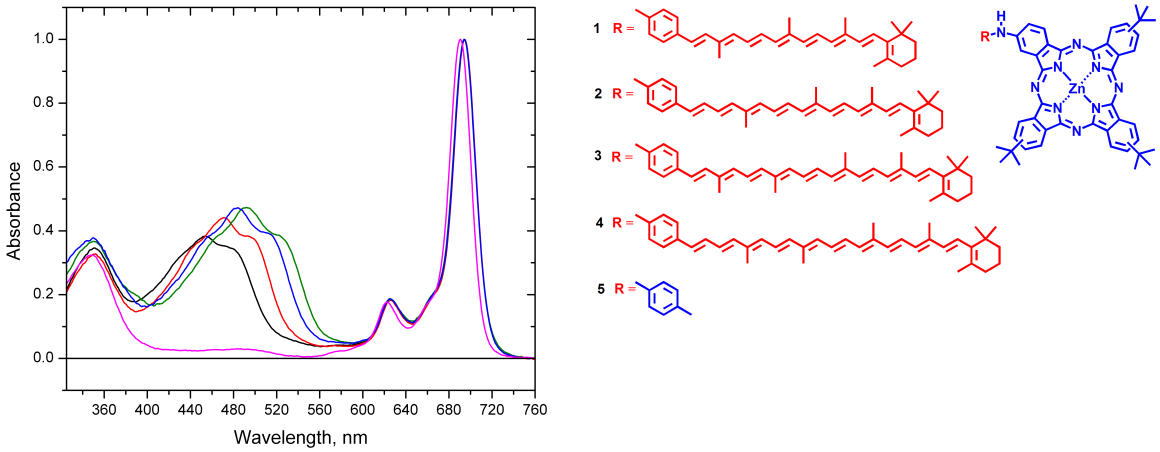

Figure1. Chemical structures and absorption spectra of Pc-Car **1 - 4** (Dyads 8-11) and model phthalocyanine **5**. Key: black, Dyad-8; red, Dyad-9; blue, Dyad-10, green, Dyad-11; magenta, model Pc.

Materials and Methods

Synthesis

The synthesis of the carotenoids bearing an amino group was achieved by a Wittig reaction with the required apo-□-carotenals and [4-*(*N-acetylamino*)*benzyl]triphenylphosphonium bromide followed by hydrolysis of the amide as previously discussed.(52) Zinc tri-*tert*-butyliodophthalocyanine was synthesized by the mixed condensation reaction of 4-iodophthalonitrile with 4-*tert*-butylphthalonitrile in a 1:3 ratio in the presence of $ZnCl_2$. From the statistical mixture of differently-substituted phthalocyanines the derivative containing one iodo group was isolated by column chromatography on silica gel in 15% yield. All tetrasubstituted phthalocyanines synthesized were obtained as mixtures of regioisomers.(53) The phthalocyanine bearing an aryl iodide was aminated with the various aminocarotenoids under conditions developed by Buchwald and co-workers.(54) Dyads

were synthesized by applying these conditions to our system using a Pd-catalyst having BINAP as a ligand. Details about the synthetic procedures are described in the Supporting Information.

Spectroscopic measurements

The spectrometer for the time resolved experiments consisted of an integrated Ti:sapphire oscillator and regenerative amplifier laser system (Hurricane, Spectra Physics) operating at 1 kHz at a wavelength of 800 nm and producing pulses of 0.6 mJ with a duration of 96 fs.(55) A portion of the light was picked to pump a home-built non-collinear optical parametric amplifier to produce excitation pulses at 670 nm. The beam was aligned through a remotely controlled delay line to set the delay between pump and probe pulses in the region from 0 to 3 ns, and subsequently led to the sample area where it was attenuated to 80 nJ per pulse. Another portion of the light was picked and focused in a CaF_2 plate to produce a broadband continuum spanning the whole visible region. The two beams were focused by 200 and 50 mm lenses, respectively and overlapped in the sample area with mutual polarization set to the magic angle (54.7˚) to avoid photoselection effects. Changes in the absorption of the sample were recorded by focusing the probe beam into the spectrograph equipped with a 256-element diode array coupled to a phase locked chopper operating at 500 Hz in the pump beam. Samples were adjusted to an absorbance of 0.7 and placed into the focus in a 1 mm path length quartz cuvette mounted in a shaking device. The spot diameter was 200 μm.

Near-IR experiments were performed on a similar spectrometer (Mira, Rega, Coherent) operating at 40 kHz with a pulse duration of 50 fs. The principal differences in these experiments were the use of sapphire plate for generation of a broad-band continuum as a more appropriate source for near IR experiments and a smaller pump pulse energy of 17 nJ enabled by the higher repetition rate.

Data Analysis

The data were globally analyzed with an R-based fitting package, TIMP.(2, 3) The femtosecond transient absorption data were globally analyzed using a kinetic model consisting of sequentially interconverting, evolution-associated difference spectra (EADS), i.e. $1\rightarrow2\rightarrow3\rightarrow...$ in which the arrows indicate successive mono-exponential decays of increasing time constant. The time constant can be regarded as the lifetime of each EADS.(2) The first EADS corresponds to the time-zero difference spectrum. This procedure allows clear visualization of the evolution of the excited and intermediate states of the system. It is important to note that a sequential analysis is mathematically equivalent to a parallel (sum-of-exponentials) analysis. The analysis program calculates both EADS and decay-associated

difference spectra (DADS) and the time constants that follow from the analysis apply to both.(2) In general, the EADS may reflect mixtures of molecular states, such as may arise, for instance, from heterogeneous ground states or branching at any point in the molecular evolution.(19, 21, 27, 56-59)

Results and discussion

Dyads in toluene

Fig. 1 shows the absorption spectra of Dyads 8-11 in toluene solution**.** Previous studies of artificial caroteno-phthalocyanine dyads and triads have shown a strong dependence of the quenching rate of ^{1}Pc by the attached carotenoid on solvent polarity.(26, 27, 60) For Dyads 8-11 of the present study, differences in the steady state fluorescence yields in various solvents also suggested a significant effect of the solvent polarity on the quenching rate (results not shown). Two different solvents, tetrahydrofuran (THF) as an example of a relatively polar solvent and toluene as a low polarity solvent, were chosen to investigate this phenomenon using the time resolved experiments.

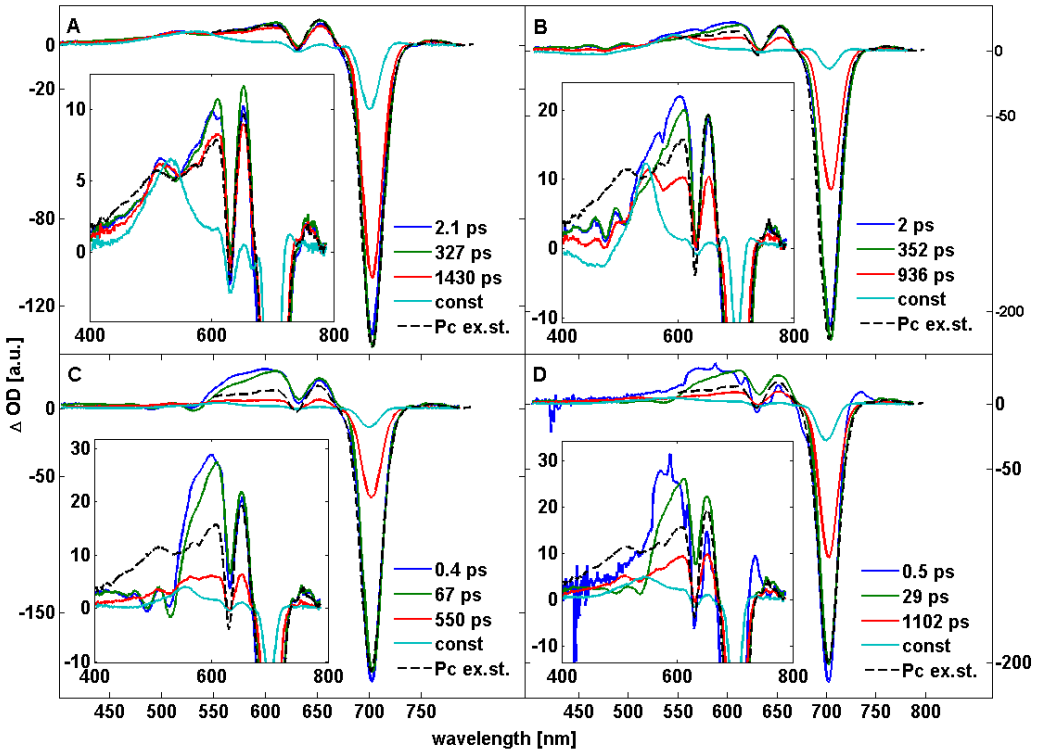

Figure 2. Evolution associated decay spectra (EADS) extracted from time resolved spectra recorded for toluene solutions of Dyad-8 (A), Dyad-9 (B), Dyad-10 (C) and Dyad-11 (D) after 670 nm excitation. The lifetime for each EADS is indicated in the panels. The black dashed lines denote the EADS of the Pc model compound, shifted by 5 nm so as to overlap with the signal of the dyad-bound Pc moieties.

Fig. 2 A-D show the evolution associated decay spectra (EADS) of Dyads 8-11 dissolved in toluene with excitation at 670 nm, together with associated time constants extracted by the global fitting analysis. A time-resolved spectroscopic examination of Pc model compound **5** revealed no significant influence of the solvent polarity on the singlet excited state lifetime, which was in both cases around 4 ns. This number represents decay of ^{1}Pc by internal conversion, fluorescence, and intersystem crossing.(61) The EADS that represents the relaxed excited state of **5** is depicted in panels A-D with the dashed black line.

In toluene, quenching of the Pc excited states in Dyads 8-11 was found to depend upon the length of the carotenoid conjugated backbone. The transient spectra required three time constants and a nondecaying component to obtain a satisfactory fit of the data to a sequential kinetic model. In Dyad-8, lifetimes of 2.1 ps, 327 ps and 1430 ps were obtained (Fig. 2A). The first EADS (2.1 ps, blue line) shows a negative band near 700 nm that results from Pc ground-state bleach and stimulated emission. At wavelengths shorter than 670 nm, a broad positive signal is observed that is due to excited-state absorption. The dip near 620 nm results from bleach of a vibronic band of the Pc Q transition (cf. Fig. 1 for the steady-state absorption spectra).

The first EADS evolves in 2.1 ps to the 2nd EADS, which has a lifetime of 327 ps (Fig. 2A, green line). The evolution in spectral shape is very minor with a very small increase in Pc ground state bleaching at 700 nm and small rise in excited state absorption between 550 and 650 nm. The origin of this spectral evolution is difficult to assign. The 1st and 2nd EADS closely resemble the excited state of the model Pc compound (Fig. 2A, black dashed line), indicating that the observed excited states in Dyad-8 represent essentially singlet-excited Pc.

The 2nd EADS evolves with a lifetime of 327 ps into the 3rd EADS, which has a lifetime of 1430 ps (Fig. 2A, red line). Their shapes are almost identical, with a 20% reduction in amplitude of the latter. The 3rd EADS evolves in 1430 ps to the nondecaying EADS (Fig. 2A, cyan line), and involves an almost 80 % drop in Pc exited state transient absorption signatures. The nondecaying EADS contains a characteristic broad peak centered near 520 nm and a small amount of Pc ground state bleaching allowing an identification of this component as a mixture of Pc and carotenoid triplet states. This observation shows that the time constant for triplet-triplet energy transfer from Pc to carotenoid is smaller than (or on the order of) that for intersystem crossing in the Pc moiety. Similar phenomena have been observed in other Pc-carotenoid dyads and triads and light-harvesting antennas of oxygenic photosynthesis. In keeping with its reduced singlet excited-state lifetime as compared to Pc, the triplet quantum yield of Dyad-8 is lower (at ~0.1-0.2 judged from its amplitude) than in Pc (~0.6).(61, 62)

These experiments show that the excited state of Dyad-8 decays multiexponentially, with a minor decay component of 327 ps and a major component of 1430 ps. We conclude that the Pc excited state is weakly to moderately quenched by the covalently attached carotenoid. In contrast to our previous work on Pc-carotenoid dyads and triads,(26, 60) we do not observe any clear spectroscopic feature of a molecular state responsible for the quenching, so we cannot draw any conclusion regarding the quenching mechanism.

Dyad-9 follows an evolution similar to that of Dyad-8 with lifetimes of 2 ps, 352 ps, 936 ps, and a nondecaying component (Fig. 2B). The 352 ps component has a larger amplitude as compared with the corresponding 327 ps component in Dyad-8. Also, the 3rd lifetime (936 ps) is somewhat shorter than in Dyad-8. These observations imply that Dyad-9 is slightly more quenched than Dyad-8.

Fig. 2C shows the results for Dyad-10. This dyad displays a clear change in its transient behavior as compared with Dyads-8 and -9. The first EADS (Fig. 2C, blue line) has a lifetime of only 400 fs. The 2nd EADS has a lifetime of 67 ps and has a shape similar to that of the 400 fs EADS. This EADS is responsible for 70% of Pc excited state decay, indicating that this component shows a 60-fold quenching of the Pc excited state (i.e., from 4 ns to 67 ps). It is followed by the 3rd EADS with a lifetime of 550 ps. This last component is responsible for about 25 % of the quenching. The nondecaying EADS again represents a mixture of Pc and carotenoid triplet states.

Dyad-10 differs significantly from Dyad-8 and the Pc model compound in the appearance of a distinct carotenoid bleaching between 400 and 500 nm and a small additional excited state absorption between 500 and 610 nm in the 400 fs and 67 ps EADS. The spectrum of the Pc model compound is flat and featureless in this spectral region. (See inset of Fig. 2C and Fig. S1C). This observation indicates that in addition to ^{1}Pc, a carotenoid excited state is populated to some extent in these EADS. In Figs. S1 and S2, we explicitly compare the signals additional to that of ^{1}Pc in Dyad-10 with the S_1 spectrum of the carotenoid as follows from direct carotenoid excitation. We conclude that the spectral shape and position of the additional bleach and induced absorption of the 67 ps component is consistent with the presence of the carotenoid S_1 state. This spectral feature does not correspond to $Car^{\bullet+}$ - $Pc^{\bullet-}$ radical pair states, as no transient carotenoid cation band is observed in the near IR (Fig. S3). Likewise, the additional absorption feature between 550 and 610 nm cannot be due to Pc excited-state absorption, because if only Pc would be excited, such absorption would not be accompanied by carotenoid ground state bleaching. The implications of these observations are discussed below.

The spectral pattern in the 400 fs component may correspond to S_1 and S* states coexisting with ^{1}Pc. The S* state, controversially discussed in the literature,(18, 19, 21, 63-65) exhibits a blue shifted shoulder at the carotenoid S_1 state excited state absorption.(19, 21, 66, 67) and disappears in 400 fs. The disappearance of the S* feature cannot be related to a

vibrational cooling process, because that would be associated with absorption loss at the red side of the S_1 absorption.(68, 69)

Dyad-11 shows characteristics similar to those of Dyad-10, with time constants of 0.5 ps, 29 ps, 1102 ps and a nondecaying component. The 0.5 ps and 29 ps EADS look essentially the same as the corresponding EADS (0.4 and 67 ps) in Dyad-10, with significant carotenoid S_1/S* features mixed in the ^{1}Pc difference spectrum (Fig. S1 and S2), although the 0.5 ps EADS is not very well resolved. The second EADS (29 ps) follows the trend of decreasing lifetime with increasing length of the carotenoid noted in the other dyads, suggesting a component that is strongly quenched. Surprisingly, the third EADS (1102 ps) does not follow such a trend at all: it is significantly longer than that of Dyad-10 (550 ps) and even slightly longer than that of Dyad-9 (936 ps). In addition, the amplitude of the 1102 ps EADS is significantly larger than that of the 550 ps EADS of Dyad-10, indicating that a larger fraction of Dyad-11 is only weakly to moderately quenched. Dyad-9 shows similar features to those of Dyad-10 and -11 in its 2 ps and 352 ps EADS (Fig. 2B), but to a lesser extent that does not allow quantitative assessment of its molecular nature.

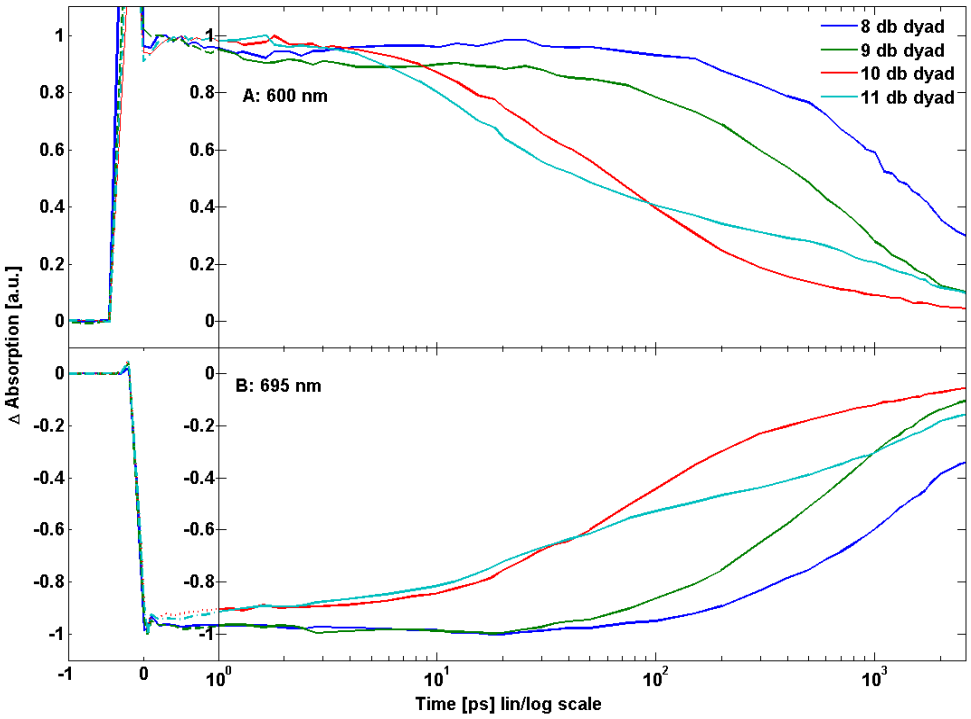

Figure 3. Normalized time traces of dyads dissolved in toluene recorded at 600 and 695 nm representing the carotenoid S_1 state absorption and Pc ground state bleach, respectively. The time axis is linear from -1 to 1 ps and logarithmic thereafter. Note that while for the first few picoseconds there are slight differences in the time evolution, at longer times the kinetics are practically identical. The kinetics in the 600 nm region are less smooth, because of relatively lower signal

intensity at this wavelength.The peak around zero delay in the kinetics at 600 nm results from coherent and cross-phase modulation artifacts and are not related to the photophysics of the Dyads.

Berera *et al.*, showed that a carotenoid can act as an acceptor of Pc excitation energy, thereby shortening the Pc singlet excited state lifetime.(26, 37) The conjugation length of the carotenoid was critical to the quenching process and the addition of only one double bond, from 9 to 10, turned the carotenoid from a non-quencher into a strong quencher. It was shown that the quenching proceeds through energy transfer from the excited Pc to the optically forbidden S_1 state of the carotenoid, coupled to an intramolecular charge-transfer state. The excited-state energy was dissipated rapidly through internal conversion from the carotenoid S_1 state to the ground state on the picosecond timescale. An important feature of the quenching phenomenon was that it proceeded through an inverted kinetic scheme, i.e., energy transfer from Pc to Car was relatively slow (on the 30 – 300 ps timescale), after which internal conversion from the Car S_1 state to the ground state occurred relatively fast, in ~5 ps. As a result, the spectral evolution was characterized by a rise of Car S_1 spectral features on the 5 ps timescale at low transient concentrations on top of Pc excited-state features, giving rise to difference spectra that are similar to those reported for the (strongly quenched) 67 ps and 29 ps EADS in Fig. 2C, D for Dyad-10 and Dyad-11, respectively.

A key difference between the present data and those of Berera *et al.(26, 37)* is that here, no obvious rise component of the Car S_1 features associated with inverted kinetics was observed. Rather, the Car S_1 (and S*) signatures were present in the transient spectra *immediately* after Pc excitation, within the time resolution of 100 fs. This can also be observed in Fig. 3, where the Pc kinetics are compared with the Car S_1 kinetics in Dyads 8-11: no rise component on a ps timescale can be discerned in the kinetics at 600 nm. This observation indicates that in the present dyads, the quenching cannot be described with a simple sequential ^{1}Pc $\rightarrow$ Car S_1 energy transfer scheme. Rather, we suggest here that the quenching may be mediated through excitonic coupling between the ^{1}Pc and the optically forbidden Car S_1 (and/or S*) state. In the excitonic case, the excited state is shared between the Pc and carotenoid immediately upon excitation. The lifetime of the collective state is then determined by the extent to which the carotenoid S_1 state is mixed with the Pc state and by the carotenoid S_1-S_0 internal conversion rate (which is in the order of picoseconds).(18) Such a mechanism differs significantly from that of Berera et al.,(26) where the excited state is localized on either of the cofactors and the Pc lifetime is determined by the rate of energy transfer from Pc to carotenoid. Despite the fact that excitonic coupling of the Car S_1 state with Pc excited states is not a generally established principle, especially because of the vanishingly low dipole strength of the former,(18, 70) there are experimental data suggesting this mechanism in natural photosynthetic antennas.(38, 71)

The question is how appreciable excitonic coupling may arise between Pc and the optically forbidden carotenoid S_1 state, as classical exciton theory predicts such coupling will be zero. First of all, it is important to note that excitonic interactions are governed by couplings essentially identical to those that govern incoherent energy transfer between closely spaced chromophores. According to traditional Förster theory, energy transfer rates that involve the carotenoid S_1 state should be rigorously zero because of the zero transition dipole moment of the latter.(72) Yet, it has been demonstrated experimentally many times that in natural and artificial light harvesting systems, Car S_1 to Chl (or for that matter, Pc) and Chl to Car S_1 can happen very rapidly on the ps and sub-ps range.(21, 26, 27, 60, 73-76) Fleming and co-workers showed that when molecules are in close contact, the point-dipole approximation breaks down and rather the interaction of the transition densities of the two molecules has to be considered.(77) In the specific case of the carotenoid S_1 state, the molecular symmetries that govern photon absorption (which applies on the wavelength scale of the photon, 0.5 – 1 microns) are not the same as the molecular symmetries experienced by closely spaced chromophores. Thus, the electronic transition to a state that is optically forbidden in an isolated molecule may exhibit considerable Coulombic coupling to transitions in chromophores at close proximity.(78, 79)

Additionally, the S_1 state may obtain dipole strength through mixing with the strongly allowed S_2 state, a mechanism that has been invoked to explain the fast (ps) energy transfer dynamics from Car S_1 states to Chl in natural LH antennas.(79, 80) In the present dyads, such an effect may be augmented by the presence of the aminophenyl group in the conjugated backbone of the carotenoid, which introduces a symmetry-breaking element in the □-electron conjugation and may result in an increased dipole strength of the Car S_1 state.

We propose that in Dyads 10-11, the Coulombic coupling is so strong that it results in delocalization of the molecular wavefunctions. Classical exciton theory predicts spectral shifts and redistribution of oscillator strength in the linear absorption spectrum upon delocalization of wavefunctions.(72) The absorption of the Pc moiety in Dyads 8-11 is red-shifted by about 100 cm^{-1} respect to the Pc model compound (Fig. 1). This shift may have an origin different from excitonic interaction, because other Car-Pc dyads that do not show excitonic interactions exhibit a similar shift.(26) The effects of large Coulombic coupling on the linear absorption spectra of coupled chromophores involving optically forbidden states remains to be investigated theoretically: the point-dipole approximation, which we know is not applicable here, is used to predict extent and magnitude of spectral shifts and redistibution of oscillator strength in classical exciton theory. Hence, the absence of obvious shifts and changes of dipole moments in the linear absorption spectra of Dyads 10-11 does not directly address the issue of excitonic interactions.

We can safely exclude the possibility that the lack of rising Car S_1 features of Figure 2 and 3 relates to an unresolved very fast energy transfer within the time resolution of 100 fs. If inverted kinetics applies as in Berera *et al*.,(26, 37) an unresolved rise component of the Car

S_1 features would actually correspond to a Car S_1 internal conversion lifetime of <100 fs, which is unrealistically short.(18) If for any reason the Car S_1 lifetime would be that short, we would not experimentally observe the carotenoid S_1 state in our spectra because with the relatively slow energy transfer from Pc (67 ps in Dyad-10, Fig. 2C), its transient concentration would become undetectably low. A direct energy transfer process from Pc to the carotenoid S_1 state within 100 fs would result in a <100 fs decay of the Pc excited state, which is not observed experimentally.

The observation of multiphasic Pc lifetimes in the dyads leads to the conclusion that the dyads may adopt multiple structural conformations leading to variable Pc-Car electronic coupling. The fitted sum of exponentials may be merely an approximation of the average dynamics observed spectroscopically despite the fact that it fully fits the data within the available signal quality. Note that in other Pc-carotenoid dyads and triads, multi-phasic decay of the Pc excited state was observed as well,(26, 27, 60, 81) although it appears more pronounced in the present study. In axially linked Si-Pc-Car triads, NMR and modeling studies confirmed that multiple conformations exist.(81) Additional conformational flexibility in the present dyads may be induced by the aminophenyl groups that link the Pc and carotenoid moieties.(82, 83)

Weak to moderate quenching is observed in Dyad-8 and Dyad-9, as well as the slow decay phases in Dyad-10 and Dyad-11. Interestingly, the EADS associated with these lifetime components (Fig. 2 A-D) are similar to those of the model Pc compound and show little (Dyad-9) or essentially no (Dyad-8) carotenoid excited-state features or signs of inverted kinetics. The quenching mechanisms of these dyad sub-populations therefore remain unknown. They may proceed through the energy transfer or excitonic mechanisms described above, but the extent of excitonic mixing or rise of transient carotenoid S_1 population remains so low that no mechanistic conclusions may be drawn. Likewise, quenching through electron transfer and recombination(60) cannot be excluded, although this option seems unlikely given the low solvent polarity of toluene.

Dyads in THF

The evolution associated decay spectra (EADS) after 670 nm excitation of Dyads 8 - 11 dissolved in THF together with associated time constants extracted by the global fitting analysis from time resolved data are depicted in Fig. 4.

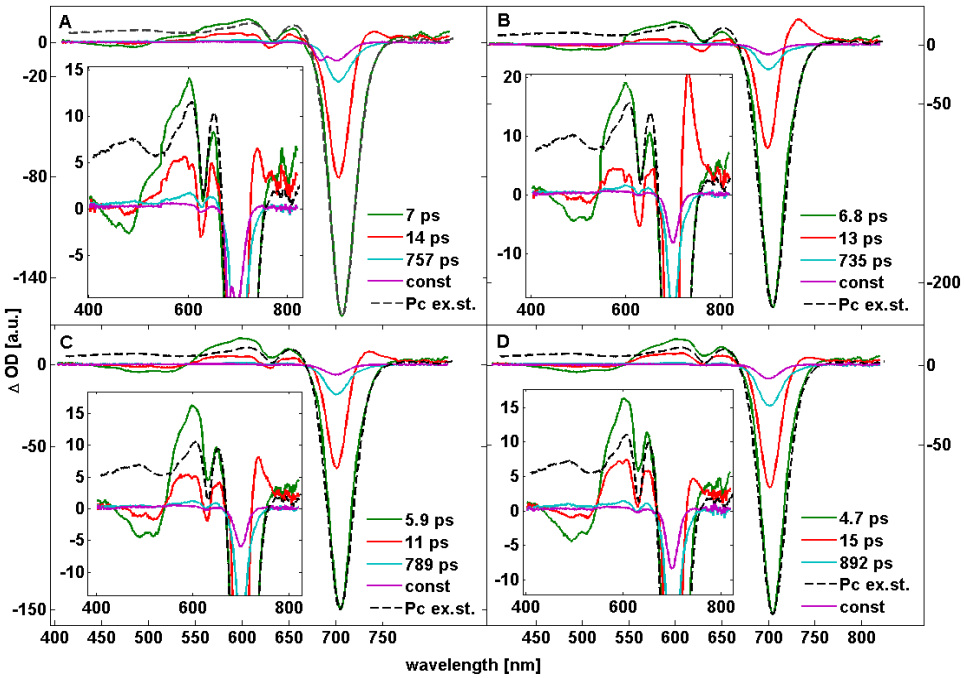

Figure 4. Evolution associated decay spectra (EADS) after 670 nm excitation extracted from time resolved spectra recorded on Dyad-8 (A), Dyad-9 (B), Dyad-10 (C) and Dyad-11 (D) dissolved in THF. The lifetime of each EADS is indicated in the panels. The black dashed lines denote the EADS of the Pc model compound **5**, shifted by 5 nm so as to overlap with the signal of the dyad Pc moieties.

All dyads dissolved in THF followed a very similar and rather complex transient evolution. Four exponentials and a nondecaying component were sufficient to fit the data. The first EADS was in the 200 fs region, was poorly resolved and hence is not shown and not further discussed. The second component (with time constant of 7, 6.8, 5.9, and 4.7 ps for Dyads-8, 9, 10 and 11, respectively, green lines in Fig. 4) shows both Car and Pc excitation signatures, which may correspond to direct sharing of the excitation between Pc and Car (see Fig. S4), similar to the situation with Dyads-10 and -11 dissolved in toluene. It comprises bleaching of the carotenoid ground state between 400 and 500 nm, bleaching of Pc ground state absorption near 700 nm and 620 nm, and broad carotenoid S_1 state absorption centering around 600 nm. The 4.7 - 7 ps EADS represent most of the quenching of the Pc excited state as may be concluded from the large drop in Pc ground state bleaching that is observed in the following EADS, which has lifetimes of 14, 13, 11 and 15 ps (for Dyads-8, -9 , -10, and -11, respectively, red lines in Fig. 4). This EADS differs from the previous one by the relative decrease of carotenoid features and the appearance of a new induced absorption shoulder near 720 nm. This EADS basically concludes the transient behavior of the dyads. A small amount of remaining excitation is contained in the fourth EADS with lifetimes 757, 735, 789, and 892 ps (for Dyads-8, -9, -10 and -11, respectively, cyan lines in Fig. 4) and also in the

nondecaying component (magenta lines in Fig. 4) representing features with lifetimes beyond the examined time window.

To investigate whether the rapid quenching proceeds through charge separation and subsequent recombination, Dyad-10 was studied in near IR region where Pc and Car radical species absorb(84, 85) (Fig. 5).

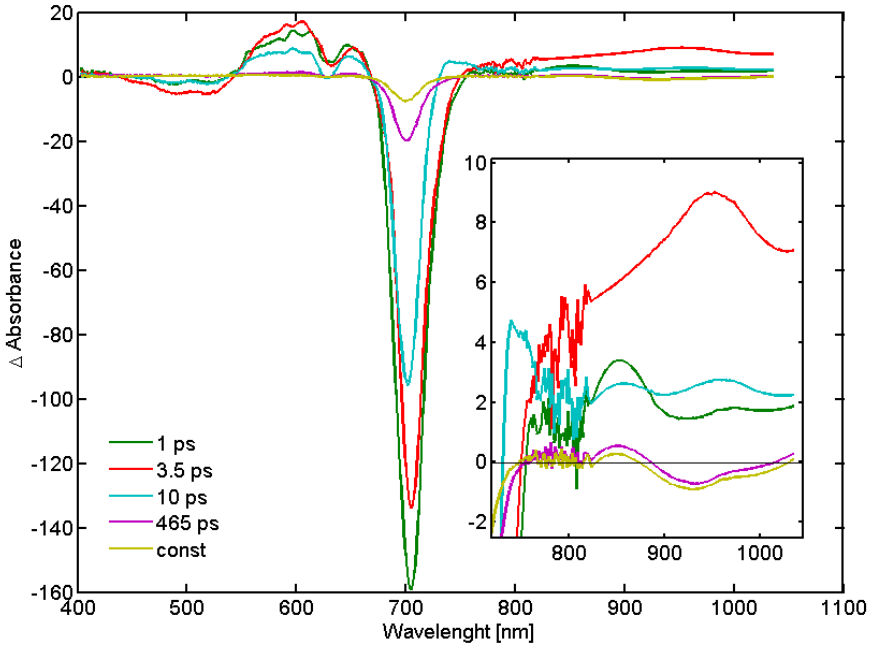

Figure. 5. Evolution-associated decay spectra of Dyad-10 in the visible and near-IR regions. The excitation wavelength was 680 nm.

Figure 5 shows the rise of a carotenoid cation radical peak around 980 nm in 1 ps, and its subsequent decay in 3.5 ps. Given the high extinction coefficient of carotenoid radical cations (~10^5 M^{-1} cm^{-1}), the low amplitude of the 980 nm peak relative to the Pc bleach near 700 nm implies a low transient concentration. The recording of a new component (1 ps) which was not resolved in the transient absorption experiments in the visible, suggests an inverted kinetics scheme, where Pc excited state (or Pc-Car coupled excited state) is slowly (5-10 ps) depopulated by charge separation followed by rapid recombination (~1 ps), resulting in a low relative concentration of radical species during the quenching process. We conclude that all dyads dissolved in THF are strongly quenched, with the majority of the Pc excited states decaying in 5 - 7 ps by this process. The quenching process is not dependent on the conjugation length of the carotenoid, which is consistent with electron transfer processes observed by Kodis *et al.* for axially linked Pc-Car triads in polar solvent.(60) We observe a Car S_1 signature in the excited-state spectra, which suggests that excitonic mixing between Pc and the carotenoid S_1 state takes place and may contribute to quenching.

In general, the electron donating ability of the carotenoids depends on the conjugation length, with a difference in the oxidation potential of the carotenoids of ~150 mV in going from carotenoids with 8 to 11 double bonds.(86-88) The amino carotenoids of this study are better electron donors that the carotenoids of refs.(86, 88) For example the midpoint oxidation potential of ~0.6 V vs. SCE for a carboxylate terminated carotenoid of 10 double bonds is ~0.3 V vs. SCE for the anilino-terminated carotenoid of the same conjugation length (not shown).(87) Thus, in every case of the systems of this study there is sufficient driving force to observe charge separation between Pc and the carotenoid, particularly in polar solvents. However, the difference in driving force between the different conjugation lengths of the carotenoids must not be sufficient to measure different quenching rates in the cases studied.

The 720 nm shoulder in the 11- 15 ps EADS of Fig. 4 and the 10 ps EADS of Fig. 5 is difficult to assign. In previous work, similar signals were associated with Pc charge-transfer processes.(89, 90) It may also be interpreted as a temporal broadening or a red shift of the main Q absorption peak of Pc. Such broadenings and red shifts are observed generally in steady state absorption spectra of dyads dissolved in high polarity solvents. In the present case, transient formation of a charge-separated $Car^{\bullet+}$ $Pc^{\bullet-}$ species results in disturbing the solvent shell. Charge recombination in a few ps may then result in a non-equilibrated solvent in such a way that the Pc Q band is broadened or red shifted showing the positive band at 720 nm, followed by solvent relaxation in 10 - 15 ps.

Conclusions

In both THF and toluene solvents, it is clearly demonstrated that in dyads that lack a carbonyl group in the carotenoid conjugated backbone, the Pc excited state is quenched by the attached carotenoid. The observed excited-state lifetimes are multiexponential, which may be attributed to ground-state heterogeneity, possibly associated with the existence of the molecule in a set of various conformations, which gives rise to a variety of quenching rates. Conformational heterogeneity around the phenyl-amine link where separate minima strongly influence Pc-car coupling may be responsible for this phenomenon.

An interesting observation is that when dissolved in THF, the quenching is, at least in part, mediated by charge separation and recombination processes, and does not show a strong dependence on the length of the carotenoid conjugated electron backbone. In toluene, on the other hand, quenching appears to be mediated by excitonic coupling between Pc and the carotenoid S_1 state and shows a clear increase in quenching rate for longer carotenoids. The transition from 9 to 10 double bond carotenoids results in an especially large increase in quenching rate, similar to observations for previously studied Pc-Car dyads.(26) In the short

carotenoid dyads (Dyad-8 and Dyad-9), weak to moderate quenching by multiexponential processes is observed. This contrasts with the previously studied 9-double bond dyad where a single exponential decay identical to that of a model Pc compound was observed.(26) Thus, the present dyads do not exhibit a clear-cut 'gear-shift' mechanism, where addition of one double bond to the carotenoid conjugated □-electron system activates the quenching.

Spectral features which could be associated with the Car S* state were observed within the first ps (Fig. 2C and D, evolution from blue to green EADS) but there is no direct evidence that this state plays a crucial role in the quenching process.

The cumulative work on artificial Pc-Car dyads and triads has led to the experimental observation of three distinct carotenoid-mediated tetrapyrrole singlet excited-state quenching mechanisms, as depicted in Fig. 6:

Electron transfer from Car to Pc followed by rapid charge recombination on the picosecond time scale (ref(60, 81) and the dyads studied here in THF). There is evidence that similar processes between Chl and xanthophylls underlie NPQ in the plant PSII antenna.(23, 33, 35, 36)

2) Energy transfer from Pc to the optically forbidden S_1 state of the carotenoid.(26) Experimental evidence for such processes between Chl and carotenoids underlying NPQ in plant PSII(24) and in the cyanobacterial IsiA protein(44) has been reported.

3) Quenching through excitonic mixing between the Pc singlet excited state and the carotenoid S_1 state. This phenomenon was directly observed here for the first time for Dyad-10 and Dyad-11 in toluene. A similar mechanism involving Chl and xanthophylls was recently proposed to account for quenching in LHCII and plant PSII.(38, 71)

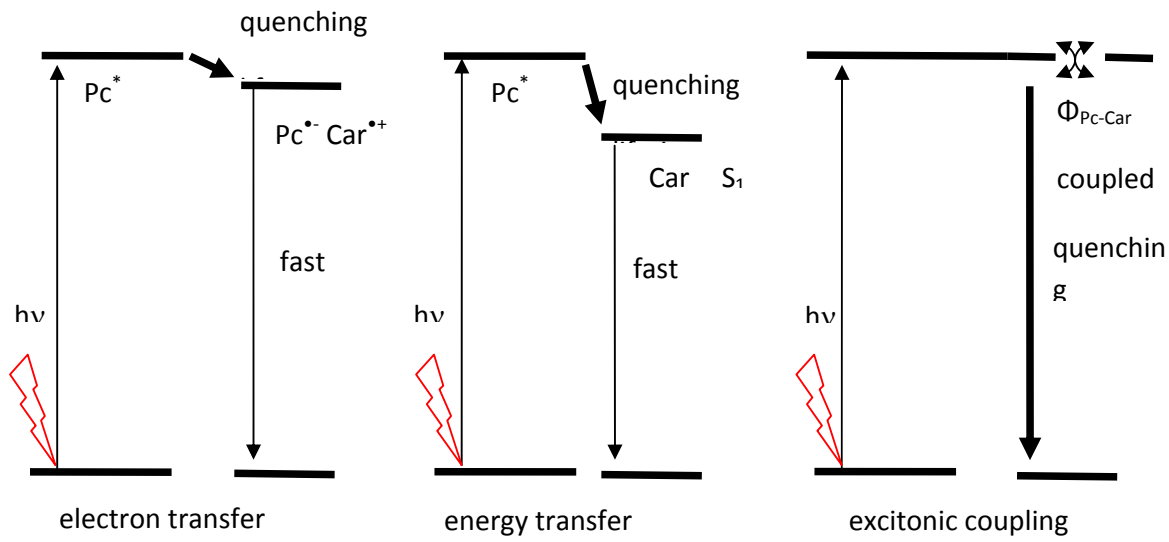

Fig. 6 Quenching mechanisms described in this paper: (1) quenching via short lived charge separated state associated with inverted kinetic scheme; (2) quenching via energy transfer to carotenoid dark S_1 state associated with inverted kinetic scheme; (3) quenching via Pc-carotenoid coupled state.

Thus, a considerable amount of evidence indicates that carotenoids can quench tetrapyrrole singlet excited states in a variety of ways, and relatively modest differences in the molecular architecture and environmental conditions can lead to a change in the quenching mechanism. The mechanistic flexibility exhibited by the artificial Pc-Car systems with regard to tetrapyrrole singlet excited state quenching suggests that any of the proposed mechanisms may operate in the various natural photosynthetic systems that display quenching. Further examination of such phenomena in artificial light harvesting systems will contribute to the understanding of the role of carotenoids in natural systems, where charge separation, energy transfer, excitonic coupling and conformational changes play their roles.

Supporting information

Supporting Information Available: Supporting figures S1-S4.
This material is available free of charge via the Internet at http://pubs.acs.org/.

4. Wavelength-modulated femtosecond stimulated Raman spectroscopy – approach towards automatic data processing

Miroslav Kloz, Rienk van Grondelle, John T.M. Kennis

This work was published in: Physical Chemistry Chemical Physics

Abstract:

A new wavelength modulator based on a custom-made chopper blade and a slit placed in the Fourier plane of a pulse shaper was used to explicitly detect the first derivative of the time-resolved femtosecond stimulated Raman spectroscopy (FSRS) signals. This approach resulted in an unprecedented reduction of the non-coherent background that results from population transfer by the Raman pump inherent to FSRS experiments. The method of Fourier peak filtering was implemented as a powerful tool for reducing both the remaining non-coherent and coherent background associated with FSRS experiments. The method was demonstrated on β-carotene and a similar synthetic aryl carotenoid. The experiments confirm earlier FSRS results on β-carotene but suggest some reinterpretation. Strong bleaching signals of ground state vibrations were observed and interpreted as an inseparable part of the time-resolved FSRS experiment. New long-lived Raman features were observed in β-carotene and the synthetic aryl carotenoid and assigned to a combination of conformational changes and solvent rearrangement. More complex wavelength modulation methods are proposed in the development of more robust FSRS experiments.

Introduction

Femtosecond stimulated Raman spectroscopy (FSRS) is a new promising tool for the ultrafast investigation of molecular vibrations.(91) Its experimental realization and underlying theory are both still in progress (12, 13, 92-96). Recently, FSRS has been used to resolve the mechanism of primary photochemistry for various photoactive molecules including proteins in great detail (97-100). It raises in importance as a complementary method to femtosecond infrared spectroscopy both because of its different selection rules and its easier experimental implementation into the standard, already broadly used visible (Vis) or near infra-red (Near-IR) time-resolved pump-probe or pump-dump-probe set-ups (101). The basis of the experiment is a proper time-spatial overlap of three pulses usually referred as: pump (Pu), a femtosecond pulse prepared to match a selected excited state energy, Raman-pump (Rp), a narrowband picosecond pulse inducing Raman scattering, and probe (Pr), a femtosecond broadband pulse stimulating the signal (light emission) towards the detection after a selected evolution time. The time resolution in FSRS is dominantly determined by the time band-widths of the Pu and Pr pulses while the spectral resolution is determined by the spectral narrowness of the Rp pulse (102). The basics of the FSRS experiment are described in the literature (92).

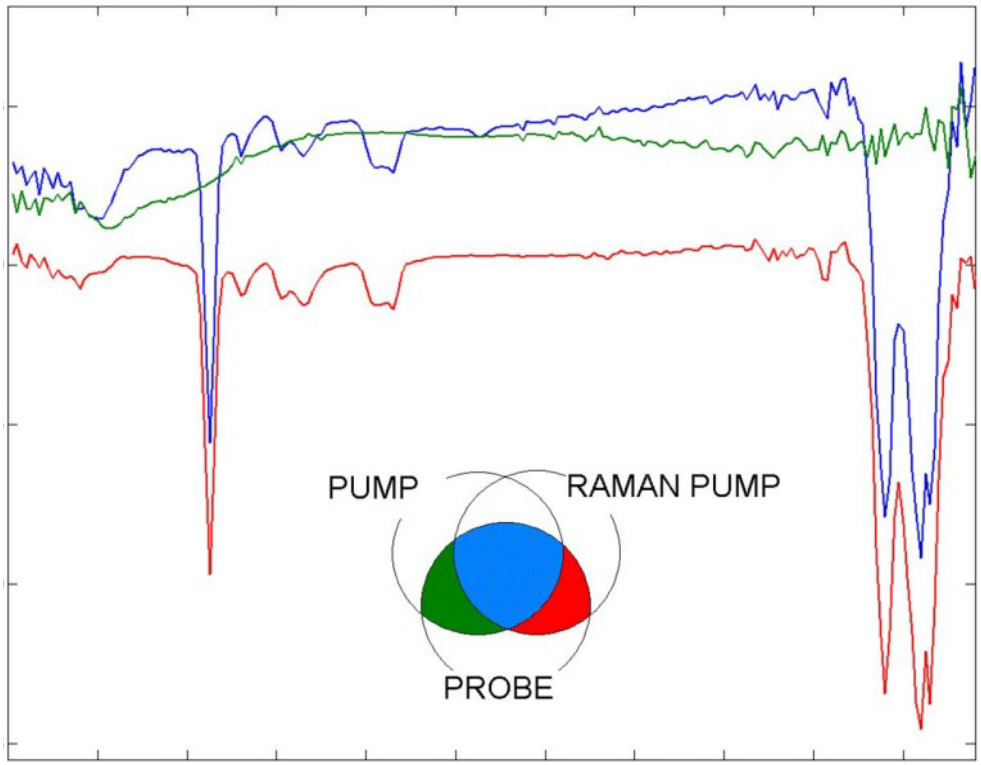

Figure 1 The transient absorption signals recorded as the three possible combinations of pulses used in a time-resolved FSRS experiment, detected by an apparatus designed for pump-dump-probe experiments(101, 103) (Rp and Pr puses were time overaped and 1.5ps delayed in respect to Pu pulse): Pu-Pr, Rp-Pr, Pu-Rp-Pr are represented by the different colors of curves defined by a diagram of overlapping pulses. The green signal represents the pump-probe signal, as no Raman-pump is applied, the red signal represents the steady state (ground-state) FSRS, as no pump is applied and the blue one represents the time resolved (excited state) FSRS, as all pulses are applied. The figure shows raw data (including the solvent originating peaks) recorded on β-carotene dissolved in THF. It demonstrates that the pump-probe signal (green) cannot fully explain the background of the time resolved FSRS signal (blue). The negative nature of Raman peaks reflects their origin in the stimulated emission as the absorption is plotted positive and emission negative.

Because the primary signal recorded by the standard FSRS experiment ($\log(I_{[Pu\text{-}Rp\text{-}Pr]}/I_{[Pr\text{-}reference]})$ (figure 1 blue) – the difference in intensity of the probe pulse alone after its propagation through the sample and of the probe pulse accompanied by pump and Raman-pump pulses – is composed of several different processes (excited state absorption, ground state bleaching, depletion of excited states, stimulated Raman scattering, stimulated emission from excited state population…), one of the challenging tasks of FSRS is the development of universal and automatic approaches towards signal processing. The goal is the extraction of the pure narrowband transient FSRS signal, or in other words: how the Raman contribution to the recorded signal changes in time during the evolution of the excited state manifold. Figure 1 shows how synchronized detection (performed by complementary chopping of Pu and Rp beams) allows a simultaneous recording of three transient absorption signals assigned to three possible combinations of applied pulses (the probe is applied always): Pu-only, Rp-only, Pu+Rp-together. The first can be considered as a combination of ground-state bleach, excited state absorption and stimulated emission, the second as FSRS of the ground state, and the third as the excited-state transient absorption features overlapped with excited-state FSRS. According to this simplified description we merely have to subtract the first two signals from the last one to acquire a transient FSRS spectrum (i.e., the difference between FSRS in excited and ground state). However, as can be concluded from the figure 1, such an approach is not sufficient and additional data processing is needed (8, 11, 94, 104). The reason is that the Rp can perturb the excited sample either by further exciting of ground state molecules and/or by dumping and re-pumping of excited molecules. In addition, the narrowband FSRS signal is affected by a broadband background originating from the coherent mixing of Rp and Pr close to zero time delay, as well as mixing of Pu and Rp pulses. The main contributions to these effects are described as resonance Raman scattering II - RRS(II), hot luminescence III and IV – HL(III) and HL(IV), and inverse Raman scattering I and II – IRS(I) and IRS(II) (12). Although deeper theoretical and experimental investigations are required, a classical interpretation of these phenomena is that together with the stimulated Raman scattering from the Rp pulse (SRS(I)), stimulated Raman scattering from the Pr pulse itself (SRS(II), IRS(I), IRS(II)) are

observed, plus contributions from the higher order coherent mixing of Rp and Pr. While these phenomena can often be neglected in steady state FSRS (i.e., stimulated Raman scattering in the absence of a Pump pulse) they gain importance under the resonance conditions where the contribution from the spectrally broadband Pr pulse can match a specific resonance and consequently be selectively enhanced. Unfortunately, during time resolved FSRS it is often difficult to work out of resonance because the absorption of excited states is typically very broad, especially for short-living states like the carotenoid S2 (1^1B_u)(8) whose excited-state absorption has significant contributions in the 800nm region where the FSRS experiment is often performed(105). This explains the experimental observation that time-resolved FSRS data suffer from a much larger background than steady-state FSRS data. The combined action of all these effects makes a straightforward separation of narrowband time-resolved FSRS from the background complicated, as the background can overwhelm the FSRS signal amplitude by orders of magnitude. So far the background correction was mostly performed by ad-hoc assumptions about the spectral shape of the background based on high order polynomial fitting(8, 99) or smoothing out the narrowband FSRS contribution from the signal (94, 100).

The problem of separating a Raman signal from the background is notorious already for steady-state (spontaneous) Raman spectroscopy, where even weak fluorescence from the sample or a contaminant can overwhelm the Raman signal. A useful approach in tackling this issue is subtracting data from two Raman experiments differing only in the scattered wavelength. If the difference between the two scattering wavelengths is infinitesimally small, the background can be usually considered identical for both experiments. Figure 2 shows how this approach results in the extraction of the first derivative of the Raman signal with a strongly or fully compensated background. The original Raman signal can be recovered by the integration of the spectra, while the process can be enhanced by some pre-integration data processing such as peak fitting (106, 107).

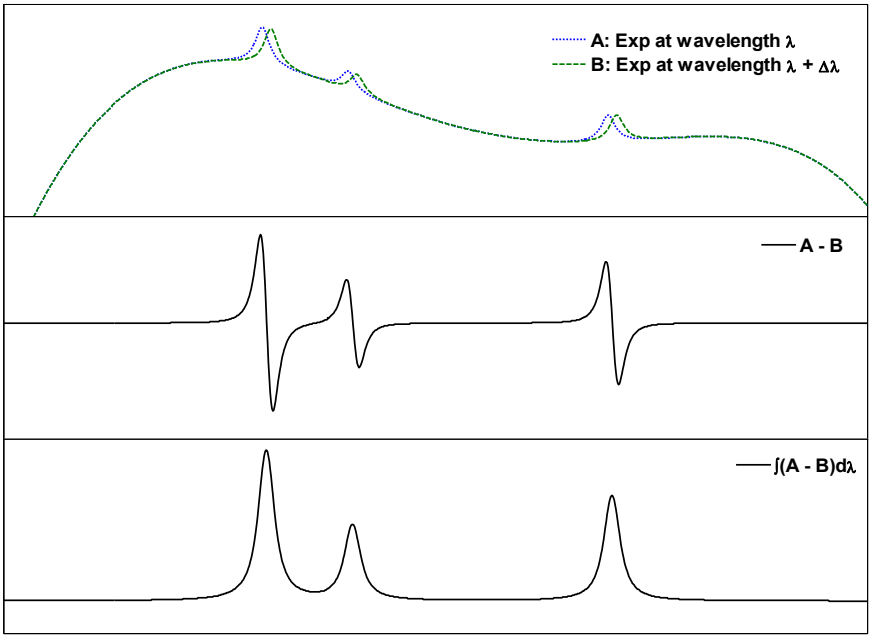

Figure 2. Concept of background subtraction through shifted Raman excitation in traditional (spontaneous) Raman spectroscopy. Subtraction of two Raman experiments with slightly shifted Raman excitation wavelengths (A, B) results in recording of the first derivative of the Raman signal (A - B) with the reduced background. The original signal is reconstructed by the integration of the difference signal (∫(A - B)dλ).

A similar approach would be useful in time resolved FSRS spectroscopy. Together with the reduction of the pump-dump-probe background (figure 1) an additional benefit is expected, namely the reduction of the broadband coherent background (RRS(II), HL(III), HL(IV)…(12)) assuming that the broad spectral structures associated with the Pr pulse scattering (FSRS induced by the Pr field instead of that from the Rp pulse) and the coherent mixing with the Rp are less sensitive to the small variation in the Rp wavelength than the narrowband FSRS signal.

For the success of this approach, it is essential to keep all conditions except the Rp wavelength identical. This includes the parameters of all involved laser pulses, the sample characteristics and other practical experimental conditions such as the spatial overlap of the pulses in the sample, thermal noise in the detector etc. A robust approach to deal with this problem is to modulate the scattering wavelength at high frequency and employing shot-to-shot detection synchronized with the modulation frequency. In this way one would explicitly record the first derivative of the signal. Any changes in the experimental parameters which occur on a timescale longer than the modulation frequency are eliminated. In fact, a similar approach based on amplitude rather than wavelength modulation is widely applied in advanced spectroscopic methods. In pulsed techniques such as pump-probe spectroscopy

or FSRS it is desirable to modulate the signal in the single pulse regime. While a well-controllable high frequency (kHz) amplitude modulation is easily achievable by the use of mechanical choppers, comparable wavelength modulation techniques need to be developed. Recently some steps towards this direction have been made (94, 108).

This paper describes a new method of fast wavelength modulation with easily controllable characteristics and its application in FSRS. It is based on the application of a chopper blade as a wavelength selector in the Fourier plane of a pulse-shaper (109). This is not an entirely new idea. To couple the chopper blade directly with the dispersive optical system was proposed earlier (94, 108), but the system presented in this paper represents an advantage over the previous one by its simplicity and the robustness of its performance. A crucial advantage is the possibility to modulate the wavelength with a smaller spectral shift than the actual spectral bandwidth. That makes it exceptionally suitable as an analog differentiator. It can be used solely as a spectrally modulated tunable optical band pass filter of the Rp pulses or as a source of wavelength modulated seed pulses for further amplification in a picosecond narrowband optical amplifier.

Methods

Femtosecond stimulated Raman spectroscopy

The system was pumped by a pulsed femtosecond Ti-Sapphire Legend amplifier (Coherent, Mountain View) with an average output of 3 W at 1 kHz, 45 fs pulse duration, centered at 800 nm. The Raman pump was prepared by direct filtering of 1W of the output through the proposed wavelength modulated spectral filter described in the Results section. The Rp intensity at the sample was 2 μJ. In the presented results, Δλ was ~0.5 nm for the β-carotene experiment and ~0.3 nm for the synthetic aryl carotenoid experiment. Another 1W of the laser output was used for pumping an optical parametric amplifier (OPA, Coherent OPERA SOLO) for creating tunable pump pulses; a small fraction was used for preparation of the probe pulse by supercontinuum generation in a 1 mm sapphire plate. The pump pulses were adjusted to a pulse energy of 500 nJ and wavelength of 530 nm. The excitation wavelength was deliberately chosen below the maximal absorption of the first vibration band. This allowed preparation of a homogenous distribution of excited molecules along the laser path in the highly concentrated sample. The probe pulses were filtered by a band pass filter for the remains of the pumping frequency (800 nm). The signal was recorded in the Stokes region through one spectral window in the near IR region (850-1000 nm). In the wavelength modulator, gratings with 1200 groves/mm blazed for 750 nm were used. In the spectrograph (Oriel MS127i™) 1/8 m, a 600 groves/mm 750 nm blazed grating was used. Detection was based on a PIN diode array (256 pixels) run byhome-built electronics and software. The sample was placed in a 1 mm quartz cuvette held by a shaker. All studied carotene molecules were dissolved to absorbance A = 2 at the excitation wavelength. β-

carotene was purchased from Fluka – Sigma Aldrich and dissolved in THF without further purification. The model carotenoid was prepared as described in [46] and dissolved in toluene. The data presented in figure 7 – 9 are based on 50 averages of single acquisition scans over the time delays in which 1000 shots were collected for each data point. The time file consisted of 92 data points leading to bulk experimental time of 4 hours for both experiments.

Data Analysis.

The data were globally analyzed with an R-based fitting package, TIMP.(2, 3) The femtosecond transient absorption data were globally analyzed using a kinetic model consisting of sequentially interconverting, evolution-associated difference spectra (EADS), i.e. $1\rightarrow2\rightarrow3\rightarrow...$ in which the arrows indicate successive mono-exponential decays of increasing time constant. The time constant can be regarded as the lifetime of each EADS.(2) The first EADS corresponds to the time-zero difference spectrum. This procedure allows clear visualization of the evolution of the excited and intermediate states of the system. It is important to note that a sequential analysis is mathematically equivalent to a parallel (sum-of-exponentials) analysis. The analysis program calculates both EADS and decay-associated difference spectra (DADS) and the time constants that follow from the analysis apply to both.(2) In general, the EADS may reflect mixtures of molecular states, such as may arise, for instance, from heterogeneous ground states or branching at any point in the molecular evolution.(19, 21, 27, 56-59)

Results

Wavelength modulation

The preparation of picosecond Rp pulses by filtering of broadband femtosecond pulses in a pulse shaper (zero dispersion pulse compressor ~ gratings or prisms are placed in the focus of a central telescope) with a slit instead of a phase mask, is a widely used method, despite its low efficiency (8, 104, 110). The wavelength modulation described in this paper originates from this approach. Figure 3 describes the key idea of the proposed method.

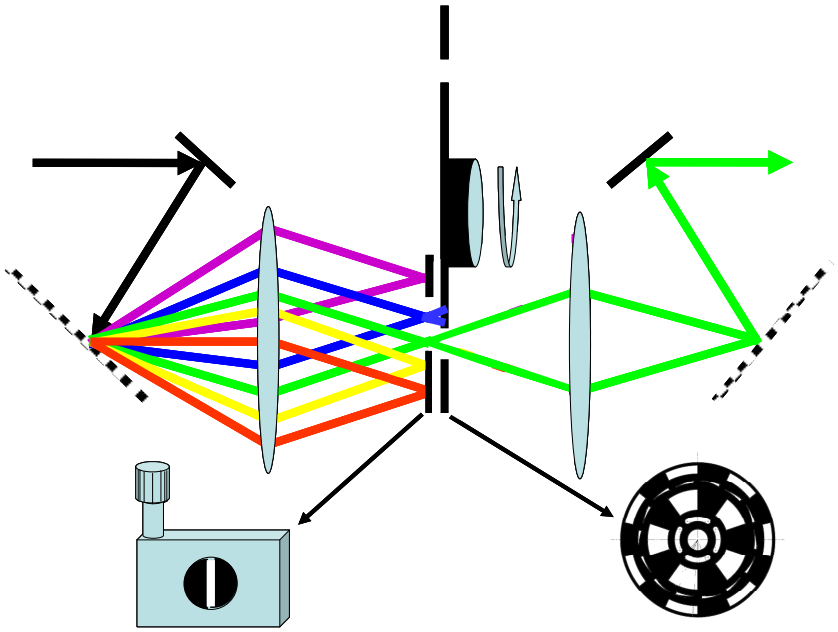

Figure 3. The principle of the wavelength modulator. A fixed adjustable slit is placed together with a custom chopper blade (with wedge shaped slits with periodically alternating orientation – see figure 4) in the focus (Fourier plane) of a pulse shaper. While the spectral content of the light blocked by the fixed slit stays constant, the fraction blocked by the chopper changes between the shots. On the picture, the blue wavelengths are blocked and green passes; for the next shot it would be the other way round. The simultaneous action of the slit and the blade results in behavior as a one slit interchanging its position in the Fourier plane in time. If both the slit and the chopper blade are placed within the Rayleigh length of the focus of the pulse shaper, the outcomming beamprofile is identical to the input profile This modulator can be used either directly as the Rp source producing Rp pulses by filtering of the broadband fs pulses or for wavelength modulation of narrowband Rp pulses.

The combination of a static adjustable slit and a specially designed chopper blade is placed into the focus of the pulse shaper. The vital principle of this device is that if the chopper blade and the slit are as close as possible to each other (within the Rayleigh length of the focus of the central telescope), they behave like a one slit oscillating in time. For ultrafast pulses the angular displacement of the blade during the time while the pulse propagates through the slit (maximally a few ps) can be neglected and when spherical lenses or mirrors are used, the dispersed wavelengths are focused in the Fourier plane to a small spot. The Fourier plane is then a long but a very narrow stripe. The combination of these effects causes that as long as the apertures in the chopper blade are periodically distributed over the circle and the chopper rotation is synchronized with the train of laser pulses the apertures in the chopper blade can have practically an arbitrary shape while still producing a stable selection of wavelengths. If those conditions are not satisfied a wavelength

modulation is still achieved but with significantly more complex output. This principle allows using of the wedge-shaped apertures in the chopper blade the way as it is described in figure 4

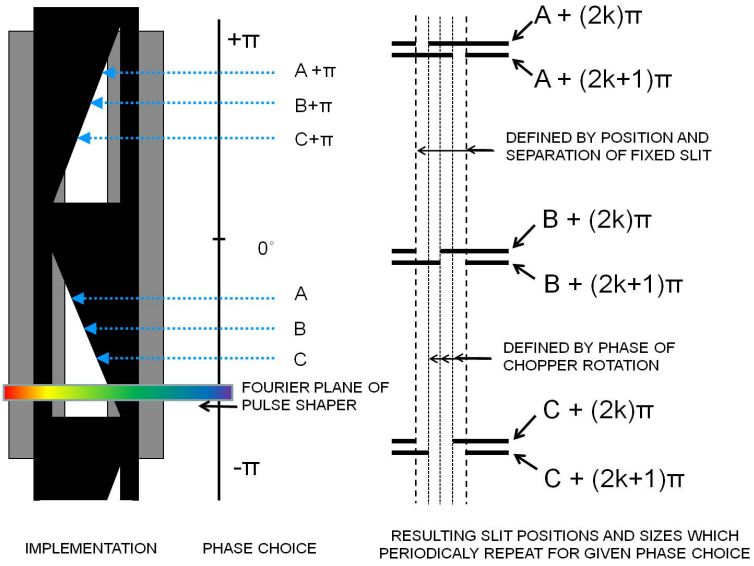

Figure 4 Schematic principle of the action of the modulator with alternating wedge-shaped slits. Dependent on the chopper phase (A, B, C) at the moment when the fs pulse hits the slit and the blade, a different part of the spectral distribution is filtered in the pulse shaper. The phase of the chopper rotation defines at which height the wedge is located when the pulse reaches the Fourier plane of the pulse shaper. If right- and left-handed wedges are periodically distributed along the chopper blade, the position of the aperture produced by the combined action of blade and slit keeps the diameter but changes its position in the Fourier plane of the pulse shaper. By setting the position and the diameter of the fixed slit, the phase of the chopper and the mutual position of the chopper and the fixed slit, the output of the modulator can be adjusted to produce two arbitrary Raman pump wavelengths, including two Raman pump wavelengths closely overlapping each other (C). For the difference signal Raman(λ) – Raman(λ+Δλ) the signal-to-noise increases with the separation (Δλ) but quality of the first derivative decreases (true derivative requires the limit where $\Delta\lambda \to 0$). The smooth adjustability of the system allows finding a compromise with regard to the studied system. Note that for clarity of the scheme, actual parameters as the tilt of the chopper slit or the height of the Fourier plane have been exaggerated compared to the actual physical situation, and the circularity of the chopper blade is neglected.

For the pulsed light synchronized with the chopper rotation, it behaves like a slit whose width can be very finely adjusted by the choice of the chopper phase. The proposed blade design (based on the alternating between the left and right oriented wedges) results in the behavior of two slits alternating their position from pulse to pulse. By adjusting the available degrees of freedom (position of the slit, width of the slit, position of the chopper, and the phase of the chopper rotation) it is possible to tune both “virtual slits” independently to the

precisely defined position and diameter (limiting is only the maximal diameter of the wedge-shaped slit). This includes the situation when the "virtual slits" partly overlap each other which cannot be achieved by the approach developed by Weigel and Ernsting (94). If the train of broadband femtosecond pulses is synchronized with the chopper and transmitted through this device, the output can be used as a wavelength-modulated Raman pump (Rp) source. The full tunability of the system allows achieving a compromise between the intensity, spectral narrowness and periodic spectral displacement of the pulses – essential for the extraction of the FSRS signal.

A standard approach of the FSRS experiment is to chop the Rp beam and record $\log(I_{[Rp\text{-}on]}/I_{[Rp\text{-}off]})$ (92). This approach results in the FSRS signal overlapped with a background as described in introduction. If instead the chopper-slit-pulse-shaper system described above is used the difference signal $\log(I_{[Rp(\lambda)]}/I_{[Rp(\lambda+\Delta\lambda)]})$ is recorded. The result is the acquisition of the first derivative of the FSRS signals almost devoid of a background, while the remaining background decreases as $\Delta\lambda$ approaches zero.

Background filtering - polynomials

Figure 5 (red line) show the FSRS difference signal recorded via the wavelength modulation approach described in the previous paragraph. While this may be not obvious from the data itself the resulting difference signal still suffers from a certain amount of remaining background. Figure 5-C and the figure 6-A2 demonstrate how the integration of the raw data accumulates the errors and results in a significant background. Various methods are available to deal with the problem of a non-vanishing background, as peak fitting (106, 107) or subtracting a polynomial fit from the raw data (figure 5A). As figure 2 shows, the first derivative of a narrow peak contains equal amounts of positive and negative amplitude. This can be used in polynomial processing of the recorded signal. When a polynomial or a sum of polynomials is directly fitted into the center of first derivative of the signal, integration of this curve yields a good background correction curve for the integrated signal. This approach is demonstrated in figure 5A. Experiments usually require polynomials of 5^{th} order or more to achieve a full background correction. This brings a certain risk of artifacts as the high order polynomials start to be badly conditioned, especially on the edges of the spectral window. Some extent of protection against this effect is fitting of several higher-order polynomials and using their average value as the background curve. This approach can be easily programmed into an automatic routine as it is relatively free of artifacts as long as the order of polynomials is kept significantly lower than the ratio between the spectral window and experimental resolution. That means that for a spectral window of 1000 cm^{-1} and resolution of 10 cm^{-1}, polynomials of order from 10 to 20 do not introduce significant risks of artifacts. The drawback of polynomial fitting is its low performance in removing

structures that steeply change its shape. This means that the polynomial treatment is very robust in removing the pump-dump-probe background, but relatively weak in removing coherent artifacts briefly described in the introduction as these artifacts may create a more steeply varying background than the background originating in transient absorption effects induced by the pulses.

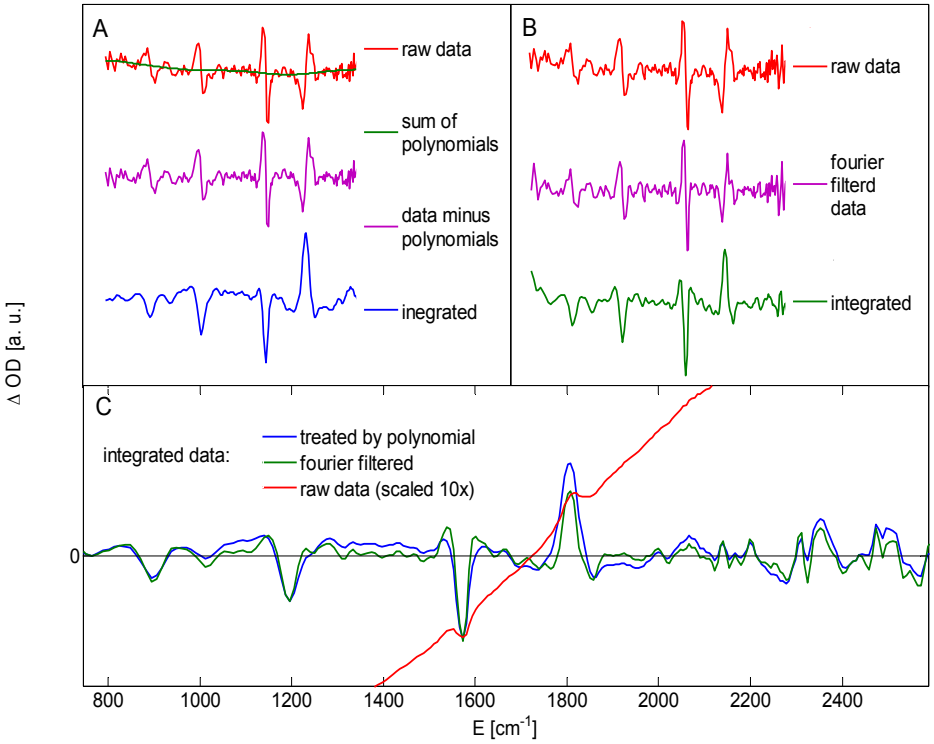

Figure 5

Comparison of alternative background correction procedures. (A) background correction through polynomial fitting; (B) background correction through Fourier filtering; (C) integrated FSRS spectrum through polynomial fitting (blue curve), Fourier filtering (green curve) and without background correction (red curve). Integration of the raw data usually leads to an offset in the integrated FSRS spectrum (panel C, red curve), its origin is treated in the main text. Fitting a polynomial or a sum of polynomials directly into the center of the first-derivative FSRS spectra (panel A) automatically finds the baseline, because the first derivative of symmetric peaks consists of equal contributions of positive and negative parts. A similarly reliable background suppression can be achieved by Fourier filtering (panel B). For details of the method see the text and Figure 6. Panel C shows that the polynomial approach is better in preserving of the peak-shapes but does not fully remove the offset even when high order polynomials are applied (see the blue line region from 1000 to 1500 cm^{-1}). The Fourier filtering method is more powerful in removing background and preserving baseline but can lead to minor artifacts in peak-shapes (see green line at 1570 cm^{-1}). This figure represents the data recorded on beta carotene at 1.7 ps after excitation. The polynomial treatment was done by fitting

series of polynomials of order from 5 to 13 and their subsequent averaging. This approach helps to compensate for artifacts associated with the fitting of high order polynomials. Fitting of higher-order polynomials leads to artifacts in peaks shapes similar to those induced by the Fourier filtering.

Background filtering – Fourier filter

To supplement the limitations of polynomial fitting, we developed an alternative method to remove the non-vanishing background from the differentiated signal. It is based on the principle that any vector of numbers can be transformed via a fast Fourier transform (FFT) into another vector which carries the same information but in a different representation. This alternative image is denoted as the Fourier image (FI) of the data. This space represents the original vector as a distribution of sinusoids of various phases and frequencies. It should be stressed that these frequencies are different quantities from the vibrational frequencies which are represented by thespectrally resolved FSRS signal. The filtering method is based on two principles: First as figure 6A1 and 6B1 show, the FI of the curve associated with the first derivative of Gaussian or Lorentzian peaks consists of a relatively small contribution from both very low and very high frequencies in Fourier space. Secondly, it employs the fact that the Fourier transform image of any function contains information about the shape of the function in the absolute value (modulus of complex number) of the frequency distribution while the position and sign of the shape is stored in the phase (imaginary and real part of the complex numbers) (111). By the combined action of these two principles, the broad band background can be removed from the raw wavelength modulated data by a Fourier filtering through the filter based on the first derivative of an ideal Gaussian peak. In terms of Raman spectra, it means that two peaks that are similar in shape but shifted in energy are composed of the same distribution of frequencies in Fourier space. Only different phases associated with this distribution result in different positions along the spectral axis where the sinusoids reconstruct back into the function when the inverse transform is applied. In this way, a Fast Fourier transform (FFT) can be used to enhance specific structures in the data regardless of their amplitude and position along the spectral axis. These principles are broadly used in various types of image processing and compression (112).

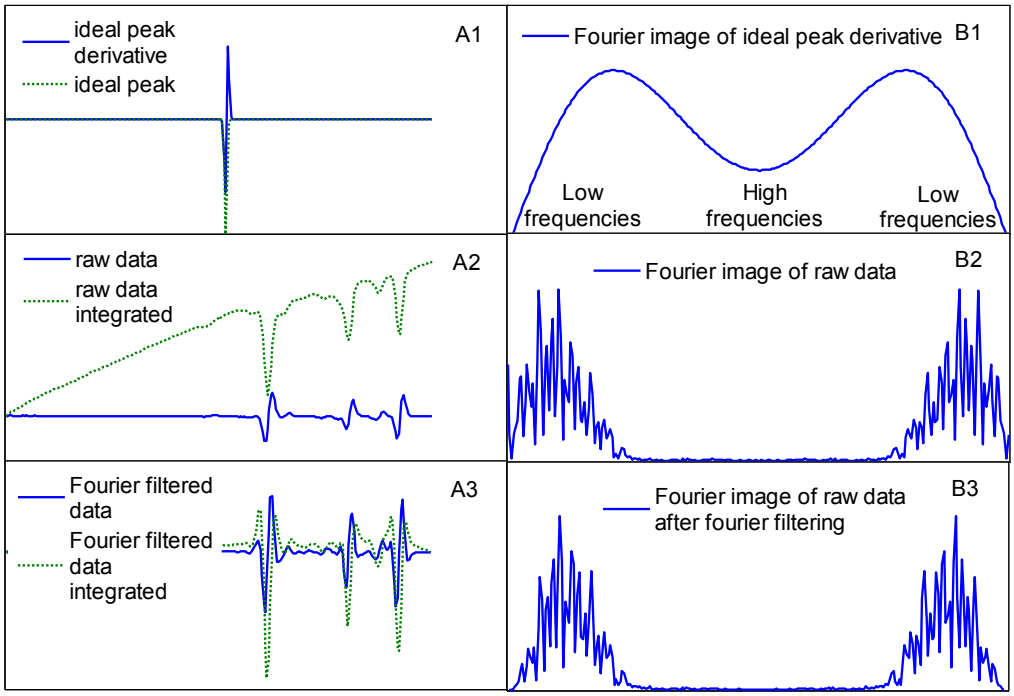

Figure 6. The Fourier filtering routine for background correction of FSRS spectra. The left part of the diagram (A) represents first-derivative and integrated FSRS signals, the right part represents absolute values of their corresponding Fourier (FFT) images (the full complex image is not represented for simplicity). The FFT image of the raw data (B2) is multiplied by the absolute value of ideal peak FFT image (B1). Note that especially the low frequencies on the edges of FFT image are suppressed. The resulting function (B3) is transformed back by the inverse Fourier transform to a first-derivative FSRS spectrum (A3). The data treated this way can be directly integrated. This procedure can lead to artifacts in the form of opposite oriented wings on the side of the peaks (panel A3, dashed line), which depends on the intensity of filtering which can be set by scaling of the B1 curve and on the difference between the bandwidth of the ideal peak that defines the filter and the actual peak shapes recorded by the experiment.

The method is described in figure 6 and involves the following steps: 1) The fast Fourier transform (FFT) image of the raw data is calculated (FI) 2) The FI of the raw data (figure 6 B2) is multiplied by the absolute value of FI of an ideal peak first derivative (figure 6 B1). The width and the shape of the ideal peak can be derived via recording the Rayleigh scattering from the actual Rp pulse. In this case the filter represents the actual instrument function of the set-up. 3) The inverse Fourier transform of treated data is performed. Step 2 suppresses the frequencies that are not associated with the desirable peak shape (figure 5 B3). The subsequent application of the inverse Fourier transform (step 3) results in the data where structures that cannot be constructed from the predefined shape (first derivative of the ideal Gaussian peak in our case) are suppressed (figure 5 A3). Although this method is not

entirely devoid of artifacts, its advantages are its continuity (no threshold is involved) and easy automatization as the FFT is numerically a very efficient procedure.

FSRS experiment on β-carotene

To test the FSRS set-up equipped with the Rp wavelength modulator we chose β-carotene, as the system currently most thoroughly investigated by the time resolved FSRS (8, 113). Figure 7-9 shows the same transient time-resolved FSRS data treated by the Fourier filter method described above plotted in various ways. Figure 7 displays the complete dataset in the form of a two-dimensional graph where the amplitude of the time-resolved Raman signal is visualized by a color scale.

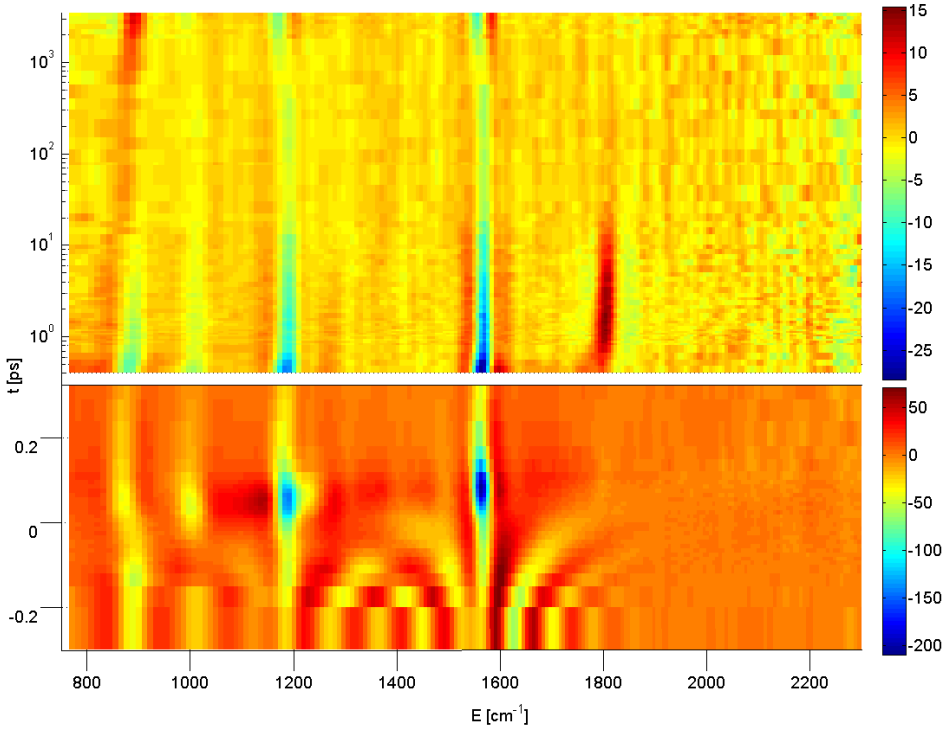

Figure 7 Time-resolved Fourier-filtered and integrated FSRS data recorded on β-carotene after excitation at 530nm on a linear-logarithmic timescale. Note the changes in the peak positions and bandwidths during the time evolution, emerging of the 1780 cm^{-1} peak after the first 500 fs and the rise of the long living structures on the ns timescale. The complicated pattern in the pre-zero signal is attributed to cross-correlation coherent artifact as all three pulses mix at this time point.

This way of data representation is useful for primary inspection of data and observation of peak shift effects. Fig 8 plots time-resolved FSRS spectra at selected time delays after the

excitation. This representation of the data presents a picture of the actual amplitudes and positions of the peaks.

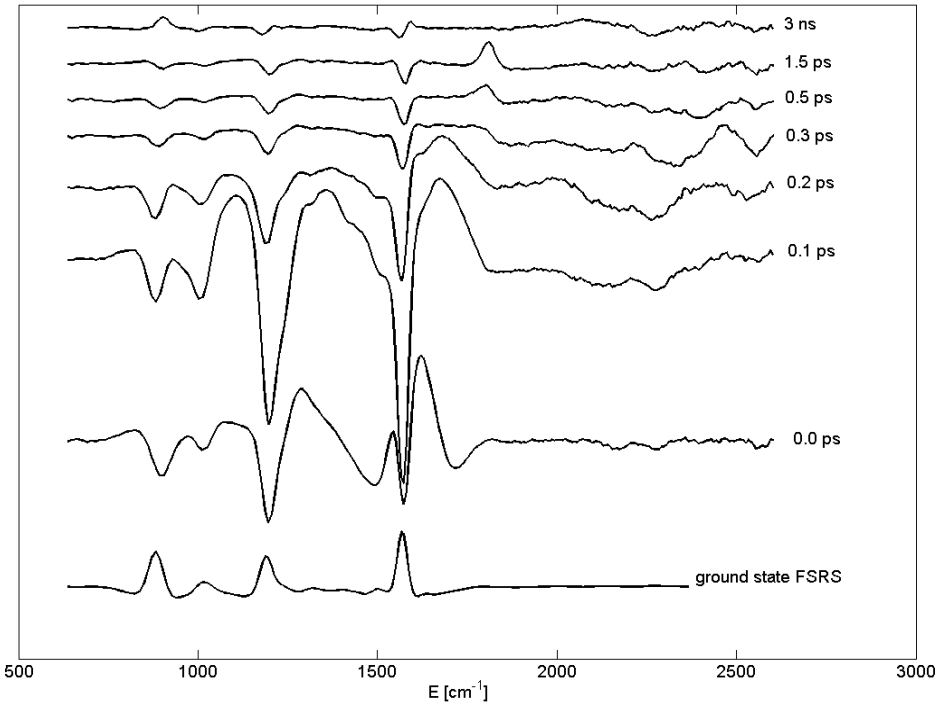

Figure 8. Selected FSRS spectra of the data on -carotene presented in fig 7. Note the evolution of the bleaching of the ground-state vibrations manifested as a negative signal and the complex spectral dynamics during the first 300 fs.

Figure 9 is the result of a global fitting analysis of the data. This approach allows one to link the peaks with specific time evolution constants. The result of this analysis facilitates assigning specific peaks to specific processes in the excited state dynamics during relaxation. As long as the fit is performed with a sufficient number of lifetimes to fully explain the dynamics, it represents the most valuable way of looking at the time resolved spectra (2) The discussion of the time-resolved spectra is dominantly based on results of this analysis. Figure 9 shows that the time evolution of the data required only 3 exponential decays to fit the data plus one final state with an infinite (on the timescale of this experiment) lifetime. This leads to 4 independently evolving spectral components. In terms of amplitude the first two largely dominate the data. The first component can be fitted with a lifetime of 200 fs which indicates that it is associated with the carotenoid S_2 (1^1B_u) state, usually observed with lifetimes in this range (67, 114-116). The amplitude of the S2 signal is markedly stronger compared to following spectral dynamics. This effect can be attributed to resonance enhancement as the S2 state of carotenoids have a strong absorption around 800

nm (105) where the FSRS experiment is performed. The second distinct structure decays with a lifetime of 8.1 ps which indicates that it is associated with the carotenoid S_1 state (117). In fig 9-10, we see that this structure does not directly rise with the decay of the previous 0.2 ps component but peaks around 1.5 ps, but no characteristic structure can be resolved in between the first 200 fs component and the 8.1ps component.

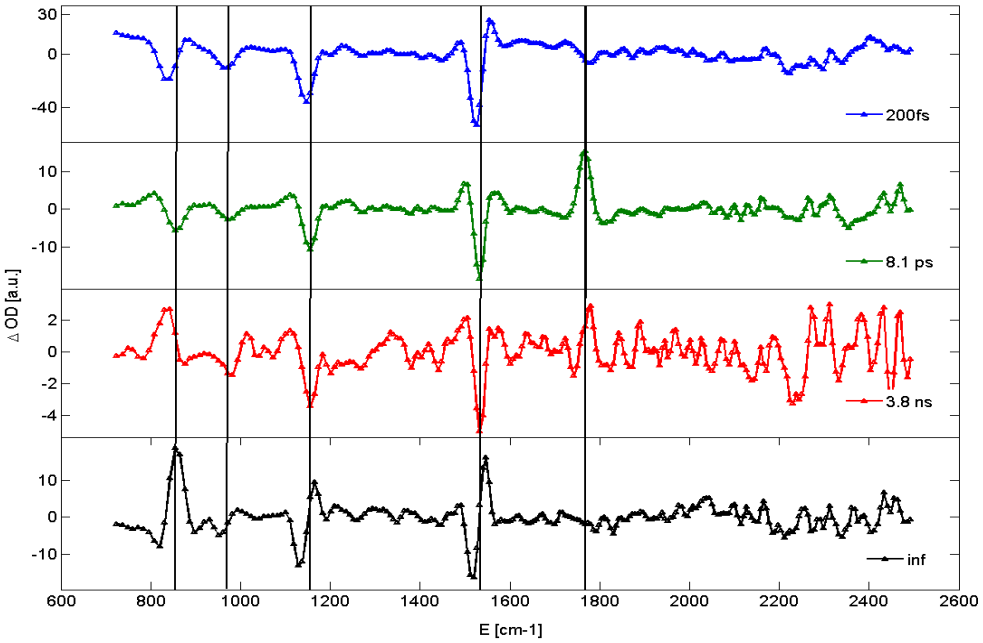

Figure 9. Evolution-associated difference spectra (EADS) that result from a global fitting analysis of the time-resolved FSRS data acquired on β-carotene. Four components were required to fit the data within the signal-to-noise ratio, with time constants indicated in the panels. The first 200 fs of the data were removed before the fitting due to nonexponential behavior, see figure 7-8 for the early time evolution. The fit shows that the long living features are not a direct product of the S1 state decay as they rise slowly with a time constant of 3.8ns.

The same trend of two step vibrational relaxation was observed also during former FSRS experiments on β-carotene(8, 102) . The features in both the S2 and the S1 components are in good agreement with previous results (8, 113, 118). Fig 9 shows that the first 200 fs component (S2) consists of three broad positive peaks with sharp negative valleys between them that we assign to the bleaching of the ground state vibrations. The S_1 signal (figure 9, 8.4 ps component) is also characterized by negative peaks (bleaching) at positions of the ground state signal, but this bleaching is significantly smaller in amplitude compared to that associated with the S_2 signal. Additionally, a new positive peak is observed around 1785 cm^{-1} which was originally observed in ps-Raman spectroscopy and attributed to the unusual C=C stretch vibrations allowed by the excitation of electrons in the carotenoid backbone (119,

120). This band was first observed in 1988 by Hashimoto and Koyama (120). Since that time there has been no progress in the assignment of this band, despite the fact that its precise spectral location varies markedly among the literature from 1760 cm^{-1} up to 1793 cm^{-1} (102, 118-120). A small positive peak can be observed around 1250 cm^{-1}. The bleaching peaks display signs of a temporal peak broadening and a slight peak shift (less than 5 cm^{-1}) towards the higher energies compared to ground state spectrum. All these features are in agreement with the previous results recorded by the FSRS or picosecond Raman spectroscopy (118-120).

A novel feature in the data presented here is recording of the bleaching of the ground state vibrations by FSRS. Implicitly this effect was already observed in the first FSRS experiments, but removed from the signal(8, 102). A recent FSRS study performed on flavin and also other studies demonstrated that transient FSRS spectra recorded in the Stokes region are dominated by the bleaching of the ground state vibrations (100, 121).

An additional novel observation is the presence of a long-living species in the FSRS spectra. Long living species were observed before in β-carotene in solution by pump-probe experiments (122). We observe a large amplitude and distinct spectral shift of peaks with this long living component. Our results are in agreement with picosecond Raman experiments that revealed significant peak shift on the scale of hundreds of ps, yet our data are different from the spectra assigned to the triplet state of carotenoids by the ps Raman experiments (119). The spectra recorded in our experiments also rise very slowly with lifetime fitted to 3.8 ns. This implies that these features are not a result of triplet formation but rather of conformational change. Recent observations of variability in ground state conformations or the presence of long living radicals are possible candidates (63, 122, 123).

Synthetic aryl carotenoid

To further test the described approach, we performed similar experiments on a synthetic carotenoid (28) containing an aryl group on one of its ends. Its structure is depicted in figure 10. The presence of conformational changes associated with the aryl carotenoids is documented, but pump-probe experiments revealed only a small effect on the excited state transient spectra (82). This makes this carotenoid a useful model for testing the performance of FSRS spectroscopy in revealing these changes. The same type of experiment as that with β-carotene was performed on this carotenoid but in a different solvent - toluene. The global fitting analysis resolved four components that clearly corresponded to those observed for β-carotene so their assignment is the same: 205 fs – S2, 8.2 ps – S1, 2.8 ns – rise of the long living species, and a long-living species. A novel observation is a 2 ps component extracted between the S2 and S1 states. Most probably, the 2 ps component is a more distinct manifestation of the phenomena observed also on β-carotene and mentioned

in the paragraph describing its transient behavior where the S1 state spectral features do not rise simultaneously with the decay of the S2 state, but rather with a certain delay. In the case of this carotenoid the delay appears to be even longer, which allows it to be included it in the fitted model. Nevertheless, this component does not contain any distinct structure except the bleach of ground state peaks. As the 2 ps lifetime is quite close to the time interval when a significant interaction between the Rp and Pu pulses is expected, the possibility arises that the origin of this component lies in the experiment itself. This idea is further supported by the fact that in this experiment a spectrally narrower Rp bandwidth than in the β-carotene experiment was applied. The Rp pulse was then naturally longer in duration and so the pump-probe delay interval during which Rp and Pu could interact with each other. Yet, only a deeper experimental and theoretical investigation of this phenomena can give a clear answer. Alternatively, a rich dynamics in the region of toluene Raman bands (124) at 784 cm^{-1}, 1002 cm^{-1}, 1028 cm^{-1}, 1208 cm^{-1}, 1378 cm^{-1}, and 1604 cm^{-1}, can be clearly observed in the data. Their interpretation is not the objective of this work, but the 2 ps component may partly originate in the response of the solvation envelope of toluene to the carotenoid excitation as this component almost entirely consists of the bleaching of the solvent bands and do not contain any new Raman peaks.

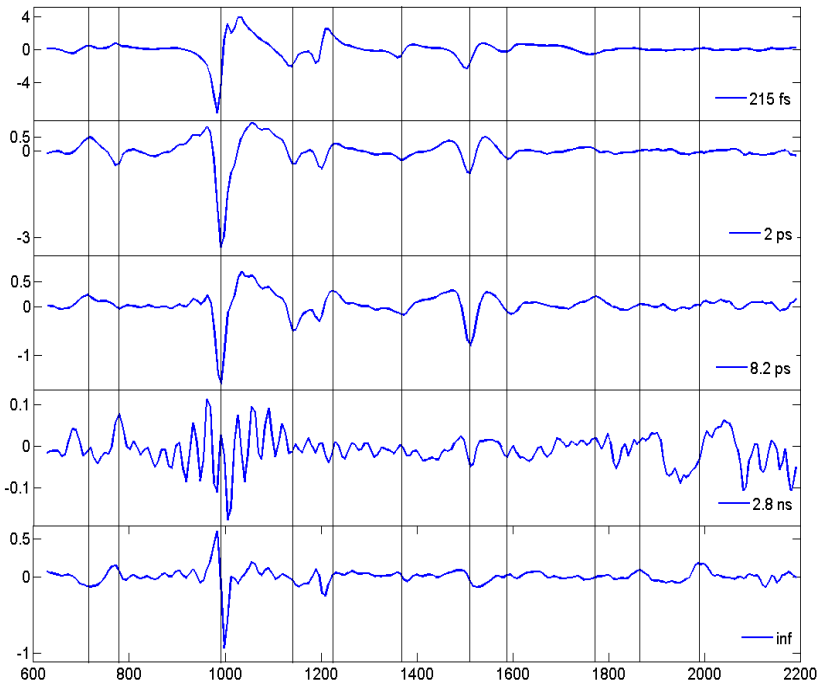

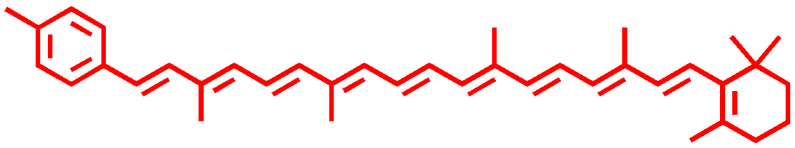

Figure 10. Evolution-associated difference spectra (EADS) that result from a global fitting analysis of the data recorded on the synthetic aryl carotenoid dissolved in toluene after excitation at 530 nm. Note the distinctly smaller amplitude of the 1780 cm^{-1} peak in the 8.2 ps component (S1 state) compared to that observed for the β-carotene in Fig. 7 - 9. The presence of a long living species was observed also for this carotenoid. Similar to the experiment with the β-carotene in THF, these long living components also display energy shifts in peaks associated with the solvent and the carotenoid.

The main difference between the behavior of the aryl carotenoid in toluene compared to that of β-carotene in THF is a significantly less pronounced S1-state associated peak at 1780 cm^{-1}. This can be judged by the comparison of 1240 cm^{-1} and 1780 cm^{-1} peak. While in both carotenoids the presence of these peaks was recorded, in β-carotene the former has an order of magnitude smaller amplitude than the latter. In the case of the aryl carotenoid they are comparable. Also the long-lived species recorded for this carotenoid differs from that of β-carotene. While in the β-carotene a general trend of shifting of peaks towards the higher energies is observed, in the case of the aryl carotenoid most of the Raman peaks seem to shift towards the lower energies which is closer to results observed by ps Raman experiments (118). It can be explained by the fact that toluene is a solvent more similar to the benzene used in those experiments. This holds both for peaks associated with the solvent and those originating in the sample.

Discussion

Wavelength modulation and background correction

The first issue requiring a further discussion is the use of the method including the Fourier filtering. The differentiating method itself proves to be very powerful in the reduction of the background associated with the time resolved FSRS. The non-coherent background (pump-probe signal and the background associated with the dumping and re-pumping excited states by Rp) were almost entirely removed. The direct recording of the difference signal also enhanced optimization of the experiment in the live acquisition mode. Yet, a small amount of the remaining background is always present. We assume that it originates partially from the finite precision of adjustment of the modulator but dominantly from the coherent nonresonant background briefly described in the introduction section. All FSRS experiments performed so far revealed that especially in the region during which the femtosecond Pu pulse still coherently interacts with the picosecond Rp pulse, a certain amount of the broadband background is produced. The temporal width of this region varies according to the experimental realization, but even under optimal conditions when the duration of Rp pulse is bandwidth-limited, the time bandwidth of the 5 cm^{-1} spectrally wide

Rp pulse is inevitably over 2 ps. This means that 1 ps after the excitation Pu pulse, it still significantly interacts with the Rp-Pr sequence used for generation of the FSRS signal. Unfortunately this is exactly the time interval where FSRS is superior to standard picosecond Raman spectroscopy by its time resolution (91, 125). Thus, the proposed approach leads to a great reduction of this effect but not to its entire elimination. Because the reduction of the background via wavelength modulation is based on the differences in sensitivity of various effects on a small change of Rp wavelength, it can be concluded that the coherent background consist of structures that are spectrally narrower than the transient absorption effects.

The reconstruction of the Raman spectra from the differentiated signal requires its integration. Numerical integration is practically a cumulative sum over the point samples through the spectrum. As figure 5C demonstrates, even minimal local deviations from the actual value are cumulating over the spectral region and lead to an offset. Because the action of polynomial fitting and subtraction is global, it is not that powerful in reduction of these contributions. Although this phenomenon is hard to quantify, thorough inspection of the blue curve in the figure 5C shows that even 12^{th} order polynomials do not produce a perfect baseline correction. The main advantage of Fourier filtering represented by the green curve in Figure 5C is that it does not induce any cumulative error to the data and minimizes artifacts based on the experimenter's subconscious input due to its fully automatic action. Nevertheless, in this simple form (as described above), it causes artifacts in the form of "after tones". They originate in the configuration when the measured peak is actually broader than the ideal peak used in designing the filter. The filter is designed for the specific bandwidth, naturally determined by the bandwidth of the Rp pulse. When the actually recorded peak has a broader bandwidth, the filter induces a deformation of the tails of the peak. In the integrated data this effect is manifested as small wings on both sides of the peaks with opposite amplitude as the main central peak (most distinct in the 1500 cm^{-1} peak - figure 8). This leads to a trade-off in the Fourier filtering. As the bandwidth of the designed filter becomes narrower, the reduction of background is more efficient but the peak shapes are becoming deformed. All these effects act only within the individual Raman bands so the spectral resolution of the experiment is still fully determined by the spectral widths of the Rp pulse.

The structures induced by the strong Fourier filtering can affect the shape of the peaks but do not directly preclude the possibility of observing effects as a peak shift or peak broadening. Yet, with increasing sensitivity and resolution of the FSRS experiments they can gain importance, specifically when the experimental resolution exceeds the intrinsic width of the vibrational bands, which is currently not common for FSRS experiments. These aspects count as a main disadvantage compared to the treating of the background by a polynomial or sum of polynomials, see figure 5 for a comparison of the Fourier filtering and polynomial approach. It has to be kept in mind that the same effect can be produced when high-order polynomials are used for the background fitting as can be seen in figure 5C. With

increasing order of the polynomial, the background curve starts to partially follow the narrow peaks. When this curve is subtracted from the data, similar wings on the tails of the peaks are formed. Generally, when a very narrow spectral region is investigated (e.g. a single specific peak), fitting a low-order polynomial is possible and may lead to reliable data as the fine structures are fully preserved. When a broader spectral region is studied and only the high order polynomials succeed in fitting of the background, the advantages of the Fourier filtering steeply rise. While the performance of the method demonstrated on peaks presented in this paper (first derivative of Gaussian peak) is already quite satisfying, the efficiency of Fourier filtering rises rapidly with the complexity of filtered peaks.

The first derivative of a Gaussian or Lorentzian peak can be considered as a very simple wavelet (112, 126). A wavelet is considered to be a structure which is a compromise between localization in the frequency and space domains. While a “narrow peak” is very localized in space and delocalized in frequency, a wavelet is less localized in space but also more localized in the frequency domain. In this light, another interpretation of the acquisition of the difference of two Raman experiments and subsequent Fourier filtering is that a basic type of wavelet-approach is applied. It uses the fact that the spectral shape of the Rp pulse has to be reflected in the Raman scattering induced by this pulse. By differential spectral modulation of Rp pulses (recording of a signal which is the difference of 2 signals stimulated by 2 different spectral masks) almost an arbitrary wavelet can be associated with the FSRS Raman peaks. This mechanism can be harnessed in a very effective filtering of the actual Raman signal from any kind of background. This suggests that a more complex wavelength modulation (realized for example by placing a spatial light modulating array into the pulse shaper (127)) leading to more complex wavelets, coupled to the subsequent Fourier filtering, can result in an even more automatic and robust FSRS experimental set-up.

Bleaching of the ground state signal

Our novel approach of data recording and processing leads to the manifestation of the ground state bleaching in the spectra as a negative signal. The phenomenon of decreasing of the ground state Raman signal after the excitation was observed already in the first time resolved FSRS experiments, but in this paper the data are presented in the raw transient form including the bleaching (8). We propose that this approach is the best option for presenting the time resolved FSRS data. In the field of time-resolved absorption spectroscopy, negative peaks are standard features in the data. Although addition of the ground state absorption species to the data is often useful to extract features solely associated with the excited state, the current convention is to interpret the data including the ground state bleaching (37). There are two main reasons for it. First, the fact that

ground state bleaching is also a source of information about the sample, and second that *ad hoc* addition of certain features (or even linear combination of features) to the data can lead to artifacts. The use of the "transient data" (data where the excited state signal minus full ground state signal is presented) greatly facilitates comparison of the different experiments or results of the same experiment acquired by different research groups. The former reason gains extra importance in FSRS, where the solvent signal is almost always recorded simultaneously with the signal from the studied molecules and varies through the excited state evolution. Following of the solvent originating features in the data, including the bleaching of ground state solvent peaks can contribute to the understanding of the dynamics that molecules undergo during the excitation and relaxation. This effect can be explained as changes in the solvation of the molecule reflecting the changes in the electronic structure of the studied molecule. Also, while the Raman peaks associated with the excited state can be quite broad, the sharp ground state bleaching features are a useful tool for distinguishing the lifetimes of involved excited states. Attempts to eliminate the bleaching can erase certain information present in the data or lead to misinterpretation. Additionally, in complex multichromophoric systems consisting of pigments with different Raman signatures connected through energy transfer, the bleaching of the ground state signal brings information on which of the chromophores are excited.

This can be demonstrated on the FSRS data recorded for the S_2 state of the β-carotene molecule. While a brief look on the data presented in this paper (figure 7) and the data presented in the past (8, 102) clearly suggests that the same type of phenomena was recorded, the interpretation differs. The signal of the S_2 (1^1B_u) state was previously described as 3 broad peaks (8). The transient signal presented in this paper implies a single broad delocalized peak overlapped with strong negative peaks of ground state vibrations bleaching which cut this broad peak in 3 parts. Figures 7-8 presenting directly the processed data also demonstrate that the rise and the decay of this positive structure do not fully coincide with the evolution of the ground state bleaching. While the positive structures practically entirely vanish within the first 250 fs, the ground state bleaching decaying with a lifetime 200 fs can be still recorded in the following few hundred femtoseconds. This suggests that additional effects apart from the Raman scattering from the S_2 excited state can be responsible for this broad positive structure, such as coherent processes mentioned in the introduction which do not lead to the narrowband Raman signal.

Long- living species

Another issue requiring a deeper discussion is the long-living spectral feature observed in -carotene and the synthetic aryl carotenoid. Analysis of the non-averaged data revealed that the amplitude of these features varied slightly during the experiment with an increasing

trend at prolonged data collection times, implying that they are probably associated with a fraction of molecules that underwent some type of photo-degradation or a photo-induced conformational change. The relative Raman amplitude of these species is almost an order of magnitude higher than the irreversible sample bleaching recorded by the linear absorption spectroscopy on the sample measured before and after the FSRS experiment. This suggests that they most probably represent some conformational changes associated with the excitation of the molecule or triplet formation rather than products of irreversible photo bleaching. However, under the assumption that the carotenoid triplet rises from carotenoid S2 or S1 state, the rise of triplet features on a nanosecond scale is not expected. Additionally, even though the spectra contain features that can be attributed to the carotenoid triplet (peaks around 960 cm^{-1}, 1005 cm^{-1}, 1190 cm^{-1}, 1260 cm^{-1}, 1340 cm^{-1}), in general they differ from previously published spectra of carotenoid triplets especially by the opposite direction of peak shift of the main carotenoids bands (1525 cm^{-1}, 1157 cm^{-1}, 1005 cm^{-1}) (118, 128). In our experiment, a shift towards higher frequencies was observed which is in contrast with the shift towards lower energies usually observed for carotenoid triplets. One of the most distinct features in those long living Raman spectra is a positive peak in the region where solvent (THF) gives a Raman signal (around 850 cm^{-1}). This observation suggests that these long living species are associated with a certain type of solvent rearrangement or a long living charge separation (122) which induces an increase in the solvent Raman signal compared to the ground state. Regardless of its origin, the existence of these species demonstrates the power of FSRS in revealing long-lifetime changes associated with the carotenoid excitation. Long-lived species were observed by pump-probe absorption spectroscopy but the transient absorption signature of these effects was rather weak (122). However, in comparing FSRS and pump-probe results it has to be kept in consideration that additional application of the Rp pulse can lead to formation of new species which are not formed during the standard Pump-probe experiment (where only Pu and Pr is applied) (101).

Conclusions

A wavelength modulator based on a custom-designed chopper blade and a slit placed in the Fourier plane of a pulse shaper was used to explicitly detect the first derivative of the femtosecond stimulated Raman signal. This resulted in an unprecedented reduction of the non-coherent background inherent to the FSRS experiment which cannot be fully filtered by the amplitude modulation of the Raman pulses. It also suggested that the wavelength modulation approach can be helpful in the reduction of the coherent background associated with the FSRS experiment (12). A Fourier filtering method for raw data treatment was proposed and applied employing the characteristic frequency trace of the first derivative of the Gaussian peaks in the Fourier image of the data. This approach is superior to polynomial or peak fitting in terms of reliability and speed but suffers from small artifacts which are not

present in former methods. A recording method of the transient FSRS signal was proposed where the direct difference between the ground state and excited state FSRS signal is presented. It essentially involves ground state bleaching as an essential and inseparable part of the time-resolved FSRS signal.

The performance of the approach was tested on the β-carotene molecule and a synthetic carotenoid terminated by an aryl group. The experiment confirmed results previously recorded on β-carotene (8, 102, 118-120) but suggested a different interpretation of some spectral features. The spectral signature of the S_2 state is interpreted as a broad peak overlapped with the bleaching of ground state vibrations. The high energy peak at 1780 cm^{-1} previously assigned to the special S_1 state (2^1A_g) C=C stretch of polyenes which is not present in the ground state Raman spectra of carotenoids has a significantly smaller amplitude in case of the synthetic aryl carotenoid.

The response of the solvent to the carotenoid excitation was recorded as additional information acquired by the FSRS experiment both in the form of the bleaching of the ground state vibration modes and the positive signal of a newly allowed vibrations. This was demonstrated by recording of a long living Raman component. This component is characterized by a slight energy shift of all Raman peaks including the solvent originating peaks. The effect is interpreted as a conformational change associated with the excitation or as an effect of the long living, probably charge-separated species. This signal may originate from altered or photo-damaged carotene molecules rather than from the dominant all-trans carotene species.

5. New light-harvesting roles of hot and forbidden carotenoid states in artificial photosynthetic constructs.

Miroslav Kloz, Smitha Pillai, Gerdenis Kodis, Devens Gust, Thomas A. Moore, Ana L. Moore Rienk van Grondelle, John T.M. Kennis

This work was published in: Chemical Science

Abstract:

We present results from fluorescence excitation and transient absorption spectroscopy on a series of artificial light harvesting dyads made up of a zinc phthalocyanine (Pc) covalently linked through a phenylamine to carotenoids with 8, 9, 10 or 11 conjugated double bonds, referred to as dyads 8 - 11. In dyad-10 and dyad-11, the energy transfer efficiency from the carotenoid S_2 state to Pc was shown to depend on the amount of excess vibrational energy in the carotenoid S_2 state. The carotenoid S_2 state lifetimes in dyad-9 and dyad-10 were several times shorter than those of model carotenoids in solution, indicating that energy transfer to Pc occurs from the S_2 state. The S_2 lifetimes lengthen with excess vibrational energy, and this correlates with a higher efficiency of energy transfer. We hypothesize that the higher energy transfer efficiency on excess vibrational excitation results either from a decreased internal conversion rate to lower-lying optically forbidden states, or from an enhanced coupling between vibrationally hot S_2 states with Pc. Ultrafast transient absorption studies revealed S* state features with unprecedented characteristics: In dyad-9, the S* state had a lifetime of only 100 fs and was observed to operate as the major mediator of energy transfer between Car and Pc. In contrast, the contribution to the energy transfer process by the optically forbidden S_1 state was negligible (5%). In dyad-10, neither S* nor S_1 appear to play a role in the energy transfer process to Pc, and all Car to Pc energy transfer proceeds through S_2. Many of the observed phenomena may be a consequence of the unusually strong electronic coupling between Car and Pc observed in the past on these particular systems.

Introduction

Energy transfer plays a crucial role in primary photosynthetic events. It allows not only maintenance of an optimal energy flow from the light harvesting complexes into reaction centers under low light conditions but also redirection of the energy towards domains with a high yield of energy dissipation in situations of excess light. It is a well-established fact that the genre of molecules known as carotenoids plays a crucial role in both functions (129-131). Indeed, with a gross primary photosynthetic production at a rate of 133 TW and 80-90% of the absorbed solar energy dissipated in regulatory processes mediated by carotenoids, an estimated 1 PW of global solar power flows through the conjugated π-electron system prior to its dissipation or photochemical conversion into biomass. While their role in light harvesting is in principle not irreplaceable, the photoprotective function of carotenoids seems to be essential for most of the thoroughly studied natural systems (132). The main feature in the molecular structure of carotenoids is a polyene chain of alternating carbon-carbon single and double bonds. Until recently, the electronic states involved in the LH function have been described by one high-lying optically allowed singlet excited state (S_2), and a low-lying, optically forbidden singlet excited state (S_1). Upon light absorption, the S_2 state relaxes to the S_1 state in 100–200 fs by internal conversion (IC), after which the S_1 state internally converts to the ground state on the picosecond time scale.(67) Excited state energy transfer (EET) from carotenoid to chlorophyll may proceed from both the S_2 and S_1 states (115, 133-141). Even though this basic two-level scheme of the carotenoid excited-state manifold showed itself useful in the interpretation of a wide range of carotenoid-involving phenomena, (142, 143) the results of recent experiments call for more extended models (19-21, 48, 50, 64, 66, 67, 144-148). The size of most carotenoids challenges the possibilities of some current *ab initio* quantum calculations (149, 150), and ultrafast spectroscopic experiments play a vital role in revealing the quantum characteristics of these molecules (67). Such experiments have clearly revealed that carotenoids present in natural systems display a wide range of excited state dynamics which are not present or, at best, difficult to definitively observe for carotenoids in solution (19, 20, 151).

Due to the enormous complexity of natural light-harvesting systems, which hampers a detailed understanding of their dynamics, significant experimental attention was recently focused on minimalistic systems such as carotenoid-porphyrin dyads and triads (52, 81, 152, 153). Experiments on these systems showed that they can mimic a wide range of processes that take place in natural light harvesting complexes with the benefit of a significantly lower uncertainty in interpretation of experimental results (26-28, 81, 154). The experimental attention directed to natural systems is increasingly more focused on the photoprotection aspects(44, 155-159) as the majority of energy in some natural systems appears to be dissipated in regulation processes (45, 160, 161). In contrast, in artificial systems there is an increasing demand for higher efficiency of energy absorption and the utilization of the

absorbed energy, as well as inclusion of photoprotection (162-166). This creates an increasing demand for a deeper understanding of hot energy transfer phenomena and regulation of energy transfer branching pathways. Of particular interest for both natural and artificial photosynthesis are the dynamics of the carotenoid hot S_2 (1^1B_u) state (142, 167, 168). This paper discusses phenomena recorded on phthalocyanine (Pc)-carotenoid (Car) dyads where a phenylamine moiety was used as a linker between the molecules (28). The chemical structure of these systems is depicted in Figure 1. Four different dyads were examined with 8 to 11 double-bonds in the carotenoid moiety. The dyads are denoted as dyad-8, dyad-9, dyad-10, and dyad-11 according to the conjugation length of the attached carotenoid. Ultrafast spectroscopic results indicate that population of a hot carotenoid S_2 (1^1B_u) state results in enhanced energy transfer to phthalocyanine and enhanced internal conversion to the carotenoid S* state as compared to the vibrationally relaxed S_2 state. Additionally, it was demonstrated that excess vibrational energy can influence the branching ratio between energy transfer to Pc and internal conversion to S_1 and S*

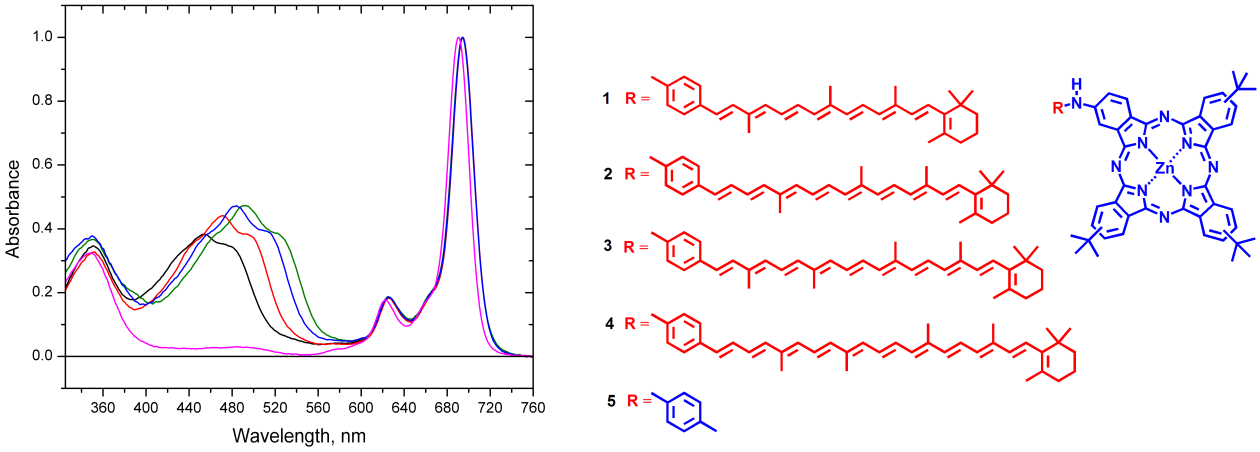

Figure 1: Chemical structures and absorption spectra of phthalocyanine–carotenoid dyads and absorption spectra of a model zinc phthalocyanine. Color key: dyad-8 black, dyad-9 red, dyad-10 blue, dyad-11 green, model phthalocyanine magenta.

Methods

Synthesis of compounds

Dyads-8 – 11 were synthesized as previously described.(28)

Spectroscopy

The fluorescence excitation spectra were recorded on a commercial fluorometer (FluoroLog Tau-3, HORIBA Jobin Yvon). The sample absorbance was adjusted to OD=0.03 cm^{-1} and measured in a fused silica cuvette of 1 cm pathlength. The spectral sensitivity of the reference detector and the minor fluorescence and scattering from the solvent were corrected by measuring blank and reference samples. Absorption spectra were recorded by an absorption spectrophotometer (Lambda-40, PerkinElmer). The time resolved studies were performed on a laboratory-built femtosecond transient absorption set-up.(158, 169) The system was pumped by a pulsed amplified femtosecond Ti:Sapphire laser system (Legend USP seeded by a Vitesse 800-2, Coherent, Mountain View) with an average output of 3.7 watts from 1 kHz, 45 fs pulses, centered at 800 nm. 1W of the output was used for pumping an optical parametric amplifier (OPA, OperA Solo, Coherent) for creating tunable pump pulses; a small fraction was used for preparation of the probe pulse by supercontinuum generation in a 2 mm sapphire plate. The pump energy was adjusted to 70 nJ with a spot size of 200 μm. Wavelengths of 515 and 530 nm were generated as a direct output of the OPA, and wavelengths of 415, 435, 469 and 475nm were prepared by second harmonic generation in a BBO crystal out of 830, 870, 938, and 950 nm pulses generated in the OPA. Both the pump and the probe pulses were filtered by interference filters for the remains of the Ti:sapphire fundamental beam (800 nm). In the spectrograph (Oriel MS127i™) 1/8m, a 300 groves/mm 500nm blazed grating was used. Detection was based on a PIN diode array (256 pixels) run by laboratory-built electronics and software including single shot statistics and noise discrimination. The signal was recorded in one 300 nm wide spectral window. The sample was placed in a 1 mm pathlength fused silica cuvette held by a shaker. All dyads were dissolved in toluene to an absorbance of 1 at the wavelength of maximal absorption of Pc. This approach resulted in an optimal absorbance of 0.4 in the region of carotenoid absorption. Free carotenoids were dissolved in THF to an absorbance of 0.4 at the maximum of their absorption. The presented data are based on 70 averages of single acquisition scans over the time delays in which 1000 laser pulse shots were collected for each data point. The dataset included 94 time points leading to a bulk experimental time of 3 hr for each experiment.

Data Analysis.

The data were globally analyzed with an R-based fitting package, TIMP.(2, 3) The femtosecond transient absorption data were globally analyzed using a kinetic model consisting of sequentially interconverting, evolution-associated difference spectra (EADS), i.e. $1\rightarrow2\rightarrow3\rightarrow...$ in which the arrows indicate successive mono-exponential decays of increasing time constant. The time constants can be regarded as the lifetimes of each EADS.(2) The first EADS corresponds to the time-zero difference spectrum. This procedure allows clear visualization of the evolution of the excited and intermediate states of the system. It is important to note that a sequential analysis is mathematically equivalent to a parallel (sum-of-exponentials) analysis. The analysis program calculates both EADS and decay-associated difference spectra (DADS) and the time constants that follow from the analysis apply to both.(2) In general, the EADS may reflect mixtures of molecular states, such as may arise, for instance, from heterogeneous ground states or branching at any point in the molecular evolution.(56, 59, 158, 170) Due to the problems associated with a precise asignment of lifetimes close to the instrument response function the shortest lifetimes were in all cases fixed to certain values estimated from a separate unrestricted fitting of the ultrafast lifetimes to facilitate the comparison of magnitudes of spectral features associated with those lifetimes for the different excitation wavelengths. This means that all data were initially fitted with full freedom and in all cases a sub-100 fs component was resolved. Because the applied time resolution was close to 100 fs, lifetimes shorter than this are strongly influenced by the instrument response function and coherent artifact which differed among the experiments as different pump pulses, generated by various approaches, were applied. In this context it is more robust for the mutual comparison of results to fit all early dynamics with a single lifetime close to the applied time resolution (100 fs). Figure 3 indicates which lifetimes were fitted and which lifetimes were fixed.

Results and discussion

Fluorescence excitation spectra – results and discussion

Figure 2 shows the fluorescence excitation spectra of dyads 8 – 11 (solid lines), along with their 1 - transmission (1 – T) spectra (dashed lines). The figure displays mismatches between the florescence excitation spectra detected in region of Pc emission (725 nm) and the (1 –T) spectra recorded from carotenoid–zinc phthalocyanine dyads linked by a phenylamine

group (see Figure 1 for the chemical structures). In general, the fluorescence excitation spectra lie well below the (1-T) spectra in the carotenoid region. While for dyad-8 and dyad-9 the shape of the (1 – T) curve is preserved in the fluorescence excitation spectra, but for dyad-10 and dyad-11 a significant loss of vibronic band amplitude with increasing wavelength is observed. The slopes of the curves suggest an increasing energy transfer efficiency from carotenoid to phthalocyanine as the excitation moves towards the higher vibronic bands of the carotenoid. Such a trend was observed on a similar system(60) but with almost negligible magnitude compared to the observation presented in Figure 2. Determination of absolute energy transfer quantum yields is not straightforward from these experiments: for these systems an efficient quenching of Pc excited state fluorescence was demonstrated (28). As a result, the fluorescence yield of the dyads is significantly lower than the fluorescence yield of the free Pc molecule (for dyad-11 and dyad-10 more than 20 times) (28). The consequence is that even a small amount of impurity in the form of free Pc molecules strongly contributes to the fluorescence excitation signal in the region of Pc absorption. Thus, differences in the amount of impurity among the samples can produce a variation in the absolute value of the energy transfer efficiency estimated from the excitation spectra normalized at the maximum of Pc absorption at 690 nm. As can be seen in Figure 2 the low and featureless absorption of Pc in the carotenoid absorption region from 400 nm to 550 nm will have a minimal effect on the shape of the excitation spectra in that region. This leads to the conclusion that the slope in the excitation spectra in the region of carotenoid absorption indicates a significant difference in energy transfer efficiency to Pc with respect to the amount of excess vibrational energy in the carotenoid S_2 state.

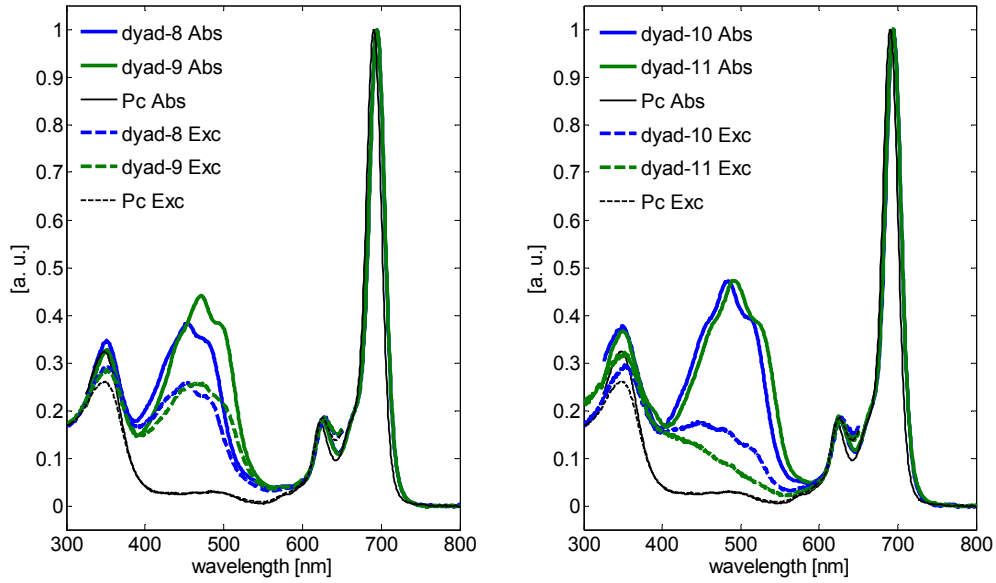

Figure 2 Normalized fluorescence excitation spectra (solid lines) and corresponding "1 – Transmission" spectra (dashed line) of phthalocyanine – carotenoid dyads dissolved in toluene. For dyad-8 and dyad-9 (blue and green curves in the left graph) the shape of the absorption curve is

preserved in fluorescence excitation spectra. For dyad-10 and dyad-11 (blue and green curve in the right graph) a significant loss of vibronic band intensity is observed. The slopes of the curves suggest increasing energy transfer efficiency from carotenoid to phthalocyanine as the excitation moves to higher vibronic bands of carotenoid.

Femtosecond transient absorption spectroscopy

For further examination of the energy transfer characteristics of the carotenoid S_2 state and possible effects of excess vibrational energy, time-resolved studies were applied. Because the excitation spectra and previous experiments on these systems (28) suggested only quantitative differences between dyads 8-9 and dyads 10-11, only dyad-9 and dyad-10 were fully investigated by femtosecond studies as representatives of these groups. For both dyads three excitation wavelengths were examined that were tuned to fit with the first, second, or fourth vibronic shoulders of carotenoid ground state electronic absorption. This included wavelengths in the region 400-470 nm, a region which is notorious for being difficult to prepare from the 800 nm pump pulses. The results are displayed in Figure 3 in the form of evolution-associated decay spectra (EADS). Five states plus one state associated with the coherent/cross phase modulation artifact for dyad-9 and six states plus the artifact for the dyad-10 were sufficient to reach an excellent agreement of the fit with the measured data. There are several qualitative differences between the behavior of dyad-9 and the dyad-10. The time evolutions following the excitation of the molecules at the various vibration bands of carotenoid S_0-S_2 transition are described in separate paragraphs.

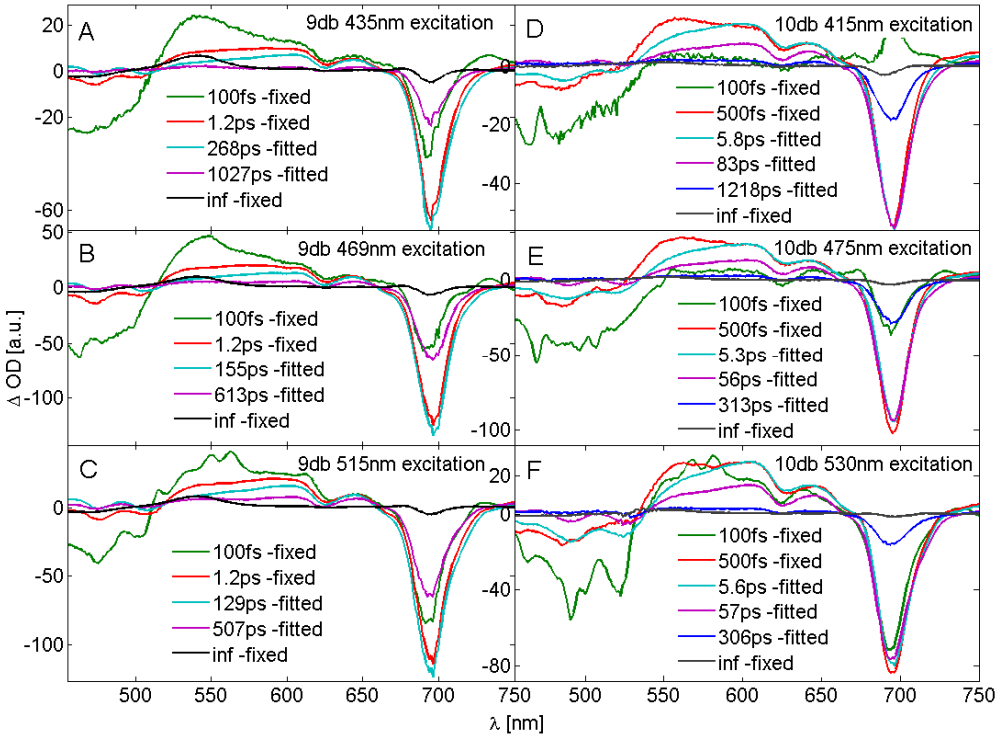

Figure 3 Evolution-associated difference spectra (EADS) fit of the time-resolved data performed on dyad-9 and dyad-10. The experiments were performed for three different excitation wavelengths corresponding to three vibronic maxima of the carotenoid moieties.

Dyad-10 results

Dyad-10 was investigated for excitation wavelengths 530, 475, and 415 nm. These wavelengths were chosen to approximately fit the first, second and fourth vibronic bands of the covalently bound carotenoid. All excitation wavelengths led to similar lifetimes in the spectral evolution but with notable variation in relative amplitudes of bands fitted within individual components. The results are plotted in Figure 3 D – F in the form of EADS. Six components were sufficient to fully fit the data. They can be characterized by their main decaying spectral features as: 1^{st} – S_2 (<100 fs), 2^{nd} – S* (500 fs), 3^{rd} – S_1 (5 ps), 4^{th} – Pc quenching 1 (55 ps), 5^{th} – Pc quenching 2 (310 ps), and 6^{th} – mixture of triplet states (>4 ns). The only feature obviously affected by the excitation wavelength is the relative magnitude of carotenoid S_1(S*) and Pc features in the 2^{nd} and 3^{rd} component. As will be explained below, this observation is consistent with the results from the fluorescence excitation spectra that relatively more energy is transferred to Pc when higher vibronic bands of the

carotenoid are excited. A detailed discussion of the assignment of these components and the excitation wavelength dependence is given in the following paragraph.

Dyad-10 discussion

The time evolution of Dyad-10 starts with a component having a lifetime and spectral signature associated with the carotenoid S_2 state (114, 171). When the lifetime is fixed to 100 fs, which is a typical lifetime for a carotenoid S_2 state,(67) there is a clear trend of increasing difficulty in resolving this component in the data acquired with longer excitation wavelengths. The interpretation is that for the shorter excitation wavelengths, the lifetime of S_2 is within the experimental time resolution, while for the longer excitation wavelengths, it is too short to be resolved. When excited at 415 nm, this component consists of carotenoid bleach with no other distinct structure in the visible spectral region which is typical of carotenoid S_2 states recorded in our systems (for reference see Figure 4 which depicts the time resolved spectral dynamics of the same carotenoids of the dyads free in solution, without attached Pc, structures shown in Supporting Information). In the case of the longest excitation wavelength (530 nm), the carotenoid S_2 features are already clearly mixed with the bleaching in the Pc region (695 nm) and absorption in the carotenoid S_1 region (around 600 nm). This shows that within the initial 100 fs, a significant fraction of energy was already transferred or internally converted to these acceptor states. These observations imply that excess vibrational energy in the S_2 state extends the S_2 lifetime.

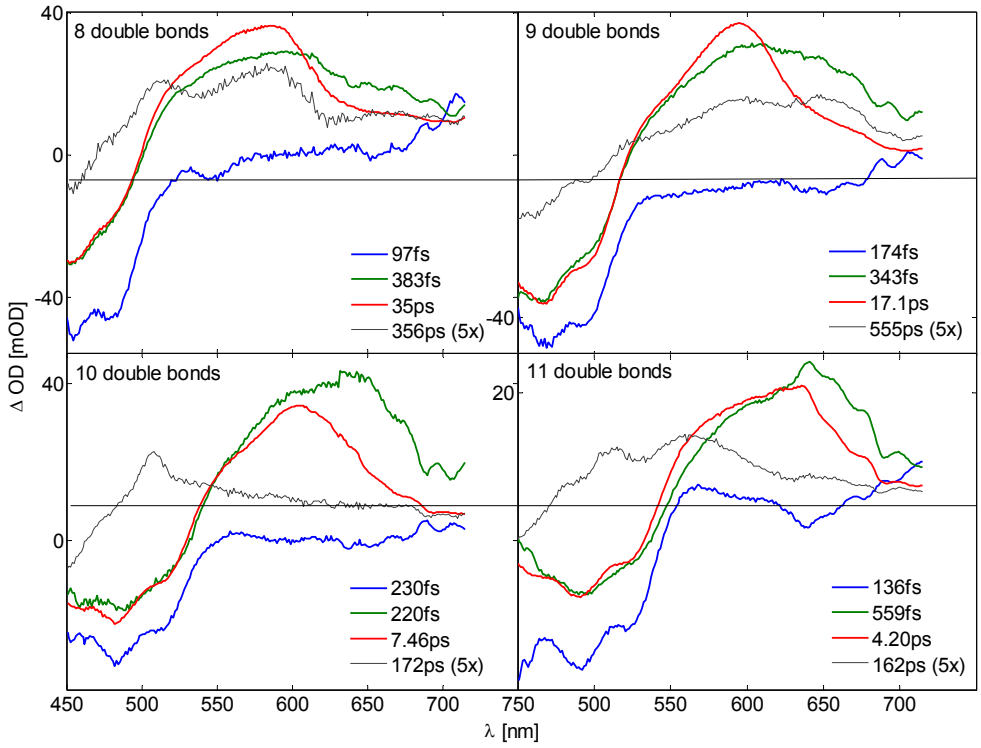

Figure 4 Evolution-associated difference spectra (EADS) fits of the time-resolved data performed on model aryl carotenoids car-8, car-9, car-10 and car-11 after excitation at 400 nm.

The S_2 state relaxes into a mixed population of Pc excited state (bleaching at 695 and 625 nm) (61), the carotenoid S* state (19, 20, 66, 172) (band at 550nm) and the carotenoid S_1 state (143, 173, 174) (a broad band spanning from 550 nm to almost 700 nm and centered around 600 nm) (67). These three products are formed for all excitation wavelengths. Interestingly, the relative amplitudes of their spectral signatures indicate that a relatively higher amount of S* and especially Pc excited state is populated when the higher vibrational levels of carotenoid S_2 are excited. In other words, relatively less S_1 is formed as compared to S* and excited Pc on excitation of the higher vibrational levels. The amplitude ratio of Pc bleach/stimulated emission at 690 nm and the S_1 absorption at 600 nm in the ~5 ps component is 4.2 :1 at 415 and 475 nm excitation, respectively, while it is 2.9 : 1 at 530 nm excitation. This observation implies that roughly 40% more S_1 is formed with 530 nm excitation as compared to the other excitation wavelengths (40% is an underestimation because the Pc excited-state absorption is ignored in this calculation). The differences in relative Pc, S_1 and S* populations do not arise from enhanced direct Pc excitation at the blue wavelengths, because at most only 9% direct Pc excitation takes place. We conclude that less internal conversion from the carotenoid S_2 state to S_1 takes place on excess vibrational excitation at 415 nm as compared to excitation in the lowest vibronic band at 530 nm.

The relaxation of the S* and S_1 states is subsequently recorded to occur with time constants around 0.5 ps and 5.5 ps respectively. Fitting revealed minor differences in those lifetimes among the different excitation wavelengths (ordered: 415 nm-475 nm-530 nm) S*: 550 fs-420 fs-390 fs and S_1: 5.9 ps-5.4 ps-5.4 ps. As mentioned, the S_1 and S* decays are not associated with an increase in Pc bleach nor any other spectral signature so further energy transfer from these states is not taking place and both excited states probably independently internally convert to the ground state.

The time evolution continues by two fitted components associated with quenching of Pc population via the carotenoid(28) and a final state that does not decay on the timescale of the experiment. In the case of 415 nm excitation, the two fitted components representing Pc quenching were 83 ps and 1218 ps. In case of 475 nm and 530 nm excitation, they were 56 ps, 313 ps and 57 ps, 306 ps respectively. The fact that the constants are almost identical for 475 nm and 530 nm excitation while significantly higher for 415nm excitation suggests that a conformational inhomogeneity exists in the sample, and that less-quenched conformers are preferentially excited at the blue edge of the carotenoid S_2 absorption. The nondecaying EADS of Fig. 3 D – F exhibit an overall very low amplitude and can be assigned to triplet states.(60)

Our observation of, on one hand, a longer carotenoid S_2 lifetime at excess vibrational excitation at 415 nm as compared to 530 nm excitation (Fig. 3 D – F) and, on the other hand, a higher yield of energy transfer to Pc on excess vibration excitation (Fig. 2) is a somewhat counterintuitive result because often higher energy transfer yields are associated with higher energy transfer rates and shorter donor state lifetimes. In the particular case of dyad-10, this apparent contradiction is explained by the fact that the carotenoid S_2 lifetime is not only determined by the energy transfer rate to Pc, but also by the IC rates to S_1 and S*. We hypothesize that vibrational relaxation of the S_2 state has to precede efficient IC from S_2 to S_1, thus slowing down the IC rate at excess vibrational excitation, while energy transfer from carotenoid S_2 to Pc can take place also from the hot S_2 states. Because S_1 does not transfer energy to Pc, the overall result is both a longer S_2 lifetime and a higher energy transfer efficiency to Pc. The previous observation of a longer S_2 lifetime on excess vibrational excitation in carotenoids in solution supports this hypothesis.(175, 176)

In an alternative model, the hot S_2 state may be more closely coupled with the Pc excited state than with the carotenoid S_1 state. In this case preparation of a hot S_2 state results in a higher amount of excitation transferred to Pc. An enhanced coupling of the carotenoid hot S_2 state with Pc may involve higher Pc-carotenoid exciton states, (28) and might be initially created as a coherently coupled system. Although this model explains the higher energy transfer yield to Pc upon excess vibrational excitation, it does not necessarily predict a longer S_2 lifetime under such excitation conditions. However, because we did not accurately record the S_2 lifetimes due to insufficient time resolution, this model cannot be excluded.

These results are summarized in Figure 5B where the pathways favored by excess vibrational energy are represented by thick blue arrows. The timescale at which the branching takes place appears to be close to or beyond the experimental time resolution so it is not possible to make a quantitative assessment of the dynamics. Yet, the observed variation in relative populations associated with S_2 energy acceptor states clearly shows that the branching ratios are significantly controlled by the amount of vibrational energy in the carotenoid S_2 state.

Dyad-9 results

Dyad-9 was investigated with excitation wavelengths 515, 469, and 435 nm. These wavelengths were chosen to approximately correspond to the first, second and third vibronic bands of the covalently bound carotenoid. All excitation wavelengths led to qualitatively the same behavior with similar lifetimes, but with notable variation in relative amplitudes of bands fitted within the first component. The variation in fitted lifetimes was more distinct than for dyad-10. The results are plotted in Figure 3 A – C in the form of EADS. Five components were sufficient to fully fit the data.

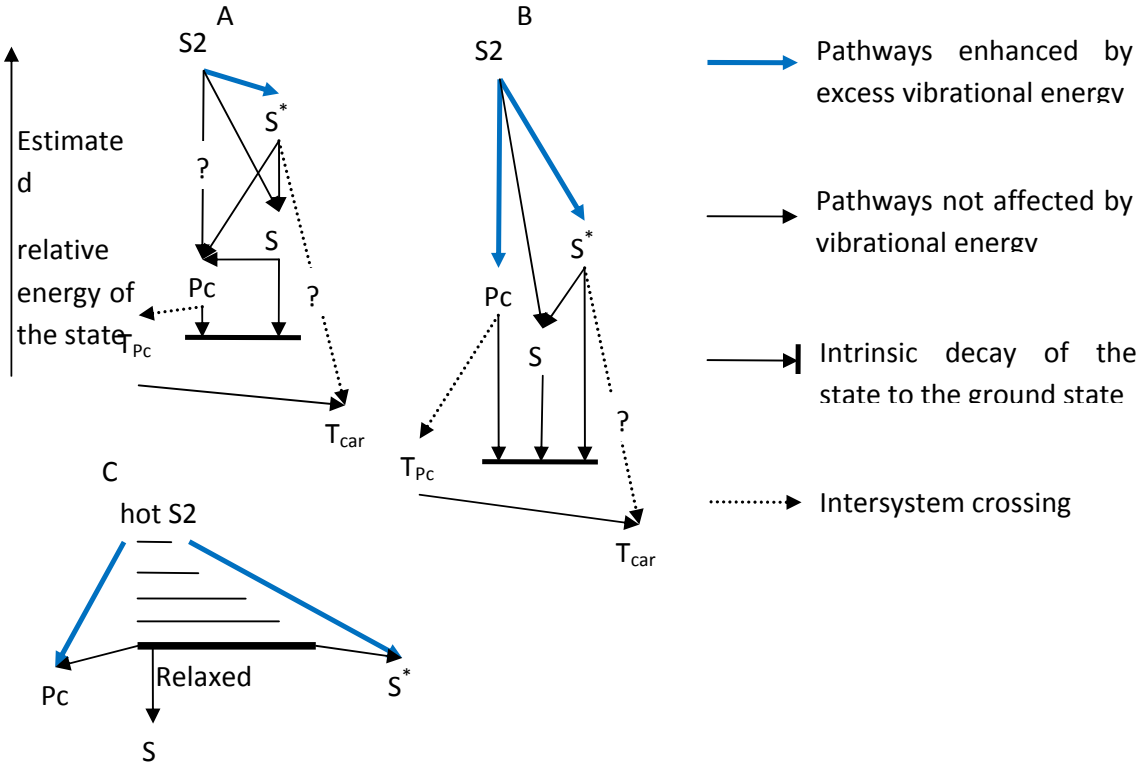

Figure.5 Energy transfer schemes. For dyad-9 (A) both S_1 and S* states transfer the energy to Pc, so the variation in branching ratios does not affect the final energy transfer efficiency. For dyad-10 (B), variation in branching ratios directly affect the amount of energy transfer to yield Pc excitation. (C) Illustration of how Pc and S* become relatively more populated than S_1 from a hot S_2 state compared to a carotenoid S_1 state. Either the hot S_2 state has enhanced coupling to these states, or internal conversion to the S_1 is preceded by vibrational relaxation of S_2.

They can be characterized by their main decaying spectral features as: 1^{st} – S_2/S* (< 100fs), 2^{nd} – S_1 (1.2 ps), 3^{rd} – Pc quenching 1 (~150 ps), 4^{th} – Pc quenching 2 (~500 ps), 5^{th} – triplet states (>4 ns). For dyad-9 it was not possible to resolve the S_2 state lifetime as the spectral shape of the 1^{st} EADS closely resembles a mixture of the carotenoid S* state with an absorption feature that is blue-shifted with respect to that of the S1 state, and the Pc excited state. We conclude that the carotenoid S_2 lifetime is extremely short in dyad-9. The relative magnitude of S* features in the 1^{st} component appear to be affected by excitation wavelength (about 30% more for 435 nm than for 515 nm excitation), although this observation should be interpreted with some caution because the associated time constant is close to the IRF, and hence its amplitude is to some degree uncertain. In contrast to the observations made on dyad-10, in dyad-9 both carotenoid S* and S_1 states act as energy donors to Pc. This is clearly manifested by the simultaneous decay of S* features with the rise of Pc features as the time evolution moves from 1^{st} to 2^{nd} component, and similarly S_1 decay and Pc rise between the 2^{nd} and 3^{rd} components, albeit with low amplitude. These observations confirm the results from the excitation spectra that no significant variation of carotenoid S_2 – Pc energy transfer efficiency takes place in response to excess vibrational energy in the carotenoid. Yet, the variation in the amplitude of the S* state signatures in the initial component among the different excitation wavelengths suggests that in this case the alterations in the carotenoid S_2 state branching also take place. The overall lack of excitation energy dependence in comparison to dyad-10 appears to be merely the consequence of all initial branches leading finally to Pc. This means that for dyad-9, excess-vibrational energy-dependent ultrafast branching may take place but it is masked by the ensuing energy transfer processes. Thus, these observations indicate that in dyad-9, the energy transfer efficiency from carotenoid to Pc is close to unity. These observations are summarized by the scheme A in Figure 5.

Dyad-9 discussion

The time evolution of dyad-9 excited in the carotenoid region starts with the component with a lifetime about 100 fs, which already displays all the signatures of S_2 state products as observed in dyad-10: S*, S_1 and the Pc excited state. This component is characterized by a high amplitude of S* state signatures (S*/S1 ratio is about three times higher than in the dyad-10). To our best knowledge such a high amount of S* compared to S_1 maximal

amplitude was never observed before. The following component displays very little or no S* state signatures at all, but a strong increase in Pc excited state signatures, especially the ground state bleaching around 695 nm. This means that the initial branching from the S_2 state, which happens within the time resolution, is followed by rapid (around or sub 100 fs) energy transfer from S* to Pc. With the amplitude ratios of Pc bleach and S* absorption in the first EADS, we estimate that roughly half of the initially excited S_2 states internally convert to S* and the energy of the other half is transferred to Pc. To our best knowledge, this observation represents the shortest S* state lifetime so far and the first documented case where S* acts as a strongly dominant energy donor; usually S* has only a minor role in light harvesting.(21, 27, 60, 177) The 100 fs lifetime of the S* state in dyad-9 implies exceptionally strong coupling with the Pc excited state and close to 100% efficiency of energy transfer from S* to Pc. The second (S_1) component has a lifetime of 1.2 ps, has overall low amplitude, and shows very little or no S* character but a clear presence of S_1 state features with amplitudes slightly varying among the examined excitation wavelengths, being highest for the 515 nm excitation. Because its 1.2 ps decay is associated with an increase in Pc bleaching, this component is assigned to energy transfer from carotenoid S_1 to Pc. The increase in the Pc bleaching associated with this component accounts only for a small fraction of the bulk energy transferred to Pc (about 5%). This means that in dyad-9, the carotenoid S_1 state plays only a marginal role in the energy transfer from carotenoid to Pc.

The following two components, assigned to quenching of Pc excitation via the carotenoid, display the same small trend of increasing lifetimes with shorter excitation wavelength as observed for dyad-10, which are probably related to conformational heterogeneity in the sample. Fitted lifetimes are: 268 and 1027 ps for 435 nm excitation; 155 and 613 ps for 469 nm excitation; 129 and 507 ps for 515 nm excitation. The assignment of these components to quenching of Pc excited states via the carotenoid is supported by the carotenoid ground state bleaching structures in the EADS. These clearly coincide with the carotenoid bleaching of the 1.2 ps S_1-component, in which the presence of carotenoid S_1 state is strongly manifested by its absorption band. As with dyad-10, these quenching processes were described in detail in a previous paper (28).

A small variation in triplet yield among the excitation wavelengths is observed for dyad-9, which is consistent with the longer Pc singlet excited-state lifetimes observed for short-wavelength excitation. Carotenoid triplets may be populated directly from carotenoid excited states through singlet fission(19) or by triplet-triplet energy transfer from the Pc triplet. For dyad-9 the latter process is the dominant source of carotenoid triplet population as indicated by the strong rise of the carotenoid triplet signature around 540 nm between the 4^{th} component (last component with fitted lifetime) and the 5^{th} (final) component. Because the Pc triplet state is not observed in the spectral evolution, triplet-triplet transfer between Pc and carotenoid is expected on a timescale comparable to or shorter than the Pc

singlet excited state lifetime, as observed previously for other carotenoid-Pc dyads and triads.(27, 60)

Model carotenoids – results

Model carotenoids for those used in the dyads possessing from 8 to 11 double bonds were dissolved in THF and examined by femtosecond pump-probe spectroscopy. The model carotenoids are denoted as car-8, car-9, car-10, and car-11 according to the number of double bonds in their conjugated backbones. Their synthesis and chemical structures are shown in Supporting Information. The results are presented in Figure 4. Excitation was tuned to 400 nm to investigate theeffects when the higher vibronic bands are excited. In all cases, transient spectra could be fitted by 4 exponential decays to obtain excellent agreement with the data. Except the last component, their interpretation is straightforward and identical for all lengths of carotenoids: 1^{st} S_2 state, 2^{nd} hot S_1 state, 3^{rd} S_1 state. Their lifetimes are: for car-8: 97 fs, 380 fs, 35 ps and 356 ps; car-9: 174 fs, 340fs, 17 ps, 555 ps; car-10: 230 fs, 220 fs, 7.5 ps, 172 ps; car-11: 136fs, 560 fs, 4.2 ps, 162 ps.

Model carotenoids – discussion

The experiments performed on model carotenoids represent important references for the data recorded on the dyads. They demonstrate that the model carotenoid S_2 decay can be clearly observed even if the S_2 lifetime is close to 100 fs. The measurements confirm the known trend of decreasing of S_1 state lifetime with the length of the carotenoid (178). The experiments largely follow the observed and predicted trend that the S_2 lifetime should be longest around car-9 (171), even though the longest lifetime was observed for car-10. The experiments provide evidence that the carotenoid S_2 lifetime is significantly shortened in dyads, in case of dyad-9 to a point where the S_2 spectral signature cannot be recovered through deconvolution with the IRF. They also show that the hot S_1 state absorbs on the red side of the S_1 spectra,(68, 69) which implies that the features assigned to the S* state in the dyads cannot be due to hot S_1. As the intrinsic S_1 lifetime of the model carotenoid with 9 double bonds was measured to be 17 ps, the lifetime of S_1 to Pc energy transfer recorded with the time constant of 1.2 ps for dyad-9 is most probably due to efficient energy transfer to Pc, although significantly more energy flows to Pc via the S* state. Car-10 shows as S_1 lifetime of 7.5 ps, which is slightly longer than that of the carotenoid in dyad-10 (5.5 ps), suggesting that some energy transfer to Pc might occur. However, the transient spectra from dyad-10 do not record this small yield (Fig. 3D – F). In all model carotenoids, a

relatively long-lived component of 160 – 550 ps at low amplitude is observed. The observation of states that are longer-lived than S_1 for carotenoids in solution is usually ascribed to population of S*.(19, 20) The longest lifetime EADS of car-8, car-10 and car-11 seem to broadly resemble the spectral signature expected for S*, with an induced absorption that is blue-shifted with respect to that of S_1.

Conclusions

The investigation of fluorescence excitation spectra and femtosecond transient absorption experiments on covalently linked carotenoid-Pc dyads indicates a dependence of the efficiency of energy transfer from the carotenoid S_2 state to Pc on the excitation wavelength. The observations are interpreted as arising from differences in the branching ratios between decay pathways of the carotenoid S_2 state leading to carotenoid S_1, carotenoid S*, and energy transfer yielding Pc excitation. When the higher vibronic bands of carotenoid are excited, the S* and energy transfer to Pc branches appear to be favored. For dyad-9 and probably also for dyad-8, this effect may be masked in the fluorescence excitation spectra by ensuing efficient energy transfer from S* and S_1 to Pc. In dyad-10 and probably also in dyad-11, both S* and S_1 states internally convert to the ground state so the effect is directly reflected in the efficiency of energy transfer to Pc and manifests itself in the fluorescence excitation spectra as an excitation wavelength-dependent energy transfer.

Figure 5C displays the most natural hypothesis about the branching which can be derived from the observations on dyad-9 and dyad-10. It is posited that vibrational relaxation of the S_2 state has to precede efficient conversion of S_2 to S_1, while the energy transfer from carotenoid S_2 to Pc can take place also from the hot S_2 state. Alternatively, the hot S_2 state may be more closely coupled with the Pc excited state and the carotenoid S* state than with the carotenoid S_1 state. In this case a preparation of hotter S_2 state results in a higher amount of excitation transferred to S* and Pc. Both of these hypotheses can explain the higher amount of S* and Pc excitation observed after preparation of a hot carotenoid S_2 state.

The S* state prominently appears in all dyads, but its role is distinctly different between dyad-9 and dyad-10. In dyad-10, an S* lifetime of 500 fs was recorded with no energy transfer to Pc. In contrast, dyad-9 showed an unprecedently large S* population of roughly 50% of initially excited S_2, which decays unusually fast (~100 fs) with associated efficient energy transfer to Pc. In essence, S* behaves similarly to the carotenoid S_2 state with regard to timescale, energy transfer and transient population. This result is very unusual given that S* is considered an optically forbidden electronic state such as S_1 (A_g^-) or B_u^- (19, 20, 64). In the molecules studied in this paper, an unusual carotenoid S_1 – Pc exciton-like behavior

was previously observed(28). The results described in this paper can be a consequence of the same peculiar conditions of the carotenoid in these systems: possibly a conformation of the carotenoid backbone, spatial proximity of Car and Pc, or both of these phenomena, that confer strong electronic coupling between the carotenoid S* state and Pc. Alternatively, an unusually strong mixing between the carotenoid S_2 and S* states may occur in this case, as proposed for S_2 and S_1 to explain the energy transfer phenomena from the S_1 state to chlorophyll.(134, 179)

6. Correction for the time dependent inner filter effect caused by transient absorption in femtosecond stimulated Raman experiment

Miroslav Kloz, Rienk van Grondelle, John T.M. Kennis

This work was published in: Chemical Physics Letters

Abstract

Femtosecond stimulated Raman spectroscopy (FSRS) is a promising multiple-pulse ultrafast spectroscopic tool whose simplest form utilizes an actinic pump, a Raman pump and a continuum probe. Here, we report that the transient absorption generated by the actinic pulse modulates the overall magnitude of the Raman signals of the photoactivated sample. As a consequence, the traditional transient FSRS signal is distorted by artifacts, which were observed in the past but left without interpretation. We propose a simple model to calculate the correct transient FSRS signals from the knowledge of transient absorption signal. The model was verified by application to experimental data.

Introduction

Femtosecond Stimulated Raman Scattering spectroscopy (FSRS) is a powerful tool for recording of molecular vibrations as a function of time (91, 92, 180). Recently even the possibility of FSRS 2D experiments was studied (14) in order to explore the vibrational couplings in complex systems. Despite its already established potential (11, 97, 98) and quite thoroughly investigated theory (10, 12, 16, 91, 181, 182) the practical aspects of FSRS experiment are still under development (9, 183, 184). One of the major experimental problems associated with realization of time-resolved FSRS is the unavoidable generation of pump-probe and pump-dump-probe signals and ground-state FSRS signal simultaneously with the desirable time resolved FSRS signal. While the separation of narrow Raman lines from the broadband transient pump-(dump)-probe envelope was recently greatly improved by wavelength modulation of Rp pulses (9, 100, 185), an intrinsic effect of this background on the magnitude of time resolved Raman signal was to our best knowledge never explicitly considered. In consequence, the extracted transient FSRS signal was usually dominated by bleaching (negative signal) at Raman shifts where the ground state gives a Raman signal (8, 9, 100, 185), that sometimes required constant *ad hoc* scaling of the subtracted ground state signal (8). In this paper we will show that this effect can arise from intensity modulation of the spectrally narrow Raman pulse by transient absorption of the sample generated by the actinic pump pulse during the time resolved experiments. A detailed discussion of the problem requires proper consideration of the actual experimental approach and recorded signals. The time resolved FSRS experiment requires three pulses (91, 92, 180): Rp (picosecond Raman pulse), Pr (femtosecond probe pulse), and Pu (femtosecond excitation-actinic pulse). The recorded signal is always a spectrally resolved logarithm of relative intensity change of the probe pulse when any additional pulses are applied (92). Synchronized chopping of Rp and Pu pulses allows simultaneous detection of three signals (186). The signals are depicted in figure 1 together with table indicating the periodic chopping sequence: A – Rp-on, Pu-on; B – Rp-on, Pu-off, C – Rp-off, Pu-on. The signal A – represents a mixture of time resolved and steady state FSRS signal, pump-probe signal and pump-dump-probe signal (result of re-pumping of excited states generated by Pu pulse by the Rp pulse); B – represents the steady state (ground-state) FSRS signal; C – represents the pump probe signals. The common way of acquiring the time resolved FSRS signal is to produce the difference signal A – (B + C). Because of this, experiments are sometimes performed by chopping only the Rp pulses (8). In this case, the Pu pulse is always on and only the difference signal A - C (mixture of time resolved and non time resolved FSRS signal) is continuously recorded. This approach saves experimental time and can be applied when no significant change of the ground state signal takes place during the experiment (no sample damage, no laser source instability). However, we would like to show in this paper that ignoring the explicit C signals (pump probe transient absorption) by direct recording the

difference signal A - C is not the best solution. The knowledge of magnitude of signal C is essential for proper data processing.

The traditional approach to time resolved FSRS experiments is by subtracting Raman spectra with the actinic Pu pulse “on” and “off”. This approach can lead to useful data but it suffers from the implicit assumption that the FSRS signal in the excited state is generated by the same pulse characteristics as in the ground state and the signals are then directly comparable. Unfortunately this assumption is not generally correct. The pulses are modulated by transient absorption changes generated by the preceding pulses. The absorption of the Rp pulse can be significantly stronger (or weaker) in the pumped sample than in non pumped sample. Such attenuation of the Rp pulse originates in transient absorption changes that evolve over time. Time resolved FSRS experiments can be understood as a six-wave-mixing process and so require stronger pumping intensities in comparison to transient absorption experiments which are just four wave mixing processes (8, 9, 11, 98-100, 102, 110, 113, 187, 188). That may lead to change in sample absorption (especially bleaching) as large as 20% (9) (This of course highly depends on specific experimental realizations and sample.

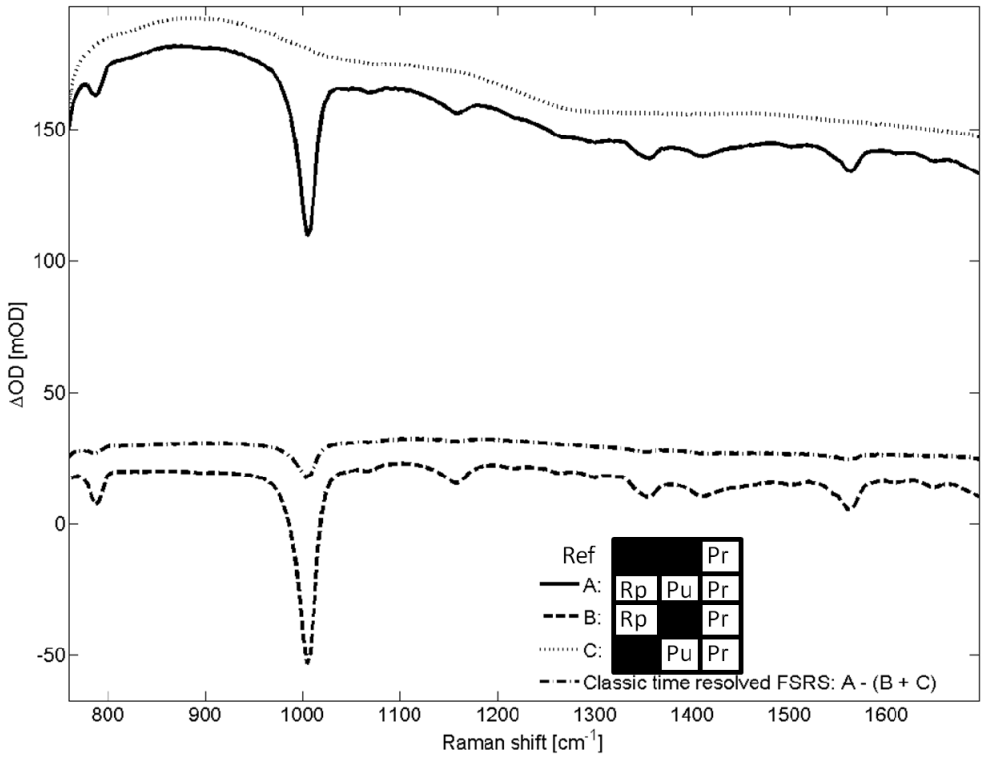

Figure 1

Three signals recorded by chopping Rp and Pu pulses during the time-resolved FSRS experiment on phthalocyanine-carotenoid dyads dissolved in THF. The legend assigning these signals also demonstrates the periodic chopping pattern required to record these signals. When all pulses are applied the desired time-resolved FSRS signal (A) is superposed on top of the steady state FSRS (B) and pump-dump-probe background (C). While the removal of the broadband background from the FSRS signal was studied quite extensively, the influence of this background on the FSRS signal itself was so far neglected. When the transient FSRS spectra are derived as simple A – (B + C), the transient signal is dominated by the bleach of the ground state Raman peaks (dash-dot line).

Systems with low extinction coefficient manifest only small bulk transient absorption change of the sample, but this is not the case for molecules such as linear polyenes (142) such as carotenoids, which are so far the most studied system by FSRS). In consequence, the time evolution of the Raman signal is convoluted with the time evolution of transient absorption. If one does not include this effect, the simple difference spectra A – (B + C) suffer from two artifacts: (i) a "spurious ground state peaks" (or "spurious bleaching", depends on the sign of transient absorption at Rp wavelength) and (ii) "spurious kinetics" (processes appear to be faster or slower than they actually are). Fortunately, with sufficient knowledge of the transient absorption pump probe signal it is possible to correct for these effects numerically by calculating the correct transient FSRS signal. In this paper we propose a simple classical model to do so. Instead of the traditional direct subtraction:

Equation 1: $\Delta FSRS_{traditional} = A_\lambda - (B_\lambda + C_\lambda)$

the transient signal is calculated as:

Equation 2: $\Delta FSRS_{corrected} = A_\lambda \cdot \frac{1}{\alpha} - (B_\lambda + C_\lambda)$

where $\alpha = \alpha(C_{\lambda\text{-}Rp}(\Delta t))$ is correction factor which differs for various pump-probe delays Δt. Factor α represents the amplitude modulation of the Raman signal in the pumped sample by transient absorption. In the paper a simple approach for calculating this correction factor from the recorded signals is proposed and a test experiment is described where we checked and proved the validity of the model. In the test experiment we managed to almost perfectly extract the time resolved FSRS signal free of spurious (produced by improper data treatment) ground state bleaching which proved the importance and robustness of including these simple corrections in FSRS experiment when a significant transient absorption is generated at the Rp wavelength.

Experimental:

The experimental set-up was pumped by a femtosecond regenerative amplifier Legend (Coherent) operating at 1 kHz producing pulses of intensity 3.6 mJ/pulse (3.6 W) and duration of 45 fs. 1 W of the output was used to pump an optical parametric amplifier (OPA, Opera Solo with Topas technology – Coherent) to produce excitation pump pulses at 500 nm. Another 1 W was used to prepare Raman pump pulses centered at 801 nm by spectral filtration in a pulse shaper. A small fraction (less than 10 mW) was used to generate broadband probe pulses by super-continuum generation in a 2 mm thick sapphire plate. The pulse energy of Raman pump pulses at the sample was 2.1 μJ and its spectral FWHM was 4 cm^{-1}, the pulse energy of excitation pump pulses was 10 μJ at the sample, and the probe pulse energy was 2 nJ. The probe and Rp pulses were joined by notch Raman filter (Semrock) and collinearly focused by an off-axis-parabolic-reflector with a focal length of 8 inches (Newport) to a focus of minimal diameter of 200 μm. Prior to analysis in spectrograph, the Rp wavelength was cut out of the probe pulse by a 850 nm long pass filter (Thorlabs). The pump pulse was applied perpendicularly to the probe from the side of the cuvette and focused by cylindrical lens into a narrow horizontal stripe intersecting the linear probed volume. A wave front tilt of the pump pulse was used to increase the time resolution (Instrument response function) in a perpendicular geometry to 1.5 ps (detailed technical description of the perpendicular FSRS experiment is beyond the scope of this manuscript; a paper solely devoted to this complicated topic is in preparation). The scheme of the experimental geometry is depicted in figure S1 in supporting materials. This non-traditional geometry was used in order to allow more direct verification of the model. Excitation of probed volume is still not fully homogeneous as the intensity in the stripe is close to Gaussian. However pumping can be considered homogeneous through the distance where the Rp and Pr pulses are most tightly focused (about 3 mm) and symmetrical around this spot where the majority of FSRS signal is generated.

The sample was prepared by dissolving dried dyads (for structure, and synthesis details of the dyads see reference (28)) in a solution of pure THF at room temperature. The sample was placed in a 1 cm pathlength quartz fluorescence cuvette and the dyad concentration was adjusted to an optical density OD = 2 mm^{-1} at 500 nm. In the ground state, the sample was transparent at the Rp pulse wavelength at 801 nm. The sample was shaken during the measurement in order to circulate sample molecules in the probed volume. The Pu pulse was focused into the sample by a convex cylindrical lens with 50 mm focal length. This lens was placed in kinematic mount on top of the translating stage to allow smooth tuning of the orientation and position of focus in order to achieve optimal overlap with the probed volume. The length of the Pu beam focus was 5 mm and minimal thickness below 300 μm. Rp and Pu pulses were aligned through a linear translating stage equipped with retroreflectors in order to allow tuning their mutual time delay without changing the beam

pointing (optical delay line). The probe pulses were analyzed in a spectrograph (Oriel MS 127i) equipped with diode array with 256 pixels and a grating with 1200 groves/mm blazed at 750nm. The diode array was operated by home built software connected to a pair of optical choppers chopping both Rp and Pr beams achieving single pulse discrimination of background noise and simultaneous detection of pump-on Rp-off, pump-off Rp-on, and pump-on Rp-on signals. 123 time delays between the pump and probe were investigated spanning from -50 ps up to 3.5 ns. Each scan through all time delays took around 4 minutes and 50 scans were averaged giving an overall experimental time of about 4 hours. All displayed spectra were recorded simultaneously.

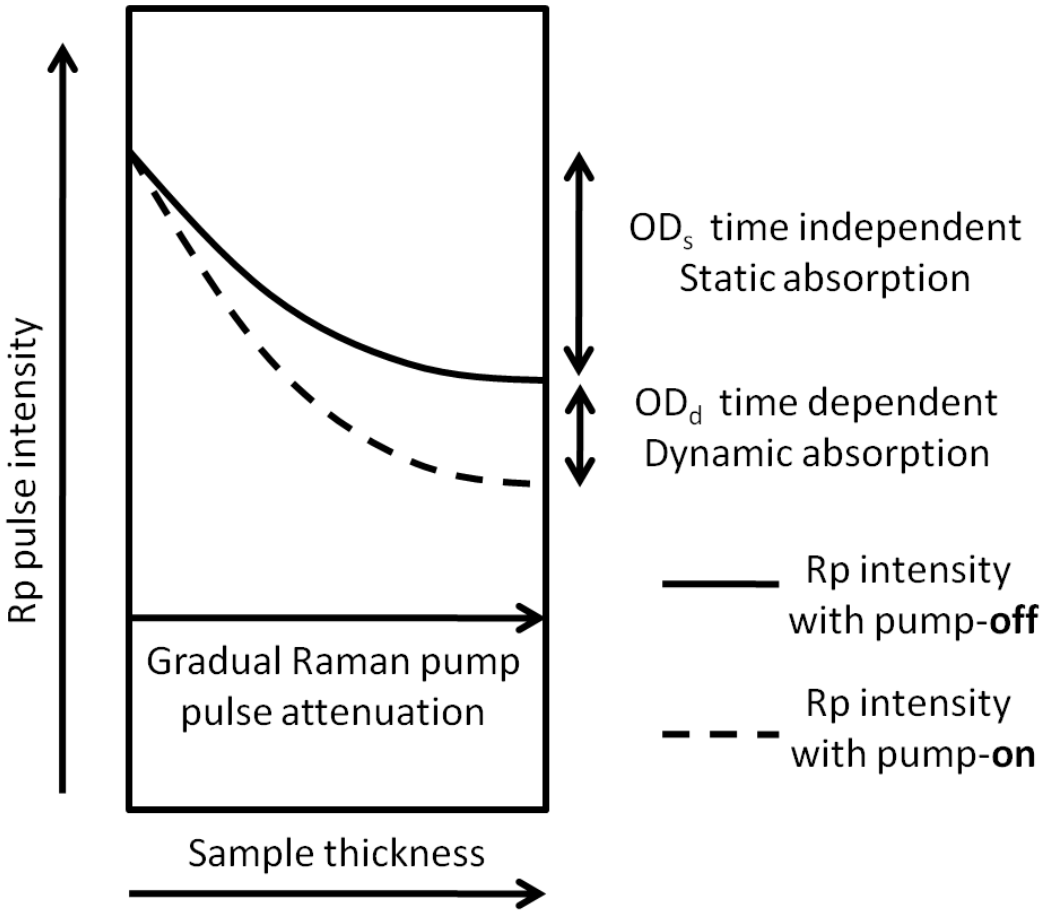

Figure 2

Definition of OD_s – static absorption and OD_d – dynamic (transient) absorption used in equations 3-4. The pulses are modulated by the transient absorption gradually during their propagation through the sample so they are modulated more at the end of the sample than at the beginning. In order to obtain the overall Raman gain, the elements of signal gain have to be integrated over the I_{Rp} distribution of Rp pulse intensity through the thickness of the sample (equation 3). The OD_d is in ideal case identical to the pump probe signal (transient absorption change) at Rp wavelength.

Results

Derivation of correction factor α

The factor α in equation 2 represents the effects of transient absorption on the Rp pulse intensity and, consequently, on the overall Raman gain signal. This constant depends only on the absorption at the Rp wavelength and it is constant for all wavelengths to which it is applied. The model proposed in this paper is based on the assumption that the Rp pulse is gradually absorbed through the sample and so its intensity is not homogeneous but exponentially decays as the pulse propagates through the sample. This is true in the condition when the actinically pumped volume is pumped homogeneously. The validity of this approximation is investigated in the Discussion section. Figure 2 schematically shows how the Rp intensity decreases due to absorption when the pulse propagates through the sample. This absorption can be divided in two parts (marked in figure 2): Static absorption (OD_s), present in a sample that is not pumped actinically, and dynamic absorption (OD_d), which changes with the time evolution of the actinically pumped, excited sample. While OD_s is always zero or positive, OD_d can be also negative, because the excitation of the sample can lead to increased absorption as well as to bleaching and stimulated emission at Rp wavelength. Because we can measure both of these values (OD_s can be measured in absorption spectrometer and OD_d is practically the pump-probe signal at Rp wavelength) the aim is to calculate how the Raman gain changes as a function of OD_d for given OD_s.

As depicted in figure 2, the Rp intensity is unaffected at the front of the sample and mostly affected at the end. This has to be included in the calculation. For mild Rp pulse intensities the relative Raman photon yield is known to be exponential in Rp intensity (92) (this means linear in ΔOD defined as logarithm of light intensities). The overall gain can be calculated by integrating the Raman gain over the Rp intensity distribution curve through the thickness of the sample. This curve can be well approximated as an exponentially decaying function directly determined by the absorbance of the bulk sample. The function $10^{-(ODd+ODs)x}$ describes spatial distribution of Rp pulse intensity in a homogeneously pumped sample of unit length where the point x = 0 lies at the front of the sample. The Raman gain is then simulated by calculating the exponential of the distribution. The choice of the base of this exponential does not have effect on qualitative aspect of the results so the base of natural logarithm was chosen for convenience. An integration of the bulk gain from 0 to 1 then produces the general result valid for any sample thickness with exponential distribution of Rp pulse intensity defined by bulk absorbance at the Rp wavelength (OD_d and OD_s). The ratio between the integrated gains when $OD_d = 0$ and when $OD_d \neq 0$ gives the change in the Raman gain induced by the pump pulse. Because the FSRS Raman signal (as well as the pump-probe) signal is usually measured as a logarithm of the actual light intensity gain (92)

we have to calculate the ratio of logarithmic gains. This ratio can be calculated analytically and represents the overall change in Raman gain due to attenuation of Rp pulse by the transient absorption induced by the Pu pulse, the correction factor α.

Equation 3:

$$\alpha = \frac{log\left[\int_0^1 f_{gain}(I_{pump-on}(x))dx\right]}{log\left[\int_0^1 f_{gain}(I_{pump-off}(x))dx\right]} = \frac{log\left[\int_0^1 e^{\left(10^{-(OD_d+OD_S)x}\right)}dx\right]}{log\left[\int_0^1 e^{\left(10^{-(OD_S)x}\right)}dx\right]} =$$

$$\frac{log\left[\left(10^{OD_d+OD_s}\right)\cdot e^{10^{-(OD_d+OD_s)}}-10^{OD_d+OD_s}\right]}{log\left[10^{OD_s}\cdot e^{10^{-OD_s}}-10^{OD_s}\right]}$$

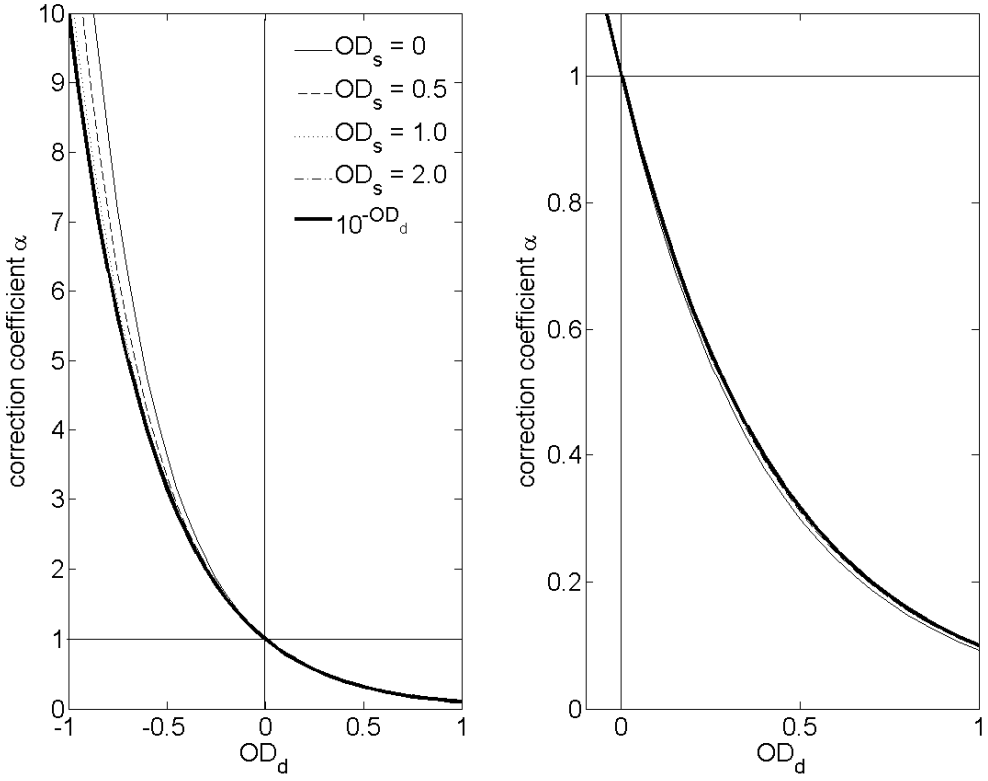

Figure 3

This graph plots the magnitude of factor α (equation 3) in dependence on the transient absorption at the Rp wavelength (OD_d) calculated for different values of the static OD_s absorption and compares them with the simple exponential 10^{-OD_d} (thick solid line). For positive values of OD_d, there is very little difference in comparison with the simple exponential. This difference further decreases with increasing static absorption so the curve for $OD_s = 2$ is entirely overlapped with the one for a simple exponential. The results generally predict that OD_s has to be considered only for high negative OD_d

values (sample bleach, stimulated emission). For small transient absorptions, a simple exponential dependence (equation 4) represents a very good approximation.

Figure 3 plots the curves representing correction factor α for OD_d spanning from -1 to +1 for various values of static absorption OD_s. We can recognize two important characteristics of factor α: The static OD_s is almost not manifested for positive transient absorption, but it is, however, quite important in conditions when a strong bleaching is produced in the transient absorption signal. Also, when the curve calculate by eq. 3 is compared with the simple exponential dependence (predictable for Rp pulse attenuation homogeneous through the thickness of the sample) there is practically no significant deviation up to OD_d = 0.2 and for even higher values of OD_d the difference stays quite marginal. This means that as far the OD_d is positive or only slightly negative the simple approximation of $\alpha \approx 10^{-OD_d}$ can be applied with negligible error. As a result for standard FSRS experiments where OD_d is kept higher than -100 mOD (including positive values) the factor α can be very efficiently approximated by the simple exponential curve:

Equation 4: $$\alpha = 10^{-k.OD_d}$$

where *k* is a phenomenological scaling constant. This can be interpreted, that the nonlinearity in the Rp pulse intensity distribution in the sample can be practically neglected for OD_s and OD_d values typically achieved in FSRS experiments. In the Discussion section it is explained why in practice the constant *k* can vary for various experimental realizations. Here we just shortly mention that constant *k* may be regarded as an "active cross section" between Pu and Rp pulses. In the case of idealized experimental realization, *k* would naturally be equal to 1. The constant has no influence on the time evolution of factor α and so it does not affect validation of the model. The negative sign in the exponent represents that Rp is attenuated when transient absorption change OD_d is positive.

Test experiment on charge separation in phthalocyanine-carotenoid dyad observed by FSRS

The proposed approach to data treatment was tested on a phthalocyanine-carotenoid dyad dissolved in THF. The chemical structure of the dyad can be found in figure 6. On this system an ultrafast charge separation and recombination was reported after excitation (28, 189), formed faster than within 1 ps and almost completely recombined within 10 ps. Because the carotenoid radical cation has a strong absorption in near IR region (84, 190) where the FSRS experiment based on 801 nm Rp is performed, this system is ideal for the study of pulse modulation by transient absorption effects. Figure 1 displays all recorded signals (A, B, C)

recorded 2 ps after excitation of the system by a 500 nm Pu pulse during the time resolved FSRS experiment. We can see that the transient absorption was as high as 200 mOD at near IR region. Figure 4 displays the pure time-resolved (transient) FSRS signal extracted from the recorded data by traditional approach described by equation 1 (figure 4A) and by approach suggested in this paper and summarized in equations 2-4 (figure 4B). For the correction the transient absorption at 850 nm was used as the kinetics at 850 nm is not expected to differ much from kinetics at 801 nm where it was not explicitly measured during the experiment (this approach is discussed in Discussion section below). The recorded signal dominantly consists of THF solvent lines and vibrational fingerprints of the dyad. The most prominent peak in the spectra is a THF ring breathing (191) mode near to 913 cm^{-1}. We can see that transient FSRS produced by the traditional approach is dominated by the evolution of the ground state bleaching of all ground state Raman lines with no other clear structure apart from it. In contrast, the data processed via the corrected approach are entirely devoid of bleach of ground state vibrations but display a small amplification of Raman bands in the region where the pump and probe pulses overlap temporally, and broadening and a slight peak shift of the Raman bands during the few picosecond after the excitation when the charge separation (carotenoid radical) exists (28). Both phenomena observed in the data extracted by our approach can be interpreted however we will treat this only briefly. An experiment on pure solvent (with no transient absorption after 500 nm excitation) showed amplification of the ring breathing THF mode Raman band when Pu and Pr pulses were overlapped (results not shown). This effect is probably due to the broad excitation of molecular low-energy vibrations and rotations via impulsive Raman scattering (192, 193) by the Pu pulse. The subsequent broadening and peak shift of the vibrational ring breathing mode of the toluene observed between 0.7 ps and 10 ps after the excitation might be the consequence of distortion of the molecular 3D structure by the temporal redistribution of electron density on the dyad. It is difficult to disentangle explicit contributions of these phenomena to the overall signal as the impulsive Raman scattering from the Pu pulse leads to general broadening and peak shift of all the Raman lines in excited state via off-diagonal enharmonic couplings of high energy modes with excited low energy modes.

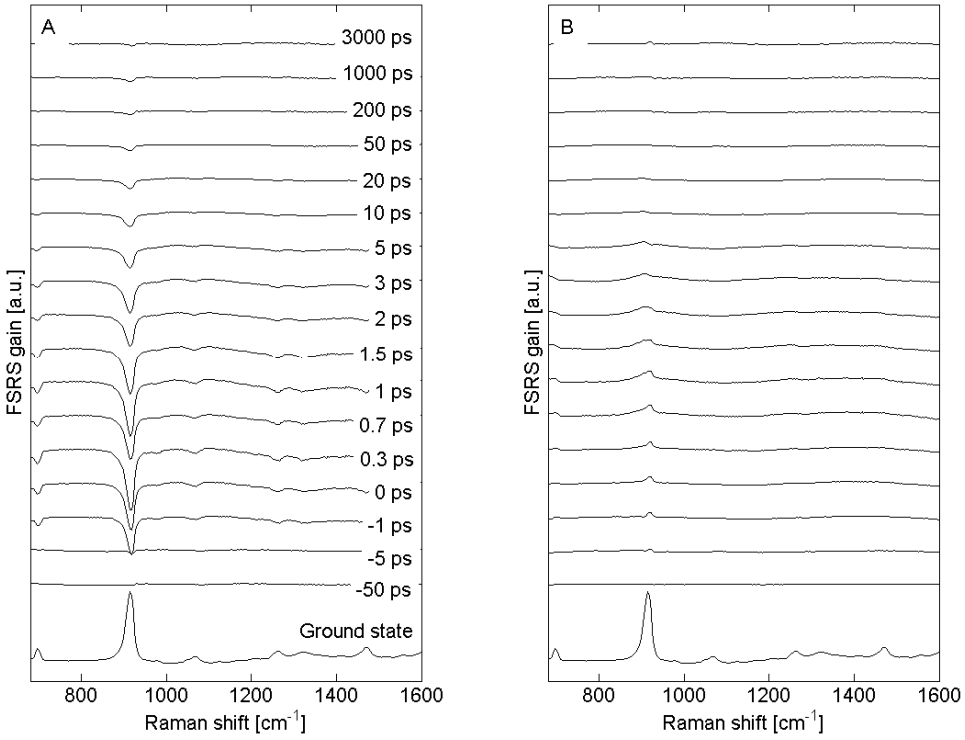

Figure 4

Comparison of traditional and corrected transient FSRS signal. Box A (left) shows transient Raman spectra obtained by the traditional approach (equation 1). Box B (right) shows spectra obtained by the corrected approach (equation 2). The time resolved transient FSRS spectra were recorded after 500 nm excitation of the sample consisting of phthalocyanine-carotenoid dyad dissolved in THF. This led to strong transient absorption in near IR region where Rp pulse propagates. Raw data from this experiment can be seen in figure 1. It is clearly shown that the ground state bleaching dynamics, which dominate the traditional spectra, entirely vanish after application of the correction. With the correction, the true FSRS signal is obtained showing slight peak broadening and shift in response to the excitation. The experiment was performed in a perpendicular geometry where the sample was pumped from the side in order to achieve a homogeneous excitation through the optically dense sample. This approach decreased the time resolution to about 1.5 ps but allowed direct verification of analytical model.

While the traditional approach leads to transient FSRS data that suggest a strong change in molecular vibrations in consequence to excitation, the proposed approach revealed that most of the effects were artifacts caused by Rp pulse modulation by transient absorption of the sample. Transient FSRS data published in the past were often dominated by bleaching of ground state signal (8, 9, 100, 185) which was sometimes treated by ad hoc scaling of subtracted ground state or solvent signals. The experiment described in this paper

represents evidence that the dominant source of this effect can be neglecting the modulation of Rp pulse by transient absorption in the data processing routine, if significant transient absorption change is generated at Rp pulse wavelength. In those situation signal can be easily improved by approach proposed in this paper.

Correction for Raman evolution of β-carotene excited state relaxation

Our recent work treating the wavelength modulated approach to FSRS spectroscopy was performed in traditional geometry (non-collinear but close to collinear crossing of focused beams in thin sample) and it would be interesting to see how the resulting transient FSRS spectra of β-carotene would look after including the correction for the inner filter effect. Unfortunately this experiment was performed with only one chopper and the explicit pump probe signal was not recorded.

In order to utilize this data in verifying the correction we applied the inverse process. We estimated the residual ground state bleach at time delays depicted in figure 8 of reference (9) and from the relative amount of this spurious background, recalculated the transient absorption change at Rp wavelength required to cause a such effect. When these values are compared with independently measured transient absorption of excited β-carotene at 850 nm a very good agreement is achieved. This is summarized in figure 5. In this figure an original spectra from reference paper (9) are presented before and after removal of ground state bleach (this leads to small dispersive structures at ground state bleach Raman shifts due to small shift of the peaks in excited sample). Figure 5C shows the comparison of calculated and measured transient absorption. The coincidence of the measured and calculated transient absorption imply that the proposed correction would have significantly improved the quality of the transient FSRS spectra even in this highly reproducible non-collinear FSRS experiment on β-carotene in solution (8, 9, 102, 188).

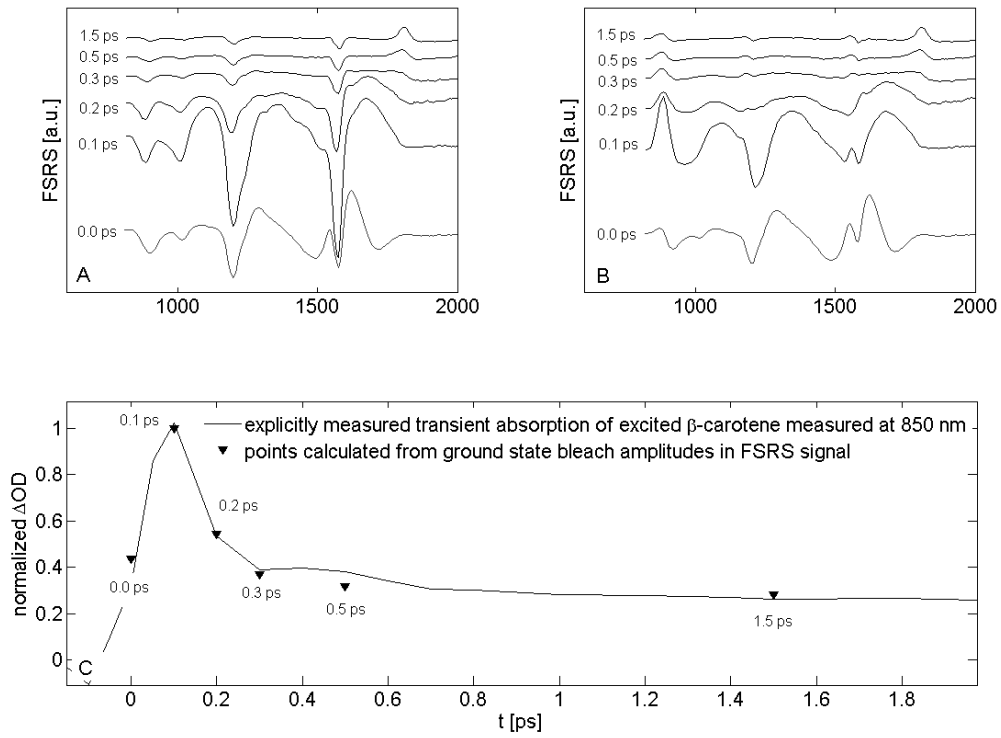

Figure 5

Panel A displays data from our past work on β-carotene (9). Panel B displays the same data after removing of the estimated magnitude of residual ground state bleach in this data (it generally leaves small dispersive structures at the old locations of ground state bleach). Panel C compares pump-probe signal measured on β-carotene at 850 nm with calculated transient absorption changes required at Rp wavelength in order to create ground state bleach corresponding to the estimated magnitude. A very good agreement between measured and calculated curve implies the validity of the correction.

Discussion

First of all it is appropriate to compare the approach described in this paper with the traditional way. In past experiments, the necessity of scaling the signals prior to subtraction was recognized (8), even though no explicit explanation was offered. Partial correction was performed by scaling the signal by an *ad hoc* chosen constant. In these previous approaches it was not recognized that the scaling factor is dynamic in origin and that it is linked with the time evolution of the activated sample. To our best knowledge, this important aspect was revealed in this paper for the first time. It has to be stressed that the magnitude of the effect varies greatly among individual experimental realizations. The detection sensitivity of each experimental set-up determines the minimal fraction of sample molecules required to

be pumped by actinic pump (Pu) in order to resolve the time dynamics on top of the ground state Raman signal. The effect is also of less importance in systems that produce very little absorption change at the Rp wavelength. This means than any experiment can be realized with various magnitude of this effect. But this also means that the correction should be generally considered in order to produce mutually comparable results. For example, the comparison of manually corrected data presented by us in figure 5B is in much better agreement with data from reference (8) than the original uncorrected data from figure 5A (9). From our test experiments it appears that some *ad hoc* scaling is necessary in order to link the recorded magnitude of the pump probe signal with the magnitude which directly acts on the Rp pulse. It is not only a product of variations in light intensity across the beam profiles but also of the experimental geometry. In a perpendicular geometry, the transient absorption change can be considered homogeneous across the probed region and so the proposed model applies very well. In a general geometry, the probed volume is pumped in-homogeneously which complicates linking the change in FSRS gain with the transient absorption change. The next paragraph is devoted to more detailed discussion of inhomogeneous pumping. Generally the "effective cross section" constant *k* (equation 4) has to be assigned phenomenologically for each experimental setting to compensate for it. But, this drawback does not put the proposed approach on the level of the simple *ad hoc* scaling as applied previously. The constant *k* has no influence on time evolution of the correction factor α which is essential in order to record the true time resolved Raman spectra and kinetics.

Another issue that requires discussion is the aforementioned inhomogeneity of the pumping. The proposed model that assumes exponential attenuation of the Rp pulse is applicable when the transient absorption change of the sample is homogeneous through the probed volume. This is certainly not the case in a collinear geometry when the optical density of the sample at Pu wavelength is higher than OD = 0.5. In this case the Pu intensity is gradually attenuated in the sample and so the front of the probed volume is pumped more efficiently and undergoes stronger transient absorption change. In our test experiment we avoided this problem by pumping the sample from the side and so achieving homogenous excitation along the probed volume. However, most FSRS experiments are performed in a geometry close to collinear and on samples with optical density close to OD = 1, which gives a motivation to discuss the problem in some detail. Including the inhomogeneity of pump dramatically increases the complexity of the model for two reasons. First, the intensity of Rp pulse generally evolves during its propagation in a rather complex way and in case of negative OD_d, it can even rise at the beginning of the sample and later drop again, because the effects of OD_d can be dominant at the beginning of the sample while effects of OD_s are homogeneous through the sample thickness. In order to estimate the inhomogeneity, a calculation of the Rp pulse intensity distribution requires, apart from OD_d and OD_s, also the knowledge of the sample absorption coefficient at Pu wavelength: OD_p. The second important complication is that the time-resolved part of the signal, the

static part of the signal (ground state signal), and the solvent signal are affected in a different way. The Raman gain derived out of calculated Rp pulse intensities has to be projected into the distribution of the pumped (or non pumped) molecules through the thickness of the sample. Pumped molecules are distributed preferentially in the front of the sample (where the Pu pulse is strongest in experimental geometry close to collinear) while non-pumped molecules reside mainly in the back of the sample. The solvent is not affected by the pump and so it is distributed homogeneously. These distributions depend also on the percentage of non-pumped molecules per unit of transient absorption: $\Delta N/(N \cdot OD_d)$. This parameter can be in principle derived from transition dipole moments (extinction coefficients) of the molecule for S0-S1 and S1-Sn transition; however, especially the extinction coefficients for S1-Sn transitions are rarely available. In consequence, including the inhomogeneity in an exhaustive way requires three additional input parameters: Absorption at pumping wavelength (OD_p), quantum yield of the pumping in dependence to transient absorption ($\Delta N/(N \cdot OD_d)$) and pure solvent FSRS (S_λ); and model would have to produce three different output parameters: dynamic (time resolved) signal correction (α_d), steady state signal correction (α_s) and solvent correction (α_{sol}). The complete correction would then be defined as:

Equation 5.1 $$\Delta FSRS_{corrected} = \frac{A_\lambda - \alpha_s \cdot B_\lambda - \alpha_{sol} \cdot S_\lambda}{\alpha_d} - C_\lambda$$

Where coefficients α are defined:

Equation 5.2 $$\alpha_i = \alpha_i \left(OD_d(t), OD_s, OD_p, \frac{\Delta N}{N \cdot OD_d} \right)$$

for the adjoined signals. In the homogeneous case when $\alpha_d = \alpha_s = \alpha_{sol}$ the model naturally simplifies to equation 2. We attempted the problem the similar way as in case of equation 3, but unfortunately did not succeeded in finding an analytical solution of the problem. The applicability of such a model would be in any case very low due to its extensive complexity. The major problem does not lie in the absence of an analytic solution, but in the drastic increase in the number of required input parameters which are often difficult to obtain. Because in practice, FSRS experiments are usually performed in a non-perpendicular but also a non-collinear geometry, for a specific experiment it would be particularly difficult to make a good approximation of the actual inhomogeneity. The application of an extensively complex model in condition of poor knowledge about its assumptions would be then an inappropriate approach.

An additional problem with the correction is that the FSRS experiment is usually performed in the region where the exact transient absorption at Rp wavelength (OD_d) is not recorded as the strong elastic scattering of Rp pulse into the sensitive detection is to be avoided (for this reasons we present kinetic at 850 nm in figure 5, the transient absorption at this wavelength was also used for all the corrections present in the paper). Because the transient electronic spectra usually consist of rather broad peaks (28) we recommend in

these situations to use the value closest to Rp wavelength, which is the transient absorption at smallest recorded Raman shift, and scale it empirically (via the constant k in equation 4) or with the knowledge of transient absorption spectra in order to estimate the transient absorption at Rp wavelength. As the kinetics of the transient absorption is usually quite the same at the Rp wavelength as few nanometers from Rp wavelength, the transient FSRS signal obtained this way can still be well corrected. However, recording of the transient absorption at the Rp wavelength is highly recommended in order to obtain a reliable correction.

We proposed only a rather simple and purely classic (no quantum assumptions involved) model of correction for FSRS experiments for modulation of applied pulses by transient absorption effects. Our test experiment clearly pointed out the importance and robustness of including the correction proposed in this paper in the data processing. While the simple exponential approximation of α is obviously quite valid for relatively small transient absorption changes (up to 200 mOD) for an arbitrary experimental geometry, most probably in case of a higher transient absorption more elaborate models have to developed for each experimental geometry. This Discussion section shows the possible direction.

Conclusions

It was both theoretically and experimentally demonstrated that in time-resolved experiments, the absolute FSRS signal amplitude acquired in an actinically pumped sample is affected by transient absorption of the sample at the Rp pulse wavelength. As a result, the transient FSRS signal cannot be derived by direct subtraction of pumped and un-pumped signal as it is common in transient absorption experiments (37). It certainly does not mean that all conclusions based on previous FSRS works have to be reconsidered, but it imply that especially the quantitative results of some past FSRS experiment may be adjusted. Our analysis suggests that FSRS signals kinetics derived by traditional approaches are actually a convolution of the actual vibrational dynamics with kinetic of the transient absorption change at the Rp pulse wavelength. This means that the significance of the effect is directly proportional to absolute magnitude of transient absorption change at the Rp wavelength.

A correction for the Rp pulse intensity modulation by transient absorption signal is proposed based on simultaneous recording of pump-probe, time resolved FSRS signal, and steady state FSRS signal (defined in figure 1 and in Introduction as signals A, B, C) with the use of equations 2 - 4. The correction factor α (used in equation 2 and derived in equation 3) corrects for modulation of the Rp pulse intensity by transient absorption change. The transient absorption evolves in time so the correction cannot be achieved by any static scaling of recorded signals. The approach was tested in an experiment where time-resolved

FSRS signals were measured in a region with strong transient absorption generated by Pu pulse and the Pr wavelength. Use of the proposed correction led to removal of ground state bleaching from the transient FSRS signal. In the test experiment, it was shown that artifacts produced by Rp pulse modulation by transient absorption were responsible for the majority of FSRS signal bleaching in transient spectra. The presence of this background was regularly noticed in previous FSRS experiments (8, 9, 100, 185) but its dynamic nature and origin was to our best knowledge never revealed. We demonstrated that in standard cases when OD_d is kept between -0.1 and 0.3, it is possible to obtain satisfying results from simple exponential correction according the equations 4. But in any case, we demonstrated the importance of including transient absorption change at Rp wavelength in data processing of time resolved FSRS experiment in order to obtain quantitatively correct Raman spectra and kinetics of excited systems. After the period of heuristic development of the FSRS technique, this work joins recent attempts to reconsider some established approaches in order to increase fidelity of the general FSRS experiment (9, 10, 96, 183).

7. High gain approach to femtosecond stimulated Raman spectroscopy and femtosecond transient absorption spectroscopy

Miroslav Kloz, Smitha Pillai, Ana L. Moore, Rienk van Grondelle, John T.M. Kennis

This work is in preparation for publication in: The Journal of Physical Chemistry

Abstract

We introduce a new approach of recording Raman molecular vibrational spectra with sub-picosecond time resolution based on the stimulated Raman process: High Gain Femtosecond Stimulated Raman Scattering (HGFSRS). The simultaneous collinear propagation of a narrowband Raman pump and a spectrally broad probe pulse through a long sample leads to exponential amplification of the probe pulse at the Raman frequencies. When the photoreaction is initiated in the sample by an actinic pump applied from the side and with a specific tilted wave front, HGFSRS can be applied to samples with virtually arbitrary density and thickness yet still with a temporal resolution of non-collinear thin sample experiment. In consequence, the proposed generalized high gain approach allows reaching arbitrary high signal gain regardless of any sample characteristics and requirements. To our best knowledge, HGFSRS appear to be currently the most powerful way of recording time resolved Raman spectra.

Femtosecond Stimulated Raman spectroscopy (FSRS)

Currently, methods such as 2D NMR or X-ray diffraction dominate the resolving structures of molecules and molecular complexes. Unfortunately, it is difficult or often even impossible to apply these methods with the time resolution at which the molecular motions actually occur, typically down to the picosecond timescale(11). In contrast, with the advent of ultrafast lasers, vibrational frequencies of any molecule can be recorded with femtosecond resolution and can be directly linked with the molecular structure. Raman spectroscopy allows recording vibration frequencies of molecules while conveniently working with visible light. While standard spontaneous Raman scattering cannot be acquired with femtosecond resolution, femtosecond stimulated Raman scattering (FSRS)(9, 12, 91, 100, 180, 181, 194) can be. FSRS is based on the time-spatial overlap of two different pulses as depicted in fig. 1 A. When a picosecond spectrally narrow pulse (Rp) is overlapped with femtosecond broadband probe pulse (Pr), the Raman signal is stimulated with femtosecond precision into the defined direction of Pr pulse(92). This approach has the benefit that the FSRS signal is imprinted in the coherently propagating beam, which can be detected at practically arbitrary distance from the sample with a 100 % yield and consequently free of randomly scattered fluorescence background. Also, the gain of the FSRS signal is improved compared to spontaneous process by several orders of magnitude (usually 104 times)(181). Importantly, FSRS is self-matching meaning that it does not have to be performed in a specific phase matching geometry as for example Coherent Antistokes Raman Scattering (CARS) and it is naturally heterodyne (phase sensitive). Thanks to these advantages, FSRS enabled to reveal the molecular nature of a variety of biological processes(8, 11, 97, 99, 100, 102).

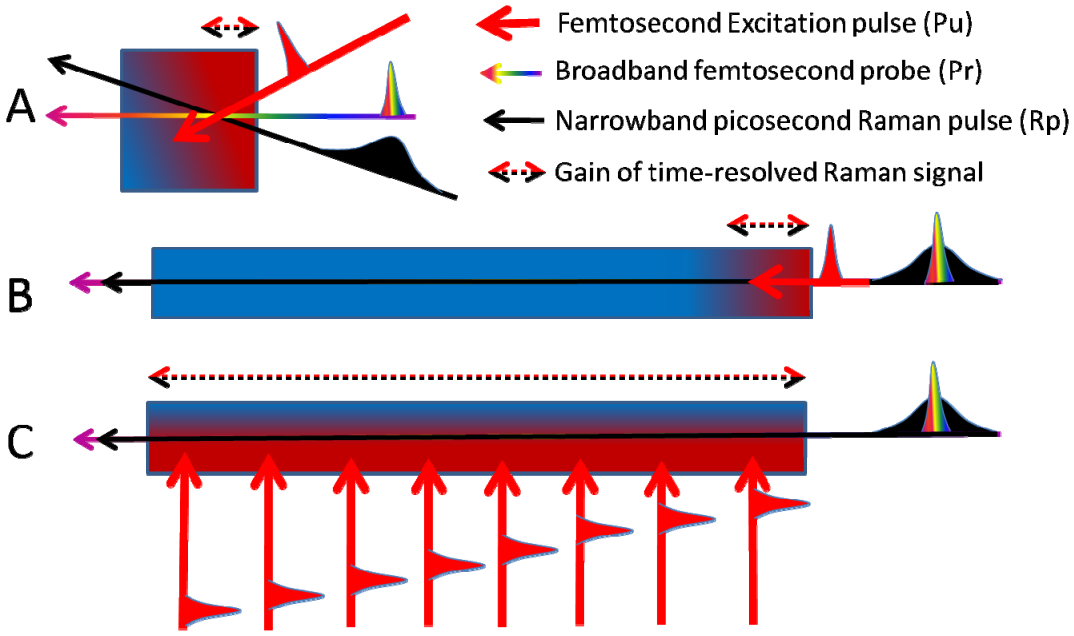

Figure. 1: Comparison of classic and High Gain Stimulated Raman experiment.

A: In the traditional approach to FSRS all involved pulses are non-collinearly crossed in a thin sample. The volume at which the pulses interact is very small B: The collinear geometry can increase the steady state signal gain greatly but the time-resolved gain is limited by absorption of the actinic pump inside the sample. C: The collinear geometry with perpendicularly applied excitation with tilted wave front not only allows obtaining high signal gains for an arbitrary concentration and extinction coefficient of studied molecules but preserves high temporal resolution of the thin sample experiment. Pulses are in this fig. represented by their temporal profiles; their spectra are schematically represented by their colors.

Traditional versus high gain FSRS

All time-resolved FSRS experiments performed so far were realized by the standard way as most femtosecond spectroscopic experiments are done nowadays, by focusing crossed beams in a thin sample(92) (fig. 1 A). In this way, the volume in which the two pulses actually interact is rather small and the gain of the vibrational signal is limited by the maximal possible density of the molecules in the sample. As a consequence usually the majority of both Rp and Pr photons is transmitted through the sample without contributing to the signal gain. For biomolecular samples the typical Raman gain of the probe pulse was close or below 10^{-3} (100, 185). This problem dramatically limits the applicability of FSRS and therefore all time resolved FSRS experiments required long averaging times to obtain reliable data. Thus, FSRS brought amazing time resolution to Raman spectroscopy but did not fully remove problems with the low gain of the Raman signal.

Rather than a scattering process, FSRS can be thought as an amplification of selected frequencies of a polychromatic Pr pulse on externally pumped vibronic transition levels of the molecule(91). When a long volume rather than a spot is pumped by a narrow frequency Raman pulse (Rp), the propagating probe pulse can be gradually amplified at frequencies resonant with the Raman shift to practically unlimited intensity, the same way as a resonant frequency is amplified in an active medium inside of a laser. In fact, a similar amplification can be achieved simply by changing the geometry of a standard FSRS experiment. Fortunately, most chromophores have electronic transitions in the UV or visible light region and vibrational transitions in the mid-infrared region, so when the Rp pulse is applied in the near-infrared region, it can freely propagate through a very long and concentrated sample without being attenuated. Then, by preparation of a collinearly propagating Rp+Pr pulse pair (fig. 1 B) the signal can be collected from a long sample volume, as depicted in fig. 2-3, with a gain rising exponentially with the length of the sample(92). Why this approach was never applied before in time resolved Raman studies if it is so powerful and easy to realize? The answer lies in the fact that as depicted in fig. 1, time-resolved FSRS requires application of an additional “actinic” pump pulse (Pu) initiating a photophysical or photochemical process with femtosecond precision. When applied out of resonance Rp+Pr pulse pair can propagate long distances in the sample without being attenuated or extensively temporally dispersed. However the pump pulse has to be applied selectively in resonance with the molecular system under study. As depicted in fig. 1B, in a collinear experiment the pump pulse is attenuated as it propagates through the concentrated sample and only a small fraction of the probed volume gives the actual time-resolved Raman signal. In contrast, by applying the pump pulse from the side (in fact similar as in many lasers) an arbitrarily long volume can be pumped (see fig 1C). Because the Rp+Pr pulse pair propagates through the long simultaneously pumped volume for many picoseconds (it takes about 3 ps for light to travel 1 mm), the time resolution would be smeared out to about 30 ps in case of a 1 cm long path and proportionally more with a longer path. We rescued the time resolution by introducing a wave front tilt to the Pump pulse(195). As depicted in fig. 1C and fig. 3, tilting of the wave front can match the moment of excitation with the collection of the FSRS signal. In this way, the FSRS spectra can be acquired at large gain while the time resolution is not directly compromised. We call the approach High Gain Femtosecond Stimulated Raman Spectroscopy (HGFSRS).

High gain Femtosecond Stimulated Raman Experiment

The HGFSRS approach is based on three critical steps depicted in fig. 2: Preparation of Rp+Pr probe pair (A), signal collection in long sample pumped from the side by the wave front tilted pump pulse (B), and separation of Rp pulse from the probe pair (C).

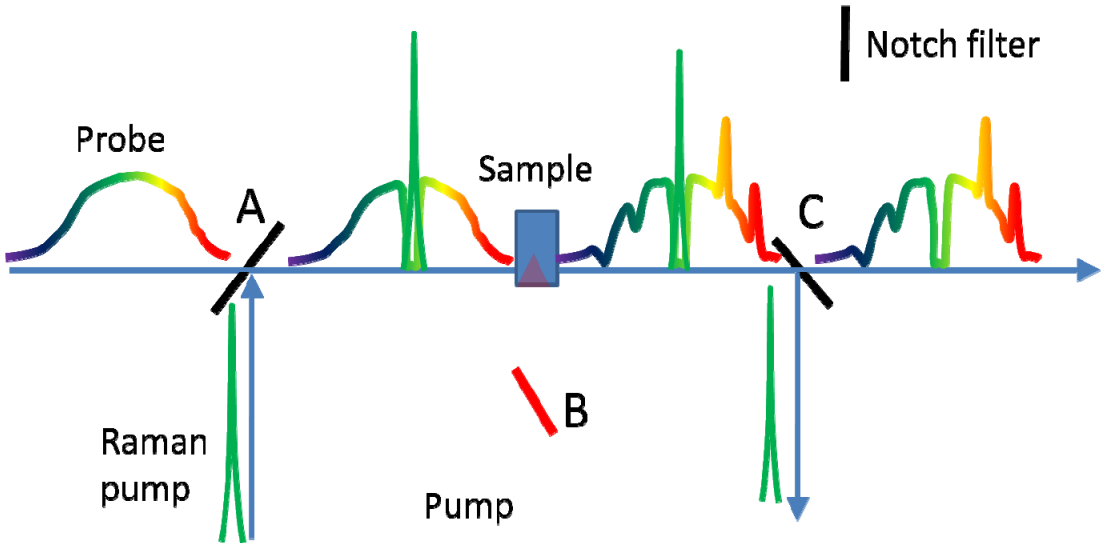

Figure 2: Three crucial steps of HGFSRS.

A: Joining of Rp and Pr pulses by the notch filter in order to create a Rp+Pr pulse pair B: Collection of FRSR signal in a long path length sample pumped by a synchronized tilted wave front. C: Removal of Rp frequency from Rp+Pr pulse pair prior to detection. In this and following figure, the pulses are represented by their spectra. For this reason, the Rp pulse is narrow and the Pr pulse broad, while in fig. 1 (which display pulses in time domain) it is the other way around.

For the preparation of the probing pulse pair, a notch filter can be used as depicted in fig. 1 A. It has to be an interference filter in order to not only block the central wavelength but also to reflect it at high efficiency. The spectral edge of the filter has to be steep in order to preserve the probe pulse intensity even at frequencies close to the Rp pulse frequency. Raman notch filters as narrow as few nanometers that can be tuned by tilting are commercially available and can be used for the purpose. The benefit from using a notch filter rather than a “cut edge” filter (a filter transmitting frequencies higher than a certain value) is the possibility to record Stokes and anti Stokes signal simultaneously (note that in

contrast to spontaneous Raman scattering in FSRS the anti-stokes signal is negative as depicted in fig. 2-3). After joining the Rp and Pr pulses, they have to be steered through the same pair of distant pinholes to achieve perfect collinearity of the beams and their spatial overlap in order to prepare simultaneously propagating Rp+Pr pulse pair. Their mutual time delay is set by means of an optical delay line. Removal of the strong Rp frequency from the Rp+Pr pulse pair after passing through the sample can be achieved by a notch or a cut-off filter.

Fig. 3 illustrates three different snapshots from the period of time when the signal is collected.

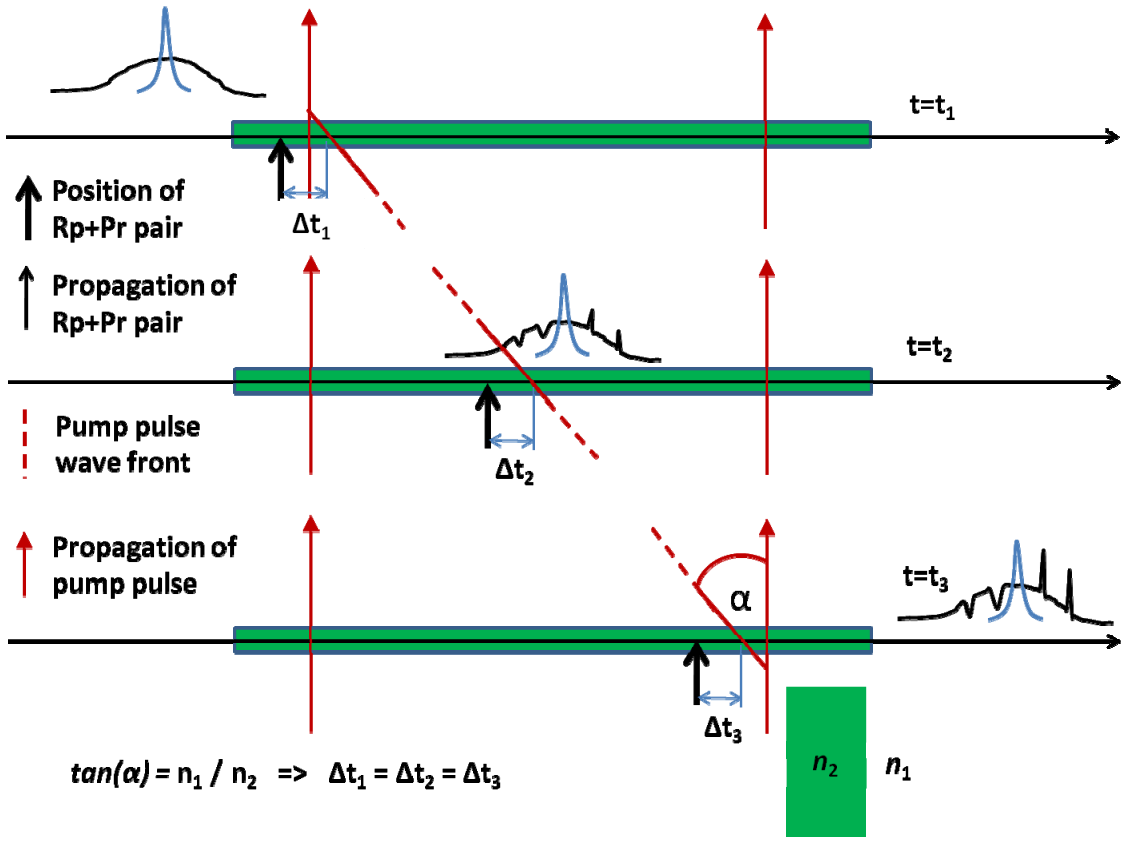

Fig. 3: Preservation of time resolution by wave front tilt

Three time snapshots from the collection of the signal inside of a long sample pumped from the side with a tilted wave front pulse. If the magnitude of the wave front tilt is chosen the right way, the cross-section of pump pulse wave front with the probed volume propagates with the same speed as Rp+Pr pulse pair. If the wave front tilt angle is bound to the refractive indices of the sample and the laboratory (n_2 and n_1) by the displayed equation, the delay between pump and probe is then preserved through the entire accumulation of signal and the resulting time resolution can greatly exceed the time during which the signal is collected. In this basic model the spectral group velocity dispersion of Pr and Pu pulse is not considered. By experimental adjustment of angle α, the instrument response function of

the experiment was successfully decreased from 30 to 0.9 ps (for recorded kinetics see figure 2 in supporting information).

The speed of propagation of the Rp+Pr pulse pair and the pump pulse is strictly determined by the refractive index of the medium. Because the Rp pulse is several picoseconds long in time and has a near-IR wavelength, the spectral dispersion of probe pulse frequencies can be neglected and the Rp+Pr pair can be considered as a single simultaneously propagating pulse. The speed at which the perpendicularly propagating pump wave front crosses the probed volume is determined also by the angle between the Pu pulse wave front and direction of propagation of Rp+Pr pair.(195) This speed can be tuned by the orientation and extent of the wave front tilt to each desired value. The wave front tilt can thus be set to a value at which the cross-section of the wave front with the probed volume and the Rp+Pr pair propagates with the same speed. As a consequence, even when the signal is collected from a long sample for many picoseconds, the delay between the pump and probe remains constant and the time resolution is preserved. The controllable wave front tilt can be generated by combining dispersive elements such as prisms and gratings with lenses. In our test experiment, we used the apparatus as depicted and explained in fig. 4 based on one grating (1800 groves/mm) and one twice magnifying telescope which simultaneously magnifies the wave front tilt introduced by the grating and projects it into the sample.

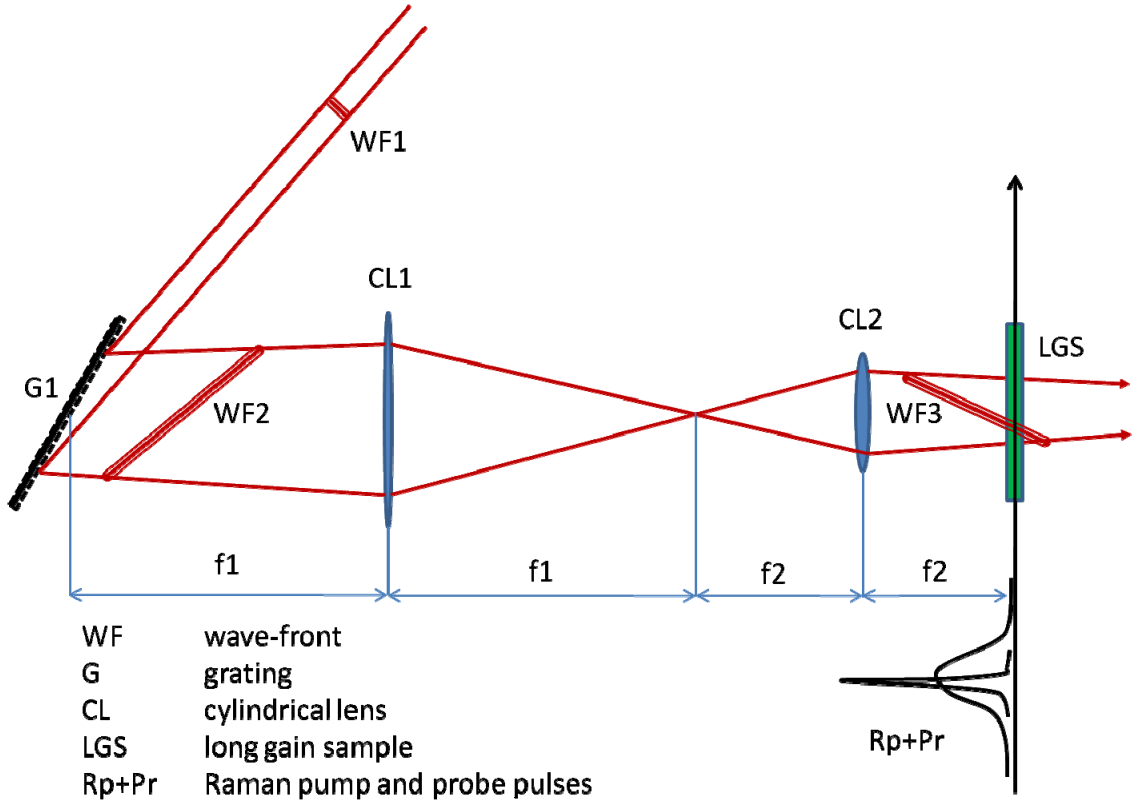

Figure. 4: Wave front tilting apparatus

The wave front tilt introduced by a grating is magnified and projected into the sample. In this way practically arbitrary wave front tilt can be achieved. The entire process happens in one plane so cylindrical lenses can be used instead of spherical. The advantage of this approach is that the telescope also refocuses the spectral dispersion introduced to the beam by the grating (for simplicity it is not displayed in the figure). The wave front tilt introduced by the grating is determined by the deviation of the diffraction angle from the normal reflection. The time delay between the left and right edge of the pulse is preserved after magnification so decreasing of the beam aperture in the telescope results in magnification of the wave front tilt angle the way that *tan(α)* (defined in figure 3) is proportional to magnification of the telescope.

The wave front tilt can be adjusted by slightly varying the angle at which the pump pulse hits the sample from the perfectly perpendicular geometry. The calculation described in fig. 3 based on basic trigonometry applied to a perpendicular geometry can set the approximate value of the required wave front tilt. Result of optimization is in figure 5B.

Generalization of high gain approach

As schematically depicted in figure 1C, the HGFSRS can be interpreted as a way of performing a collection of standard thin sample femtosecond experiments synchronized by the wave front tilt of the excitation pulse in a way that they can all be probed simultaneously and the signal is accumulated within a single probe pulse. In the presented approach, a stronger signal is reached by increasing the bulk active cross section of studied molecules by elongation of the sample and not by subjecting molecules to stronger photon densities. From this perspective, the same approach can be used also in other femtosecond spectroscopic techniques such as pump-probe transient absorption in situations where high signal gain and low excitation density are required simultaneously.

Increased requirement for pump pulse intensities

While the Rp+Pr pulse pair can be constructed from exactly the same Rp and Pr pulses as would be used in a non-collinear thin sample experiment, the intensity of excitation pump has to be increased proportionally to the sample thickness. The generalized high gain approach is then a way to transfer all the abundant laser intensity into the signal. But, the signal gain per unit of input photons (from the amplified laser system feeding the experimental set-up) is for HGFSRS much higher that summing of equivalent of thin sample FSRS experiments. First, the signal in the probe is accumulated exponentially(92) compared to a linear summation from set of thin samples. Second, due to the strict spectral narrowing

in a pulse shaper, the generation of a strong Raman pulse (Rp) is usually the most complicated and inefficient part of the experimental set-up(92, 187). Hence, it is usually easier to prepare a strong Pu pulse and a moderate Rp pulse rather than the other way round. Also, the HGFSRS uses just one Rp pulse for many thin sample experiments. In this context, while for most femtosecond experiments our “high gain” approach is also valid but only as a way to transfer all available laser power into a signal, for stimulated Raman experiments it means also a dramatic qualitative improvement.

Time resolution

The wave front tilt largely improves the time resolution of thick sample experiment, but it probably has a practical limit. It is largely dependent on flexibility in generation of wave front tilt. In the simple perpendicular geometry as applied in our test experiment, we found the instrument response function to be 0.9 ps in a 1 cm thick sample (figure 5B), as followed from global fitting. For complete time traces of the recorded signals see supporting information. The reduction of the instrument response function from more than 30 ps, which is the time the probe needs to cross a 1 cm long sample, to 0.9 ps is certain experimental evidence that the wave front tilt can be used to compensate for the long time during which the signal is collected in the HGFSRS technique and to our opinion represents convincing proof of the principle of the HGFSRS approach. The instrument response function achieved in our experiments is not connected to the length of the sample but rather to our current implementation of HGFSRS. Non-perpendicular geometry of side pumping should be in principle capable of perfect overlap of Pu and probe wave fronts in the sample. However this approach is severely limited by difficulties in generating a tunable wave front tilt. One of the possibilities would be use of tunable telescope within the wave front tilting apparatus, but this possibility waits for experimental examination.

As we did not directly proved that HGFSRS can benefit from superior time resolution of FSRS process, two aspects of FSRS have to be mentioned. First, FSRS was believed to offer literarily unlimited time resolution by circumventing traditional time-bandwidth limitation of femtosecond spectroscopy(91), but the meaning of <100 fs time resolution of FSRS was disputed recently(96). We believe that the future of FSRS experiments lies more in possibility of recoding time resolved Raman spectra with close 100% yield and so in shorter experimental time (thanks to directionality of the signal), with higher sensitivity and probably even with higher spectral resolution(196) rather than in potentially deeply sub-picosecond time resolution associated with complicated interpratations(10). Second, all pulses applied collinearly with the Rp+Pr pair can act even on the long sample with high time resolution, which allows the extension of HGFSRS to powerful 2D FSRS techniques requiring the application of series of pulses with well controllable time delays(14). This extension is not possible in time resolved techniques based on spontaneous Raman

scattering even when they may have time resolution comparable with purely realized HGFSRS.

Tests of performance

In figure 5 the results from testing the crucial parameters of HGFSRS (high signal gain and high time resolution) are presented. In figure 5 A are plotted spectrally resolved probe pulse intensities with and without the simultaneous propagation of Rp pulse in solution of toluene. It can be seen that amplification at Raman lines is comparable with overall intensity of probe pulse at this wavelength. This leads to the Raman gains as high as 0.6. Figure 5 B shows the Instrument Response Function of the pump probe signal from the 10 mm thick sample of styril-9 laser dye after approximate setting of the wave front tilt based on equations in figure 3 and after optimization by adjustment of incidence angle. It can be seen that IRF was thanks to wave front tilt pushed close to 1 ps bandwidth.

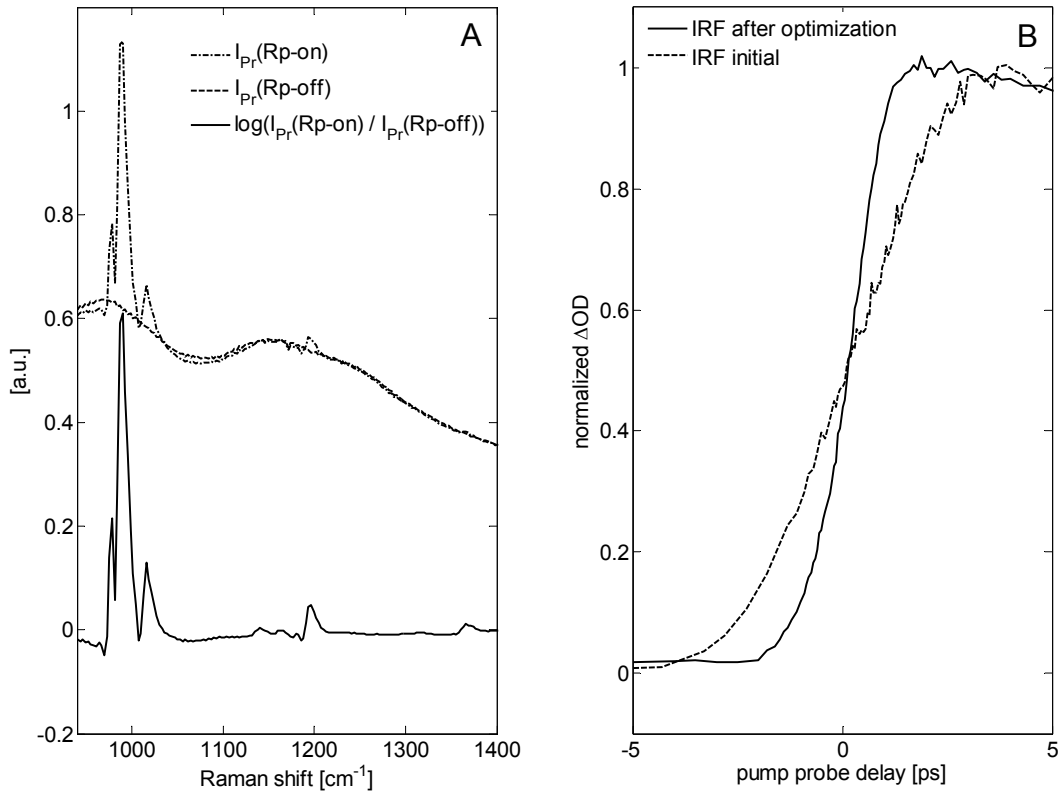

Figure 5: Recorded parameters of HGFSRS experiment

A: Spectrally resolved intensity of freely propagating probe pulse (dashed) and after co propagation with Rp pulse (dashed-dot) together with resulting Raman gain spectrum (solid). B: Measured instrument response function in 1cm thick cuvette. After initial setting (dashed) and after optimization (solid).

We performed various experiments to test the applicability of the approach. This included repeating some well studied FSRS experiments. Overview of these experiments is depicted in figure 6.

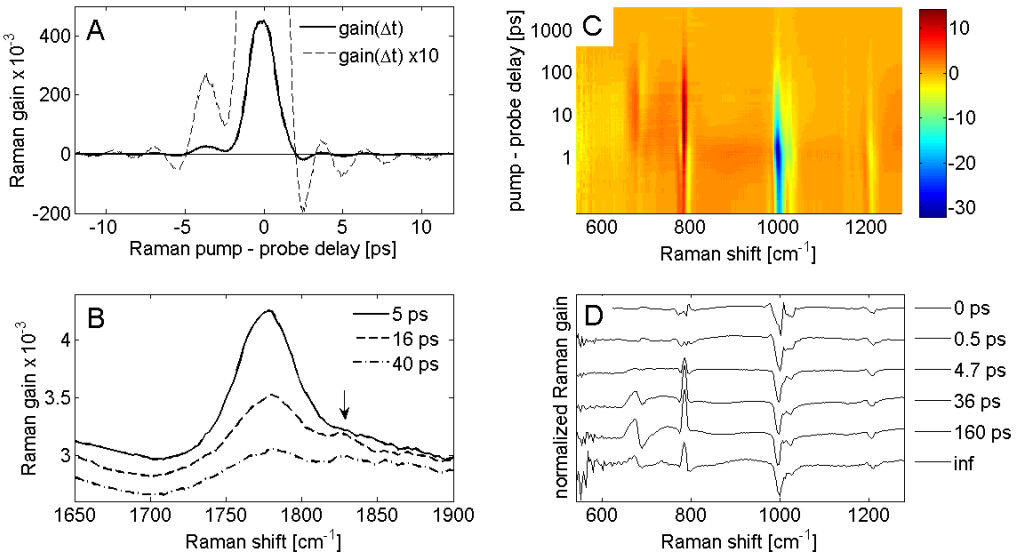

Figure 6: Selected results from testing of HGFSRS approach

A: Raman gain dependence on Rp probe time overlap B: β-carotene excited state vibration at long time delays. Arrows highlight a long living shoulder. C: Complete time resolved FSRS spectra acquired after 500 nm excitation of toluene solution of phthalocyanine dyads. D: Spectral components fitted from the time resolved spectra (see supporting information for actual kinetics and the fit).

In all presented preliminary results an increased sensitivity HGFSRS approach was manifested by recording phenomena which were beyond resolving power of past experiments. In this short letter we will describe results only briefly highlighting the achievement of HGFSRS. Each of shown results is currently subject of further investigation and its interpretation will deserve a separate publication. In case of repeated experiments we refer to the older works. An interested reader may compare referenced works with our results in order to judge the benefits of HGFSRS. Note that all presented data are free of any smoothing or peak fitting procedures.

First presented result is from investigating the dependence of FSRS gain on the Rp and Pr time overlap in HGFSRS configuration. The test medium was 1 cm thick sample consisting of pure toluene solution at room temperature. Results can be seen in figure 5 A. Our results confirmed the phenomena observed in past(182). Namely we repeated observations of maximal gain in condition of slightly advanced probe in comparison to Rp pulse peak and overall shape of Rp-Pr dependence function close to Gaussian curve. However the increased sensitivity of HGFSRS allowed investigation of broader range of Rp-Pr delays. Interestingly

we observed an oscillatory pattern in the gain at high temporal separation between the pump and probe pulses (both positive and negative). Origin and dependence of this phenomena on the experimental conditions is subject of further investigation however a careful examination of data presented in the referenced work(182) reveal small but clear hint of the same phenomena which was left uncommented in that study.

Second presented results are from investigation of high energy vibration of diethyl ether dissolved β-carotene dark $2Ag^-$ (S1)(18) excited state assigned to vibrational coupling of ground and excited state via C=C stretch mode(197). This 1770-1790 cm^{-1} (solvent dependent) vibration is well separated from ground state vibrations. Also the dynamic of β-carotene excited states(18) in exceptionally fast. Thanks to it this Raman active vibration with lifetime as short as few picoseconds became a sort of etalon for testing ultrafast Raman techniques (9, 102, 113, 119, 120). High signal gain of HGFSRS allowed investigation of this vibration mode at long Pu-Pr delays when the amplitude drops beyond the sensitivity of past techniques. In figure 5 B it can been seen a presence of small long lasting shoulder on the high energy tale of this peak (highlighted in figure 5 B by arrow). There is implication that this observation (to our best knowledge recorded for the first time) is related to phenomena of additional dark excited state of carotenoids usually denoted as S*(18, 19, 66). There is high controversy about the nature of S* phenomena(20, 63, 123) despite the broad scientific enthusiasm to resolve it. Our findings are still subject of further examination however if they were proven relevant to S* state it would suggest that S* phenomena can be merely S1 state of different carotenoid conformation.

Our third presented result was chosen to demonstrate the general capability of HGFSRS and high signal to noise ratio. In figure 5 C we present complete time resolved FSRS spectra recorded after 500 nm excitation of toluene solution of carotenoid-phthalocyanine dyad(28). In figure 5 D are presented the evolution associated decay spectra (EADS) extracted from the Raman data shown above. The fitted spectra highlight the observation detectable also in the box C. Excitation of the dyad led to temporary amplification of 787 cm^{-1} toluene ring vibrational mode. Origin of this effect is subject of further investigation.

Prospects of HGFSRS

We believe that the simple experiments we performed to test and demonstrate our idea is only a taste of future possibilities. The power, stability, size, robustness, and availability of femtosecond lasers improved dramatically during the last couple of years and it is still expanding. In established time resolved vibrational techniques such as femtosecond infrared transient absorption spectroscopy, the signal gain is directly related to the sample's extinction coefficient and maximal optical density and therefore these techniques cannot directly benefit from the recent improvement of amplified laser systems. In contrast, the HGFSRS as an emissive technique can, in abundance of laser power, in principle produce an

arbitrary strong signal out of any sample concentration, optical density or Raman cross section. Hence, we believe that HGFSRS opens a new dimension to the applicability of the Stimulated Raman process as a way to investigate the vibrations and consequently even the chemical and 3D structure of molecules and molecular complexes with high resolution and sensitivity and the time resolution spanning from femtoseconds up to the long biological time scales.

Methods:

The experimental set-up was pumped by a femtosecond regenerative amplifier Legend (Coherent Company) operating at 1 kHz, producing pulses of intensity 3.6 mJ/pulse (3.6 W) and duration of 45 fs. 1 W of the output was used to pump an optical parametric amplifier (OPA, Opera with Topas technology – Coherent company) to produce excitation pump pulses at 500 nm. Another 1 W was used to prepare Raman pump pulses centered at 801 nm by spectral filtration in a pulse shaper. A small fraction (less than 10 mW) was used to generate a broadband probe pulses by super-continuum generation in 2 mm thick sapphire plate. The pulse energy of the Raman pump pulse at the sample was 2.1 μJ, the pulse energy of excitation pump pulses was 3 μJ at the sample, and the probe pulse energy was 2 nJ. For preparation of Rp+Pr pulse pair a Raman notch filter centered at 808 nm was used (Semrock). The probing pulse pair was focused by off-axis-parabolic-reflector with focal length of 8 inches (Newport) to a focus of minimal diameter of 200 μm. The sample was placed in 1 cm thick quartz fluorescence cuvette and adjusted to an optical density OD = 2 mm^{-1} at 500 nm. The sample was shaken during the measurement in order to circulate sample molecules in the probed volume. In the wave front tilting apparatus, a grating with 1800 groves/mm blazed to 500 nm was used. The telescope projecting the wave front into the sample consisted of a convex cylindrical lens with focal length of 300 mm and another convex cylindrical lens with 150 mm focal length in order to magnify the wave front tilt twice. The probe pulse was focused into the sample by a convex cylindrical lens with 50 mm focal length and a curvature perpendicular to cylindrical lenses used for the wave front tilt generation. This lens was placed in a kinematic mount on top of a translation stage to allow smooth tuning of the orientation and position of focus in order to achieve optimal overlap with the probed volume. The length of the focus was 5 mm and the minimal thickness below 300 μm. The Rp and Pump pulses were aligned through a linear translation stage equipped with retro reflectors to allow tuning their mutual time delay without changing the beam pointing (optical delay line). The probe pulses were analyzed in a spectrograph (Oriel MS 127i) equipped with a diode array of 256 pixels and a grating with 1200 groves/mm blazed at 750 nm. The diode array was operated by home-built software connected to a pair of optical choppers chopping both Rp and Pr beams to achieve single-pulse discrimination of background noise and simultaneous detection of the pump-probe and pump-dump-probe background. 123 time delays between the pump and probe were investigated, spanning from -50 ps up to 3.5 ns. Each scan through all time delays took around 4 minutes and 50 scans were averaged to smooth the time kinetics from the noise originating from instability of the laser pulse power, giving a total experimental time of about 4 hours. All displayed spectra were recorded simultaneously. The data were analyzed in free fitting package TIMP running under R environment.

8. Direct observation of anharmonic couplings in β-carotene through Three-pulse frequency-domain two-dimensional stimulated Raman spectroscopy

Miroslav Kloz, Rienk van Grondelle, John T.M. Kennis

This work is in preparation for publication

Abstract

We propose and experimentally investigated a new approach for recording frequency-domain 2D Raman spectra using three ultrashort laser pulses only, two spectrally narrow picosecond pulses and one spectrally broad femtosecond pulse. A systematic scan of energy difference between the two picosecond pulses produces the 2D spectra. On a test sample of β-carotene dissolved in THF clear diagonal and off-diagonal peaks were recorded, very likely manifesting an anharmonic shift due to the coupling of vibrational modes in the recorded region from 860 cm^{-1} to 1600 cm^{-1}. To our best knowledge, this represents the first demonstration of successful recording of frequency-domain 2D Raman spectra based on femtosecond stimulated Raman mechanism and over the broad spectral window.

Introduction

Two dimensional (2D) spectroscopies including 2D Raman techniques form the backbone of the frontier research in (bio) molecular femtosecond spectroscopy (14, 198-208). The main motivation for development of 2D techniques is their capability to disentangle a complicated manifold of mutually interacting quantum states of the system, perhaps even shed some light on the general role of quantum coherence in nature (209-211). While both theoretical and practical aspects of 2D spectra acquisition are usually quite complicated, (5, 212) from the user perspective the link between the recorded spectra and the actual molecular dynamics becomes often more straightforward in comparison to their 1D counterpart. This effect grows in importance with the complexity of the system making the 2D spectroscopy highly desirable for study of extensive biopolymers such as proteins. Unfortunately, optical 2D spectroscopies still need significant progress and development in order to catch up with 2D–NMR techniques in terms of robustness, applicability and a general adoption by the scientific community.

There are two approaches towards 2D spectroscopy. In “time-domain” 2D spectroscopy all states are excited simultaneously and the time evolution of the system is recorded in a form of coherent quantum beats of all interfering processes. Fourier transform of this evolution yields the 2D spectra including the anharmonicities originating in couplings. In “frequency domain” 2D spectroscopy the states are excited selectively and 1D spectra are recorded for each excitation. A collection of recorded spectra for all the scanned frequencies forms the 2D spectra. From a purely theoretical perspective, the time domain approach can achieve a higher time-spectral resolution and also deeper insight into the system as it can benefit from the possibility of an explicit control over the formed train of coherences and populations by complex pulse sequences, for example by recording photon echoes (213, 214). In practice, the time-domain techniques have to deal with the extremely short periods of optical transitions (~1 fs for electronic and ~20 fs for vibrational transitions) and at room temperature with very short decoherence times (~100 fs for electronic and ~1000 fs for vibrational states).

While pulses of about 100 fs are nowadays easily available at practically all possible wavelengths from near UV to mid-IR, with even shorter pulses (<30fs) the technical complications rise drastically, especially because of the inevitably very broad spectral bandwidth of such short pulses. Despite this experimental limitation, time-domain experiments are readily attempted, harnessing phase matching rules and heterodyne detection in order to filtrate the desired signals (201, 215, 216). Time domain 2D spectra are thus recorded, but their interpretation becomes a very delicate issue often requiring non-intuitive modeling as the idealized models (successfully used in NMR) do not apply, especially for the electronic states (217). “Frequency-domain” experiments do not allow an explicit coherent control over the system and generally offer a worse time resolution, but

are balanced by a higher experimental robustness, a more straightforward data treatment and usually also by a broader spectral window at which they can be acquired (212).

At present 2D-IR vibrational spectroscopy probably is the most developed optical 2D spectroscopy (212), then follows the 2D-VIS electronic spectroscopy (201, 215), both realized in either "time-domain" and "frequency-domain" forms. Only very recently, also "time-domain" 2D-Raman vibrational spectroscopy was attempted (14-16). Thus, the only 2D-spectroscopy that has not been experimentally tested with spectral resolution so far is frequency-domain 2D-Raman spectroscopy, following the generally delayed evolution of femtosecond Raman techniques. The reason for this delay is largely historical. The crucial mechanism in all femtosecond Raman techniques is a combined action of the broadband femtosecond white light continuum (probe - Pr) and a narrowband picosecond pulse (Raman pump - Rp) (91, 180). Preparation of such a pulse pair of a sufficient intensity requires advanced photonics (especially strong femtosecond laser amplifiers, capable of pumping a multiple optical amplifiers at the same time) which is now easily available even on a commercial basis but which was difficult to be accessed for molecular spectroscopists just a decade ago. With up-to-date experimental equipment we had the opportunity to conduct a pioneering exploration of the last fully untested 2D technique, frequency-domain 2D Raman spectroscopy. As there are in principle many ways how to perform a frequency domain 2D Raman experiment the specific approach we are proposing in this paper will be from now called "three-pulse frequency-domain 2D femtosecond Stimulated Raman spectroscopy" (3PFD2D-FSRS).

Methods

The experimental set-up was pumped by commercial Ti:sapphire fs amplifier (Libra, Coherent Inc., Mountain View CA) tuned to 800 nm, generating 45 fs pulses at 1 kHz at 4.5 W output power. 1 W of the output was spectrally filtrated in a pulse shaper producing Rpi (see Results section for abbreviations) pulses centered at 804.4 nm and 20 cm^{-1} broad. Another 1 W pumped a second harmonic bandwidth compressor producing narrowband 400 nm pulses feeding a ps OPG (TOPAS-400-WL – Light conversion) producing about 12 cm^{-1} broad and 2.9 ps long pulses tunable from 480 nm to 2500 nm. This source was used for generation of Rpd pulses. 100 mW of pumping power was picked and attenuated in order to produce a probing (Pr) white light continuum by focusing it into a 2 mm thick sapphire plate. All three pulses (Rpi, Rpd, Pr) were non-collinearly focused into a 1 mm thick sample cuvette. Foci were overlapped and both Rpd-probe and Rpi-probe spatial overlap was optimized by independent recording of pump-probe signals on a laser dye sample. Polarization of all involved pulses was set to parallel to each other. The timing of the pulses was optimized by independently maximizing FSRS signal originating from both Rpd and Rpi pulses by their delaying in a pair of optical delay lines. The experiment was performed by manually scanning the ps OPA between 710 nm and 752 nm in roughly 0.3 nm steps and

simultaneously recording FSRS spectra from the Rpi pulse in the carotenoid window (860-1650 cm^{-1}, corresponding roughly to 860-920 nm). Rpi pulses were focused onto a 100 µm wide spot and kept at the same intensity of 1.4 µJ/pulse for all investigated Rpd wavelengths. The Rpd pulses were focused onto a 200 µm spot and their intensity was continuously checked and adjusted by a continuous neutral density filter to 3 µJ/pulse for all scanned wavelengths. The probe pulse was analyzed by a spectrograph and a 256 pixel silicon detector array operating in a single pulse regime. The detection was synchronized with a pair of choppers operating at 500 Hz and 250 Hz in Rpi and Rpd path respectively in order to achieve simultaneous recording of Rpi-Pr, Rpd-Pr, and Rpd-Rpi-Pr signals. The sample (β-carotene) was dissolved in THF into OD~ 15/mm at maximal absorption wavelength (~450 nm). Such a concentration has still minimal absorption in the spectral region from 700-1000 nm so for all applied pulses (Rpi, Rpd, Pr), the sample was virtually transparent. Simultaneous application of Rpd and Rpi pulses led to transient absorption in the near IR of about 50 mOD, probably due to two photon excitation of β-carotene S1 state (73). Considering the concentration of the sample and high extinction coefficient of carotenoids, it was relatively a minor effect (less than 1% of molecules is expected to be two-photon excited derived from amplitude of transient absorption signal in low concentration sample at saturating light intensity). No two photon absorption was recorded when only one Rp pulse was applied.

Results

Mechanism of the FSRS and the time domain 2D-FSRS experiment

As mentioned in the introduction, the basis of femtosecond stimulated Raman scattering (FSRS) process is the simultaneous action of a broadband Pr pulse and a narrowband Rp pulse on the sample (12, 91, 180, 181). The combination of two interactions with the Rp field (one <Bra| and one |Ket>) and one interaction with the Pr field (|Bra>) (Figure 1) produces a coherence resulting in emission of a photon into the probe field at Stokes region (180); the situation is little bit more complicated for the anti-Stokes signal (12, 13). This four wave mixing process is strongly enhanced for the Rp-Pr energy shifts which are in resonance with the actual Raman active (vibrational) states of the sample. Amplification of the Pr pulse then has a spectral profile proportional to the Raman signature of the medium in which SRS occurs. An important property of the SRS process is that it does not leave the molecule in an initial state but it results in deposition of an energy and momentum quantum into the molecule; its value is equivalent to the difference between the Rp and Pr photons.

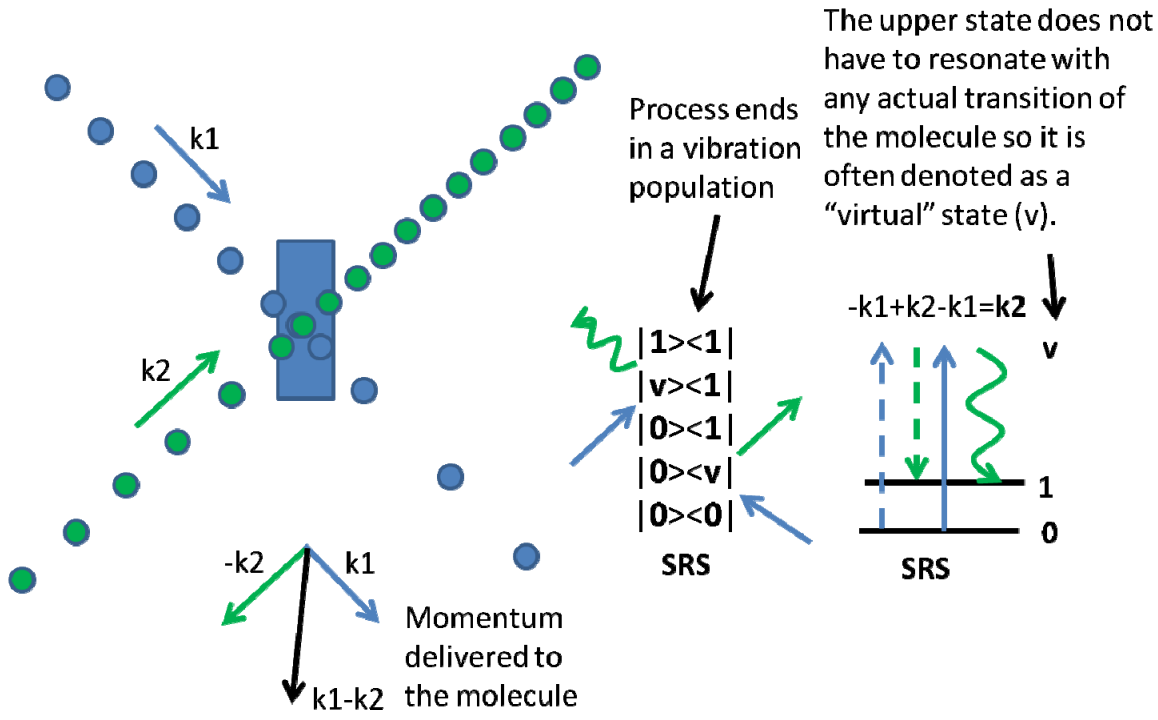

Figure 1

In the simplest way stimulated Raman scattering (SRS) can be viewed as an exchange of a photon between two fields of non-equal frequency with a particular molecular system serving as a resonator. The field of the higher frequency is absorbed and the field of the lower frequency is amplified. The excess energy and momentum is dumped into the molecule. Both the wave mixing energy level diagram and the double sided Feynman diagram for the process are presented.

This property is illustrated in figure 1 both by means of a double sided Feynman diagram and the corresponding wave mixing energy level diagram (WMEL). The multidimensional Raman spectroscopies are based on this property of the SRS process that results in vibrational state population. In the recently investigated time domain Femtosecond stimulated Raman spectroscopy (2D-FSRS)(14, 16) a third ultra short pulse (impulsive pump) is applied prior to recording of FSRS spectra. This pulse (when sufficiently spectrally broad and temporally compressed) induces so-called “impulsive stimulated Raman scattering” which means a special type of FSRS where the pulse acts as the Raman pump and the Probe at the same time. This leads to the simultaneous excitation of all Raman active transitions within the pulse spectral bandwidth (ΔE between the longest and shortest pulse wavelength). For a 15 fs short pulse it means vibrational (and rotational) modes from 0-1500 cm^{-1}, for 10 fs pulse vibrations up till 3000 cm^{-1}. The coherent oscillations in the FSRS spectra are then recorded as function of an impulsive pump - probe delay. Their Fourier transform yields the 2D spectra the same way as it does in all the time domain 2D techniques.

Principle of the frequency domain FSRS – experimental approach

A natural way to perform frequency domain 2D-FSRS would be to use two narrowband pulses prior to recording of the FSRS spectra. This would lead to excitation of a selected vibrational band via the SRS process between the pulses defined by the frequency difference between the fields (7). This is a four-pulse experiment (figure 2).

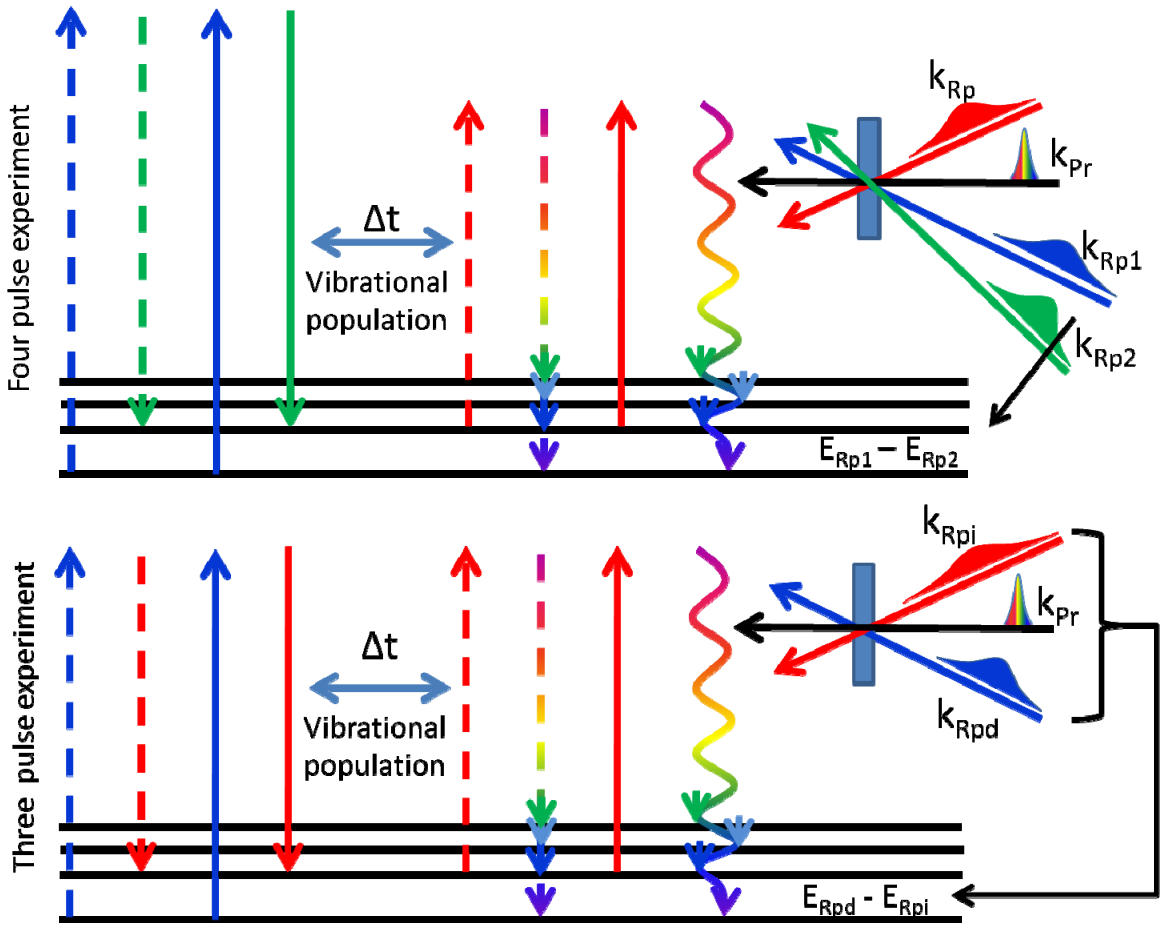

Figure 2

The most natural way of performing a frequency-domain 2D Raman experiment is to use one SRS process to selectively pump a vibration by a pair of narrowband pulses (Rp1 and Rp2) and subsequently probe the system by standard FSRS using one Rp and one Pr pulse. This is a four-pulse experiment where the signal is linear in all involved pulses. An alternative is to mediate the same process by only three pulses where one of them (Rpi) act both in the excitation and the detection. The signal should then be quadratic in the Rpi intensity. This type of experiment is explored in this work.

However, an interesting option exists because the Rp pulse is spectrally narrow enough that its temporal envelope spans the times far before the Pr pulse. An excitation then can be triggered just by a one additional narrowband pulse applied before the Pr pulse. The Rp pulse then would act both in excitation and detection of Raman modes. This is illustrated in figure 2 via an experimental scheme and WMEL diagram. The 3PFD2D-FSRS experiment is a 2D experiment derived from the standard steady state FSRS experiment by including only one additional pulse in a similar way as it does in the time domain 2D-FSRS experiment (14). The only difference is that while in time domain 2D-FSRS a third pulse is short in time, broad in spectra and scanned over time, in 3PFD2D-FSRS a third pulse is temporally long, spectrally narrow and scanned over wavelengths. The 3PFD2D-FSRS experiment can be viewed as a FSRS experiment performed with two Rp pulses acting at the same time. From now the Rp pulse with the higher energy will be denoted as the Rpd (from drudge, because it is going to be scanned) and the one with a smaller energy, expected to act both in excitation and detection, the Rpi (from idler, because it is going to stay at the same frequency). The SRS process then can happen not only between the Rp and Pr pulses but also between Rpi and Rpd pulses. Because Rpi and Rpd are both spectrally very narrow, the Raman interaction is restricted to the conditions when the Rpd-Rpi energy difference matches some Raman active transition of the sample. This is illustrated in figure 2. The scanning of the Rpd pulse wavelength starting from Rpi wavelength towards the shorter wavelengths is then a systematic scan over the excited vibrational states of the system. Application of the broadband femtosecond continuum results in recording of FSRS spectra from both of the Rp pulses, but while the Raman spectrum originating in Rpi pulse is fixed in terms of wavelength the Raman scattering from the Rpd pulse slides together with the scan of the Rpd pulse over the wavelengths. This is described in figure 3. A more thorough discussion of the underling mechanism forming the 2D signal is in the following paragraph. Certainly there is not just one but multiple “self matching” 8-wave mixing (figure 2) and 6-wave mixing (figure S1 in supplementary information) processes that involve interaction of the sample with all the three applied pulses and should result in photons scattered in the Pr pulse direction. As the spectrally narrow picosecond Rpi and Rpd pulses have about 2 ps long overlap in time (quite comparable with a vibration decoherence times and more than 100 times longer than the period of a typical vibrational coherence) the uncertainty in timing of interactions responsible for initiation of vibrational coherences is rather high. For this reason it is expected that the dominant signal would be a population formation via the process described in the Figure 2. The systematic scan of the Rpd pulse wavelength, coupled with the recording of the Raman spectra from the Rpi pulse then yields a matrix which should reflect the connectivity (coupling) among the vibrational modes within the system. This data we call Three Pulse Frequency Domain Two Dimensional Femtosecond Stimulated Raman spectroscopy (3PFD2D-FSRS).

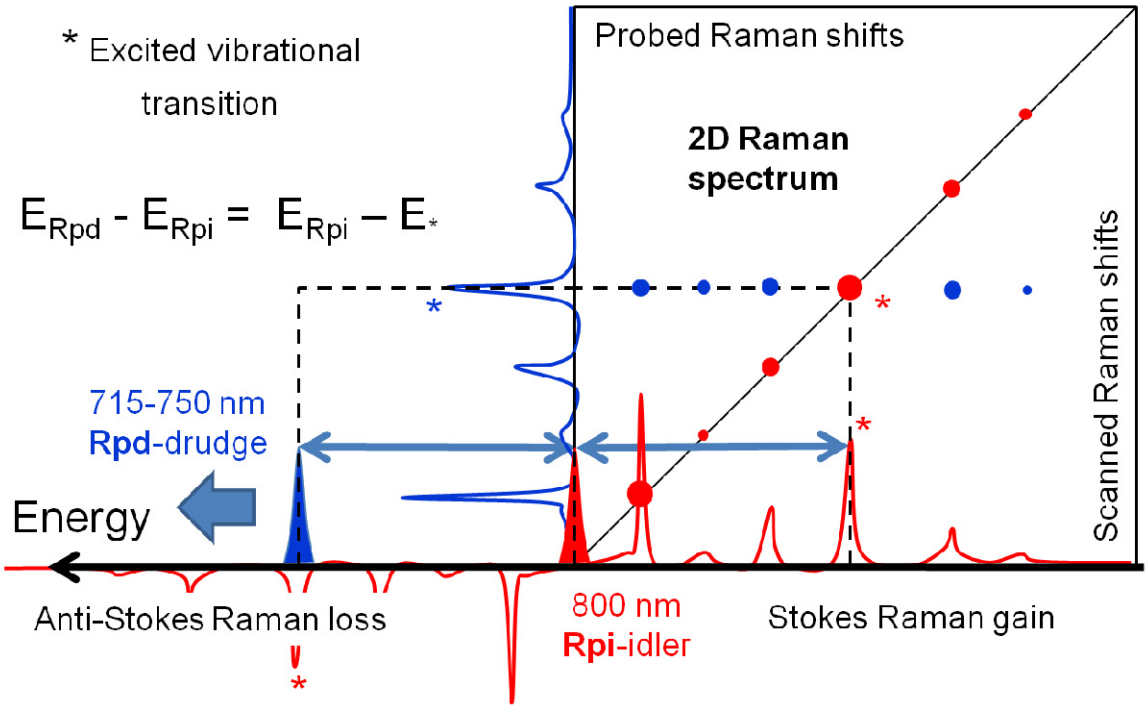

Figure 3

Experimental principle of 3PFD2D-FSRS

In 3PFD2D-FSRS, a standard FSRS experiment is performed but with one extra Raman pumps pulse. While one of pump pulses (for distinction called Rpi) is applied all the time at the same wavelength, the other (called Rpd) is scanned towards the higher energies (shorter wavelengths). When the Rpi – Rpd energy difference matches a certain Raman transition of the studied system, this transition is selectively excited via stimulated Raman process. This selective excitation of the vibration is manifested in standard FSRS spectra recorded through interaction of the Rpi and Pr pulses. A systematic scan over Rpd – Rpi spectral energy difference forms the 2D spectrum. Note that while the Rpd pulse role is merely for excitation, the Rpi pulse acts both in excitation (mixed with Rpd) and detection process (mixed with probe). The expected eight wave mixing mechanism is described in figure 2.

Principle of frequency domain FSRS – underlying mechanism

To our best knowledge, the first theoretical attempt to investigate a similar type of frequency domain 2D Raman experiment was proposed in 1997 by Cho and coworkers (202) and denoted as COTRAS (coherent 2D Raman scattering), with very little further

development (218, 219). In that work it was proposed that at least three different fields are required to perform the experiment, which was suggested as a "non self matching" transient grating type of experiment performed with 3 noncollinear spectrally narrow pulses and detected in the 4th direction defined by phase matching angle $3k_1 - k_2 - k_3$ for the corresponding wave vectors of applied pulses. Our approach is fundamentally similar, however with the crucial difference that a white light continuum is used as a third field and only the self matching interactions emitted in the white light probe field direction are recorded. In COTRAS it was suggested to record a 2D signal from a 6-wave mixing process which seems to be the most natural way. However, our approach is expected to follow rather an 8-wave mixing process. Some six wave mixing processes can potentially generate a self-heterodyned signal in our experimental configuration (see figure S1 in supplementary information), but none of them emits the signal into the Stokes region of the signal originating in the Rpi field: The six wave mixing process such as the one depicted in the supplementary figure S1 emits the signal into the Rpd originating Stokes region and may hence be excluded from the spectral detection window. Additionally, all six-wave mixing processes produce a 2D signal based on at least one double-vibrational transition which is in the ideal case not permitted for symmetry reasons (harmonic approximation). Also in frequency domain 2D IR spectroscopy (which is an analogy of the presented Raman technique) there are typically no cross peaks observed from the pathways that has a coherence as an intermediate state (212). Because of these reasons our 2D signal is expected to be dominated by an 8-wave mixing process forming a vibrational population as an intermediate state such as the one depicted in figure 2, despite it formally represents a process of a higher nonlinearity than a 6-wave mixing process.

Test experiment

The 3PFD2D-FSRS spectra acquisition was tested on a solution of β-carotene molecules dissolved in THF. The Rpi pulse was centered at 804.4 nm while the Rpd pulse was scanned in roughly 6 cm^{-1} steps over the region from 752 nm to 710 nm in order to record the 2D spectra in the square region between 860 cm^{-1} and 1650 cm^{-1} where the FSRS spectra of the system were continuously recorded. The spectrally resolved Pr intensity was measured synchronized with the chopping of Rpi and Rpd pulses with different frequencies so the Rpi-Pr, Rpd-Pr, and Rpi-Rpd-Pr signals were recorded simultaneously as a logarithm of the probe pulse intensity change induced by each of these pulse sequences (92, 186). The 2D spectra were produced as (Rpi-Rpd-Pr) – (Rpi-Pr) – (Rpd-Pr) difference signal in order to extract the 2D signal from the 1D four wave mixing process (processes where only one of the Raman pulses interacted with the probed molecule). Unfortunately, the overall amplitude of the FSRS signal from the Rpi significantly decreased (in our experiment by 30%) in conditions when the Rpd pulse was applied. This probably originates in the inner filter effects (220) and other phenomena associated with the strong field intensities inside of the sample where

both the pulses were applied. Baseline problems are very peculiar of FSRS experiments (9) and reach beyond the scope of this paper. An ad-hoc scaling of signals was applied to (Rpi-Pr) and (Rpd-Pr) signals prior to their subtraction. The scaling constants were chosen by minimization of the (Rpi-Rpd-Pr) – k_1 x (Rpi-Pr) – k_2 x (Rpd-Pr) signal at the off-resonant Rpi-Rpd energy shifts. This approach is based on the assumption that when the Rpd-Rpi energy difference is not matching any Raman transition of the system, no 2D signals are expected. One pair of constants (k_1 and k_2) was applied to the entire data set producing an almost flat signal for all off-resonant excitations, but giving signal in all the resonant excitations. This observation implies at least a partial validity of the applied data treatment approach. The extracted spectra still suffered from moderate baseline problems (narrowband lines were superposed on a broadband slowly varying baseline comparable in magnitude with recorded narrow peaks) so all the spectra were straighten by fitting a third order polynomial in order to straighten the baseline. The 2D spectra extracted by the described process are displayed in figure 4.

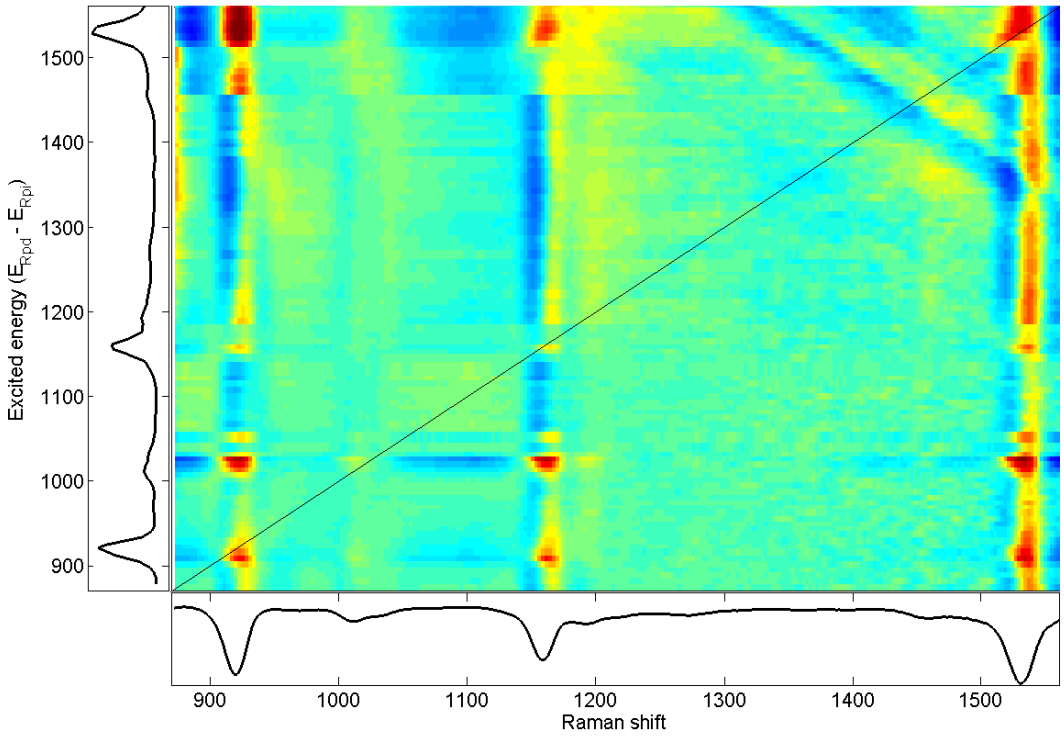

Figure 4

3PFD2D-FSRS spectra of β-carotene dissolved in THF recorded via the experiment described in figure 1. The horizontal axis represents FSRS spectra from the Rpi pulse, the vertical axis is a result of scanning of Rpd pulse. It can be clearly seen that tuning of the Rpd – Rpi shift into resonance with the Raman transitions of the sample leads to clear 2D signals manifested mostly by dispersive peaks in the probed (horizontal) dimension (see figure 5 and supporting figure S2 for the selected traces).

Several sharp steps in the data (manifested most notably as sharp horizontal edges at 1450 and 1510 cm^{-1}) result from experimental set-up optimization during the experiment. The anti-diagonal lines in the right upper corner are residual of high-frequency FSRS solvent signals (2940 cm^{-1} and 2875 cm^{-1}) stimulated from Rpd pulse. The color scale was adjusted in favor of resolving fine structures. For the actual magnitudes of prominent peaks see figure 5 and supplementary figure S2.

The 2D spectra displayed clear on- and off-diagonal peaks at Raman active vibration modes of the sample (see figure 4 for the entire 2D matrix and figure 5 for details of excitation of 1005 cm^{-1} methyl rock of β-carotene (221, 222)). Despite probably a significant portion of a nonspecific amplification of ground state FSRS in the 2D signal (see the Discussion for possible interpretation) 2D peaks have a strongly dispersive shape (negative side bands at the low energy tails of ground state Raman peaks), characteristic for 2D signals in 2D IR spectroscopy (figure 5) most probably originating in anharmonic shift, as the driven oscillator follows the driving force with a phase shift (14-16).

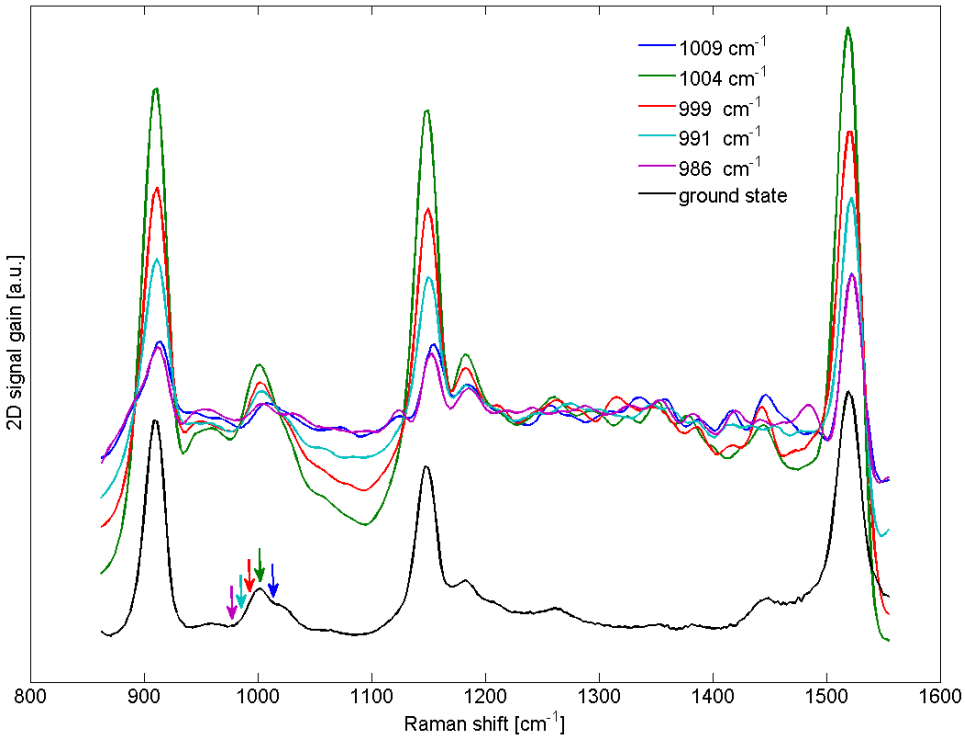

Figure 5

Comparison of static FSRS spectra of a β-carotene solution in THF with traces from the 3PFD2D-FSRS acquired after sliding excitation frequency over the 1005 cm^{-1} methyl rock mode of β-carotene. Graphs record 2D spectra in roughly 6 cm^{-1} steps. Approaching of the resonance can be distinguished by changes in amplitudes of the 2D signal at ground state signal frequencies and by formation of negative sidebands, probably originating in anharmonic coupling of modes.

The appearance of newly formed bands at spectral Raman shifts clearly out of the ground state signal regions is questionable and was not convincingly observed, however, the overall structure of 2D spectra including relative amplitudes of peaks is clearly different for various excited Raman modes. See supporting figure S2 for comparison of 2D spectra after excitation of various Raman transitions. This strongly implies that the recorded 2D spectra at least to a substantial degree reflect connectivity and coupling within the system. In case that the 2D signals would originate from the third order cascading processes the relive structure of signal (mutual peak amplitudes and shapes) would be identical for all excitations. However the interpretation of 3PFD2D-FSRS peak shapes and amplitudes waits for a theoretical development in order to extract the coupling effects out of all the other effects associated with application of Rpi and Rpd at the same time.

In the right upper corner of the 2D spectra in figure 4 we can see a set of antidiagonal lines (see also the blue line in supporting figure S2). This is a parasite FSRS from 2875 cm^{-1} and 2940 cm^{-1} solvent (THF) lines (191) scattered from the Rpd pulse. These prominent bands are strongly suppressed as a part of (Rpi-Rpd-Pr) – k_1 x (Rpi-Pr) – k_2 x (Rpd-Pr) baseline subtraction procedure but do not entirely vanish, partially also because the spectra from the Rpd pulse are expected to manifest a fraction of spectral anharmonic energy shifts and other 6- and 8-wave mixing phenomena similar to the Rpi originating signal. However, this Rpd signal does not overcome the actual 2D spectra from the Rpi pulse in terms of intensity. It is partially the price to pay for the fact that Rpi pulse plays the role both in exciting and probing Raman modes and the 2D Raman signals can be recorded with three pulses only. This tight configuration with the limited degrees of freedom strictly defines the spectral position of the Rpd pulse in respect to Rpi in order to excite the selected transition. In frequency domain experiments using more pulses (as it was proposed in past (207)) this problem can be in principle avoided. The issue of background signals originating in Rpd-probe FSRS signal will be treated more thoroughly in the Discussion section.

It is clear that the experiments produced 2D spectra with diagonal and off-diagonal peaks that most likely result from anharmonic coupling, and these peaks cannot be easily interpreted as a mere nonselective amplification of Raman spectra. Figure S2 in supporting information displays other selected slices from the 2D spectra normalized on the carotenoid peak at 1157 cm^{-1} in order to highlight the variation in mutual peak amplitudes and shapes for the different excited vibrations. These observations lead us to believe that we conducted the first successful frequency-domain stimulated Raman experiment in which a coupling of vibration modes was recorded..

Discussion

Comparison with similar methods

The essential advantage of 3PFD2D-FSRS as compared to time domain Raman techniques and 2D IR is practically an unrestricted range in which the 2D Raman spectra can be collected within a single experiment. While time domain 2D-FSRS has trouble to excite the high energy vibrations dealing with ultra short pulses of less there 15 fs, 2D IR spectroscopy is difficult to be applied out of the typical "fingerprint region" for technical restrictions to both the pulse generation and detection. It is quite easy to prepare Rpi and Rpd pulses of an arbitrary energy shift in 0-4000 cm^{-1} regime(186, 187, 223). The overlap of the 2D signal with Rpd parasite can be the issue at certain configurations, but this issue will be probably suppressed by experimental configuration with high Rpi and low Rpd intensity (see "pulse intensities" paragraph below). A scan over the wavelengths also does not require the delicate interferometric stability essential for recording of coherent beats in the time domain experiment. Given the possibility to work in the convenient visible or near IR region and the potential freedom in choice of Rpi and Rpd wavelengths to match the sample requirements, an approach such as the described 3PFD2D-FSRS experiments represents a reasonable candidate for a very robust experimental 2D vibrational technique, especially if the notorious FSRS baseline problems (8, 9) will eventually be sorted out. In our case we generated Rpi pulse by spectral filtration of the direct output from a Ti:sapphire amplifier, while the Rpd was taken as signal from picosecond collinear OPA. In fact there is a possibility to use certain types of picosecond OPA device for generation of both Rp pulses using signal and idler pulses generated simultaneously in OPA as Rpd and Rpi respectively. The Rpi would then drift together with Rpd but in a highly defined way that can be easily incorporated within the data processing.

The crucial drawback of 3PFD2D-FSRS most probably hides in the interpretation of measured signal which, at least in its current simple form, represents no match for highly selective signals generated by pulse sequences in advanced 2D-IR techniques. However, the complementary nature of Raman spectroscopy makes development of 2D Raman techniques important in order to study vibrations with low or zero transition dipole moment. Theoretical investigation of all the measured phenomena is probably a formidable task and it is not the objective of this paper. The following paragraphs attempt to briefly analyze the main actual or potential problems encountered during the realization of the 3PFD2D-FSRS experiment.

Baseline definition and signal normalization

An important unresolved issue is the baseline problem. As mentioned above, the 2D spectra required phenomenological scaling of subtracted signals and fitting of a 3rd order polynomial in order to achieve a signal consisting of sharp peaks on a flat base. Baseline problems strangle FSRS spectroscopy in general from its very beginning (8, 188). However there is no implication that it would not be possible to find a robust solution combining wavelength and amplitude modulation (9, 220). In general, the baseline problems encountered in the presented experiment were rather moderate in comparison to what is regularly observed in other FSRS experiments where a 3rd order polynomial was usually insufficient in order to remove the broadband background (100, 220). In practice, the acquisition of 2D spectra is expected to be synchronized with specific photo activation of a studied sample. In this case the relative difference measurement between the 2D spectra of an activated and non-activated sample would be recorded rather than evolution of the absolute magnitude of 2D Raman spectra. This relative difference signal is expected to be less sensitive to normalization of components subtracted in order to acquire the 2D spectra but highly selective to genuine 2D coupling effects.

Interpretation of recorded signals

The crucial question of the proposed 3PFD2D-FSRS method is which Liouville pathways derived from perturbative expansion of a density matrix (5) significantly contribute to the recorded signal. In multi-pulse Raman experiments, there is a risk of generation of cascading signals which result in off-diagonal peaks carrying no actual information about the couplings within the studied system (14, 16, 224). In the frequency domain experiment only one vibration is excited at the same time so there is no risk that the signal would be globally overlapped with cascading signals as it is typical for time domain 2D-FSRS (14, 16, 17). We identified, however, one potential cascade-like process: the overall amplification of ground state Raman bands may be ascribed to a phenomenon we call a stimulated Raman cascade (SRS-cascade). Its expected mechanism is illustrated in figure 6. When Rpd and Rpi are tuned to match a resonance with any vibrational transition, the Rpi field is generated (gets amplified) and this field result in nonspecific amplification of FSRS stimulated from the Rpi pulse. However, this signal is expected to form solely a constant background signal and only at the location of ground state peaks. But in any way its elimination has to be resolved.

Another issue is the question whether the signal is spoiled by undesired four wave missing processes such as coherent antistokes Raman scattering (CARS) and coherent stokes Raman scattering (CSRS). We attempted recording of the 3PFD2D-FSRS matrix also in a collinear geometry (all the pulses were applied collinearly) where practically all processes are self matched. The result is depicted in supporting figure S3. The signal differs from the data

presented in figure 4 by a large amount of nonspecific broadband signal in resonant conditions and also by evident CSRS signal which is manifested as a wavy diagonal line in the data. The complete absence of these effects in the fully non collinear conditions suggests that in this case the signal is entirely free of signals of these nonspecific 1D signals. Presence of additional signals of complicated origin cannot be easily entirely excluded however the coupling signal does not seems to be overwhelmed by unknown effects.

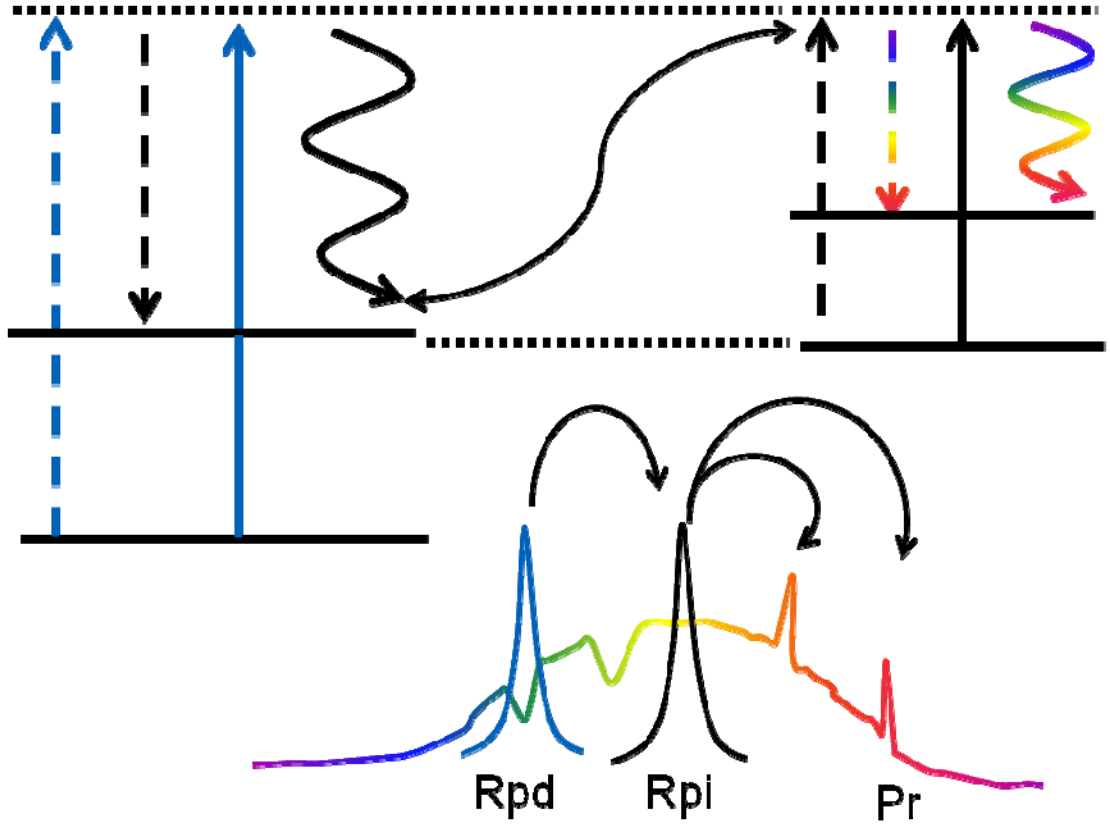

Figure 6

Cascade linking two SRS processes. When the Rpd pulse is tuned into the resonance with the Rpi pulse the Rpi field is amplified via SRS process. As a result, the entire 2D signal is amplified when Rpd and Rpi matches a resonance. However this signal does not provide any information about the couplings.

Pulse intensities

For a selected trace in the 2D spectra (namely the excitation of the 1157 cm^{-1} mode of β-carotene) a power series was performed in order to investigate the evolution of the 2D signal in respect to intensity of both Rpi and Rpd pulses. The spectra were recorded for the

Rpd intensity: 0.3 μJ, 0.6 μJ, and 1.1 μJ and Rpi intensity: 2 μJ, 2.5 μJ, 3.2 μJ. The results can be seen in supplementary figure S4. The scheme presented in figure 2 predicts that the recorded signal should be quadratic in the Rpi intensity while linear in the Rpd intensity. From the recorded data the signal does not seems to be linear in Rpd intensity but rather almost independent to intensity only manifesting a rapid change of the signal structure at the highest Rpd intensity. This implies that at these intensities saturation was approached. We chose the Rpd intensity quite high in order to generate the standard ground state four wave mixing FSRS signal stimulated from this Rpd pulse. This is principally not necessary and even not desirable as the FSRS signal from the Rpd pulse is a parasite on genuine 2D signals. The idea behind this configuration was observing the Rpd-originating FSRS signal as an evident reference over Rpd and Pr pulse overlaps during the long experiment as the 2D signal is not clear prior to data processing. For pioneering purposes we also deliberately aimed for saturation of the excitation to guarantee recording maximum number of both desirable and undesirable signals. Most probably, selective excitation of bands by the SRS process between two narrowband picosecond Rpd and Rpi fields can be saturated with much lower intensities that those required for Rp pulses in the standard FSRS experiment.

The situation is different in case of the Rpi pulse. An ideal quadratic dependence of signal on a Rpi intensity predics relative rise of the signal within the recorded power series in ratio 1/1.6/2.6 derived from the respective Rpi intensities 2/2.5/3.2 μJ as their quadrates forms ratio: 4/6.3/10.2 ~ 1/1.6/2.6. From the 2D signal amplitude in figure S3 it was derived the ratio 1/1.5/2.6 which is in an excellent agreement with the prediction. This means that the Rpi field contributes to the signal mostly with quadratic dependence and so the dominant source of the 2D signal can actually be the process like the one described in figure 2. Collective information gathered from varying both Rpd and Rpi intensity suggest that while the Rpi intensities have to be kept very high due to the quadratic contribution of Rpi field to the signal (perhaps more than we used) the Rpd intensity contributes linearly and it can be quite moderate, probably even significantly lower than it was in the experiments presented in this paper.

While the sample was very stable when the Rpd or Rpi pulse was applied only, their simultaneous action induced slow sample degradation. A possible explanation for this effect is two photon excitation of the β-carotene S1 state allowed by excessively high photon densities inside of the sample. Even though the fraction of excited β-carotene molecules was rather small (less than 1%, estimated from the known transient absorption amplitude of the carotenoid S1 state) these electronically excited and consequently in far-Red and near IR absorbing molecules were probably repumped by strong Rpd and Rpi intensities leading to charge separation (23, 28) and other damaging photo-degradation effects. This implies that 3PFD2D-FSRS is probably difficult to be applied in resonance with any transition of the sample and pulse intensities have to be kept safe from the two-photon effect. This should be possible as our power series investigation presented in the paragraph above implied that intensities we applied in our experiment were probably unnecessarily high. Also a relative

freedom in choice of absolute value of Rpd and Rpi wavelengths can be exploited in order to tune the experiment out of resonance with the electronic states absorption.

Outlook

Raman active vibrational modes are typically of a low or zero transition dipole moment. That means that Raman techniques are indispensable in their complementary nature to IR spectroscopy which senses only vibrations with a transition dipole moment. Thus, for highly symmetric molecules femtosecond Raman spectroscopy is the only tool capable to shed some light on their structural activity in vivo. For example the photo-physics of bound carotenoids (both in biological and artificial systems) was discovered to be dramatically more complex than in solution or vacuum(18-20, 28, 38, 189, 225). Resonance Raman spectroscopy was successfully used to shed some light on carotenoid conformations in light harvesting proteins(226), but still very little is known about the actual function-conformation relation of these important molecules as they give practically no signal in the IR. The proposed 2D Raman technique should offer sufficient combination of structural and temporal resolution in order to challenge such tasks. For this reason we believe that the approach is truly worth of further development. In photosynthetic light-harvesting systems, carotenoids play a key role in light harvesting and photo protection processes. The excited-state manifold of carotenoids bound to such systems is remarkably complex with optically forbidden states exhibiting unexpectedly strong couplings with nearby pigments. Hence, from 3D X-ray structures and advanced quantum chemical calculations alone the function of carotenoids is difficult to predict. Static and time-resolved 2D Raman may prove an important tool to accurately map out such interpigment interactions through their anharmonic vibrational couplings, and thus map the structural changes and spatial interactions.

Conclusions

We proposed en experimental approach for recording of frequency domain 2D Raman spectra using three pulses only, two spectrally narrow picosecond pulses and one spectrally broad femtosecond pulse. We called the approach “three-pulse frequency-domain two-dimensional femtosecond stimulated Raman spectroscopy” - 3PFD2D-FSRS. The crucial mechanism is a combined action of one picosecond pulse both in excitation and detection while one picosecond pulse acts only for excitation. Phenomenologically the procedure can be described as a standard FSRS experiment performed with two Raman pump pulses with a controllable mutual spectral gap. The expected mechanism is an 8-wave mixing process forming a vibrational population prior to recording of FSRS spectra. In a test experiment the 3PFD2D-FSRS spectra were recorded on β-carotene molecules dissolved in THF. Spectra

contained very clear diagonal and off diagonal peaks at the Raman shifts of main Raman active vibrational modes of the system and also out of the ground state vibration regions, proving a strong implication that the actual 2D signal originating in anharmonic coupling of vibration modes was recorded despite some contamination of signal from parasitic effects is expected. The experimental observations, technical aspects and data processing are discussed in this paper, which sets the stage for a detailed theoretical investigation of the method and presented results.

Acknowlegments

M.K. was supported by the Netherlands Foundation of Scientific Research (NWO) via the Council of Earth and Life Sciences (ALW). RvG was supported by an ERC Advanced Investigator grant. J.T.M.K was supported through the Chemical Sciences council of NWO (NWO-CW) through a VICI grant.

Supporting information

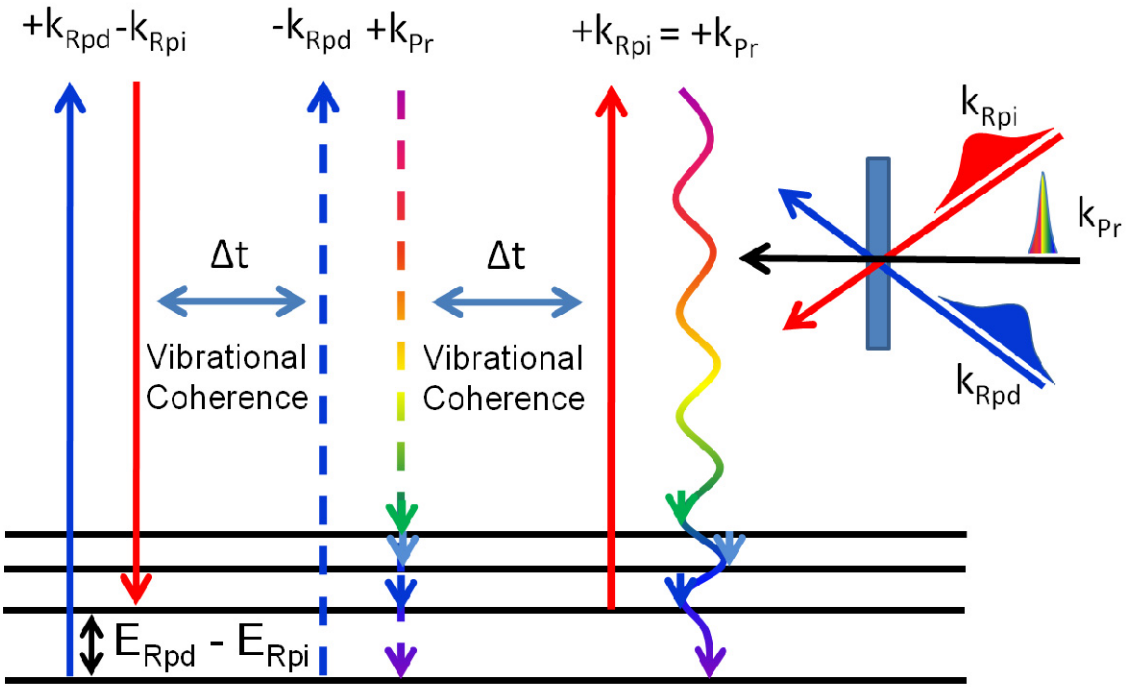

Figure S1

Wave mixing energy level diagram (WMEL) for the self matching six wave mixing process expected to contribute to the 3PFD2D-FSRS signal, however to a minor extent. The <bra| interactions are plotted as dashed arrow, while |ket> interactions are described by full arrows. Following the "vertex": Interaction with Rpd and Rpi field generates a vibrational coherence between the ground and excited vibrational state. Because of the narrow bandwidth of Rpd and Rpi pulses, this state can be excited in a highly selective way. The following interaction with Rpd and broadband Pr field generates a second vibrational coherence, this time between the initially excited and any other possible vibrational state (denoted by multiple arrows). The following interaction with Rpi field results in free induction decay leading to absorption of a Raman scattered photon in the probe field direction. Note that while the interaction with the probe field (k_{Pr}) is highly localized in time, the other interactions are quite delocalized in time as both Rpi and Rpd pulses are several picoseconds long. In consequence, when some vibration is selectively excited by combined action of Rpd – Rpi, the recorded signal represents an average over the broad distribution of vibrational coherence times Δt between excitation and emission of signal photons and so the signal is most probably averaged to zero.

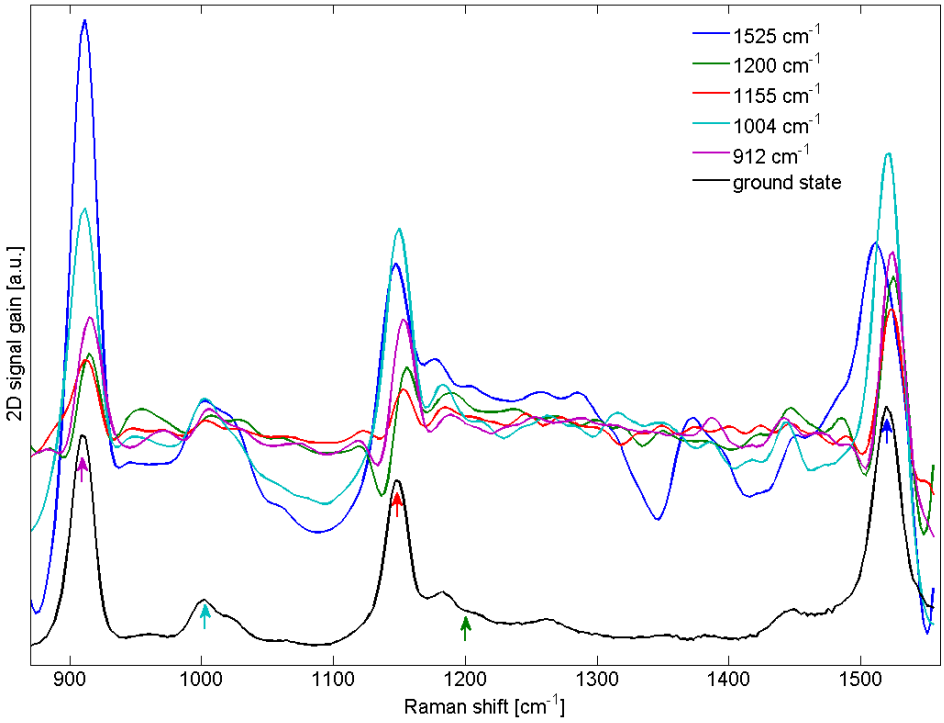

Figure S2

Comparison of selected traces from 3PFD2D-FSRS spectra for various excitations energies resonant with Raman transitions of the sample. It can be clearly seen that the relative amplitude of the peaks as well as their precise spectral position clearly differs for various excited Raman modes. This can be explained as various degree of coupling among different states.

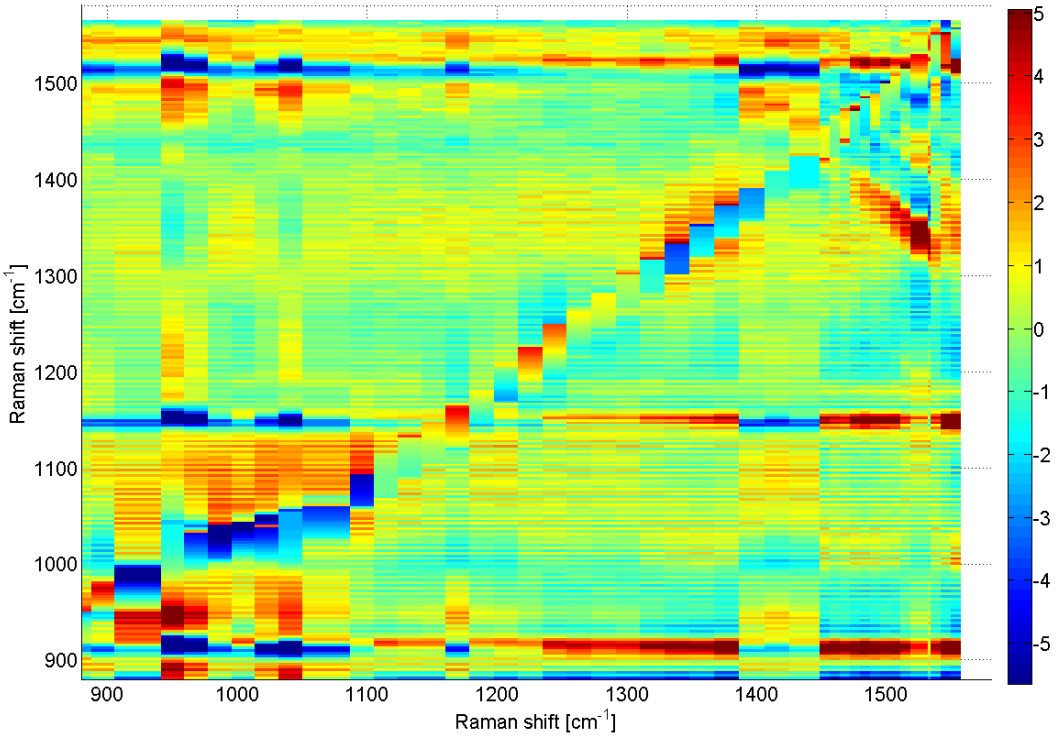

Figure S3

3PFD2D-FSRS spectra recorded in a similar experiment as the spectra depicted in figure 4 but in a fully collinear geometry (all pulses were applied collinearly). The cross peaks are way less pronounced and the diagonal is spoiled by a strong nonresonant CSRS signal.

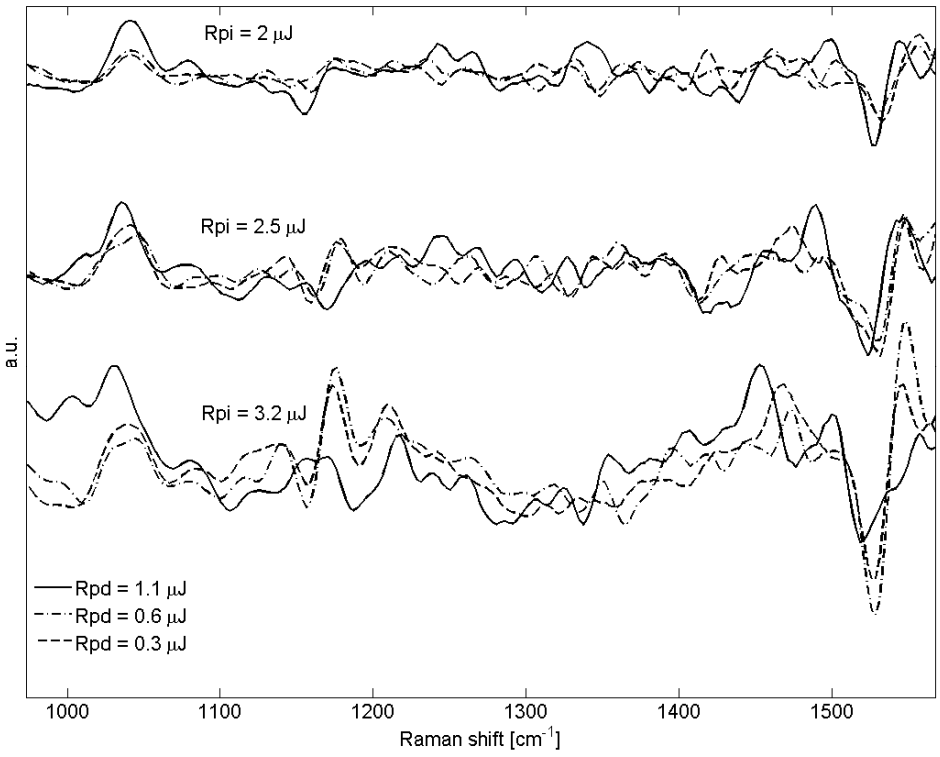

Figure S4

Power series investigating 3PFD2D-FSRS signal for 1157 cm^{-1} excitation for various intensities of Rpd and Rpi pulse. It can be seen that even for Rpd intensities as low as 300 nJ a clear 2D signal can be observed. 2D signal amplitude rises quadratically with Rpi intensity.

8. List of references

1. Strickland D & Mourou G (1985) Compreession of amplified chirped optical pulses. (Translated from English) *Opt. Commun.* 56(3):219-221 (in English).
2. van Stokkum IHM, Larsen DS, & van Grondelle R (2004) Global and target analysis of time-resolved spectra. *Biochimica Et Biophysica Acta* 1657(2-3):82-104.
3. Mullen KM & van Stokkum IHM (2007) TIMP: An R package for modeling multi-way spectroscopic measurements. *J. Stat. Softw.* 18(3).
4. Snellenburg JJ, Laptenok SP, Seger R, Mullen KM, & van Stokkum IHM (2012) Glotaran: A Java-Based Graphical User Interface for the R Package TIMP. (Translated from English) *J. Stat. Softw.* 49(3):1-22 (in English).
5. Mukamel S (1999) *Principles of Nonlinear Optical Spectroscopy* (Oxford University Press) (English) p 576.
6. Hamm P & Zanni MT (2011) *Concepts and Methods of 2D Infrared Spectroscopy* (Cambridge Unversity Press, Cambridge).
7. Baggen M, Exter Mv, & Lagendijk A (1987) Time-resolved stimulated Raman scattering in a diamond anvil cell. *The Journal of Chemical Physics* 86(4):2423-2427.
8. Kukura P, McCamant DW, & Mathies RA (2004) Femtosecond time-resolved stimulated Raman spectroscopy of the S-2 (1B(u)(+)) excited state of beta-carotene. (Translated from English) *Journal of Physical Chemistry A* 108(28):5921-5925 (in English).
9. Kloz M, Grondelle Rv, & Kennis JTM (2011) Wavelength-modulated femtosecond stimulated raman spectroscopy-approach towards automatic data processing. *Physical Chemistry Chemical Physics* 13(40):18123-18133.
10. McCamant DW (2011) Re-Evaluation of Rhodopsin's Relaxation Kinetics Determined from Femtosecond Stimulated Raman Lineshapes. *The Journal of Physical Chemistry B* 115(29):9299-9305.
11. Kukura P, McCamant DW, Yoon S, Wandschneider DB, & Mathies RA (2005) Structural Observation of the Primary Isomerization in Vision with Femtosecond-Stimulated Raman. *Science* 310(5750):1006-1009.
12. Zhigang S, J. L, Dong HZ, & Soo-Y. L (2008) Quantum theory of (femtosecond) time-resolved stimulated Raman scattering. *Journal of Chemical Physics* 128(14):144114.
13. Umapathy S, Mallick B, & Lakshmanna A (2010) Mode-dependent dispersion in Raman line shapes: observation and implications from ultrafast Raman loss spectroscopy. (Translated from English) *J Chem Phys* 133(2):024505 (in English).
14. Wilson KC, Lyons B, Mehlenbacher R, Sabatini R, & McCamant DW (2009) Two-dimensional femtosecond stimulated Raman spectroscopy: Observation of cascading Raman signals in acetonitrile. *The Journal of Chemical Physics* 131:214502.
15. Kukura P, Frontiera R, & Mathies RA (2006) Direct Observation of Anharmonic Coupling in the Time Domain with Femtosecond Stimulated Raman Scattering. *Physical Review Letters* 96(23):238303.
16. Mehlenbacher RD, Lyons B, Wilson KC, Du Y, & McCamant DW (2009) Theoretical analysis of anharmonic coupling and cascading Raman signals observed with femtosecond stimulated Raman spectroscopy. *The Journal of Chemical Physics* 131(24):244512.
17. Tewari NP & Sharma PK (1969) A THEORETICAL APPROACH TO CASCADE PHENOMENON IN SCATTERING WITH SPECIAL REFERENCE TO RAMAN EFFECT. (Translated from English) *Indian J. Pure Appl. Phys.* 7(7):516-& (in English).
18. Polivka T & Sundstrom V (2004) Ultrafast dynamics of carotenoid excited states - From solution to natural and artificial systems. *Chemical Reviews* 104(4):2021-2071.

19. Gradinaru CC*, et al.* (2001) An unusual pathway of excitation energy deactivation in carotenoids: Singlet-to-triplet conversion on an ultrafast timescale in a photosynthetic antenna. *Proc. Natl. Acad. Sci. U. S. A.* 98(5):2364-2369.
20. Polivka T & Sundstrom V (2009) Dark excited states of carotenoids: Consensus and controversy. (Translated from English) *Chem. Phys. Lett.* 477(1-3):1-11 (in English).
21. Papagiannakis E, Kennis JTM, van Stokkum IHM, Cogdell RJ, & van Grondelle R (2002) An alternative carotenoid-to-bacteriochlorophyll energy transfer pathway in photosynthetic light harvesting. *Proc. Natl. Acad. Sci. (USA)* 99(9):6017-6022.
22. Smith MB & Michl J (2010) Singlet Fission. (Translated from English) *Chemical Reviews* 110(11):6891-6936 (in English).
23. Holt NE*, et al.* (2005) Carotenoid Cation Formation and the Regulation of Photosynthetic Light Harvesting. *Science* 307(5708):433-436.
24. Ruban AV*, et al.* (2007) Identification of a mechanism of photoprotective energy dissipation in higher plants. *Nature* 450(7169):575-578.
25. Demmig-Adams B (1990) Carotenoids and photoprotection in plants: A role for the xanthophyll zeaxanthin. *Biochimica et Biophysica Acta (BBA) - Bioenergetics* 1020(1):1-24.
26. Berera R*, et al.* (2006) A simple artificial light-harvesting dyad as a model for excess energy dissipation in oxygenic photosynthesis. *Proc. Natl. Acad. Sci. U. S. A.* 103(14):5343-5348.
27. Berera R*, et al.* (2007) Energy transfer, excited-state deactivation, and exciplex formation in artificial caroteno-phthalocyanine light-harvesting antennas. *Journal of Physical Chemistry B* 111(24):6868-6877.
28. Kloz M*, et al.* (2011) Carotenoid Photoprotection in Artificial Photosynthetic Antennas. *J. Am. Chem. Soc.* 133(18):7007-7015.
29. Horton P, Ruban AV, & Walters RG (1996) Regulation of light harvesting in green plants. *Annual Review of Plant Physiology and Plant Molecular Biology* 47:655-684.
30. Niyogi KK (1999) Photoprotection revisited: Genetic and molecular approaches. *Annual Review of Plant Physiology and Plant Molecular Biology* 50:333-359.
31. Cogdell RJ, Monger TG, & Parson WW (1975) CAROTENOID TRIPLET-STATES IN REACTION CENTERS FROM RHODOPSEUDOMONAS-SPHAEROIDES AND RHODOSPIRILLUM-RUBRUM. *Biochimica Et Biophysica Acta* 408(3):189-199.
32. Truscott TG, Land EJ, & Sykes A (1973) IN-VITRO PHOTOCHEMISTRY OF BIOLOGICAL MOLECULES .3. ABSORPTION-SPECTRA, LIFETIMES AND RATES OF OXYGEN QUENCHING OF TRIPLET-STATES OF BETA-CAROTENE, RETINAL AND RELATED POLYENES. *Photochemistry and Photobiology* 17(1):43-51.
33. Ahn TK*, et al.* (2008) Architecture of a charge-transfer state regulating light harvesting in a plant antenna protein. *Science* 320(5877):794-797.
34. Amarie S*, et al.* (2007) Carotenoid radical cations as a probe for the molecular mechanism of nonphotochemical quenching in oxygenic photosynthesis. *Journal of Physical Chemistry B* 111(13):3481-3487.
35. Avenson TJ*, et al.* (2009) Lutein Can Act as a Switchable Charge Transfer Quencher in the CP26 Light-harvesting Complex. *Journal of Biological Chemistry* 284(5):2830-2835.
36. Avenson TJ*, et al.* (2008) Zeaxanthin radical cation formation in minor light-harvesting complexes of higher plant antenna. *Journal of Biological Chemistry* 283(6):3550-3558.
37. Berera R, van Grondelle R, & Kennis J (2009) Ultrafast transient absorption spectroscopy: principles and application to photosynthetic systems. *Photosynth. Res.* 101(2):105-118.
38. Bode S*, et al.* (2009) On the regulation of photosynthesis by excitonic interactions between carotenoids and chlorophylls. *Proc. Natl. Acad. Sci. U. S. A.* 106(30):12311-12316.
39. Standfuss R, van Scheltinga ACT, Lamborghini M, & Kuhlbrandt W (2005) Mechanisms of photoprotection and nonphotochemical quenching in pea light-harvesting complex at 2.5A resolution. *Embo Journal* 24(5):919-928.

40. Valkunas L, van Stokkum IHM, Berera R, & van Grondelle R (2009) Exciton migration and fluorescence quenching in LHCII aggregates: Target analysis using a simple nonlinear annihilation scheme. *Chemical Physics* 357(1-3):17-20.
41. Olaizola M, Laroche J, Kolber Z, & Falkowski PG (1994) NONPHOTOCHEMICAL FLUORESCENCE QUENCHING AND THE DIADINOXANTHIN CYCLE IN A MARINE DIATOM. (Translated from English) *Photosynth. Res.* 41(2):357-370 (in English).
42. Ruban AV*, et al.* (2004) The super-excess energy dissipation in diatom algae: comparative analysis with higher plants. *Photosynth. Res.* 82(2):165-175.
43. Lohr M & Wilhelm C (1999) Algae displaying the diadinoxanthin cycle also possess the violaxanthin cycle. *Proc. Natl. Acad. Sci. U. S. A.* 96(15):8784-8789.
44. Berera R*, et al.* (2009) A Mechanism of Energy Dissipation in Cyanobacteria. *Biophysical Journal* 96(6):2261-2267.
45. Wilson A, Boulay C, Wilde A, Kerfeld CA, & Kirilovsky D (2007) Light-induced energy dissipation in iron-starved cyanobacteria: Roles of OCP and IsiA proteins. *Plant Cell* 19(2):656-672.
46. Boulay C, Abasova L, Six C, Vass I, & Kirilovsky D (2008) Occurrence and function of the orange carotenoid protein in photoprotective mechanisms in various cyanobacteria. *Biochimica Et Biophysica Acta-Bioenergetics* 1777(10):1344-1354.
47. Wilson A*, et al.* (2008) A photoactive carotenoid protein acting as light intensity sensor. *Proc. Natl. Acad. Sci. U. S. A.* 105(33):12075-12080.
48. Zigmantas D*, et al.* (2004) Effect of a conjugated carbonyl group on the photophysical properties of carotenoids. *Physical Chemistry Chemical Physics* 6(11):3009-3016.
49. van Stokkum IHM*, et al.* (2009) Inter-pigment interactions in the peridinin chlorophyll protein studied by global and target analysis of time resolved absorption spectra. *Chemical Physics* 357(1-3):70-78.
50. Zigmantas D, Hiller RG, Sundstrom V, & Polivka T (2002) Carotenoid to chlorophyll energy transfer in the peridinin-chlorophyll-a-protein complex involves an intramolecular charge transfer state. *Proc. Natl. Acad. Sci. U. S. A.* 99(26):16760-16765.
51. Ruban AV, Lee PJ, Wentworth M, Young AJ, & Horton P (1999) Determination of the stoichiometry and strength of binding of xanthophylls to the photosystem II light harvesting complexes. *Journal of Biological Chemistry* 274(15):10458-10465.
52. Gust D*, et al.* (1992) TRIPLET AND SINGLET ENERGY-TRANSFER IN CAROTENE PORPHYRIN DYADS - ROLE OF THE LINKAGE BONDS. (Translated from English) *Journal of the American Chemical Society* 114(10):3590-3603 (in English).
53. Maya EM, Vazquez P, & Torres T (1999) Synthesis of alkynyl-linked phthalocyanine dyads: Push-pull homo- and heterodimetallic bisphthalocyaninato complexes. *Chemistry-a European Journal* 5(7):2004-2013.
54. Wolfe JP & Buchwald SL (2000) Scope and limitations of the Pd/BINAP-catalyzed amination of aryl bromides. *Journal of Organic Chemistry* 65(4):1144-1157.
55. Sytina OA*, et al.* (2008) Conformational changes in an ultrafast light-driven enzyme determine catalytic activity. *Nature* 456(7224):1001-U1089.
56. Bonetti C*, et al.* (2010) Identification of excited-state energy transfer and relaxation pathways in the peridinin-chlorophyll complex: an ultrafast mid-infrared study. *Physical Chemistry Chemical Physics* 12(32):9256-9266.
57. Bonetti C*, et al.* (2008) Hydrogen Bond Switching among Flavin and Amino Acid Side Chains in the BLUF Photoreceptor Observed by Ultrafast Infrared Spectroscopy. *Biophysical Journal* 95(10):4790-4802.
58. Kennis JTM & Groot ML (2007) Ultrafast spectroscopy of biological photoreceptors. *Current Opinion in Structural Biology* 17(5):623-630.

59. Toh KC, Stojkovic EA, van Stokkum IHM, Moffat K, & Kennis JTM (2010) Proton-transfer and hydrogen-bond interactions determine fluorescence quantum yield and photochemical efficiency of bacteriophytochrome. *Proc. Natl. Acad. Sci. U. S. A.* 107(20):9170-9175.
60. Kodis G*, et al.* (2004) Light harvesting and photoprotective functions of carotenoids in compact artificial photosynthetic antenna designs. *Journal of Physical Chemistry B* 108(1):414-425.
61. Savolainen J, van der Linden D, Dijkhuizen N, & Herek JL (2008) Characterizing the functional dynamics of zinc phthalocyanine from femtoseconds to nanoseconds. (Translated from English) *Journal of Photochemistry and Photobiology, A: Chemistry* 196(1):99-105 (in English).
62. Bishop SM, Beeby A, Parker AW, Foley MSC, & Phillips D (1995) THE PREPARATION AND PHOTOPHYSICAL MEASUREMENTS OF PERDEUTERO ZINC PHTHALOCYANINE. *Journal of Photochemistry and Photobiology A Chemistry* 90(1):39-44.
63. Jailaubekov AE, Song SH, Vengris M, Cogdell RJ, & Larsen DS (2011) Using narrowband excitation to confirm that the S* state in carotenoids is not a vibrationally-excited ground state species. *Chemical Physics Letters* 487(1-3):101-107.
64. Niedzwiedzki D*, et al.* (2007) Ultrafast dynamics and excited state spectra of open-chain carotenoids at room and low temperatures. (Translated from English) *Journal of Physical Chemistry B* 111(21):5984-5998 (in English).
65. Wohlleben W*, et al.* (2004) Pump-deplete-probe spectroscopy and the puzzle of carotenoid dark states. *Journal of Physical Chemistry B* 108(10):3320-3325.
66. Papagiannakis E*, et al.* (2003) Light Harvesting by Carotenoids Incorporated into the B850 Light-Harvesting Complex from Rhodobacter sphaeroides R-26.1: Excited-State Relaxation, Ultrafast Triplet Formation, and Energy Transfer to Bacteriochlorophyll. *Journal of Physical Chemistry B* 107(23):5642-5649.
67. Polívka T & Sundstrom V (2004) Ultrafast Dynamics of Carotenoid Excited States: From Solution to Natural and Artificial Systems. *Chem. Rev.* 104(4):2021-2072.
68. Billsten HH, Zigmantas D, Sundstrom V, & Polivka T (2002) Dynamics of vibrational relaxation in the S-1 state of carotenoids having 11 conjugated C=C bonds. *Chemical Physics Letters* 355(5-6):465-470.
69. de Weerd FL, van Stokkum IHM, & van Grondelle R (2002) Subpicosecond dynamics in the excited state absorption of all-trans-beta-Carotene. *Chemical Physics Letters* 354(1-2):38-43.
70. Andersson PO, Bachilo SM, Chen R-L, & Gillbro T (1995) Solvent and Temperature Effects on Dual Fluorescence in a Series of Carotenes. Energy Gap Dependence of the Internal Conversion Rate. *ChemInform* 99(44):16199-16209.
71. van Amerongen H & van Grondelle R (2000) Understanding the Energy Transfer Function of LHCII, the Major Light-Harvesting Complex of Green Plantsâ€ *Journal of Physical Chemistry B* 105(3):604-617.
72. Van Amerongen H, Valkunas L, & Van Grondelle R (2000) *Photosynthetic Excitons* (World Scientific Publisher Co., Singapore).
73. Walla PJ, Linden PA, Hsu CP, Scholes GD, & Fleming GR (2000) Femtosecond dynamics of the forbidden carotenoid S-1 state in light-harvesting complexes of purple bacteria observed after two-photon excitation. *Proc. Natl. Acad. Sci. U. S. A.* 97(20):10808-10813.
74. Walla PJ, Linden PA, Ohta K, & Fleming GR (2002) Excited-state kinetics of the carotenoid S-1 state in LHC II and two-photon excitation spectra of lutein and beta-carotene in solution: Efficient car S-1 -> Chl electronic energy transfer via hot S-1 states? *Journal of Physical Chemistry A* 106(10):1909-1916.
75. Walla PJ, Yom J, Krueger BP, & Fleming GR (2000) Two-photon excitation spectrum of light-harvesting complex II and fluorescence upconversion after one- and two-photon excitation of the carotenoids. *Journal of Physical Chemistry B* 104(19):4799-4806.

76. Zhang JP*, et al.* (2000) Mechanism of the carotenoid-to-bacteriochlorophyll energy transfer via the S-1 state in the LH2 complexes from purple bacteria. (Translated from English) *Journal of Physical Chemistry B* 104(15):3683-3691 (in English).
77. Krueger BP, Scholes GD, & Fleming GR (1998) Calculation of Couplings and Energy-Transfer Pathways between the Pigments of LH2 by the ab Initio Transition Density Cube Method. *Journal of Physical Chemistry B* 102(27):5378-5386.
78. Frahmcke JS & Walla PJ (2006) Coulombic couplings between pigments in the major light-harvesting complex LHC II calculated by the transition density cube method. *Chemical Physics Letters* 430(4-6):397-403.
79. Hsu CP, Walla PJ, Head-Gordon M, & Fleming GR (2001) The role of the S-1 state of carotenoids in photosynthetic energy transfer: The light-harvesting complex II of purple bacteria. *Journal of Physical Chemistry B* 105(44):11016-11025.
80. Damjanovic A, Ritz T, & Schulten K (1999) Energy transfer between carotenoids and bacteriochlorophylls in light-harvesting complex II of purple bacteria. *Physical Review E* 59(3):3293-3311.
81. Palacios RE*, et al.* (2006) Tetrapyrrole singlet excited state quenching by carotenoids in an artificial photosynthetic antenna. *J. Phys. Chem. B* 110(50):25411-25420.
82. Fuciman M*, et al.* (2010) Excited state properties of aryl carotenoids. *Physical Chemistry Chemical Physics* 12(13):3112-3120.
83. Takamitsu F, Shigetsugu H, & Nagao K (2005) Deformed Phthalocyanines: Synthesis and Characterization of Zinc Phthalocyanines Bearing Phenyl Substituents at the 1-, 4-, 8-, 11-, 15-, 18-, 22-, and/or 25-Positions. *Chemistry--A European Journal* 11(18):5205-5216.
84. Getoff N (1999) Radical anion of [beta]-carotene studied by pulse radiolysis in ethanol-water and tert-butanol-water mixtures. *Radiation Physics and Chemistry* 55(4):395-398.
85. Nyokong T, Gasyna Z, & Stillman MJ (1987) Phthalocyanine .pi.-cation-radical species: photochemical and electrochemical preparation of [ZnPc(-1).+ in solution. *Inorganic Chemistry* 26(4):548-553.
86. Fungo F*, et al.* (2003) Correlation of fluorescence quenching in carotenoporphyrin dyads with the energy of intramolecular charge transfer states. Effect of the number of conjugated double bonds of the carotenoid moiety. *Physical Chemistry Chemical Physics* 5(3):469-475.
87. Fungo F*, et al.* (2001) Photoelectrochemistry of a pigment used in artificial photosynthesis: An anilinocarotenoid. *Journal of Physical Chemistry B* 105(21):4783-4790.
88. Visoly-Fisher I*, et al.* (2006) Conductance of a biomolecular wire. *Proc. Natl. Acad. Sci. U. S. A.* 103(23):8686-8690.
89. Fukuzumi S*, et al.* (2008) Control of Photoinduced Electron Transfer in Zinc Phthalocyanineâ^'Perylenediimide Dyad and Triad by the Magnesium Ion. *Journal of Physical Chemistry A* 112(43):10744-10752.
90. Ogunsipe A & Nyokong T (2004) Effects of substituents and solvents on the photochemical properties of zinc phthalocyanine complexes and their protonated derivatives. *Journal of Molecular Structure* 689(1-2):89-97.
91. Kukura P, McCamant DW, & Mathies RA (2007) Femtosecond Stimulated Raman Spectroscopy. *Annual Review of Physical Chemistry* 58(1):461-488.
92. McCamant DW, Kukura P, Yoon S, & Mathies RA (2004) Femtosecond broadband stimulated Raman spectroscopy: Apparatus and methods. (Translated from English) *Rev. Sci. Instrum.* 75(11):4971-4980 (in English).
93. Shim S & Mathies RA (2008) Femtosecond Raman-induced Kerr effect spectroscopy. *Journal of Raman Spectroscopy* 39(11):1526-1530.
94. Weigel A & Ernsting NP (Excited Stilbene: Intramolecular Vibrational Redistribution and Solvation Studied by Femtosecond Stimulated Raman Spectroscopy. (Translated from English) *J. Phys. Chem. B* 114(23):7879-7893 (in English).

95. Frontiera RR & Mathies RA (2011) Femtosecond stimulated Raman spectroscopy. (Translated from English) *Laser Photon. Rev.* 5(1):102-113 (in English).
96. Mukamel S & Biggs JD (2011) Communication: Comment on the effective temporal and spectral resolution of impulsive stimulated Raman signals. *The Journal of Chemical Physics* 134(16):161101.
97. Fang C, Frontiera RR, Tran R, & Mathies RA (2009) Mapping GFP structure evolution during proton transfer with femtosecond Raman spectroscopy. *Nature* 462(7270):200-204.
98. Dasgupta J, Frontiera RR, Taylor KC, Lagarias JC, & Mathies RA (2009) Ultrafast excited-state isomerization in phytochrome revealed by femtosecond stimulated Raman spectroscopy. *Proc. Natl. Acad. Sci. U. S. A.* 106(6):1784-1789.
99. Shim S, Dasgupta J, & Mathies RA (2009) Femtosecond Time-Resolved Stimulated Raman Reveals the Birth of Bacteriorhodopsin's J and K Intermediates. *Journal of the American Chemical Society* 131(22):7592-7597.
100. Weigel A*, et al.* (2011) Femtosecond Stimulated Raman Spectroscopy of Flavin after Optical Excitation. *Journal of Physical Chemistry B* (115):3656–3680.
101. Larsen DS*, et al.* (2003) Excited state dynamics of [beta]-carotene explored with dispersed multi-pulse transient absorption. *Chemical Physics Letters* 381(5-6):733-742.
102. McCamant DW, Kukura P, & Mathies RA (2003) Femtosecond Time-Resolved Stimulated Raman Spectroscopy: Application to the Ultrafast Internal Conversion in β-Carotene *Journal of Physical Chemistry A* 107(40):8208-8214.
103. Kennis JTM*, et al.* (2004) Uncovering the hidden ground state of green fluorescent protein. *Proc. Natl. Acad. Sci. U. S. A.* 101(52):17988-17993.
104. McCamant DW, Kukura P, & Mathies RA (2003) Femtosecond broadband stimulated Raman: A new approach for high-performance vibrational spectroscopy. (Translated from English) *Applied Spectroscopy* 57(11):1317-1323 (in English).
105. Zhang J-P, Skibsted LH, Fujii R, & Koyama Y (2001) Transient Absorption from the 1Bu+ State of All-trans-β-carotene Newly Identified in the Near-infrared Region. 73:219-222.
106. Cherepy NJ, Shreve AP, Moore LJ, Boxer SG, & Mathies RA (1997) Electronic and Nuclear Dynamics of the Accessory Bacteriochlorophylls in Bacterial Photosynthetic Reaction Centers from Resonance Raman Intensities. *Journal of Physical Chemistry B* 101(16):3250-3260.
107. Cherepy NJ, Shreve AP, Moore LJ, Boxer SG, & Mathies RA (1997) Temperature Dependence of the Qy Resonance Raman Spectra of Bacteriochlorophylls, the Primary Electron Donor, and Bacteriopheophytins in the Bacterial Photosynthetic Reaction Centerâ€ *Biochemistry* 36(28):8559-8566.
108. Bhattacharyya J, Ghosh S, & Arora BM (2005) Wavelength modulation spectroscopy using novel mechanical light chopper blade designs. *Review of Scientific Instruments* 76(8):083903-083903-083906.
109. Weiner AM (2000) Femtosecond pulse shaping using spatial light modulators. *Review of Scientific Instruments* 71(5):1929-1960.
110. Mallick B, Lakshmanna A, Radhalakshmi V, & Umapathy S (2008) Design and development of stimulated Raman spectroscopy apparatus using a femtosecond laser system. (Translated from English) *Current Science* 95(11):1551-1559 (in English).
111. Felinger A, Pasti L, & Dondi F (1990) Fourier analysis of multicomponent chromatograms. Theory and models. *Analytical Chemistry* 62(17):1846-1853.
112. Trzasko J & Manduca A (2009) Highly Undersampled Magnetic Resonance Image Reconstruction via Homotopic l0-Minimization. *IEEE Transactions on Medical Imaging* 28(1):106-121.
113. Shim S & Mathies RA (2008) Development of a Tunable Femtosecond Stimulated Raman Apparatus and Its Application to ß-Carotene. *Journal of Physical Chemistry B* 112(15):4826-4832.

114. Shreve AP, Trautman JK, Owens TG, & Albrecht AC (1991) Determination of the S2 lifetime of [beta]-carotene. *Chemical Physics Letters* 178(1):89-96.
115. Holt NE, Kennis JTM, & Fleming GR (2004) Femtosecond fluorescence upconversion studies of light harvesting by beta-carotene in oxygenic photosynthetic core proteins. *J. Phys. Chem. B* 108(49):19029-19035.
116. Macpherson AN & Gillbro T (1998) Solvent dependence of the ultrafast S-2-S-1 internal conversion rate of beta-carotene. (Translated from English) *Journal of Physical Chemistry A* 102(26):5049-5058 (in English).
117. Wasielewski MR & Kispert LD (1986) Direct measurement of the lowest excited singlet state lifetime of all-trans-[beta]-carotene and related carotenoids. *Chemical Physics Letters* 128(3):238-243.
118. Hayashi H, Noguchi T, Tasumi M, & Atkinson GH (1991) Vibrational spectroscopy of excited electronic states in carotenoids in vivo. Picosecond time-resolved resonance Raman scattering. (Translated from English) *Biophysical Journal* 60(1):252-260 (in English).
119. Hashimoto H & Koyama Y (1989) Raman spectra of all-trans-[beta]-carotene in the S1 and T1 states produced by direct photoexcitation. *Chemical Physics Letters* 163(2-3):251-256.
120. Hashimoto H & Koyama Y (1989) The C=C stretching Raman lines of [[beta]-carotene isomers in the S1 state as detected by pump-probe resonance Raman spectroscopy. *Chemical Physics Letters* 154(4):321-325.
121. Schmierer T, Bley F, Schaper K, & Gilch P (2010) The early processes in the photochemistry of ortho-nitrobenzyl acetate. *Journal of Photochemistry and Photobiology A: Chemistry* 217(2-3):363-368.
122. Zhang J-P*, et al.* (2001) The 1Bu-type singlet state of [beta]-carotene as a precursor of the radical cation found in chloroform solution by sub-picosecond time-resolved absorption spectroscopy. *Chemical Physics Letters* 348(3-4):235-241.
123. Lukes V, Christensson N, Milota F, Kauffmann HF, & Hauer J (2011) Electronic ground state conformers of β-carotene and their role in ultrafast spectroscopy. *Chemical Physics Letters* 506(1-3):122-127.
124. Hitchcock AP & Laposa JD (1975) Vibrational frequencies of toluene-d5. *Journal of Molecular Spectroscopy* 54(2):223-230.
125. Hopkins JB & Rentzepis PM (1986) Picosecond transient Raman spectroscopy of excited-state dynamics. *Chemical Physics Letters* 124(1):79-83.
126. Unser M & Aldroubi A (1996) A review of wavelets in biomedical applications. *IEE Proceedings. Nanobiotechnology* 84(4):626-638.
127. Monmayrant A & Chatel B (2004) New phase and amplitude high resolution pulse shaper. *Review of Scientific Instruments* 75(8):2668-2671.
128. Ohashi N*, et al.* (1996) The structures of S-0 spheroidene in the light-harvesting (LH2) complex and S-0 and T-1 spheroidene in the reaction center of Rhodobacter sphaeroides 2.4.1 as revealed by Raman spectroscopy. (Translated from English) *Biospectroscopy* 2(1):59-69 (in English).
129. Cogdell RJ & Frank HA (1987) HOW CAROTENOIDS FUNCTION IN PHOTOSYNTHETIC BACTERIA. (Translated from English) *Biochimica Et Biophysica Acta* 895(2):63-79 (in English).
130. Young AJ & Frank HA (1996) Energy transfer reactions involving carotenoids: Quenching of chlorophyll fluorescence. (Translated from English) *Journal of Photochemistry and Photobiology B* 36(1):3-15 (in English).
131. Koyama Y (1991) STRUCTURES AND FUNCTIONS OF CAROTENOIDS IN PHOTOSYNTHETIC SYSTEMS. (Translated from English) *Journal of Photochemistry and Photobiology B* 9(3-4):265-280 (in English).
132. Niyogi KK, Bjorkman O, & Grossman AR (1997) The roles of specific xanthophylls in photoprotection. (Translated from English) *Proc. Natl. Acad. Sci. U. S. A.* 94(25):14162-14167 (in English).

133. Walla PJ, Linden PA, Hsu CP, Scholes GD, & Fleming GR (2000) Femtosecond dynamics of the forbidden carotenoid S-1 state in light-harvesting complexes of purple bacteria observed after two-photon excitation. *Proceedings of the National Academy of Sciences (USA)* 97:10808-10813.
134. Zhang J-P*, et al.* (2000) Mechanism of the carotenoid-to-bacteriochlorophyll energy transfer via the S-1 state in the LH2 complexes from purple bacteria. *Journal of Physical Chemistry B* 104:3683-3691.
135. Gradinaru CC, van Stokkum IHM, Pascal AA, van Grondelle R, & van Amerongen H (2000) Identifying the pathways of energy transfer between carotenoids and chlorophylls in LHCII and CP29. A multicolor, femtosecond pump-probe study. *Journal of Physical Chemistry B* 104:9330-9342.
136. Shreve AP, Trautman JK, Frank HA, Owens TG, & Albrecht AC (1991) Femtosecond Energy-Transfer Processes in the B800-850 Light- Harvesting Complex of Rhodobacter-Sphaeroides-2.4.1. *Biochimica Et Biophysica Acta* 1058(2):280-288.
137. Gobets B*, et al.* (2001) Excitation energy transfer in dimeric light harvesting complex I: A combined streak-camera/fluorescence upconversion study. *J. Phys. Chem. B* 105(41):10132-10139.
138. Holt NE, Kennis JTM, Dall'Osto L, Bassi R, & Fleming GR (2003) Carotenoid to chlorophyll energy transfer in light harvesting complex II from Arabidopsis thaliana probed by femtosecond fluorescence upconversion. *Chem. Phys. Lett.* 379(3-4):305-313.
139. de Weerd FL, Kennis JTM, Dekker JP, & van Grondelle R (2003) beta-carotene to chlorophyll singlet energy transfer in the photosystem I core of Synechococcus elongatus proceeds via the beta-carotene S-2 and S-1 states. *J. Phys. Chem. B* 107(24):5995-6002.
140. Croce R, Muller MG, Bassi R, & Holzwarth AR (2001) Carotenoid-to-chlorophyll energy transfer in recombinant major light-harvesting complex (LHCII) of higher plants. I. Femtosecond transient absorption measurements. *Biophysical Journal* 80(2):901-915.
141. Peterman EJG, Monshouwer R, vanStokkum IHM, vanGrondelle R, & vanAmerongen H (1997) Ultrafast singlet excitation transfer from carotenoids to chlorophylls via different pathways in light-harvesting complex II of higher plants. *Chemical Physics Letters* 264(3-4):279-284.
142. Tavan P & Schulten K (1987) Electronic excitations in finite and infinite polyenes. *Physical Review B* 36(8):4337.
143. Frank HA*, et al.* (1994) PHOTOPHYSICS OF THE CAROTENOIDS ASSOCIATED WITH THE XANTHOPHYLL CYCLE IN PHOTOSYNTHESIS. (Translated from English) *Photosynth. Res.* 41(3):389-395 (in English).
144. Bautista JA*, et al.* (1999) Excited state properties of peridinin: Observation of a solvent dependence of the lowest excited singlet state lifetime and spectral behavior unique among carotenoids. *J. Phys. Chem. B* 103(41):8751-8758.
145. Niedzwiedzki DM*, et al.* (2009) Spectroscopic Investigation of Peridinin Analogues Having Different pi-Electron Conjugated Chain Lengths: Exploring the Nature of the Intramolecular Charge Transfer State. *J. Phys. Chem. B* 113(41):13604-13612.
146. Polivka T & Frank HA (2010) Molecular Factors Controlling Photosynthetic Light Harvesting by Carotenoids. *Accounts of Chemical Research* 43(8):1125-1134.
147. Alexandre MTA*, et al.* (2007) Triplet state dynamics in peridinin-chlorophyll-a-protein: A new pathway of photoprotection in LHCs? *Biophysical Journal* 93(6):2118-2128.
148. Gall A*, et al.* (2011) Molecular Adaptation of Photoprotection: Triplet States in Light-Harvesting Proteins. *Biophysical Journal* 101(4):934-942.
149. Shao Y*, et al.* (2006) Advances in methods and algorithms in a modern quantum chemistry program package. (Translated from English) *Physical Chemistry Chemical Physics* 8(27):3172-3191 (in English).

150. Dreuw A, Fleming GR, & Head-Gordon M (2003) Charge-transfer state as a possible signature of a zeaxanthin-chlorophyll dimer in the non-photochemical quenching process in green plants. (Translated from English) *Journal of Physical Chemistry B* 107(27):6500-6503 (in English).
151. Rademaker H, Hoff AJ, Vangrondelle R, & Duysens LNM (1980) CAROTENOID TRIPLET YIELDS IN NORMAL AND DEUTERATED RHODOSPIRILLUM-RUBRUM. (Translated from English) *Biochimica Et Biophysica Acta* 592(2):240-257 (in English).
152. Carbonera D*, et al.* (1998) EPR investigation of photoinduced radical pair formation and decay to a triplet state in a carotene-porphyrin-fullerene triad. (Translated from English) *Journal of the American Chemical Society* 120(18):4398-4405 (in English).
153. Osuka A*, et al.* (1993) SYNTHESIS AND PHOTOEXCITED-STATE DYNAMICS OF AROMATIC GROUP-BRIDGED CAROTENOID PORPHYRIN DYADS AND CAROTENOID PORPHYRIN PYROMELLITIMIDE TRIADS. (Translated from English) *Journal of the American Chemical Society* 115(21):9439-9452 (in English).
154. Kodis G*, et al.* (2003) Light Harvesting and Photoprotective Functions of Carotenoids in Compact Artificial Photosynthetic Antenna Designs. *Journal of Physical Chemistry B* 108(1):414-425.
155. Holt NE*, et al.* (2005) Carotenoid cation formation and the regulation of photosynthetic light harvesting. *Science* 307(5708):433-436.
156. Ahn TK*, et al.* (2008) Architecture of a charge-transfer state regulating light harvesting in a plant antenna protein. *Science* 320(5877):794-797.
157. Ruban AV*, et al.* (2007) Identification of a mechanism of photoprotective energy dissipation in higher plants. *Nature* 450(7169):575-U522.
158. Berera R, van Grondelle R, & Kennis JTM (2009) Ultrafast transient absorption spectroscopy: principles and application to photosynthetic systems. *Photosynth. Res.* 101(2-3):105-118.
159. Wilson A*, et al.* (2008) A photoactive carotenoid protein acting as light intensity sensor. *Proc. Natl. Acad. Sci. U. S. A.* 105(33):12075-12080.
160. Muller P, Li XP, & Niyogi KK (2001) Non-photochemical quenching. A response to excess light energy. (Translated from English) *Plant Physiology* 125(4):1558-1566 (in English).
161. Wilson A*, et al.* (2006) A soluble carotenoid protein involved in phycobilisome-related energy dissipation in cyanobacteria. *Plant Cell* 18(4):992-1007.
162. O'Regan B & Gratzel M (1991) A low-cost, high-efficiency solar cell based on dye-sensitized colloidal TiO2 films. *Nature* 353(6346):737-740.
163. Li G*, et al.* (2005) High-efficiency solution processable polymer photovoltaic cells by self-organization of polymer blends. *Nat Mater* 4(11):864-868.
164. Park SH*, et al.* (2009) Bulk heterojunction solar cells with internal quantum efficiency approaching 100%. *Nat Photon* 3(5):297-302.
165. Straight SD*, et al.* (2008) Self-regulation of photoinduced electron transfer by a molecular nonlinear transducer. *Nature Nanotechnology* 3(5):280-283.
166. Terazono Y*, et al.* (2011) Mimicking the Role of the Antenna in Photosynthetic Photoprotection. *J. Am. Chem. Soc.* 133(9):2916-2922.
167. Pang Y & Fleming GR (2010) Branching relaxation pathways from the hot S2 state of 80-apo-b-caroten-80-al. *Physical Chemistry Chemical Physics* 12(25):6782-6788.
168. Billsten HH*, et al.* (2005) Excited-State Processes in the Carotenoid Zeaxanthin after Excess Energy Excitation. *The Journal of Physical Chemistry A* 109(31):6852-6859.
169. Bonetti C*, et al.* (2009) The Role of Key Amino Acids in the Photoactivation Pathway of the Synechocystis Slr1694 BLUF Domain. *Biochemistry* 48(48):11458-11469.
170. van Stokkum IHM, Larsen DS, & van Grondelle R (2004) Global and target analysis of time-resolved spectra. *Biochimica Et Biophysica Acta-Bioenergetics* 1657(2-3):82-104.
171. Kosumi D*, et al.* (2009) The dependence of the ultrafast relaxation kinetics of the S-2 and S-1 states in beta-carotene homologs and lycopene on conjugation length studied by

femtosecond time-resolved absorption and Kerr-gate fluorescence spectroscopies. (Translated from English) *Journal of Chemical Physics* 130(21):8 (in English).
172. Jailaubekov AE, Song SH, Vengris M, Cogdell RJ, & Larsen DS (2010) Using narrowband excitation to confirm that the S* state in carotenoids is not a vibrationally-excited ground state species. *Chemical Physics Letters* 487(1-3):101-107.
173. Polivka T, Herek JL, Zigmantas D, Akerlund H-E, & Sundstrom V (1999) Direct observation of the (forbidden) S1 state in carotenoids. *Proc. Natl. Acad. Sci. U. S. A.* 96(9):4914-4917.
174. DeCoster B*, et al.* (1992) Low-lying electronic states of carotenoids. *Biochimica et Biophysica Acta* 1102(1):107-114.
175. Akimoto S, Yamazaki I, Takaichi S, & Mimuro M (1999) Excitation relaxation of carotenoids within the S-2 state probed by the femtosecond fluorescence up-conversion method. (Translated from English) *Chemical Physics Letters* 313(1-2):63-68 (in English).
176. Buckup T*, et al.* (2006) Pump-probe and pump-deplete-probe spectroscopies on carotenoids with N=9-15 conjugated bonds. (Translated from English) *J. Chem. Phys.* 125(19):7 (in English).
177. Wohlleben W, Buckup T, Herek JL, Cogdell RJ, & Motzkus M (2003) Multichannel carotenoid deactivation in photosynthetic light harvesting as identified by an evolutionary target analysis. *Biophysical Journal* 85(1):442-450.
178. Chynwat V & Frank HA (1995) The application of the energy gap law to the S1 energies and dynamics of carotenoids. *Chemical Physics* 194(2-3):237-244.
179. Hsu CP, Walla PJ, Head-Gordon M, & Fleming GR (2001) The role of the S(1) state of carotenoids in photosynthetic energy transfer: The light-harvesting complex II of purple bacteria. *J. Phys. Chem. B* 105(44):11016-11025.
180. Yoshizawa M & Kurosawa M (2000) Femtosecond time-resolved Raman spectroscopy using stimulated Raman scattering. (Translated from English) *Physical Review A* 61(1):art. no.-013808 (in English).
181. Lee S-Y, Zhang D, McCamant DW, Kukura P, & Mathies RA (2004) Theory of femtosecond stimulated Raman spectroscopy. *Journal of Chemical Physics* 121(8):3632-3642.
182. Yoon S*, et al.* (2005) Dependence of line shapes in femtosecond broadband stimulated Raman spectroscopy on pump-probe time delay. *Journal of Physical Chemistry* 122:024505.
183. Ploetz E, Marx B, & Gilch P (2011) Origin of spectral interferences in femtosecond stimulated Raman microscopy. *Journal of Raman Spectroscopy* 42(10):1875-1882.
184. Challa JR, Du Y, & McCamant DW (2012) Femtosecond Stimulated Raman Spectroscopy Using a Scanning Multichannel Technique. (Translated from English) *Applied Spectroscopy* 66(2):227-232 (in English).
185. Weigel A & Ernsting NP (2010) Excited Stilbene: Intramolecular Vibrational Redistribution and Solvation Studied by Femtosecond Stimulated Raman Spectroscopy. (Translated from English) *Journal of Physical Chemistry B* 114(23):7879-7893 (in English).
186. Laimgruber S, Schachenmayr H, Schmidt B, Zinth W, & Gilch P (2006) A femtosecond stimulated raman spectrograph for the near ultraviolet. (Translated from English) *Applied Physics B-Lasers and Optics* 85(4):557-564 (in English).
187. Co DT, Lockard JV, McCamant DW, & Wasielewski MR (2010) Narrow-bandwidth tunable picosecond pulses in the visible produced by noncollinear optical parametric amplification with a chirped blue pump. (Translated from English) *Applied Optics* 49(10):1880-1885 (in English).
188. Yoshizawa M, Aoki H, & Hashimoto H (2001) Vibrational relaxation of the 2A(g)(-) excited state in all-trans-beta-carotene obtained by femtosecond time-resolved Raman spectroscopy. (Translated from English) *Physical Review B* 63(18):4 (in English).
189. Kloz M*, et al.* (2012) New light-harvesting roles of hot and forbidden carotenoid states in artificial photosynthetic constructs. *Chemical Science*.

190. Getoff N (2000) Pulse Radiolysis Studies of ß-Carotene in Oxygenated DMSO Solution. Formation of ß-Carotene Radical Cation. *Radiation Research* 154(6):692-696.
191. Shurvell HF & Southby MC (1997) Infrared and Raman spectra of tetrahydrofuran hydroperoxide. *Vibrational Spectroscopy* 15(1):137-146.
192. Yan Y (1985) Impulsive stimulated scattering: General importance in femtosecond laser pulse interactions with matter, and spectroscopic applications. *Journal of Chemical Physics* 83(11):5391.
193. Wahlstrand JK, Merlin R, Li X, Cundiff ST, & Martinez OE (2005) Impulsive stimulated Raman scattering: comparison between phase-sensitive and spectrally filtered techniques. *Optics Letters* 30(8):926-928.
194. Lee S-Y & et al. (2006) Femtosecond Broadband Stimulated Raman Spectroscopy. *Journal of Physics: Conference Series* 28(1):36.
195. Bor Z, Szatmári S, & Müller A (1983) Picosecond pulse shortening by travelling wave amplified spontaneous emission. *Applied Physics B: Lasers and Optics* 32(3):101-104.
196. Ramos Á*, et al.* (2009) Lineshape analysis of stimulated Raman spectra of the near-nozzle region of free jet expansions. *Journal of Raman Spectroscopy* 40(9):1249-1256.
197. Haley LV & Koningstein JA (1983) Space-resolved and time-resolved resonance-enhanced vibrational Raman-spectroscopy from a femtosecond-lived singlet excited-state of β-carotene. (Translated from English) *Chemical Physics* 77(1):1-9 (in English).
198. Zanni MT & Hochstrasser RM (2001) Two-dimensional infrared spectroscopy: a promising new method for the time resolution of structures. (Translated from English) *Curr. Opin. Struct. Biol.* 11(5):516-522 (in English).
199. Jonas DM (2003) Two-dimensional femtosecond spectroscopy. (Translated from English) *Annu. Rev. Phys. Chem.* 54:425-463 (in English).
200. Zhang WM, Chernyak V, & Mukamel S (1999) Multidimensional femtosecond correlation spectroscopies of electronic and vibrational excitons. (Translated from English) *J. Chem. Phys.* 110(11):5011-5028 (in English).
201. Brixner T, Stiopkin IV, & Fleming GR (2004) Tunable two-dimensional femtosecond spectroscopy. (Translated from English) *Opt. Lett.* 29(8):884-886 (in English).
202. Cho M, Okumura K, & Tanimura Y (1998) Coherent two-dimensional Raman scattering: Frequency-domain measurement of the intra- and intermolecular vibrational interactions. *J. Chem. Phys.* 108(4):1326-1334.
203. Zhuang W, Hayashi T, & Mukamel S (2009) Coherent Multidimensional Vibrational Spectroscopy of Biomolecules: Concepts, Simulations, and Challenges. (Translated from English) *Angewandte Chemie-International Edition* 48(21):3750-3781 (in English).
204. Cho M (1999) Two-dimensional vibrational spectroscopy. III. Theoretical description of the coherent two-dimensional IR-Raman spectroscopy for the investigation of the coupling between both IR- and Raman-active vibrational modes. *J. Chem. Phys.* 111(9):4140-4147.
205. Biggs JD, Zhang Y, Healion D, & Mukamel S (2012) Two-dimensional stimulated resonance Raman spectroscopy of molecules with broadband x-ray pulses. *J. Chem. Phys.* 136(17):174117.
206. Hamm P & Savolainen J (Two-dimensional-Raman-terahertz spectroscopy of water: Theory. *J. Chem. Phys.* 136(9):094516.
207. Mukamel S, Piryatinski A, & Chernyak V (1998) Two-dimensional Raman echoes: Femtosecond view of molecular structure and vibrational coherence. *Acc. Chem. Res.* 32(2):145-154.
208. Mukamel S, Piryatinski A, & Chernyak V (1999) Semiclassical simulations of multidimensional Raman echoes. (Translated from English) *J. Chem. Phys.* 110(3):1711-1725 (in English).
209. Cheng YC & Fleming GR (2009) Dynamics of Light Harvesting in Photosynthesis. *Annu. Rev. Phys. Chem.,* Annual Review of Physical Chemistry, (Annual Reviews, Palo Alto), Vol 60, pp 241-262.

210. Leitner DM (Quantum localization and protein-assisted vibrational energy flow in cofactors. (Translated from English) *New Journal of Physics* 12:17 (in English).
211. Ishizaki A & Fleming GR (2012) Quantum Coherence in Photosynthetic Light Harvesting. *Annual Review of Condensed Matter Physics, Vol 3,* Annual Review of Condensed Matter Physics, ed Langer JS (Annual Reviews, Palo Alto), Vol 3, pp 333-361.
212. Hamm P & Zanni M (2011) *Concepts and Methods of 2D Infrared Spectroscopy* (Cambridge University Press, Cambridge) 1 Ed p 286.
213. Kurnit NA, Hartmann SR, & Abella ID (1964) OBSERVATION OF PHOTON ECHO. (Translated from English) *Phys. Rev. Lett.* 13(19):567-& (in English).
214. Mukamel S (2000) Multidimensional femtosecond correlation spectroscopies of electronic and vibrational excitations. (Translated from English) *Annu. Rev. Phys. Chem.* 51:691-729 (in English).
215. Zigmantas D*, et al.* (2006) Two-dimensional electronic spectroscopy of the B800-B820 light-harvesting complex. (Translated from English) *Proc. Natl. Acad. Sci. U. S. A.* 103(34):12672-12677 (in English).
216. Shim SH, Strasfeld DB, Ling YL, & Zanni MT (2007) Automated 2D IR spectroscopy using a mid-IR pulse shaper and application of this technology to the human islet amyloid polypeptide. (Translated from English) *Proc. Natl. Acad. Sci. U. S. A.* 104(36):14197-14202 (in English).
217. Cheng YC, Engel GS, & Fleming GR (2007) Elucidation of population and coherence dynamics using cross-peaks in two-dimensional electronic spectroscopy. (Translated from English) *Chem. Phys.* 341(1-3):285-295 (in English).
218. Okumura K & Tanimura Y (1997) Interplay of inhomogeneity and anharmonicity in 2D Raman spectroscopy of liquids. *Chem. Phys. Lett.* 277(1â€“3):159-166.
219. Nagata Y, Hasegawa T, & Tanimura Y (2006) Analyzing atomic liquids and solids by means of two-dimensional Raman spectra in frequency domain. *J. Chem. Phys.* 124(19):194504.
220. Kloz M, Grondelle Rv, & Kennis JTM (2012) Correction for the time dependent inner filter effect caused by transient absorption in femtosecond stimulated Raman experiment. *Chemical Physics Letters* 544:94-101.
221. Tschirner N*, et al.* (2009) Resonance Raman spectra of β-carotene in solution and in photosystems revisited: an experimental and theoretical study. *Physical Chemistry Chemical Physics* 11(48):11471-11478.
222. Merlin JC (1985) Resonance Raman-spectroscopy of carotenoids and carotenoid-containing systems. (Translated from English) *Pure Appl. Chem.* 57(5):785-792 (in English).
223. Pontecorvo E*, et al.* (2011) Femtosecond stimulated Raman spectrometer in the 320-520nm range. *Opt. Express* 19(2):1107-1112.
224. Jansen TlC, Snijders JG, & Duppen K (2001) Interaction induced effects in the nonlinear Raman response of liquid CS[sub 2]: A finite field nonequilibrium molecular dynamics approach. *The Journal of Chemical Physics* 114(24):10910-10921.
225. Liao PN*, et al.* (2011) On the role of excitonic interactions in carotenoid-phthalocyanine dyads and implications for photosynthetic regulation. (Translated from English) *Photosynth. Res.* 111(1-2):237-243 (in English).
226. Gall A*, et al.* (1999) Effects of mutagenesis on the detailed structure of spheroidenone in the Rhodobacter sphaeroides reaction centre examined by resonance Raman spectroscopy. Photosynth. Res. 59(2):223-230.

Summary

This thesis consists of eight chapters. The first describes the author's personal opinion on the general place of biophysics, femtosecond spectroscopy and photosynthesis in the context of natural science. The second chapter is a theoretical introduction to the spectroscopic techniques used in works described in the rest of the thesis. It includes a brief summary of spectroscopic properties of carotenoids. The third chapter describes transient absorption experiments performed on carotenoid-phthalocyanine dyads, investigating energy transfer from phthalocyanine to carotenoids of various lengths. The results suggest the existence of excitonic couplings between dark states of carotenoids and excited states of phthalocyanine. The fourth chapter is dedicated to a wavelength modulation approach to the femtosecond stimulated Raman experiment as a way to reduce undesired background signal. This includes the measurement of time resolved vibrational dynamics of β-carotene after excitation by blue light. The fifth chapter extends the study of molecules described in the third chapter for the study of the reverse process: carotenoid to phthalocyanine energy transfer. The energy transfer efficiency was discovered to be strongly dependent on the excessive vibrational energy. Additionally it was discovered that this effects can be masked by the subsequent dynamics of lower lying excited states. The sixth chapter describes a theoretical study of the inner filter effect as a source of artifacts in femtosecond stimulated Raman experiments. The seventh chapter is focused on the examination of a femtosecond stimulated Raman experiment performed in collinear geometry actinically pumped from the side. The goal of this approach is to achieve a higher signal gain and thus facilitate more sensitive femtosecond Raman experiments. Chapter eight proposes a two-dimensional Raman experiment based on interaction of two narrowband picosecond pulses and one broadband femtosecond pulse. The approach was also experimentally tested on a solution of β-carotene.

Samenvatting

Dit proefschrift bevat acht hoofdstukken. Het eerste hoofdstuk beschrijft de mening van de auteur over de algemene plaats van biofysica, femtoseconde spectroscopie en fotosynthese in de context van de natuurwetenschappen. Het tweede hoofdstuk is een theoretische introductie van de spectroscopietechnieken die worden gebruikt in het onderzoek dat in de volgende hoofdstukken wordt beschreven. Het bevat een korte samenvatting van de spectroscopische eigenschappen van carotenen. Het derde hoofdstuk beschrijft tijdopgeloste absorptie experimenten van caroteen-phtalocyanine moleculen. Hierbij wordt de energie-overdracht van phtalocyanine naar carotenen van verschillende lengte onderzocht. De resultaten wijzen op het bestaan van excitonische koppelingen tussen donkere staten van caroteen en geexciteerde staten van phtalocyanine. Het vierde hoofdstuk is gewijd aan het gebruik van golflengte modulatie in femtoseconde gestimuleerde Raman experimenten als een methode om ongewenst achtergrond signaal te verminderen. Het bevat een meting van de tijdopgeloste vibrationele dynamica van β-caroteen nadat het is geexciteerd met blauw licht. Het vijfde hoofdstuk is een uitbreiding van de studie naar de moleculen uit hoofdstuk drie met een onderzoek naar het omgekeerde proces: energie-overdracht van caroteen naar phtalocyanine. Hierbij werd ontdekt dat de efficiëntie van energieoverdracht sterk afhangt van de overtollige vibrationele energie. Daarnaast werd gevonden dat dit effect kan worden gemaskeerd door de hierop volgende dynamica van de lager liggende geëxciteerde staten. Het zesde hoofdstuk beschrijft een theoretische studie van het binnenste filter effect als een bron van artefacten in femtoseconde gestimuleerde Raman experimenten. Het zevende hoofdstuk is gericht op de studie van een femtoseconde gestimuleerde Raman experiment in collineaire geometrie, actinisch gepompt vanaf de zijkant. Het doel van deze benadering is het behalen van een grotere signaal sterkte, waardoor meer subtiele femtoseconde Raman experimenten kunnen worden uitgevoerd. Hoofdstuk acht beschrijft het voorstel van een tweedimensionaal Raman experiment, gebaseerd op interactie van twee nauwbandige picoseconde pulsen en één breedbandige femtoseconde puls. Deze methode is experimenteel getest op een β-caroteenoplossing.